STRUCTURE - PROPERTY BEHAVIOR OF SOL-GEL DERIVED HYBRID MATERIALS

by

Raymond Hans Glaser

Dissertation submitted to the Faculty of the
Virginia Polytechnic Institute and State University
in partial fulfillment of the requirements for the degree of
DOCTOR OF PHILOSOPHY
in
Materials Engineering Science

APPROVED:

Garth L. Wilkes, Chairman

Mark E. Davis

James L. McGrath

Larry T. Taylor

Richard H. Zallen

October, 1988

Blacksburg, Virginia

STRUCTURE - PROPERTY BEHAVIOR OF

SOL-GEL DERIVED HYBRID MATERIALS

by

Raymond Hans Glaser

Garth L. Wilkes, Chairman

Materials Engineering Science

(ABSTRACT)

Structure-property studies were carried out on a number of different hybrid sol-gel materials. Multifunctional silicon ethoxides were prepared and studied by solid state ^{29}Si NMR and Raman spectroscopy to determine the type of silicate structures formed and the degree of conversion attained by the sol-gel process under previously established reaction conditions. New procedures were developed to incorporate titaniumisopropoxide as well as Al, Zr and Zn acetylacetonates into functionalized poly(tetramethylene oxide) modified sol-gel systems. The physical properties of titanium containing poly(tetramethylene oxide) modified sol-gel materials were studied in detail and correlated to morphological and structural information gained from dynamic mechanical analysis, small angle x-ray scattering and scanning electron microscopy. The incorporation of titanium was found to increase the measured Young's modulus and stress at break relative to comparable materials based solely on TEOS.

To Indra

Acknowledgements

I wish to thank Professor Garth L. Wilkes for directing my research and for introducing me to the sol-gel process. He allowed me the freedom to pursue my interests in this area without any "unwanted" advice for which I am very grateful; his suggestions were always timely and worthwhile.

I wish to thank the secretaries in the Chemical Engineering office for helping with all of the "little things" that become "BIG THINGS" if not taken care of - thanks , and ! A special thanks goes to the head of the department Prof. William Conger who took care of my bureaucratic "problems" although, as an MESC student, I was not officially a part of Chemical Engineering.

I wish to thank my colleagues in Prof. Wilkes lab for all the stimulating discussions; in particular, I would like to thank the "Sol-Gel Gang" past and present for sharing their thoughts and ideas on THE PROJECT.

I also wish to thank the Phillips Petroleum Company for the fellowship support provided during my graduate school tenure at VPI & SU.

Finally, I am indebted to Dr. Hao-Hsin Huang who graciously provided his samples and data for comparison with my materials and who collected all of the SAXS profiles presented in this dissertation.

One last note; my friends and colleagues in Prof. Wilkes lab as well as those throughout the university will be missed; they made my stay in Blacksburg a pleasant one.

Table of Contents

List of Illustrations

List of Tables

CHAPTER I

INTRODUCTION

1.1 Definition of Sol-Gel

The objective of the ensuing work is to develop an understanding of the structure-property relationships in materials made by the so called "sol-gel process". This chemical process, well known to ceramic engineers, results in the formation of a three dimensional metal oxide network from a liquid metal alkoxide precursor. In such a process, a solution or "sol" (liquid) becomes a network solid or "gel". In principle, any crosslinking process by which a "molecular" liquid becomes a "network" solid can be considered to be a sol-gel process. Within the context of this text, however, the term "sol-gel", by definition, will refer only to the process by which an inorganic oxide network is made from monomeric metal alkoxides or related materials such as metal acetylacetonates.

The sol-gel process as just defined is not new. A review of the scientific literature confirms that the sol-gel process has been known for over one hundred years [1]. This process has proven to be a very useful method for preparing mixed inorganic oxide powders which can, in turn, be fired at relatively low temperatures (~900°C rather than ~1500°C or higher)

to form high purity glasses or ceramics of controlled chemical composition. For this and other related purposes, sol-gel chemistry has long been utilized.

1.2 Hybrid Sol-Gel Materials

In recent years, the sol-gel process has been used as a means of creating different types of novel hybrid materials. In the most general terms, these materials are either organically modified inorganic oxides or matrices comprised of inorganic oxides covalently linked to polymer molecules [1-20]. The potential advantages that such hybrid sol-gel materials may provide over conventional ceramic or polymeric materials are numerous. The most obvious advantage is improved mechanical performance relative to either pure ceramic or pure polymer. The inorganic component of the hybrid material promises hardness, high modulus and good thermal stability while the polymeric component promises variable flexibility and toughness. The combination of these properties in a homogenous material would be most desirable; increased thermal stability and high performance (strength and toughness) should be the result. Such materials could prove immediately useful as coatings and/or structural adhesives. The unique chemical nature of inorganic oxide/polymer hybrid materials promises many other advantages as well, particularly with regards to chromatography. These systems could be potentially useful as ion exchange resins or as customized column packings for gas and/or liquid chromatography. The sol-gel process is one possible route to achieving hybrid materials of this kind. Understanding the details of the overall process is important in determining how it can be utilized to produce new types of materials with specifically "tailored" properties.

The chemistry involved in the sol-gel process, sometimes incorrectly referred to as the sol-gel "reaction", is deceivingly simple. The process resembles a step-growth polymerization comprised of two reactions: hydrolysis and condensation. These reactions are schematically

HYDROLYSIS

$$Si(OR)_4 + 4H_2O \xrightarrow{H^+} Si(OH)_4 + 4ROH$$

CONDENSATION

$$Si(OH)_4 + Si(OH)_4 \xrightarrow{H^+} (HO)_3Si\text{-}O\text{-}Si(OH)_3 + H_2O$$

R = an organic function

Figure 1. Sol-gel reaction scheme

illustrated in Figure 1. Initially, a metal alkoxide - usually TEOS, $Si(OCH_2CH_3)_4$ - is hydrolyzed generating metal hydroxide (or metaloid) species - silanol in the case of silicon alkoxides. The hydroxide species can then, in turn, undergo stepwise polycondensation forming a three-dimensional network in the process. In the ideal case, all of the reactive sites on the metal alkoxide react fully each forming one network link. This, of course, is not actually the case; many factors influence the chemistry of these reactions the consequences of which determine the type of network structure formed.

Based on this chemistry at least three different types of hybrid material can be made. The metal alkoxide can be chemically modified at a functional site to include an organic (or inorganic) moiety which would then modify the properties of the final gelled material [1-6]. Alternately, a polymer system can be swollen with a metal alkoxide monomer; the swollen system, after the sol-gel process, would form a hybrid material in which the oxide may or may not be covalently linked to the polymer matrix [7-13]. Finally, a third possibility would be to covalently link the modifying component (organic/inorganic, monomer/polymer) directly to the oxide network using sol-gel chemistry [14-20].

It seemed reasonable to expect that appropriately functionalized long chain molecules would ***connect*** to the silicate network being formed ***during*** the sol-gel process. Hybrid materials incorporating functionalized oligomers/polymers with silicon alkoxides can in fact be made by this method. The first such materials, incorporating silanol terminated polydimethylsiloxane (PDMS) with tetraethylorthosilicate (TEOS), were successfully made in the laboratory of G.L.Wilkes in 1985 [14, 15]. These new materials proved to be unique in that they exhibited a high degree of optical clarity as well as physical properties unlike those of glass filled siloxane polymers [9, 10]. The novel mix of **cera**mic and poly**mer** nature prompted GLW to coin the descriptive term "CERAMER" to name these systems; they have been considered a new class of material.

At the time the first "CERAMER" type hybrid silicate-siloxane sol-gel materials were made, they were not well understood. Specifically, the type of silicate structures present in the material matrix was not known. Also, the degree of dispersion of the silicate structures

in the material matrix was not known except in an indirect manner. In order to determine the structure-property relationships governing these hybrid sol-gel materials, the degree of reaction in the silicate forming component and the degree of dispersion of that component in the material matrix has to be determined.

This is not a simple undertaking. Many factors are known to affect not only the chemistry of the sol-gel process but the morphology of the resulting gels as well. The amount and type of catalyst, the solvent system, the concentration as well as the amount of water available for hydrolysis are but a few of the obvious factors that influence the structure of the final materials. All of these factors can not be reasonably fathomed during the course of one study. Of necessity, then, certain reaction parameters were taken as "standard" or as reference conditions during the course of the study that follows. In this work, gels formed within the framework of the standard conditions set by prior work [14, 15] were studied to determine the type of silicate structures and morphology formed.

1.3 Objectives

There were four primary objectives that motivated the following research. The first objective was to determine the degree of completion of the overall sol-gel process in gels made under the reaction conditions established for the original hybrid "CERAMER" materials. The pursuit of this objective, it was hoped, would generate some understanding regarding the types of silicate structures and morphologies possible in "CERAMER" systems [14, 15]. The second objective was to make new and different hybrid materials. Several routes were explored in pursing this objective. New materials were attempted by incorporating non-silicon metal alkoxides as well as silicon alkoxides of varying functionality into existing oligomer modified TEOS systems. Also attempted were materials made by incorporating incompatible oligomers/polymers into silicate and modified silicate systems. In conjunction with the first

objective, successful incorporation of these modifying components, in particular the metal alkoxides, would provide a basis for "tailoring" specific features into new materials. This would be accomplished, in the case of metal oxide incorporation, by controlling the chemical composition of the inorganic oxide thereby "tailoring" the properties of the resulting material. The third objective was to characterize the various hybrid materials made in terms of their physical and mechanical properties. From these studies, it was hoped, one could determine the effects of chemical composition on the mechanical behavior of hybrid systems. The fourth and "final" objective was to take all data collected for the various sol-gel systems studied and formulate structure-property relationships. If clear-cut structure-property relationships exist and can be determined, they would provide a basis for designing and producing specialized new hybrid materials.

Several approaches were taken in attempt to meet the ambitious goals set forth. Model compounds were made and studied by Raman and NMR spectroscopy, as well as by dynamic mechanical analysis (DMA), in order to establish the nature of the silicate structures formed under the conditions used to synthesize the "CERAMER" materials. Hybrid sol-gels were also studied using these methods. To a lesser extent, other analytical techniques were applied to determine the morphological features of the sol-gel systems. These techniques included small-angle x-ray scattering (SAXS), scanning electron microscopy (SEM), and wide-angle x-ray scattering (WAXS).

Reaction schemes were devised to allow incorporation of metals, other than silicon, into hybrid sol-gel oxide materials. In particular, titanium(IV) isopropoxide, aluminum tri-sec-butoxide, aluminum acetylacetonate, zirconium(IV) acetylacetonate and zinc acetylacetonate hydrate were utilized as precursors for incorporation into transparent hybrid monolithic gels. Titanium(IV) isopropoxide was extensively used as a precursor for making mixed metal hybrid materials. The resulting materials were studied to observe the effects of metal oxide "heterogeneity" on the final material properties. These properties being, primarily, the thermo-mechanical and tensile stress-strain behavior.

An aging phenomenon that had been observed in hybrid materials made using functionalized poly(tetramethylene oxide) (PTMO) polymers [18, 20] was studied also. The change in certain physical properties was closely followed for a series of titanium containing multifunctional PTMO (defined in Chapter III) sol-gel hybrids. The thermo-mechanical (glass transition, T_g, behavior), tensile mechanical properties (Young's modulus, ultimate stress and ultimate strain) and the extraction as well as swelling behavior were all followed as a function of "aging" time for selected hybrid materials. Such information, it was hoped, would provide additional insight with regards to the "mechanism" of network formation in hybrid materials.

At this point, motivation for the ensuing research efforts should be clear. However, before the above mentioned studies can be meaningfully presented, a brief review of the pertinent sol-gel literature is in order.

CHAPTER II

LITERATURE REVIEW

2.1 Introduction

As mentioned in the previous chapter, the sol-gel process is not new. Schmidt et al. [1] pointed out that silicate sol-gel chemistry was first recognized by Ebelmen in 1844 and later studied by Friedel, Landenburg and Crafts in the years between 1860 and 1870. Study of the sol-gel process has continued steadily since that time, increasing dramatically in recent years. Indeed, a computer aided literature search covering just the past five years generated thousands of references (~4000) when given the general search heading of "sol-gel". For the most part, these publications address glass and/or ceramic precursors made using sol-gel techniques. The materials studied are generally in the form of oxide powders that have been pressed and scintered at elevated temperatures but studies of monolithic gelled materials are also present. Among this group of publications are also a number of general review articles [1, 5, 6, 21-25]. Specific topics of these reviews range from the chemistry to the processing and potential uses of sol-gel derived materials.

Though a desirable end, it is beyond the scope or intent of this chapter to comprehensively review this large body of literature. Also, as was pointed out, a number of general review articles on the subject of the sol-gel process already exist. Another such review is, then, somewhat unnecessary. Therefore, it is intended that this chapter present an overview to the general literature in the sol-gel area, reviewing in detail only topics of specific interest. In so doing this chapter will, hopefully, indicate the current level of scientific understanding (or lack thereof) in this area and serve as a prelude to the work that follows.

Two particular topics of interest that will be emphasized throughout this review are the chemistry and the structures of materials made by the sol-gel process. The materials studied in the work to be presented, relies on the acid catalyzed reaction of tetraethylorthosilicate (TEOS) in an alcohol based solvent. Accordingly, this review will be focused on papers addressing related sol-gel systems and will include studies on materials ranging from the liquid state up to and including the gelled state.

2.2 Sol-Gel Chemistry

The importance of the sol-gel process has grown rapidly since the synthesis of multicomponent glasses was first reported around 1970 [21]. Applications for specialized glass/ceramic materials made by the sol-gel process have burgeoned since then. Some of the reasons for this "enthusiastic" interest in sol-gel materials are obvious; some are not. In either case, sol-gel methods for producing specialized materials have gained popularity as a direct result of the compositional and structural control afforded by the chemistry of the overall process. It is worthwhile, for this reason, to review the deceivingly "simple" reactions that take place during the course of a typical sol-gel process.

2.2.1 Reactions

Typically, a sol-gel process starts out with a monomeric precursor: most often a tetrafunctional metal alkoxide such as TEOS. This precursor is usually diluted with a suitable solvent to which is added a certain amount of free water and a catalyst. The sol-gel process then begins - frequently at room temperature (~ 25°C) though sometimes at slightly elevated temperatures (~ 40-60°C) - and continues until all of the reactive sites have been utilized or the system can no longer react.

Figure 2 on page 11 gives a schematic representation of the various reactions possible for a tetrafunctional silicon alkoxide under typical sol-gel conditions. In this figure, "R", stands for an alkyl group and the open ended "bonds" stemming from the silicon atoms, ≡Si-OR & ≡Si-OH, (Figure 2 e & f) signify a connection to another -O-Si≡, an HO- or an RO- function. Note that if R = $-CH_2CH_3$, then $Si(OR)_4$ is tetraethylorthosilicate (TEOS) and ROH is ethanol.

The initial reaction, hydrolysis of one of the alkoxy groups, generates one hydroxide function on the alkoxide monomer and produces one equivalent of the corresponding "R" alcohol per functional group reacted. Figure 2 also illustrates the different levels or stages of hydrolysis that a four functional metal alkoxide (silicon alkoxide in this case) can, in principle, attain. Each hydrolysis step is actually an equilibrium reaction and is, therefore, properly characterized by two rate constants and an equilibrium constant. To fully describe the overall hydrolysis process in terms of just these four simple hydrolysis steps one would need twelve different constants.

Once the hydrolysis of a functional site has taken place, condensation reaction between an alkoxide and a hydroxide site can take place. Once several alkoxide sites have hydrolyzed, condensation between two hydroxide sites can take place (Figure 2 e & f). In each case, one equivalent of "R" alcohol or water is liberated per condensation reaction. It should be noted that hydrolysis need not be completed for these condensation reactions to begin; all that is

$$Si(OR)_4 + H_2O \leftrightarrows HOSi(OR)_3 + ROH \quad (a)$$

$$HOSi(OR)_3 + H_2O \leftrightarrows (HO)_2Si(OR)_2 + ROH \quad (b)$$

$$(HO)_2Si(OR)_2 + H_2O \leftrightarrows (HO)_3SiOR + ROH \quad (c)$$

$$(HO)_3SiOR + H_2O \leftrightarrows Si(OH)_4 + ROH \quad (d)$$

$$\equiv SiOR + HOSi\equiv \leftrightarrows \equiv Si\text{-}O\text{-}Si\equiv + ROH \quad (e)$$

$$\equiv SiOH + HOSi\equiv \leftrightarrows \equiv Si\text{-}O\text{-}Si\equiv + HOH \quad (f)$$

Figure 2. Schematic of sol-gel reactions

required for condensation to occur, to satisfy the ***simplified*** reaction scheme in Figure 2 on page 11, is the hydrolysis of one alkoxide function.

As the condensation proceeds, the average number of ≡Si-O-Si≡ links per silicate molecule increases. This process is analogous to a "standard" step-growth by polycondensation polymerization known for hydrocarbon polymers [26]. The weight average molecular weight, $<M_W>$, of the silicate molecules formed increases as the polycondensation progresses until, ultimately, it reaches infinity. At this point the system undergoes a transition from a solution of "large particles" (molecules if you will) to a network gel. For silicate systems this is generally considered to be a non-reversible transition [23].

After the sol to gel transition, *if* the hydrolysis and condensation reactions both go to completion, the molecular structure of the resultant network should be that of amorphous silica i. e. tetrahedral SiO_2. Under "normal" experimental conditions this would be highly unlikely since one hundred percent completion of any reaction is generally difficult to obtain. Even under the best of conditions, ultrahigh conversions are not trivial, especially for polycondensation reactions. However, unlike linear monomers, to reach the gel point (infinite $<M_W>$) with a four-functional monomer such as TEOS, does not require a degree of conversion equal to unity. Rather, to form a gel from a four-functional precursor would only require the polycondensation process go to $\simeq$ 40 percent completion if one assumes a Bethe lattice (no cyclization) is formed [26]. After the sol-gel process has run its course, there are still, undoubtedly, many unreacted sites left on silicon centers throughout the gel. The gel structure actually formed is, therefore, somewhere between that of high molecular weight silica particles (polymers) and pure tetrahedral silica.

Based on the seemingly simple reaction scheme presented in Figure 2, it becomes apparent that during the sol-gel process, as the metal alkoxide of interest first hydrolyzes then condenses, a host of intermediate species are formed. The possibility of condensed ring-like silicate species complicates the scheme further. What these intermediate species are, how they influence the course of the oxide network formation and whether or not they are present in the final gelled or vitrified materials are three fundamental issues that are addressed in

most of the existent sol-gel literature. The mechanical integrity, porosity and other properties of gelled and subsequently fired materials hinge on the presence (or absence) of the above said intermediates. Pursuit of these structures provides insight to the reaction mechanisms which, in turn, identifies the important experimental parameters governing the sol-gel process.

2.2.2 Reaction Mechanisms

Since hydrolysis and condensation are the two critical reactions in the sol-gel process, they have been the subject of a certain amount of study [27-33]. Schmidt et al. gave a brief history of the reactions of silicon alkoxides in their review on the sol-gel process [1]. In that review, Schmidt and co-workers postulated that the hydrolysis of silicon alkoxides, under acidic conditions, proceeds through the rate limiting formation of a three coordinate siliconium ion transition state ($(RO)_3Si^+$). The basis for this postulated transition state was, primarily, rate data obtained for substituted ethyl silicates [1, 5]. Others have postulated hydrolysis and condensation intermediates/transition states (i. e. mechanisms) based on kinetic [22, 23, 34] and growth data [24 27, 35-43] as well. In the later studies, the structure of the polymerizing silicate species was tied to the mechanisms of hydrolysis and condensation [27, 35-39]. Structural data from reactions involving stereochemical compounds were also reviewed [44, 45]. In all of the studies it was found that the mechanism for hydrolysis, in particular, was dependent on the type of catalyst used, acid or base.

The common approach taken in all these studies was to explain the reactions of silicon alkoxides in terms of mechanisms developed for carbon chemistry [1, 29, 34, 44, 45]. Silicon being of the same elemental group as carbon makes it reasonable to expect certain similarities in the chemistry of the two. Hence, the same rationale used to explain the mechanism of a reaction at a carbonyl carbon (in particular an ester carbonyl) can be and is applied to the analogous reaction of a silicon alkoxide. Hydrolysis of a silicon ester, for example, has

been explained in terms of mechanisms established for the hydrolysis of a hydrocarbon ester. After this "convention", the two mechanisms that have been postulated most often for the hydrolysis of silicon alkoxides are nucleophilic [1, 29, 34, 35, 36, 44, 45] and (incorrectly this author believes) electrophilic substitution [35, 36]. Condensation, on the other hand, has been generally thought to proceed by only a nucleophilic substitution mechanism [29, 36].

In the most general sense, the distinction between "electrophilic" and "nucleophilic" substitution lies in the nature of the attacking and leaving groups as well as the nature of the reactive site [46]. A nucleophilic substitution reaction involves the attack of an electron "rich" group (Lewis base) at an electron "poor" center (Lewis acid) generating, ultimately, an electron "rich" leaving group. The attacking group in such a reaction is known as the "nucleophile"; the reaction center is the "electrophile". In an electrophilic substitution reaction the attacking and leaving groups are the electrophiles and are electron "poor" while the reaction center is considered the "nucleophile" and is electron "rich" (the exact reverse of the nucleophilic reaction). In both cases, the nucleophiles and electrophiles may or may not carry an actual charge depending on the relative strength of the leaving group and/or the reaction center. In this manner, a neutral moiety can act as a nucleophile or an electrophile provided the proper circumstances exist. For example, a neutrally charged moiety may act as a nucleophile if the reaction site is strongly electrophilic (electron deficient or electropositive) and/or the leaving group is a weaker nucleophile than the attacking moiety [46].

The two classes of mechanisms, nucleophilic and electrophilic, can each be subdivided into unimolecular and bimolecular reactions. This gives rise to four inherently different substitution reactions. Using the notation "S" for substitution, subscript "N" or "E" for nucleophilic or electrophilic and "1" or "2" for unimolecular or bimolecular to identify the four reactions gives: S_N1, S_N2, S_E1 and S_E2. A bimolecular nucleophilic substitution reaction, S_N2, in carbon chemistry, always proceeds through a five coordinate transition state which results in the inversion of the reactive center [46]. The rate limiting step in an S_N2 mechanism is the formation of the coordinated transition state by "backside" attack of the nucleophile; "backside", here, refers to a position on the reactive center opposing the eventual leaving group. A

bimolecular electrophilic reaction, S_E2, also proceeds through a five coordinate transition state, the formation of which is the rate limiting step. However, the coordinated transition state in an S_E2 reaction is not necessarily formed by a "backside" attack of the electrophile. Therefore, an S_E2 mechanism can result in inversion or retention of configuration at the reactive center [46]. A unimolecular mechanism, either S_N1 or S_E1, by contrast, proceeds through a planar charged intermediate which results in the "racemisation" of a chiral reactive center [46].

In principle, the different substitution mechanisms presented should be distinguishable on the basis of their chemistry. The stereochemistry of unimolecular reactions should produce racemic mixtures of enantiomers for reactions at chiral centers. The kinetics for these mechanisms should be first order overall [46]. The rate of reaction should be dependent only on the concentration of the reacting substrate. The stereochemistry of bimolecular mechanisms should not result in the racemisation of chiral centers. S_N2 reactions should result in inversion of configuration at the chiral center while S_E2 reactions should result in either retention or inversion of configuration but no racemisation. Both bimolecular mechanisms are expected to follow second order kinetics overall [46]. The rate of reaction should be proportional to the product of concentration of the substrate and attacking group. In this manner, the four different types of substitution mechanisms presented can be distinguished from one another based on the chemical identity of the substituting groups (nucleophiles or electrophiles), the stereochemistry at the reaction center and/or the kinetics of the reaction. In practice these distinctions, for a variety of reasons, are not always easy to make.

The first notable kinetic studies of the sol-gel process were carried out by Aelion, Loebel and Eirich in 1950 [34]. These researchers studied the rate of hydrolysis and condensation for ethyl silicates under both acidic and basic conditions. Schmidt and co-workers conducted similar kinetic studies ~30 years later extending the scope to include the hydrolysis and condensation of alkyl substituted silicates as well [1, 5]. Sommer and co-workers, rather than studying the kinetics, studied the stereochemistry of substituted **chiral** silicate compounds reacted under a variety of conditions [44, 45]. Stereochemical information obtained from these

reactions were attributed to specific mechanisms. In addition to these three groups, a host of other researchers have also studied the sol-gel process under different reaction conditions [27, 28, 30, 33, 35, 36]. These researchers have postulated mechanisms based on early work reported in the literature (primarily Aelion et al. [34]) and their own "structural" results.

Aelion et al. observed that the rate of hydrolysis, at ~20°C under acidic conditions and excess water, was dependent on the concentration of ethyl silicate and the amount of water in the reaction mixture [34]. The hydrolysis rate was found to be proportional to the acid concentration and the strength of the acid as well. In strongly acidic solutions the hydrolysis was observed to be fast and complete with no unreacted monomer. In weakly acidic solutions the rate was observed to be slow and the hydrolysis incomplete. Under neutral conditions, hydrolysis of ethyl silicates was found to be extremely slow and reached only 15% completion. Furthermore, weak organic acids, such as acetic acid, did not accelerate or "catalyse" the hydrolysis as well as did strong inorganic or "mineral" acids such as nitric or hydrochloric.

Under basic conditions at ~20°C and excess water, the rate of hydrolysis was also observed to be dependent on the concentration of ethyl silicate. Additionally, hydrolysis under basic conditions was observed to be dependent on the concentration of base but independent of the amount of water. Aelion and co-workers found that, except for very high acid concentrations, hydrolysis was the fastest step in acid catalysed ethyl silicate reactions; condensation or "dehydration" lagged behind [34]. On the other hand, in base catalysed reactions condensation proceeded rapidly. Further, in base catalysed systems, phase separation was observed at higher ethyl silicate concentrations (which confused some of the kinetic results) [34].

Aelion Loebel and Eirich also studied the effect of solvent on the reaction rates of ethyl silicates [34]. In acid catalysed reactions, changing the solvent from ethyl alcohol to methyl alcohol or even dioxane was found to have little effect on the hydrolysis rate. This was taken by Aelion et al. as an indication that transesterification with these alcohol solvents (solvolysis) is negligible under acidic conditions [34]. This also implied that perhaps the active species and mechanism of acid catalysed hydrolysis are such that they are not significantly affected

by the nature of the solvent. In base catalysed systems, unlike acid catalysed systems, a marked dependence on the nature of the solvent was discovered. The hydrolysis rate observed in dioxane was much slower than that in ethanol which, in turn, was slower than that observed in methanol [34]. These results implied that the base catalysed reaction proceeds by a mechanism involving species strongly affected by the solvent media.

From the experimental results outlined above, Aelion and his colleagues [34] were able to draw several conclusions concerning the hydrolysis of ethyl silicates. Under acid catalysed conditions, using a strong acid and a given acid concentration, the overall hydrolysis kinetics were second order with respect to the ethyl silicate and water content. On the other hand, under base catalysed conditions the hydrolysis kinetics were first order with respect to the concentration of the ethyl silicate and also first order with respect to the concentration of base. Since the concentration of base determines the concentration of HO^- (a reactive species in the hydrolysis) the observed rate dependence on the base concentration implied that hydrolysis under basic conditions is second order overall. In light of the observed reaction kinetics, Aelion et al. proposed two possible mechanisms for hydrolysis in acidic media: "general acid catalysis" and "oxonium ion catalysis" [34]. The base catalysed reaction, it was concluded, proceeds through the nucleophilic displacement of an alkoxy function by a hydroxide ion [34].

The "general acid catalysis" proposed by Aelion and co-workers is simply a textbook acid catalysed S_N2 mechanism known for hydrocarbon esters [46]. In this mechanism, a protonated alkoxy oxygen helps make the silicate center a "better" electrophilic site for the subsequent nucleophilic attack of a water molecule. Such a mechanism is consistent with the observed rate dependence on acid strength and concentration since the equilibrium level of protonation of the alkoxy functions is governed by the pH (acidity) of the reaction media. The acid catalysed S_N2 mechanism can, therefore, be considered termolecular in nature since three separate "molecules" are necessary for the reaction to begin: an ethyl silicate, an acidic proton and a water molecule.

The postulated "oxonium ion catalysed" mechanism also superficially resembles an acid catalysed S_N2. However, instead of an independent protonation of an alkoxide function fol-

lowed by the nucleophilic attack of a water molecule, the postulated oxonium ion mechanism is bimolecular in nature and involves the attack of a coordinated water-acid species - i.e. a hydronium ion. This coordinated species attaches to the unshared pairs of electrons at the ester oxygen and silicon atoms to form a five coordinate transition state. The transition state then rearranges and dissociates to form a silanol, the corresponding alkoxy alcohol and one mole of acid (which would rapidly reform a hydronium ion).

The rate dependencies observed by Aelion et al. for hydrolysis of ethyl silicates under acidic conditions hint that the reaction is termolecular in nature - there is a concentration dependence on three different species. A termolecular reaction, in turn, would favor general acid catalysis over an oxonium ion mechanism. However, an acid catalysed (termolecular) mechanism can also be reconciled with second order kinetics. For a given acid concentration, since H^+ remains relatively constant throughout the reaction, the rate is dependent on only the ethyl silicate and water concentration - second order kinetics. Therefore, the observance of "second order" kinetics does not rule out the "general acid catalysed" (S_N2) mechanism.

Schmidt et al. [1, 5] repeated the kinetic work of Aelion et al. [34] on ethyl silicates but extended the study to include substituted silicates of the type $R_XSi(OC_2H_5)_{4-X}$. In general, the observations of Aelion and his co-workers [34] were verified. Specifically, Schmidt and his co-workers found that in acidic media H^+ does play a catalytic role in the hydrolysis of ethyl silicates. In their work Schmidt and co-workers also demonstrated that, under acid (HCl) catalysed conditions, the relative rates of hydrolysis for substituted silicate esters is: R_3SiOR > $R_2Si(OR)_2$ > $RSi(OR)_3$ >> $Si(OR)_4$ [1, 5]. Under base (NH_4OH) catalysed conditions this order was observed to be reversed. Schmidt et al. also noted that the relative rates of hydrolysis for substituted alkoxy silanes under acid hydrolysis slow down as the R group becomes larger (for a homologous series of alkyls) [1].

The rate results for acid catalysed hydrolysis of alkyl substituted silicate esters led Schmidt and his co-workers to postulate a mechanism that proceeds through a siliconium ion intermediate [1]. The rationale was that methyl groups on the silicate ester help stabilize the positive charge of a siliconium ion intermediate through an inductive effect (this is a well re-

cognized effect [46]). Stabilization of the charged intermediate lowers the activation energy which, in turn, increases the rate of the hydrolysis reaction. Each additional methyl function on the silicate ester should, therefore, serve to make the remaining alkoxy functions more reactive towards acid catalysed hydrolysis [1]. This rationale is consistent with the observed increase in acid catalysed hydrolysis rate with increasing methyl substitution. However, Schmidt and his co-workers [1], recognized that a nucleophilic mechanism for hydrolysis is consistent with the kinetic results of Aelion et al. [34] whereas a siliconium ion intermediate is not.

Schmidt et al., based on reaction rate data, postulate a bimolecular nucleophilic substitution mechanism for base catalysed hydrolysis [1, 5]. A bimolecular nucleophilic substitution, or S_N2, mechanism is consistent with the observation that tetraorthosilicate esters hydrolyse much faster than alkyl substituted esters under basic conditions [1, 5]. The rationale used to explain these results in terms of a S_N2 mechanism is much the same as that involked for the formation of a siliconium ion. Methyl substituents contribute electron density to the silicon center making it less positive and, therefore, less reactive towards nucleophilic attack by a hydroxide ion. Each successive methyl substituent renders the silicon center less "electrophilic" further reducing the reactivity towards base catalysed hydrolysis in the process. The observed hydrolysis rates for substituted silicate esters under basic conditions support this rationale: the di and tri methyl substituted orthoesters did not even hydrolyze [1, 5].

Sommer and co-workers studied the substitution reactions of a variety of optically active (chiral) silicon compounds providing evidence for the S_N2 hydrolysis mechanism in the process [44, 45]. In their work, the optical activity of the reaction products were studied to determine whether inversion, retention or racemisation of the chiral center took place during the substitution. Compounds with the general formula R_3Si^*X were reacted under conditions ranging from basic to neutral pH while the solvent polarity and the substituting species were varied [44, 45]. Sommer et al. found that inversion took place for reactions in which X was a good leaving group (-OCOR or -Cl) for which the conjugate acid had a pKa $< \simeq 5$ [45]. For

reactions involving poor leaving groups, (-H, -OCH_3, or -OH) whose conjugate acids had pKa values > ≃10, the stereochemistry resulted in either retention or inversion of configuration depending on a number of unspecified factors [45]. Sommer and his colleagues concluded that these reactions need to be evaluated on an individual basis. One such reaction of note was the substitution of methoxide (-OCH_3) by hydroxide (-OH) in a basic solution of water and acetone, i.e. base catalysed hydrolysis of a silicon alkoxide. These conditions produced an inversion of the chiral silicon center which is indicative of a bimolecular nucleophilic substitution or S_N2 reaction [45]. Unfortunately, reaction conditions comparable to the acid catalysed hydrolysis used in many sol-gel processes were not studied. Otherwise, as for base catalysed hydrolysis, definitive stereochemical information would have been available to aid in the determination of the acid catalysed hydrolysis mechanism.

Keefer also proposed a nucleophilic mechanism for base (HO^-) catalysed hydrolysis [36]. Keefer, however, proposed an "electrophilic" mechanism for acid (H^+) catalysed hydrolysis in apparent contrast to the work of Aelion et al. which was cited [34]. Upon close inspection though, the electrophilic substitution mechanism presented by Keefer [36] for silicon ester hydrolysis in acidic media turns out to be the oxonium ion mechanism postulated by Aelion et al. [34] for those conditions. According to the previously given definitions of "nucleophilic" and "electrophilic", Keefer [36] was incorrect in terming the proposed mechanism "elecrophilic". In the mechanism proposed, the oxygen from the attacking hydronium ion is attached to the silicon center after substitution is complete; there is no substitution at the alkoxide oxygen (unless one considers rearrangement of the oxonium ion after the actual hydrolysis). The R-O bond of the alkoxy group is not broken during the reaction. The labelled oxygen substitution experiments of Khaskin confirm this last point; hydrolysis of $(CH_3)_2Si(OR)_2$ by $H^{18}OH$ demonstrated that the R-O bond remains intact. (as cited by Schmidt et al. [1]). Since hydrolysis involves substitution at the silicon center, the mechanism postulated should indicate the nature of the reaction at the silicon center ***not*** at the alkoxy oxygen. Therefore, because the "substitution" is at the silicon center rather than the alkoxy oxygen, it is technically incorrect to label this overall hydrolysis process "electrophilic". It would be

more accurate to label this postulated hydrolysis process as an S_N2 mechanism. It should be recognised though, that the differences between one author's "oxonium ion catalysed" mechanism and the other's "electrophilic" mechanisms are, in this case, due more to differences in terminology than in substance.

Keefer and his colleagues have provided a connection between the mechanisms of reaction and the structure of the silicate "particles" formed [35-39, 43, 47]. Using small-angle x-ray scattering (SAXS), these researchers observed "fractal" or open, "linearlike", silicate growth in acid catalysed systems but dense highly branched "particulate" silicate growth in base catalysed systems. It was reasoned that the observed scattering particle growth can be directly related to the reaction mechanisms by which the polysilicates are formed. The rationale invoked is that basic or alkaline conditions promote the formation of silicic acid ($Si(OH)_4$) while acidic conditions do not promote the formation of silicic acid. The condensation of silicic acid under alkaline conditions forms highly crosslinked silicates [36]. On the other hand, condensation under acidic conditions begins prior to the completion of the hydrolysis to silicic acid resulting in the formation of "loosely" crosslinked linear silicates [36].

The mechanism for hydrolysis and condensation under alkaline conditions was postulated to be nucleophilic substitution by backside attack of the nucleophile [36]. Base catalysed hydrolysis would be expected to proceed rapidly towards the formation of silicic acid. As each successive alkoxide function is hydrolysed the silicon center becomes more positive (electrophilic) in nature and the remaining alkoxide functions become more reactive (see earlier explanation of the S_N2 mechanism). The condensation process, also proceeding by an S_N2 mechanism, for these same reasons favors the reaction of partially condensed silicates with uncondensed silicic acid. Partially condensed silicates, due to the inductive contribution of electron density to the silicon center, are nucleophilic relative to silicic acid. Silicic acid, being reactive at four sites, would, therefore, be expected to condense into tightly crosslinked silicate molecules.

Hydrolysis under acidic conditions was postulated by Keefer [36] to proceed by an oxonium ion catalysed mechanism (discussed earlier). This proposed mechanism would be

sensitive to the electron density surrounding the silicon center (as would a "normal" acid catalysed S_N2 mechanism [46]). As the electron density around the silicon center is decreased, the alkoxide oxygen atoms are less apt to form the five coordinate transition state since their relative electron density is decreased also (they are less susceptible to protonation or attack by a hydronium ion complex). The acid catalysed reaction slows as each successive alkoxide group is hydrolysed since hydroxy groups do not contribute as much electron density to the silicon center as do alkoxy groups. For this reason, unreacted tetraorthosilicates should be the fastest hydrolysing alkoxide species. The end result is that under acidic conditions, condensation reactions should begin before hydrolysis is completed. The average number of reactive sites (functionality) in the condensing silicate species should be, in turn, less than the maximum value of four as observed for silicic acid. The acid catalysed process would, therefore, be expected to produce less highly crosslinked silicates than the alkaline process simply due to the lower functionality of the condensing species.

On the whole, the kinetic results of Aelion et al. [34] for the hydrolysis of different silicates under acidic and basic conditions are consistent with those expected for bimolecular processes. A bimolecular nucleophilic substitution mechanism for base catalysed reactions based on kinetic information has not been disputed. This mechanism has been supported by stereochemical evidence as well. On the other hand, kinetic evidence alone has not been sufficient to determine the exact mechanism for acid catalysed reactions. The kinetic evidence has indicated some kind of bimolecular process, thereby making a siliconium ion intermediate an unlikely pathway for the acid catalysed hydrolysis of ortho silicates. There exists, however, no stereochemical data to support the choice of one mechanism over the other. A strong likelihood is that more than one type of reaction mechanism is possible during acid catalysed hydrolysis. Which particular mechanism dominates the hydrolysis will be very dependent on the experimental conditions used - a "complicating" factor that, in the interest of simplicity, has been tacitly ignored up to this point.

2.3 Experimental Conditions

As implied, the sol-gel process can be carried out under many different experimental conditions. Numerous reaction parameters as well as post gel "processing" parameters can be altered or "adjusted" to obtain, often times, vastly different final materials. The type of alkoxide, the amount of water available for the initial hydrolysis, the type of catalyst - either acid or base - and the chemical nature of the solvent are all reaction parameters commonly "adjusted" for this purpose. The rate and extent of solvent removal and thermal treatment (pre and/or post gel), on the other hand, are processing parameters commonly used to control the final material matrix. A review of these various reaction and processing parameters and their individual effects on the gelled materials produced could prove insightful.

Not surprisingly, different types of alkoxides are known to have different reactivity towards hydrolysis [1, 2, 5, 6, 22, 23, 29, 48]. In relative terms, the reactivity of a metal alkoxide can be judged by comparing three of its chemical/structural features with those of TEOS, $Si(OC_2H_5)_4$ (an arbitrary standard). The base "metal", the chemical structure of the alkoxy functions as well as the number and type of non-reactive functional groups all control the reactivity of a metal alkoxide as does the solvent system used and other experimental parameters (the latter two will be addressed shortly). In addition to affecting the reactivity, the afore mentioned features have a direct bearing on the type of network structure that can be formed by a particular metal alkoxide when gelled.

Of the three chemical/structural features that govern the reactivity of an alkoxide, the most influential is the choice of base "metal". Here the term "metal" is being used in its broadest sense. Many elements, including non-traditional "metals" (silicon for example), can be and have been used as precursors in sol-gel processes. In a recent review, Dislich included a periodic table highlighting the different elements that had been employed in sol-gel processes [21]. Most elements and every elemental group, save for the noble gases, were represented in this highlighted set. The choice of sol-gel precursor is, then, in no way re-

stricted to silicon alkoxides. A change from silicon as the base "metal", however, would change the electron affinity, hence the charge density, of the alkoxide core and could also result in a change in the coordination number [29, 48]. Differences of this nature should be reflected in the chemistry of the "altered" alkoxide.

Indeed, changing the metal has been known to drastically alter the reactivity of the alkoxide. For example, titanium alkoxides have been found to be much more reactive towards hydrolysis than the corresponding silicon alkoxides [2-6, 22, 23, 25, 48-52]. This has also been found true for zirconium [53-56] and aluminum [30, 54, 57-59] alkoxides when compared to their silicon counterparts. Further, the reactivities of the various metal alkoxides change in a systematic fashion. Hubert-Pfalzgraf noted that the stability of "d" block transition metal alkoxides of the general formula $M(OR)_n$ (where M = a metal atom and R = a saturated or an unsaturated organic group), decreases as one moved to the right of the periodic table: i. e. with decreasing "n". Moreover, the number of such alkoxides also decreases as the coordination number, "n", decreases [22]. Hubert-Pfalzgraf concluded that hydrolysis seemed to be favored by the electropositivity of the metal in the alkoxide, though the conditions for hydrolysis were unspecified (but are of critical importance as will be demonstrated shortly) [22]. In general, silicon alkoxides are the slowest hydrolyzing and most stable of the metal alkoxides [2, 4, 22, 52].

The chemical nature of the metal atom in question not only effects the reactivity of the alkoxy functions but the structure of the resultant gel network as well. For example, silicon oxides, such as quartz. typically have the chemical composition: SiO_2, where the silicon atoms are four-fold coordinate (tetrahedral geometry) [29, 48]. Zirconium and titanium can also form oxides of similar chemical composition where the metal atoms are four coordinate: ZrO_2 & TiO_2. However, titanium and zirconium can also exist as six coordinate (octahedral geometry) as well as four coordinate species [60, 61]. On the other hand, aluminum oxides are generally of the composition Al_2O_3 while those of zinc are of the form ZnO [22, 59, 62, 63]. It is intuitively obvious that gels containing oxides of these different metals would have dif-

ferent network geometries simply by virtue of their bonding configurations. Hence, such gels should have different structures and, more than likely, different properties.

Another factor demonstrated to effect the hydrolysis mechanism and reactivity of an alkoxide is the chemical makeup/structure of the alkoxy groups. The electron donating or withdrawing capability of the alkoxy function is reflected in the polarity of the metal-alkoxy bond; the polarity, in turn, determines both the reactivity of the bond towards hydrolysis and the mechanism of that reaction [5, 22, 44, 45, 48]. Alkoxy groups that can withdraw electron density from the metal center, creating a partial positive charge in the process, promote nucleophilic attack at the metal center. Conversely, alkoxy groups that can donate electron density, preventing a partial positive charge from developing, render the alkoxide less sensitive to nucleophilic attack [36]. Also, the nature of the alkoxy group as a leaving group generated by a bimolecular nucleophilic substitution has a significant bearing on the hydrolysis of an alkoxide (provided the reaction proceeds by an S_N2 mechanism). It has been demonstrated that alkoxy functions with a conjugate acid pKa lower than that of the surrounding reaction mixture make good leaving groups and favor hydrolysis. The reverse has been demonstrated for functions with a conjugate acid of high pKa [45]. In the same vein, Hubert-Pfalzgraf noted that the hydrolysis rates for $Si(OR)_4$ increased as the R group changed from a primary to a tertiary alkyl (though the pH of the reaction medium was not specified) [22]. The "bulkiness" of the alkoxy structure has also been demonstrated to play a major role in determining the reaction rate as well as the mechanism [1, 5, 22, 29, 44, 45, 48]. Large alkoxy functions sterically hinder the approach of potential reactants to the active site of the metal alkoxide thereby slowing or preventing any reaction from taking place. In this manner the chemical nature as well as the physical structure of the alkoxide function effect the rate and mechanism of the hydrolysis reaction.

The final consideration regarding the reactivity of metal alkoxides concerns the number of reactive functions on the alkoxide in question. Non-reactive (non-hydrolyzable) sites on the metal alkoxide are known to have a bearing on the reactivity of the alkoxide sites. In a study discussed previously (section 2.2.2), Schmidt and co-workers measured the relative rates of

hydrolysis of a series of substituted alkoxides of the type $(CH_3)_XSi(OC_2H_5)_{(4-X)}$ [1, 5]. Increasing the number of methyl groups attached to the silicon atom was found to increase the acid catalyzed hydrolysis rate relative to $Si(OC_2H_5)_4$. The reverse was found to be true for base catalysed hydrolysis.

The qualifier to all of the above discussion is that the reactivity of any given metal alkoxide is highly dependent on the experimental conditions employed. Changing the nature of the reaction media and/or the catalyst has been demonstrated to effect the chemistry of the sol-gel process in numerous ways. The rate and mechanisms (discussed in section 2.2.2) of the hydrolysis and condensation reactions, it has been shown, are determined by the type of catalyst, the amount of water available for hydrolysis and the nature of the solvent media.

Many authors have studied the effects of using various amounts of water and/or one type of catalyst over the other [5, 6, 21-24, 27, 28, 30-33, 35-43, 47, 48, 64-66]. The amount of water in the reaction mixture plays a key role in determining the type of silicate structures formed during the sol-gel process. This point has been generally agreed upon [1, 5, 6, 21-24, 27, 31, 32, 35-43, 64-66]. When run under conditions that provide insufficient amounts of water to completely hydrolyze the silicon alkoxide (TEOS in most cases), most authors conclude that the silicate structures formed are linear or polymeric in nature. The precursor alkoxide, under such conditions it has been reasoned, can not fully hydrolyse before condensation begins. Once the condensations have begun, generating water in-situ, hydrolysis can continue. However, since the endgroup alkoxides of condensed species are the most reactive towards continued hydrolysis, the reacting system produces more linear polymeric silicates rather than dense highly crosslinked silicates. Hubert-Pfalzgraf (as well as many others) noted that if the ratio "h" is less than "n", where "h" = $H_2O/M(OR)_n$ and "n" is the number of reactive functions on the metal alkoxide, fibers (chains) and coatings can be formed by the sol-gel process; if "h" is greater than "n", gels or three dimensional networks are formed [22].

It should be noted, though, the above conclusions were based on acid catalysed systems. Base catalysed systems, it has been demonstrated, generate more highly branched dense silicate structures [24, 35-43]. For this reason, the type of catalyst employed, acid or base,

plays probably the most important role of all the experimental factors in determining the structure of the condensing silicate. Specifically, polymeric or linear structures have been attributed to reaction limited cluster - cluster growth in low water/acid catalyzed systems by Brinker and his colleagues [35-39, 43]. Dense highly branched silicate particles have been attributed to monomer - cluster growth in base catalysed systems by these same authors though Duran et al. [33] have observed what they deemed to be "polymeric growth" in base catalyzed systems. The rationale behind the observed differences in silicate structure is a change in the hydrolysation mechanism from acid catalysed to base catalysed substitution (mechanisms are discussed in detail in section 2.2.2).

The chemical nature of a solvent and its effects on reactions have often been overlooked or tacitly ignored. Generally solvents have been chosen for their ability to dissolve the reactants and keep the reaction intermediates and products in solution. However, it has been demonstrated that the solvent can, under the appropriate conditions, participate directly in the hydrolysis reaction [22, 28, 36]. An important potential competing reaction not shown in Figure 2 on page 11 is transesterification, or solvolysis, of the metal alkoxide with the alcohol solvent. Though solvolysis has not generally been considered a problem, it has been shown to be dependent on the choice of alcohol solvent, the nature of the alkoxide and the hydrolysis conditions employed [28, 36]. Solvolysis was found to be particularly sensitive to whether acid or base catalysis was employed. In base catalysed hydrolysis, transesterification was non-existent whereas in acid catalysed hydrolysis it was observed to be, potentially, a troublesome side reaction [28, 36]. Dilution of the reactants has also been known to effect the molecular structure and degree of polymerisation. Yoldas demonstrated by ^{29}Si NMR and gpc that, all things being equal, higher dilution results in more Si-O-Si bridging links and a higher degree of polymerization [32]. For these reasons, in sol-gel systems, the solvent plays an important role in governing the hydrolysis reaction in addition to solvating the different reacting species.

Dilution and solvolysis (discussed above) are properly considered as "solvent effects" on the sol-gel process as is complexation. The ability (or inability) of a solvent to "solvate" or form complexes with reacting species can control a reaction. For example, the hydrolysis rate

of ethyl silicates in base catalysed reactions was observed to decrease as the solvent was changed from methanol to ethanol to dioxane due to a decrease in the ability of the solvent to solvate the leaving groups generated (discussed in section 2.2.2) [34]. The so-called "drying control chemical agents" or DCCAs also fall, correctly, under the same general heading: "solvent effects". Within the framework of a given reaction mechanism, the observed effects of the DCCAs can be explained in terms of their ability to solvate the various reacting species [22, 33]. Artaki Zerda and Jonas studied the effects of DCCAs on the reactions of ethyl silicates under slightly acidic conditions [33]. These researchers found that polar DCCAs, both protic (water, methanol and formamide) and aprotic (acetonitrile and dimethylformamide), solvate the reactive nucleophile thereby slowing the S_N2 condensation reaction. Nonpolar DCCAs, such as dioxane, do not interfere with the reactive nucleophile and condensation proceeds rapidly [33]. Solvents are, therefore, not strictly an "inert" media; the term "solvent" properly covers all species (including "DCCAs") in the reaction mixture.

2.4 Analysis of Structure

The experimental conditions employed in the sol-gel process manifest themselves in the types of gel that are formed. Klein and Garvey, in their review, gave definitions of the common classifications of sol-gel as determined by the experimental conditions employed during the gelation and/or drying process [23]. An "alcogel" is one made from the hydrolysis and condensation of a silicon alkoxide in an alcohol/water medium. By contrast, a "hydrogel" is one made from ion-exchanged sodium-silicate solutions. A "xerogel" is one in which the solvent has been removed through "ordinary" means: evaporation at ambient or under vacuum. An "aerogel", on the other hand, is one in which the solvent has been removed by "extraordinary" means, namely, hypercritical evacuation. The last two categories differ in the observed microporosity as a direct result of the manner in which they were dried. Aerogels,

because of the hypercritical removal of the solvent, have been postulated to retain larger pores than the xerogels [67]. The larger pores, it has been speculated, are the reason aerogels densify more readily to monoliths than the xerogels [67].

The degree of completion of the hydrolysis and condensation reactions, the nature of the unreacted groups and the amount of solvent and/or reaction by-products "trapped" in the matrix all reflect the experimental conditions under which the gels were made. Also, notably, the "superstructure" of the gels has been observed to vary as a function of the experimental conditions. The result is that various pore sizes, distributions of pore sizes and overall porosity are possible in sol-gel derived materials. The size distribution and nature of the porosity in a gel (closed or open pores) is important for applications as catalyst supports or as separations media. Porosity has also been demonstrated to be a determining factor in the densification of gelled materials, particularly in determining the temperature at which the gel vitrifies and whether or not that vitrification results in a crack-free monolith [47, 67]. Determination of the gel structure and relating it to the experimental conditions used is an important multifaceted problem that has required the use of several analytical techniques.

The overall structure of a gel made by the sol-gel process (or any other process for that matter) contains microstructure of interest on several size scales. Structures at the molecular level provide information concerning the chemical state of the atoms in question, including the number and type of bonds. For example, a silicon center in an alkoxide derived sol-gel could contain unreacted alkoxide, hydroxide, or crosslinking bonds (-OR, -OH, or -OSi≡, see Figure 2 on page 11) and also, possibly, bonds to solvent molecules or reaction by-products. Structures on the next larger scale, the macromolecular level (i. e. several atomic "units"), give an indication of the level of crosslinking in the network. Specifically, cyclic versus long linear structures or even "fishnet" type structures of tetrahedral silicate crosslinks would be observed at this scale. Additionally, on the macromolecular level, small pores, on the order of 10Å, should be detected if present. Finally, at the "supermolecular" level (~ 50 Å and larger) pore structure and phase separation (if any) should be observable. To gain a thorough understanding of sol-gel structures, from the smallest to the largest, from molecular to

macromolecular to, ultimately, "supermolecular", requires analytical techniques sensitive in each size regime.

2.4.1 NMR Spectroscopy

Nuclear magnetic resonance (NMR) spectroscopy is an ideal technique for probing the chemical nature of structures on the atomic scale. NMR is inherently sensitive to the chemical state of the atom being studied since this technique actually probes the nucleus of the atom in question. For the study of silicon based sol-gel systems, ^{29}Si NMR is the method of choice. The ^{29}Si NMR experiment allows direct observation of the silicon center as the hydrolysis and co-condensation processes occur. Supporting ^{13}C and ^{1}H NMR spectra can supply useful information regarding the chemical nature of carbon and hydrogen containing components in the reacting alkoxides.

Several types of NMR experiment have been applied to the study of sol-gel systems. In addition to multinuclear NMR, ^{29}Si, ^{13}C, ^{1}H , solution and/or solid state experiments have been or are being utilized. Solution NMR experiments have been used extensively for studying the hydrolysis reactions in sol-gel systems [28, 32, 38, 42, 65, 68, 69, 70]. Condensation reactions, though, can only be followed up to the point of gelation by the solutions NMR method (for reasons given below). In general, gelled materials and have been studied using solid state NMR experiments [71-75].

Assink and Kay [65] and coworkers [38] studied the hydrolysis and polycondensation kinetics of TEOS using proton NMR of solutions. The ethyl silicate (TEOS) was reacted in an ethanol/water mixture using a two stage catalysis process: 1) HCl followed by 2) water and either more HCl or NH_4OH [35-39, 65]. In these studies the methylene proton signals of the silicon ethoxide and the "free" ethanol were followed as a function of time. Integration of the observed resonances allowed Assink et al. to determine the relative rates of reaction for the different reaction conditions [65]. After the second step addition of acid, hydrolysis of the re-

maining alkoxide functions was completed well before gelation occured. Reactions to which base was added in the second step hydrolysed much slower, and gelled before hydrolysis was completed [65]. Rate data obtained from reactions to which there was nothing added in the second step demonstrated two distinct regions of different slope. Using this data, Assink and Kay calculated the hydrolysis rate, 0.025 liters/mole-min, and the condensation rate, 0.002 liters/mole-min, for an acid catalysed TEOS system [65].

Peace, Mayhan and Montle also used proton NMR of solutions to study the acid catalysed hydrolysis of TEOS [28]. Ester interchange of the TEOS alkoxides with various alcohol solvents was studied. Methanol, Cellosolve (ethylene glycol mono ethyl ether), isopropanol and t-butanol were found to behave differently with regards to interchange. In particular it was found that in isopropanol at 25°C, ~35% of the alkoxide sites underwent transesterification (solvolysis) and ~63% of the sites hydrolysed [28]. Methanol and Cellosolve were found to promote similar levels of transesterification (~45% and ~46% respectively) while t-butanol prevented transeseterification from occuring. Using deuterated ethanol as a solvent resulted in an even distribution deuterated sites between silicate and solvent. Further, it was discovered that increasing the reaction temperature to 110°C was observed to have little influence on the hydrolysis - transesterification distribution [28].

Yoldas used the ^{29}Si solutions NMR experiment to study the hydrolytic polycondensation reactions of TEOS [32]. The effect of dilution on the silicate structures formed by the sol-gel process was directly observable by this method as was the effect of acid catalyst concentration. Increased dilution of the reaction mixture resulted in a decreased number and intensity of resonances attributed to condensed silicate structures [32]. Yoldas attributed the observed decrease in the number of condensed structures to a higher intermolecular spacing between silicates during the sol-gel process. The NMR data also showed that the hydrolyzation rate of TEOS increased with increasing acid catalyst (HNO_3) concentration; a maximum in the rate of hydrolysis was reached at $\simeq$1.25 g $HNO_3/Si(OR)_4$ [32].

Artaki et al. used the ^{29}Si solutions NMR experiment to study pressure effects on the acid catalysed reaction kinetics of TMOS (tetramethoxysilane) [42]. The effect of formamide (a so

called DCCA) on the hydrolysis process of TMOS at atmospheric pressure was studied by Artaki et al. as well [70]. Zerda, Artaki and Jonas also studied the reaction kinetics of TMOS catalysed over a wide range of pH (1-9) using the ^{29}Si solutions NMR technique [68]. In each of these three papers, the effect of the particular parameter being studied was determined by following the changes in the NMR spectra with time. Detailed knowledge of the chemical shift assignments for the various hydrolysis products allowed correlation between changes in the NMR spectra and the appearance (or disappearance) of certain structural groups. In this manner, it was determined that increasing pressure accelerates the hydrolysis and polycondensation of TMOS under acid catalysed conditions without changing the reaction mechanism [42]. Changing the pH of the reaction mixture, on the other hand, changed the rate of polymer formation; at pH = 2 the reaction mixtures contained 92% polymers midway to gelation while at pH = 9 the reaction mixtures contained only 42% polymers (43% monomers and 15% oligomers) [68]. It was also determined that TMOS systems containing formamide hydrolyse at a greatly reduced rate and to a much lower degree than systems containing no formamide [70].

Kelts, Effinger and Melpolder undertook similar experiments studying pH effects on the reactions of TEOS as well as TMOS using ^{1}H NMR and ^{29}Si NMR [69]. As in the above mentioned articles, these researchers were able to attribute changes in the NMR spectra with time to specific silicate structures. Kelts et al. concluded from their NMR data that the polycondensation of silicate esters under the conditions studied was most accurately described by a linear growth model. In addition, they determined that there were three distinct pH regimes in terms of hydrolysis rates. At pH < 1, hydrolysis was fast and complete before gelation occured. At pH > 6, condensation and gelation occured before hydrolysis was complete. At intermediate pH ~4-6, hydrolysis and condensation occured concurrently resulting in a wide variety of species being present at the gel point (monomers, oligomers as well as polymers) [69]. Proton spectra provided evidence to support these conclusions gleaned from the silicon NMR experiments.

The degree of condensation achieved in the final gelled state (i. e. number of crosslinks per unit volume) is of prime interest in determining structure - property relationships. Unfortunately, the solutions NMR experiment loses resolution in solid samples [70]. This is primarily due to the large anisotropic chemical shift in the solid state [71-74]. Solutions ^{29}Si NMR experiments on condensing sol-gel systems sufferred the further complication of spectral overlap; the spectral region of glass NMR tubes coincides with the spectral region of condensed silicates [70]. Thus, in order to determine the degree of reaction in gelled materials using NMR, solid state experiments are necessary. Solid state NMR requires special probes and is not yet a "routine" experiment [71, 72, 74]. It is, therefore, not surprizing that only one solid state ^{29}Si NMR study on sol-gel type system has been published [75].

Beshah and co-workers used solid state ^{29}Si cross-polarization (CP) NMR to study the model junctions in sol-gel crosslinked polydimethylsiloxane (PDMS) systems [75]. The CP/MAS NMR allowed these researchers to resolve a number of different silicon structures corresponding to difunctional PDMS silicons as well as tetrafunctional silicates from fully and partially reacted TEOS crosslinks. Nonconnected PDMS chains or dangling ends were identifiable in the NMR spectra as were several other Si structures. Beshah et al. proposed several types of silicate structures to account for the observed NMR resonances. In particular, "butterfly" and "bowtie" silicate structures were proposed for fully reacted TEOS to account for an observed "triplet" at ~ -105 ppm [75].

2.4.2 Vibrational Spectroscopy

Vibrational spectroscopy, both infrared (IR) and Raman, is ideally suited to probe structures of molecular and macromolecular dimensions. These techniques allow not only a "fingerprint" indentification of certain chemical functions, such as an alkoxide or hydroxide function, but the identification of certain "molecular groupings" as well. For example, cyclic silicate "defect" structures that have been predicted by Galeener [76, 77] have been observed

in Raman spectra by Tallant et al. [78]. Because of their versatility, both IR [64] and Raman [33, 68, 79], have been used in conjunction with NMR as a means of following the progess of the overall sol-gel "reaction" (i. e. hydrolysis and condensation). These techniques have also been used to follow changes in silicate sol-gels as they are densified at elevated temperatures [64, 70, 80-82].

Duran et al. utilized infrared spectroscopy to observe chemical changes in gels produced using different water to TEOS ratios: R = H_2O/TEOS [64]. These researchers were able to detect residual alkoxy functions that were not hydrolysed at a water/TEOS ratio of R = 1.0. At higher water to TEOS ratios (R = 20) the hydrolysis went to completion and dense silicate structures were formed. It was demonstrated that during vitrification, regardless of the water/TEOS ratio, $Si\text{-}O^-$ functions disappeared while Si-O-Si linkages increased [64]. This result indicated that the condensation process continued towards completion during vitrification. Bertoluzza et al. used both IR and Raman to arrive at the same conclusion [82]. Krol et al. [80], and Gottardi et al. [81] also conducted vitrification studies on TEOS gels with similar results using Raman rather than infrared spectroscopy.

2.4.3 X-Ray Scattering

Wide-angle x-ray scattering (WAXS) and small-angle x-ray scattering (SAXS) are ideal analytical probes with which to study structures on the order of ~ 1 - 20 Å (WAXS) and ~ 10 - 10^4 Å (SAXS). Wide-angle scattering is able to detect scattering arising from crystal planes that satisfy Bragg's equation:

$$\frac{1}{d} = \frac{2}{\lambda}\sin(\frac{\theta}{2}) \qquad (2.1)$$

where, d, is the spacing between crystal planes, λ, is the wavelength of the x-rays and, θ, is the radial scattering angle. Whereas SAXS, with the exception of the Bragg region which is

really WAXS, detects scattering arising from electron density fluctuations that do not have, necessarily, a high degree of order. Therefore, WAXS is generally used to detect and characterize crystallinity while SAXS is generally used to study multiphase or heterogeneous materials.

As such, WAXS is best suited for studying vitrified sol-gel systems in which there may be crystalline phases present. As will be detailed in section 2.5, WAXS has been used by several authors to detect the different crystalline phases of TiO_2 [50, 54, 61], ZrO_2 [54, 56] and Al_2O_3 [59, 62, 63, 83] containing sol-gel systems. The conclusion common to all of the WAXS results in these studies is that materials made by the sol-gel process were amorphous in their "as gelled" state. Wide angle x-ray scattering has also demonstrated that polymer modified sol-gel systems are amorphous in their as gelled state [20].

Small-angle x-ray scattering consists of four distinct regions. Progressing from very small to very large scattering angles ($\simeq 0°$ to $\simeq 90°$) they are: the limiting, the Guinier, the Porod and the Bragg regions. SAXS data can be presented as a plot of log I (K) against log KR where, I (K), is the measured scattering intensity at a given Fourier spatial scattering frequency, K, and, R, is the average radius of gyration of the scattering macromolecule (using the notation of Schaefer and Keefer [37]). The Fourier spatial scattering frequency, K, is given by:

$$\frac{1}{K} = \frac{2\pi}{\lambda} \sin\left(\frac{\theta}{2}\right) \tag{2.2}$$

where, λ, is the wavelength of the x-rays and, θ, is the radial scattering angle. Using the dimensions K^{-1}, R and ξ (where ξ = length of a monomeric unit) the limits of the four scattering regions can be defined as follows [37]: $KR << 1$ is the limiting region, $KR \leq 1$ is the Guinier region, $R >> K^{-1} >> \xi$ is the Porod region and $K\xi = 1$ is the Bragg region. The limiting region of the small angle scattering curve provides the weight average molecular weight of a macromolecule while the Guinier region provides the radius of gyration and the Bragg the "d" spacing of crystal planes. Careful analysis of the Porod or power law scattering region can

provide the exponent of the scattering decay which has been shown to be directly related to the dimensionality of the scattering particle [37].

The SAXS method is relied upon heavily by Schaefer and his colleagues to determine the growth habits of sol-gel systems under different reaction conditions [35-39]. The Porod region of the scattering curves prove particularly useful for this purpose. In these papers, Schaefer and co-workers obtained SAXS curves as a function of time for TEOS systems catalysed under both acidic and alkaline conditions using different levels of water. Porod analysis of the SAXS curves demonstrated that under acidic conditions the growing silicate exhibits dimensionality characteristic of a Gaussian polymeric system, $D \simeq 2.0$ [37]. The growing silicate "particles" are not space filling; their structure is open. This type of structure is mass fractal since the mass does not scale as the cube of a characteristic linear dimension such as the radius of the particle (a non-fractal spherical particle would have a dimensionality, D, of 3.0). Under basic conditions, Porod analysis of the SAXS curves indicated that the growing silicates are more dense than their acid catalysed counterparts (D is slightly greater than 2.0 rather than slightly less than 2.0 [37]) but are still polymeric rather than colloidal.

Guinier analysis of the low angle region of the SAXS curves of acid catalysed and base catalysed ethyl silicates were distinctly different. The radius of gyration of the silicate particles in acid catalysed systems remained constant throughout the reaction whereas in base catalysed systems the radius of gyration increased steadily [35]. To explain these results, Brinker et al. proposed two growth models: monomer-cluster growth and cluster-cluster growth [35-39]. Base catalysed sol-gel reactions were postulated to grow by a monomer-cluster mechanism; clusters grew with time at the expense of the monomers in the system. In acid catalysed systems reactions, the clusters reached their "mature" size very early in the reaction and did not grow with time, gelation was effected by cluster-cluster interaction initiated by the second step of the reaction process [39]. Keefer, based on these random growth models, proposed mechanisms for the hydrolysis and condensation reactions of ethyl silicates (discussed in section 2.2.2) [36].

Invariant analysis of SAXS data, though not as common as Porod or Bragg analysis, is also an important technique used to analyze two phase systems such as hybrid sol-gel materials (discussed in section 2.6). In a very rudimentary sense, the intensity of the observed scattering in a SAXS experiment is dependent on the degree or "sharpness" of the separation between phases of different electron density. The sharpness this electron density fluctuation is related to an "invariant" value which can be calculated from measured SAXS profiles. If there is no electron density fluctuation, as in a perfectly homogeneous material, the value of the "measured" invariant would be zero. Conversely, high values of the "measured" invariant indicate a relatively high degree of phase separation. The limiting value would be for a perfectly separated system of two phases in which case an invariant can be calculated from theory. Therefore, the degree to which the "measured" value matches the theoretical limit is an indication of how well the two phases are separated or, from the opposite perspective, how homogeneous the overall system is (or is not).

Invariant analysis performed on slit smeared SAXS data have been used to determine the degree of homogeneity (or phase separation) in hybrid "Ceramer" systems [20]. Huang and Wilkes performed such an invariant analysis on a series of poly (teramethylene oxide) (PTMO) modified "Ceramer" materials to determine the effect of acid catalyst level on the relative homogeneity of the sol-gel produced. The invariant analysis demonstrated that the relative homogeneity of these systems increases as the acid concentration is increased (the invariant decreases with increasing acid concentration) [20].

2.4.4 Electron Microscopy

Scanning electron microscopy (SEM) and transmission electron microscopy (TEM) in combination can resolve structures in the size range of tens of angstroms to those visible by the unaided eye (~ 0.1 mm). Porosity at various size scales can be readily observed using scanning electron microscopy, whereas electron density fluctuations due to phase separation

can be observed using transmission electron microscopy. TEM and SEM, because of their large range of usefulness, are both complimentary to several other techniques including: SAXS, light scattering and optical microscopy.

Brinker et al. utilized both TEM and SEM to observe the differences in the silicate structures formed from two step acid-acid as opposed to acid-base reaction conditions [35]. Photomicrographs taken from TEM and SEM show that the silicate structures formed in acid catalysed media are extremely fine (~50 Å) and not particulate in nature. In direct contrast, silicate structures on two size scales are formed from basic media. An extremely coarse structure is observed (~900 Å) which, in turn, seems to consist of smaller finer structures ($\leq$100 Å) [35].

Duran and co-workers used SEM to study the fracture surfaces of SiO_2 vitrified gels (800°C) made using different H_2O/TEOS ratios [64]. Gels made using a 1 to 1 water to TEOS ratio showed surfaces that were fibrous in nature whereas those made at a 4 to 1 ratio showed sheetlike structures (for both acid and base catalysis). Gels made at a ratio of 20 to 1, water to TEOS, showed ribbons and layers in the fracture surfaces [64]. These observations were consistent with the conclusions derived from the IR spectroscopy (discussed in section 2.4.2). Namely, at low water to TEOS ratios linear structures are formed, at intermediate ratios higher density structures are formed and at high water to TEOS ratios high density structures are formed [64].

Mark et al. were able to observe SiO_2 particulates in TEM studies of their hybrid siloxane materials (discussed in section 2.6.2) [10]. In situ SiO_2 particles formed under alkaline conditions could be resolved in the TEM studies while structures formed using acetic acid were much less well defined (no distinct particles could be resolved). Distinct particles $\simeq$10 nm in size were visible in the TEM photographs of the alkaline system. The TEM photographs indicated that under basic conditions TEOS phase separated from the silicone based polymer. The acid catalysed morphology, being less distinct, indicatived a more homogeneous system - at least when compared to the base catalysed system.

2.5 Mixed Metal Oxides

A primary driving force for making mixed metal oxides has been to obtain materials with "improved" mechanical and chemical properties relative to pure silicon oxides. Certain physical properties of a material, such as density, coefficient of thermal expansion or refractive index, can be tailored to meet specific requirements by controlled mixing of metal oxides. The sol-gel method has proven to be useful in this respect. In fact, the ability to make such multicomponent oxide glasses was a major factor behind the dramatic increase in sol-gel related research.

Not only has the sol-gel technique provided a low temperature method for obtaining mixed oxide glasses of high purity and homogeneity, this technique has also enabled researchers to achieve compositions heretofore unattainable for certain oxide combinations [22, 53, 58, 83]. The sol-gel process has also proven to be a general method for making a wide range of composite oxides. Dislich pointed out that elements from virtually every group in the periodic table have been incorporated into sol-gel materials [21]. Three of the most commonly incorporated elements are aluminum, titanium and zirconium. These three elements are of particular interest for a number of reasons specific to each metal oxide and the applications for which that oxide system could be used (applications are discussed in section 2.7). Aluminum, zirconium and especially titanium are also of interest in making hybrid polymer - metal oxide materials.

Several publications in the mixed metal literature reviewed addressed the sol-gel synthesis of alumina (Al_2O_3) and other aluminum containing mixed metal oxides [25, 30, 57, 59, 62, 63, 83, 84]. The remaining publications addressed the sol-gel synthesis of titanium and zirconium oxides [2-6, 13, 16, 22, 25, 49-56, 58, 60, 61, 85]. The majority of these efforts focused on making mixed oxide materials that can be used as ceramics or glasses. Concern was not generally given to the formation of monolithic structures; the criterion of importance was the formation of homogeneously mixed oxides that could be densified into useful materials. As

a result, many of the sol-gel procedures for incorporation of mixed metal alkoxides with silicon alkoxides generated powdered "gels" or cracked monoliths.

Metal alkoxides, in general, have been found to be much more reactive towards hydrolysis than are silicon alkoxides (section 2.3) [1-6, 22, 23, 25, 30 48, 52]. It should be recognised that incorporation of metal alkoxides into a silicon based sol-gel scheme has not been trivial. Mukherjee reported that successful incorporation of metal alkoxides into silicate systems required alteration of conventional sol-gel processes in order to overcome a large difference in reactivities; conventional processes, unaltered, often result in precipitation of molecular metal oxides [25]. Also, it was noted, the addition of water in the reaction schemes was critically important. In order for fast reacting metal alkoxides to be successfully combined with slow reacting alkoxides, the timing and amount of water addition had to be carefully regulated [2-5, 16].

Several methods have been developed to achieve the successful combination of metal alkoxides with silicon alkoxides. The methods developed each embrace at least one of two basic approaches to solving the problem of mismatched reactivities. These being: 1) regulate the amount and timing of water addition, 2) regulate the timing of metal alkoxide addition. Both of these approaches, for similar reasons, can prevent the metal alkoxide from precipitating out of the reaction mixture as a molecular oxide.

Mukherjee proposed that the water required for hydrolysis be added at a later point in the reaction scheme to prevent rapid hydrolysis and precipitation of fast reacting alkoxides such as those containing Al, Ti or Zr [25]. The delayed addition of water would allow the reactants to mix thoroughly prior to any reaction taking place. Subsequent addition of small amounts of water, such as that from atmospheric moisture, would allow only partial hydrolysis of the fast reacting metal alkoxide. These "feed starved" conditions would allow the slower alkoxide time to hydrolyse before precipitation of a metal oxide could occur. The simultaneous presence of hydrolysed sites on different alkoxide species would tend to promote co-condensation.

Schmidt and coworkers also developed a process on the basis of "feed starving" the hydrolysis reaction in order to incorporate titanium and zirconium alkoxides into ORMOSIL

materials (discussed in section 2.6.1) [2-5]. Their so called "CCC" (chemically controlled condensation) method involves the generation of controlled amounts of water in situ, followed by the addition of excess water at a later time. The small amount of water generated in situ is well dispersed since it is a by-product from the esterification of an organic acid with the alcohol in the solvent media. This technique effectively "feed starves" the initial hydrolysis of the fast reacting alkoxide species thereby preventing it from precipitating out of solution. However, partial hydrolysis and co-condensation with surrounding silicate esters can still take place, though at a slow rate. Once stable partially condensed species have been formed, an excess of water can be introduced to complete the sol-gel process without fear of inducing phase separation or precipitation of molecular oxides.

Parkhurst and co-workers took a different tack [16]. These researchers made use of a delayed addition of the fast reacting titanium(IV)ethoxide species to facilitate incorporation into a partially reacted silicate system [16]. In their procedure, the silicate ester and polymer modifying component are allowed to partially react under conventional acid catalysed sol-gelconditions. After a given amount of time, the titanium alkoxide is added to the mixture and allowed to react. Rather than being "feed starved", the titanium species is free to hydrolyse and condense at an unrestricted rate. At the time of addition, however, the silicate species has already formed partially hydrolysed and condensed moieties that contain reactive sites for the metal species to co-condense with. The result is that the titanium species condense with the silicate particles instead of precipitating out of solution.

All of methods mentioned have had a certain amount of success in the incorporation of specific metal alkoxides into silicate sol-gel schemes. Though universally applicable in principle, these methods in practice are, in many cases, "alkoxide specific".

2.5.1 TiO_2-SiO_2 Oxides

Titanium oxides have a number of desireable characteristics that make them prime candidates for incorporation into silicate systems. The incorporation of small amounts of titania (TiO_2) into silica (SiO_2) materials is known to reduce the coefficient of thermal expansion. For example, a composition of 7.6 wt% TiO_2 in a vitrified titania-silica glass is known to exhibit a coefficient of thermal expansion of zero [61]. Also, titania has been known to increase chemical resistance to alkali [54], strengthen glass-ceramics and act as a nucleating agent for crystallization [58]. All three are desireable characteristics for many ceramic applications. In nonvitrified sol-gel materials, the incorporation of titanium alkoxides has other advantages as well. The refractive index of titania containing hybrid materials have been demonstrated to be higher than that of pure silica containing hybrid materials, the difference being a function of the titania content [2]. Additionally, titania has been known to act as a condensation catalyst during the sol-gel process [3].

Primarily for these reasons, different authors have attempted to make titania containing materials using sol-gel technology. Philipp and Schmidt incorporated TiO_2 in their hybrid ORMOSIL materials (to be discussed in section 2.6.1) to improve scratch resistance as well as to control the refractive index [2, 3, 4]. Wang and Mark further toughened their siloxane systems by extending their in situ silica technique (to be discussed in section 2.6.2) to include titania fillers [13].

Titanium containing sol-gel materials have been made from a number of titanium alkoxides. Yamane and coworkers studied the reactivity of titanium(IV)ethoxide, titanium(IV)isopropoxide, and titanium(IV)teramyloxide with TEOS and TMOS under alkaline conditions (pH = 11.2-11.3) [51]. These researchers found that the longer branched titanium alkoxides were less sensitive to hydrolysis and were more apt to co-react with the silicate species. Yamane et al. also preferred to use TMOS as the silicate precursor, it reacts faster than TEOS thereby bringing the reactivities of the silicate and the titanate closer together [51].

Yoldas also studied the reactions of the same alkoxides under slightly acidic (HCl & HNO_3) and basic (NH_4OH) conditions [50]. The results of both studies were consistent; tertiary alkoxides were less reactive than secondary alkoxides which were less reactive than primary alkoxides. Yoldas also noted that upon addition of a slight amount of the acid, cloudy slurries cleared and remained stable for several weeks [50]. Kamiya, Tanimoto and Yoko also noted that the addition of HCl prevents flocculation of titanium isopropoxide in the reaction mixture [49]. These researchers used a delayed dropwise addition of a titanium alkoxide solution to make TiO_2 fibers using a sol-gel process. Already mentioned, several researchers have also successfully incorporated titanium alkoxides into hybrid silicate materials. Schmidt et al. [2-5] and Parkhurst et al. [16] have incorporated titanium alkoxides into silicate based modified sol-gels as well.

A major concern in mixed metal alkoxide sol-gel processes is the potential formation of separate oxide phases. This is particularly true for systems, such as those containing TiO_2, ZrO_2 and Al_2O_3, in which one or more components can readily "self-react" and, potentially, crystallize. Rather than forming one homogeneous oxide composite, these metal oxides may, for thermodynamic reasons, phase separate as they attempt to crystallize into "pure oxide" phases. Phase separation could manifest itself in two ways in such systems. It could occur during the sol-gel process or later during high temperature crystallization.

Titanium oxide can exist in two crystalline forms, anatase and rutile. Yoldas reported that titania made by the sol-gel method from alkoxides is amorphous but tends to crystallize to the anatase form as low as 150-190°C [50]. The anatase form, it was noted, gives way to the rutile crystalline form at higher temperatures (as low as ~500°C [50]). Emili and coworkers used extended x-ray absorption fine structure (EXAFS) and x-ray absorption near edge spectroscopy (XANES) to study silica-titania oxides of 4.5, 10 & 19 wt% TiO_2 content [61]. From their work, these researchers were able to determine that the Ti^{4+} ions are only four coordinate in amorphous TiO_2-SiO_2 sol-gels [61]. These results confirmed the suggestion that TiO_2 is "dissolved" into the SiO_2 network at compositions below ~19wt% Ti [61]. At elevated temperatures, as crystallization began to occur, an "intermediate" phase was discovered.

Octahedral Ti sites were observed in partially crystallized (anatase form at 1200°C) materials of high (19wt%) titania content [61]. It can be concluded in general though, that sol-gel derived titania containing materials are amorphous and homogeneous unless subjected to an elevated temperature.

2.5.2 ZrO_2-SiO_2 Oxides

The incorporation of zirconia (ZrO_2) into silica systems generates many of the same beneficial effects as the incorporation of titania. Zirconia containing glasses are known to exhibit increased strength, fracture toughness and chemical durability (especially with regard to alkali) when compared to pure silica glasses [55, 56]. In addition, like titania, the incorporation of zirconia has been shown to result in a monotonic increase in the refractive index [55] as well increased scratch resistance in hybrid materials [2, 3, 4].

Different methods have been demonstrated to be successful in the incorporation of zirconium into silicate sol-gel systems. Klein used zirconium isopropoxide to make ZrO_2 - SiO_2 glasses [53] as did Nogami and his colleagues [55, 56]. The approach used by Nogami et al. [55, 56] to incorporate zirconium isopropoxide into a TEOS based glass resembles the approach taken by Parkhurst et al. [16] to incorporate titanium alkoxides. Nogami and coworkers slowly add the zirconium alkoxide to a prereacted acid catalysed TEOS/alcohol/water system. The slowly added zirconium isopropoxide then reacts with the polysilicate rather than precipitating out of solution. Schmidt et al. used the "CCC" method discussed earlier to incorporate zirconium alkoxide into their ORMOSIL materials [2-5].

Nogami and Tomozawa found, by x-ray diffraction, that their ZrO_2-SiO_2 gels remained amorphous up to 800°C (crystalline bands were not observed) [56]. Also, by infrared spectroscopy and molar refractivity, these researchers have demonstrated that the Zr^{4+} ions are in the intersticies of the SiO_2 network (Si-O-Zr bands at ~600 cm^{-1} were not present in the IR spectra) [55]. The sol-gel derived zirconia-silica materials are therefore homogeneous.

Thermogravimetric analysis performed on these gels showed a loss of water occuring at ~100°C followed by a steady increase in shrinkage until ~800°C at which point the shrinkage increased dramatically [55]. Heat treatment of the zirconia-silica gels between 1000° and 1200° C allowed crystallization of tetragonal ZrO_2. In these materials Nogami and coworkers were able to relate the high fracture toughness to a morphological change: tetragonal ZrO_2 to monoclinic ZrO_2 [56].

2.5.3 Al_2O_3-SiO_2 Oxides

Alumino-silicates are the basis for zeolite structures [22]. The prospect of using the sol-gel technique (as defined in the context of this work) as a means of synthesizing custom zeolites is one driving force for attempting Al_2O_3-SiO_2 glasses. Another reason for incorporating aluminum into ceramic oxide systems is to impart machinability and thermal shock resistence to the final materials [83].

Yoldas reported transparent alumina gels made from aluminum alkoxides in 1975 [59]. An excess of water was used in the reaction mixture along with HNO_3 or HCl to clarify the solutions. The reaction was then boiled until a critical volume was reached at which point a gel formed. The resulting materials were noted to be amorphous by x-ray analysis and highly porous (60%) with a final chemical composition of $\simeq$AlO(OH): which was calculated to be 82-85 wt% equivalent of alumina [59]. On heating, the alkoxide derived alumina exhibited a 16wt% loss between 150°C and 500°C. Yoldas also found that the pore size, transparency and critical gelation volume of the sol-gel derived alumina were dependent on the pH of the reaction media (which is consistent with the findings for silicate sol-gels - see section 2.2.3). Despite the promising findings of Yoldas, Coltrain notes that aluminum alkoxides are extremely difficult to incorporate into hybrid sol-gel materials [86]. Covino and Nissan used aluminum propionate and the sol-gel process to make Al_2O_3 powders. These gelled powders were found to be amorphous (like Yoldas' materials), with the exception of sonicated powders which

crystallized in the γAl_2O_3 form. After heating to ~800°C the alumina was observed to crystalize in the αAl_2O_3 form [62, 63].

2.5.4 Other Mixed Metal Oxide Systems

Sol-gel derived oxide systems that include metals not mentioned above have been attempted and may prove particularly useful in certain cases. Synthetic spinels are one such case because of their optical and magnetic properties. Spinels (magnesium aluminum oxides) have been known to exhibit excellent mechanical and thermal shock resistence and are resistent to chemical corrosion [83]. In this vein, Debsikar was able to produce transparent gels of controlled stoichiometry: $MgAl_2O_4$ [83]. These transparent "spinel" gels were made using aluminum secondary butoxide and magnesium acetate tetrahydrate as precursors; the magnesium salt was used in lieu of a magnesium alkoxide. Of note, Debsikhar adds a tautomerising compound, acetylacetone, to help regulate the hydrolysis and polycondensation of the aluminum butoxide [83]. Gels made by this sol-gel procedure proved to be amorphous by WAXS [83]. Also, subsequent thermal treatment of the gelled materials past 2000°C showed no signs of phase separation; the spinel crystallized according to the stoichiometry of the gel [83]. Hölland and coworkers used the sol-gel route and magnesium acetate tetrahydrate to incorporate magnesium into a sol-gel scheme [58]. Alumino-silicates of the composition SiO_2-Al_2O_3-MgO had been found to exhibit "good" machinability.

Ternary (or higher) mixtures of the above mentioned metal oxides have certain advantages also. Zhu and his colleagues used zirconium nitrate pentahydrate as a sol-gel precursor for making ternary glasses of the type: ZrO_2-TiO_2-SiO_2 [54]. Using zirconium nitrate pentahydrate along with titanium butoxide and TEOS allowed these researchers to make transparent glass pieces. The x-ray diffraction patterns for these ternery systems demonstrated that the materials were amorphous and homogeneous [54]. Infrared spectroscopy on these gels as a function of temperature and composition led Zhu and his colleagues conclude

that zirconia acts as a network modifyer (no Zr-O-Si bonds were observed by IR) while titania acts as a network former (Ti-O-Si bonds were observed by IR) [54].

2.6 Hybrid Materials

In the previous chapter hybrid sol-gel materials that combined the properties of organic and/or polymeric components with those of inorganic oxides were briefly introduced. These hybrid sol-gel materials represent a significant departure from the pure inorganic-oxide sol-gel materials reviewed up to this point. Unlike the pure oxide systems, the hybrid sol-gels are not intended to be vitrified by a secondary processing step. Although a post gelation thermal curing or annealing will, no doubt, be employed in any commercial process utilizing hybrid systems; these materials will not be heat treated at the extreme temperatures common for preparing glasses or ceramics from sol-gel precursors (~ 900°C). The limiting factor for hybrid systems being the temperature stability of the organic and/or polymeric component. The hybrid materials are, for the most part, intended to be used in their "as gelled" state (or at least at temperatures below ~450°C).

2.6.1 ORMOSILs

Schmidt and coworkers reported hybrid sol-gel materials in which organic components had been incorporated into inorganic oxides [1-6]. These hybrid materials were made by allowing substituted silicon alkoxides, in which one alkoxy group had been replaced by an organic group, to undergo the sol-gel process. The acronym ORMOSIL for ORganically MOdified SILicate was appropriately given to such systems [5, 6]. The ORMOSIL approach allowed

these researchers to generate new materials with specifically tailored properties through incorporation of select organic functions into inorganic oxides.

The use of alkoxides that contained organic functions with reactive side groups, such as an epoxy or vinyl group, allowed the possibility of post gelation crosslinking or copolymerization with appropriate monomers [2, 3, 4]. Philipp and Schmidt used such alkoxides to make a hard contact lens material by the sol-gel process [3, 4]. Specifically, allyl substituted alkoxides were used that could be crosslinked (or polymerized) free radically with methylmethacrylate after gelation to form a hard transparent material. The incorporated polymethylmethacrylate, in addition to flexibility, contributed the oxygen permeability required for use as a contact lens material [3, 4].

Specific properties of a material were also tailored using the sol-gel process to "adjust" the chemistry of the oxide components. Development of a "CCC" reaction scheme (discussed in section 2.5) allowed the incorporation of mixed metal alkoxides into the sol-gel process. Philipp and Schmidt combined the CCC procedure with their ORMOSIL approach to gain control over the oxide composition in the final materials. In this manner, by controlled incorporation of TiO_2 or ZrO_2, Philipp and Schmidt were able to improve the scratch resistance and control the refractive index of the silicate-PMMA contact lens material mentined previously [3, 4].

2.6.2 SiO_2 Reinforced PDMS Networks

Mark et al. were able to use the sol-gel process as a means of forming in-situ glass particles to toughen siloxane elastomer systems [7-10]. The starting crosslinked polydimethylsiloxane elastomer networks could be obtained a number of different ways by endlinking capped PDMS oligomers [11, 12]. The reinforcing glass "filler" particles were introduced by swelling the siloxane elastomer network in TEOS then initiating the sol-gel proc-

ess to form SiO_2 in situ. Phase separated hard "particles" of SiO_2 were desired for this type of hybrid sol-gel system in order for the networks to be toughened.

A number of catalysts systems were attempted to determine which conditons best promoted the formation of the desired particulate SiO_2 morphology from the sol-gel process [8]. Acid catalysed systems were found to produce brittle materials (possibly due to random scission and ring-chain equilibrium of the PDMS) while base catalysed systems produced materials that were observed to be strong or toughened [8]. Specifically, the alkaline catalyst ethylene diamine was found to promote the desired SiO_2 particulate formation [9, 10]. TEM micrographs of the ethylene diamine catalysed systems showed well dispersed distinct SiO_2 particles of $\simeq$ 10nm size [9, 10]. Systems catalysed in acetic acid, on the other hand, did not show distinct particles in the TEM micrographs [10].

2.6.3 CERAMERs

Wilkes, Orler and Huang created a new type of hybrid material by introducing functionalized polymeric components into silicate systems formed by the sol-gel process [14, 15, 17]. The first such materials combined silanol terminated polydimethylsiloxane (PDMS) with TEOS and were reacted under acid catalysed conditions. Gels formed in this manner were optically transparent and displayed a considerable amount of flexibility. These materials were observed to be more flexible than pure SiO_2 glass (ceramic) yet stiffer than pure PDMS polymer. The acronym CERAMER standing for CERAmic polyMER was coined by GLW to describe these new sol-gel derived materials [14, 15, 17]. Figure 3 on page 50 gives a schematic representation of the network system formed by the incorporation of a functionalized oligomer into a sol-gel process with TEOS.

Dynamic mechanical spectra of the first CERAMER materials distinguished them from filled systems (such as those prepared by Mark et al. [7-10]) and demonstrated their hybrid nature. Instead of displaying a sharp glass transition, T_g, at $\sim$ -120°C (expected for pure

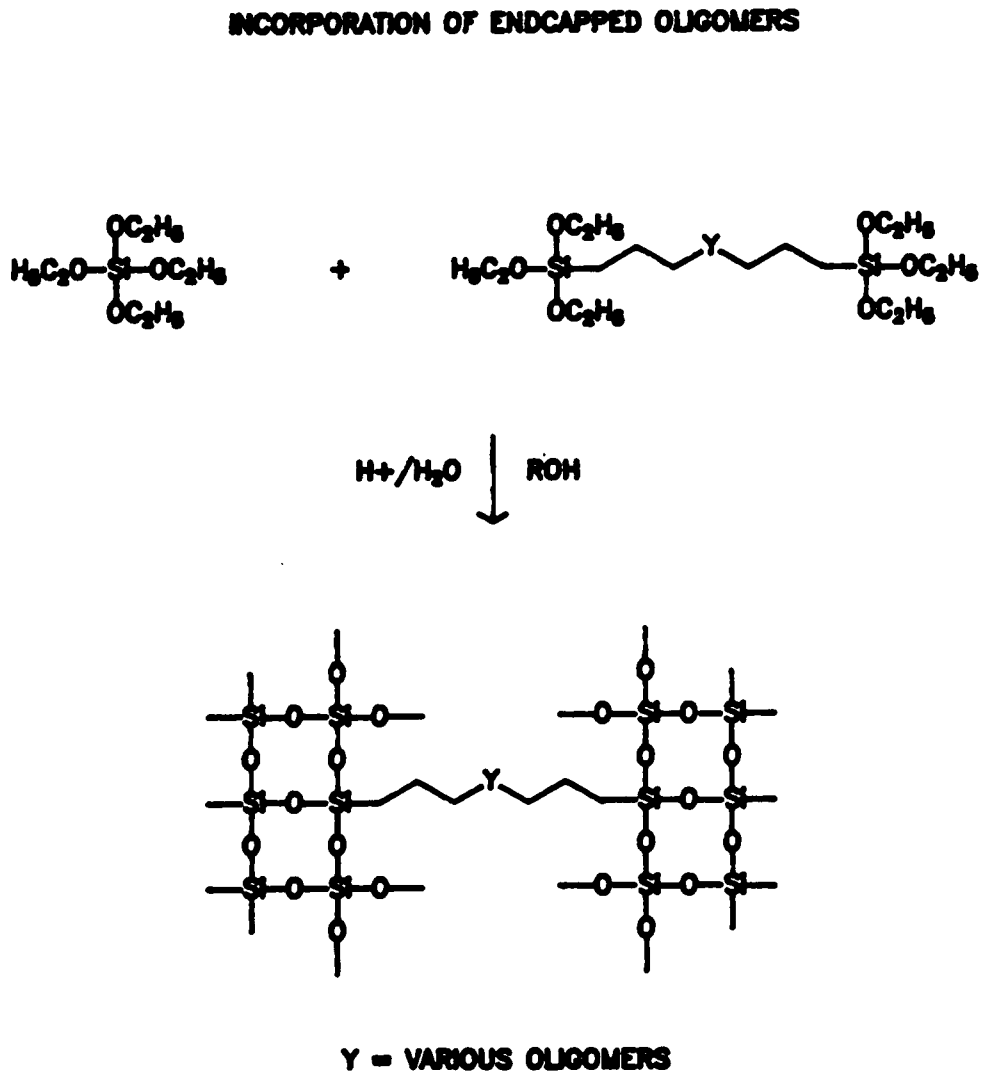

Figure 3. Schematic of silicate sol-gel network formation.

PDMS), the transitions for 48wt% TEOS 52wt% 1700Mw PDMS materials were often bimodal and were broadened considerably spanning well past room temperature in several cases. The broadening effect on the glass transition of the PDMS component was even more dramatic for the 60 wt% TEOS material in which transitions were shifted to as high as 100°C [17]. The observed broadening and shifting of the T_g transition was interpreted as an indication that the PDMS component was well dispersed throughout the material matrix. SAXS studies on the PDMS CERAMERS showed no indication of well defined phase separation which also indicated that the systems are homogeneous or uniform in nature (however, there may not be sufficient electron density difference between PDMS and the TEOS network to actually be able to measure any scattering from phase separation) [17].

The schematic in Figure 3 implies that the process by which the first CERAMERs were made is general. Such is the case. In addition to "compatible" polymers such as PDMS, noncompatible polymers can be and have been incorporated into this scheme giving rise to new generations of "CERAMERs". Materials incorporating functionalized poly(tetramethylene oxide) (PTMO) [18, 20] and polyetherketones (PEK) [19] into the sol-gel scheme have been demonstrated. The non-compatible polymers/oligomers, not surprisingly, phase separate. Small-angle x-ray scattering profiles of the PTMO containing materials display distinct maxima corresponding to ≃20nm interdomain spacing [18, 20]. Hybrid CERAMER materials containing PTMO, though, were also observed to be optically transparent [18, 20]. Finally, Parkhurst et al. demonstrated the utility of the "CERAMER" method by making materials that incorporated TiO_2 as well as silanol terminated PDMS into the sol-gel scheme [16].

2.7 Applications

Applications of the various types of sol-gel materials discussed have been purposely left to the end of this review. During the process of introducing the chemistry, physical properties

and structural aspects of sol-gel derived materials, many potential applications have come to light. Customized ceramics alone could generate an unlimited number of applications of the sol-gel process. Hybrid materials only serve to increase this number, expanding the types of applications feasable for sol-gel derived materials. In terms of their useage, sol-gel materials can be classified into two catagories: vitrified gels and non-vitrified gels.

2.7.1 Vitrified Gels

Vitrified or "fired" gels have the greatest potential in "traditional" glass and/or ceramic applications. These materials, having been vitrified at temperatures of ~900°C or higher, are generally dense and hard. Hubert-Pfalzgraf gives a comprehensive table that presents many applications for mixed inorganic oxide materials that are desireable [22]. This table lists the general area of potential use (electronics, biomaterials...), the type material desired (superconductor, insulator...) and examples of oxide compositions that would be required. For example, in the general area of electronics, β-Al_2O_3 is listed as one desired composition for a superionic conductor [22]. This list shows that inorganic oxides have applications as ceramic engine components, piezoelectrics, dielectrics, insulators, thermistors, nuclear waste storage media and as catalysts in addition to those applications mentioned already [22]. Mixed inorganic oxide powders (which can be formed by the sol-gel route) that are subsequently pressed and vitrified have found much use in such applications. Blum cites applications of sol-gel materials in microelectronics as low temperature sealants (~450°C) or as piezoelectrics (lead zirconate titanate) [87]. Alkali ion conductors (NASCION) both fibers and films, also exemplify electronic applications of sol-gel derived materials [23, 53]. In addition, sol-gel derived mixed metal oxides of specific composition have found applications as optical coatings for waveguides and for use in mirrors or windows for aerospace applications [22, 83]. Further, sol-gel technology is touted as a useful method for making hard coatings or ceramic monoliths of specific shape [21, 22, 23]. Spin coating of thin sheets [85] and drawing of TiO_2 fibers [49]

are two examples of this versatility. Finally, it must be said that if, after looking through all the above possibilities, no application can be found for a particular sol-gel material, it can always fill that all time favorite application: "lab curiosity" [23].

2.7.2 Non-vitrified Gels

Sol-gel derived materials used "as gelled" or with minimal post gel treatment (gentle heating or evacuation for solvent removal for example) fall into the catagory of non-vitrified gels. Such materials would retain much of the porous microstructure formed during the sol-gel process. Controlled porosity would lend these "as gelled" systems to applications as catalyst supports or as separations media [21, 22, 23]. Gallagher & Klein synthesized silica membranes, using the sol-gel method, which could serve as permselective membranes in gas separations [88]. Along a similar vein, Schmidt and coworkers, by controlling the sol-gel chemistry of their ORMOSIL materials (discussed in section 2.6.1), were able to make a hard contact lens material of controlled oxygen permeability [1-5]. Another factor encouraging sol-gel use is the toughening effect on hybrid polymeric systems. Silicones toughened by in-situ sol-gel "reinforcing" (discussed in section 2.6.2) have been reported by Mark and coworkers, though specific applications have not been mentioned [7-13]. A series of hybrid polymer modified sol-gel materials have been synthesized in the laboratory of G. L. Wilkes (the so called "Ceramers" discussed in section 2.6.3) which bridge the gap between polymers and ceramics and could see applications as coatings and/or structural adhesives [14, 15, 17-20]. Although by no means exhaustive, these are all of the known applications for non-vitrified sol-gels. However, it should be recognised that the relative paucity of published applications in the area of non-vitrified sol-gels is not indicative of a lack of potential; it is merely indicative of a very new field, open for development.

2.8 Summary

The impressive potential applications for oxide based materials, whether vitrified or non-vitrified, are a powerful incentive to pursue sol-gel technology. The literature just reviewed demonstrated the diversity of materials possible using this technology. Mastery of the sol-gel chemistry and the structure - property relationships involved would provide the scientific base necessary for making revolutionary new materials by this method. The literature just reviewed represents the current status of this scientific base. An accurate condensed summary of this literature provides the means to predict the effects of certain experimental parameters on the structure and properties of sol-gel derived materials.

Depending on the type of materials desired, different experimental parameters have been shown to be important. If the desired material is only constrained to being a homogeneous mixture of oxides (i. e. powders are acceptable), a relatively wide range of experimental conditions will prove successful. If, however, the desired material is a non-vitrified homogeneous monolithic gel, the experimental "window" of conditions available for which the sol-gel process produces an acceptable material becomes limited. The specific materials of interest in the ensuing work are non-vitrified homogeneous monolithic gels. Close attention was paid to conditions in the literature that produced monolithic materials for this reason. Also, since mixed metal oxide materials are also desired, attention was paid to methods of incorporating metal oxides into silicate systems. Several "key" guidelines have been gleaned from the literature.

1. Acid catalysed sol-gel processes using less than the stoichiometric amount of water produce linear, lightly branched polymeric silicates.
2. Mineral or strong acids catalyse the hydrolysis better than weak organic acids.
3. The reactivity of alkoxides in acidic media decreases as the size of the alkoxy group increases.

4. Acid catalysed sol-gel processes produce materials with small uniform interconnected pores (~5-30Å [40]) and high bulk density relative to base catalysed sol-gels.
5. The hydrolysis mechanism is, more than likely, an acid catalysed S_N2; condensation also proceeds by an S_N2 mechanism.
6. Monolithic materials are possible from acid catalysed systems.
7. Alkaline catalysed processes are independent of water concentration and produce condensed highly branched silicates.
8. The reactivity of alkoxides in alkaline media increases as the size of the alkoxy group increases.
9. Alkaline catalysed systems produce materials with a bimodal pore distribution highly dependent on the base concentration (~10-30Å & ~50-500Å [40]) and a lower relative bulk density relative to acid catalysed sol-gels.
10. Hydrolysis and condensation under alkaline conditions both proceed by S_N2 mechanisms.
11. Powders are generally obtained from alkaline catalysed systems.
12. Metal alkoxides generally hydrolyze much more readily than their silicon alkoxide counterparts.
13. Incorporation of metal oxides into silicate systems using alkoxides can be accomplished by generating small amounts of water in situ or by late addition of water or metal alkoxide to the reaction mixture.
14. Acetylacetonates and nitrates can be used in the sol-gel process to make mixed metal oxides.
15. Hybrid materials incorporating inorganic oxides with functionalised organic and/or polymeric molecules can be made using silicate sol-gel chemistry.

The above listed guidelines "distilled" from the literature reviewed were used as references in guiding the sol-gel research that follows.

CHAPTER III

EXPERIMENTAL METHODS

3.1 Introduction

Precedent in the laboratory of G. L. Wilkes has been to study sol-gel materials made from silicon ethoxides which have been allowed to gel at room temperature (~ 22°C). These systems were reacted, generally, in an alcohol based solvent (isopropanol:THF) containing a given amount of deionizied water and an acid catalyst (HCl) [14, 15]. Hybrid networks formed under these conditions, it was postulated, would possess sufficient flexibility to produce large, stable and crack-free monolithic gels. Also, it was hoped, the structure of the forming silicate would allow good dispersion of the oligomeric/polymeric modifying component in the final material matrix. Taken into consideration during the development of the reaction procedure were: the relative reactivities of silicon ethoxides, the type of structure formed under acid catalysis and the solubilities of the various reactants in different solvent media. In light of these considerations and the success achieved in making hybrid sol-gel materials, the previously used procedures were taken as a reference on which to base new designs. In this chapter, the experimental procedures developed to make new types of sol-gels will be de-

tailed. Also, the various materials and analytical techniques used throughout this study will be discussed.

3.2 Materials

The nomenclature used to identify the hybrid systems and their precursors involved several abbreviations for the sake of expediency. Table 1 on page 58 gives the chemical abbreviations used to identify the different material components used in this study.

3.2.1 Metal Oxide Precursors

Table 2 on page 59 lists the metal oxide precursors used to produce the hybrid sol-gel materials that were studied. This table gives some of the physical properties as well as the main supplier of the alkoxide and acetyl acetonate precursors used. Silicon ethoxides and methoxides were purchased from Petrarch Systems Inc. and were used as shipped; whenever possible, the highest purity grade (99% + distilled over quartz) was obtained. Reagent grade titanium(IV)isopropoxide, 98 + % $Al(i\text{-}pr)_3$, 97% $Al(s\text{-}bu)_3$, 99% $Al(acac)_3$, 98% $Zn(acac)_2$, and 98% $Zr(acac)_4$ were also used as shipped and were all obtained from the Aldrich Chemical Company Inc..

3.2.2 Polymer and Oligomer Modifying Components

Table 1. Chemical abbreviations

Chemical Reagent	Abbreviation
dimethyldiethoxysilane	DMDEOS
dimethyldimethoxysilane	DMDMOS
ethyltriethoxysilane	ETEOS
methyltriethoxysilane	MTEOS
methyltrimethoxysilane	MTMOS
tetraethoxysilane	TEOS
tetramethoxysilane	TMOS
aluminum tri-isopropoxide	$Al(i\text{-}pr)_3$
aluminum tri-secondarybutoxide	$Al(s\text{-}bu)_3$
titanium (IV) isopropoxide	$Ti(i\text{-}pr)_4$
aluminum acetyl acetonate	$Al(acac)_3$
zinc acetyl acetonate hydrate	$Zn(acac)_2$
zirconium (IV) acetyl acetonate	$Zr(acac)_4$
polydimethylsiloxane	PDMS
poly(tetramethylene oxide)	PTMO
tetrahydrofuran	THF
isopropyl alcohol	IPA

Table 2. Metal alkoxide and acetylacetonate precursors

Material	Mw	bp (°C)	mp (°C)	d (g/ml)	Supplier
DMDEOS	148.3	114-115	--	0.840	Petrarch
DMDMOS	120.2	82	--	0.865	Petrarch
ETEOS	192.3	158	--	0.896	Petrarch
MTEOS	178.3	141-143	--	0.815	Petrarch
MTMOS	136.2	102-103	--	0.955	Petrarch
TEOS	208.3	169	--	0.934	Petrarch
TMOS	152.2	121-122	--	1.032	Petrarch
$Al(s\text{-}bu)_3$	246.33	200-206*	--	0.967	Aldrich
$Al(i\text{-}pr)_3$	204.25	--	138-142	1.036	Aldrich
$Ti(i\text{-}pr)_4$	284.26	218†	--	0.955	Aldrich
$Al(acac)_3$	324.31	315	190-193	--	Aldrich
$Zn(acac)_2$	263.59	--	136-138	--	Aldrich
$Zr(acac)_4$	487.66	--	--	--	Aldrich

* at 10mm Hg
† at 30mm Hg

Table 3. Oligomers used to modify sol-gel oxides

Oligomer ID	<Mn>	Mw/Mn	wt%*	-Si(OEt)$_3$†	Source
PDMS(1700)	1700	--	--	2	Petrarch
PTMO(1000)	1000‡	--	--	2	3M
PTMO(2000)	2000‡	--	--	2	3M
PTMO(2900)	2900‡	--	--	2	3M
PTMO(2)	5736	2.50	40.3	2	3M
PTMO(3)	5575	2.88	34.0	3	3M
PTMO(4)	5632	2.83	43.0	4	3M
PTMO(5)	5763	2.85	38.0	5	3M

* weight percent solids in THF solution
† number of triethoxy functional ends (PDMS oligomers were hydroxy terminated)
‡ molecular weight prior to endcapping

Table 3 on page 60 lists the oligomer and polymer modifying components used to make modified sol-gels, their key properties and the supplier of the functionalized material. In this table, values under the column, -Si(OEt)$_3$, except for PDMS(1700), represent the number of triethoxysilane units attached to the oligomer/polymer backbone. In the PTMO oligomers (1000, 2000, 2900), trifunctional silane groups are attached to the chain ends. These oligomers are referred to as "endcapped" and are distinguished from each other by their molecular weight. For example, PTMO(2900) is the designation given to identify the 2900 Mw PTMO oligomer. The pendant or multifunctional PTMO polymers are approximately the same molecular weight (Mn = 5575-5763), though, and can not be readily distinguished on that basis. The multifunctional PTMO polymers do, however, contain from 2-5 triethoxysilane groups "randomly" attached along the backbone by which they can be distinguished. For example, PTMO(5) is the designation used to identify the 5763 Mn PTMO polymer with five triethoxysilane groups.

Silanol terminated PDMS oligomers were purchased from Petrarch Systems Inc. and were used as shipped. Triethoxysilane endcapped PTMO oligomers as well as triethoxysilane endcapped and branched polymers were specially prepared, characterized and generously supplied by Dr. James G. Carlson of the 3M Company.

Figure 4 on page 62 gives a schematic representation of the chemistry used to endcap PTMO oligomers with triethoxysilane functions. Figure 5 on page 63 shows the components used to make the multifunctional or branched PTMO polymers listed in Table 3 on page 60. The exact procedures used to make and characterize these materials have been presented elsewhere [20]. The number of "randomly" distributed triethoxysilane branches and the molecular weight of the functionalized PTMO polymers were both determined by the reaction composition used. Adjusting the ratio of the butanediol to the trimethylol propane, allowed the number of dangling -OH "pendant" groups to be controlled. The amount of isophorone-diisocyanate added, in turn, determined the molecular weight of the polymers formed. Once the pendant PTMO polymers had been formed, 3-isocyanato-propyl-triethoxysilane was added to cap the -OH functions with triethoxy groups. The capping reaction (analogous to that shown

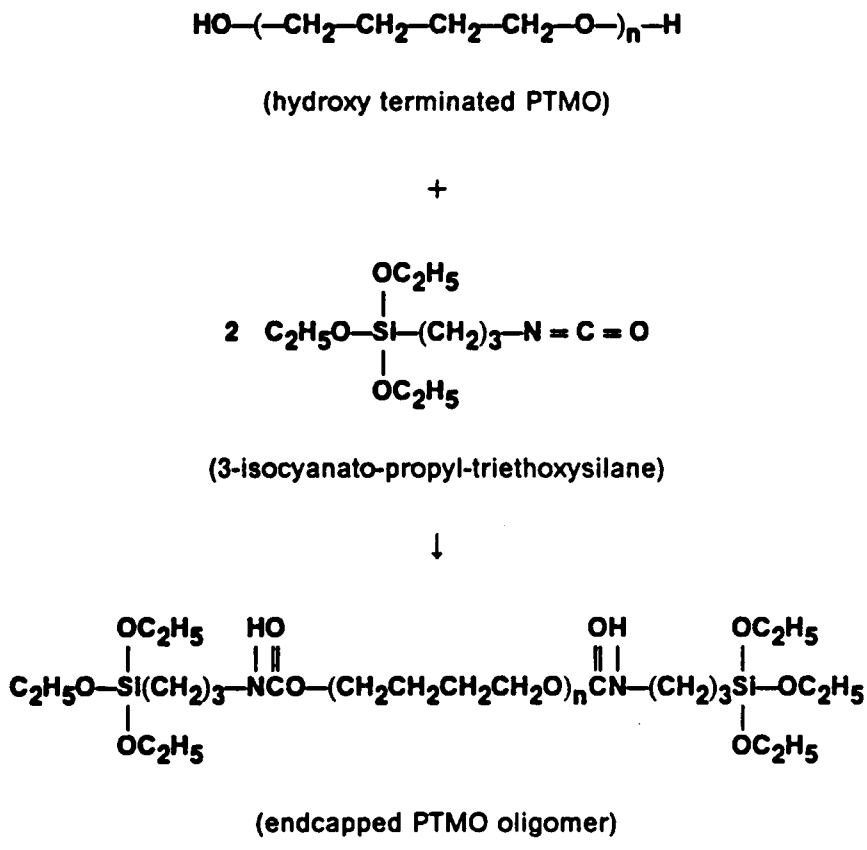

Figure 4. Schematic of PTMO endcapping procedure

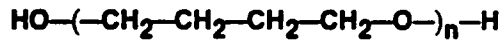

(hydroxy terminated PTMO)

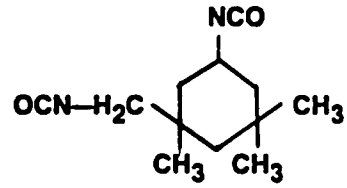

(isophorone-diisocyanate)

(butanediol)

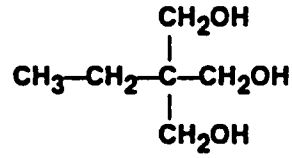

(trimethylol propane)

Figure 5. Components used to make multifunctional PTMO polymers

in Figure 4 on page 62) served to functionalize the hydroxy chain ends as well as the hydroxy pendant groups distributed along the polymer backbone.

3.2.3 Apparatus and Quantities Used

The reaction apparatus used for making the sol-gel materials studied consisted of a two-neck round-bottom flask fitted with a reflux condenser (with drying tube) and a nitrogen purge. Magnetic stirrers were employed for mixing while reactions were heated either in a thermostated oil bath, used for constant temperature at 80±5°C, or on a heating mantle. All reactions were carried out in a vented hood and were set up to produce 10-20 grams of gelled material. Unless otherwise specified, all solids were dispensed by weight; all liquids were dispensed by volume. Weights were measured to the nearest 0.1 gm on an electric balance while volumes were measured to the nearest 0.05 ml with disposable graduated serological pipets. Concentrations, when given, are either weight or volume percent of reactants in solution and are calculated based on the amount of materials added.

3.3 Procedures

3.3.1 Multifunctional Silicate Sol-Gel Glasses

The sol-gel glass materials used in this study were made using, primarily silicon-ethoxides of differing functionality blended together in various concentrations. The three silicon-ethoxides used to make the multifunctional glasses were: TEOS known as tetraethylorthosilicate (or tetraethoxysilane), MTEOS known as methyltriethylorthosilicate (or

methyltriethoxysilane) and DMDEOS known as dimethyldiethylorthosilicate (or dimethyldiethoxysilane). Glasses were also made from silicon methoxides as well. All of the gelled materials were made using the following reaction scheme (which is analogous to that previously reported for oligomer modified sol-gel materials [14, 15, 17]):

1. The various alkoxide reactants were measured into a clean dry roundbottom flask in sufficient quantity to produce 10-20 grams of gel.
2. The mixture was diluted to ≃56 vol% reactants with a solvent blend of 3:1, IPA to THF.
3. 1/2 the stoichiometric amount of distilled water required to completely hydrolyze the metal alkoxide functional groups was added.
4. A specified amount of HCl catalyst per mole alkoxide group was added (0.014 moles HCl per mole alkoxide group was the standard used for most systems).
5. The reaction mixture was heated to 80±5°C and allowed to reflux under vigorous stirring.
6. After ~1/2 hour of refluxing the reaction mixture was cast into Teflon coated glass petri dishes and covered.
7. Once gelation had occurred, the covers were removed and the gels were allowed to air dry at ~22°C.

3.3.2 Hybrid Sol-Gel Materials: Metal Alkoxide Incorporation

The incorporation of titaniumisopropoxide into the TEOS based glass network posed one major experimental problem. Unlike the silicon alkoxides such as TMOS (tetramethoxysilane) or TEOS (tetraethoxysilane) which readily form an oxide network (SiO_2) the titanium alkoxides react rapidly with water to form a "molecular" or non-network oxide: titaniumdioxide (TiO_2). As a consequence, the previously used procedure for making PDMS/TEOS and PTMO/TEOS hybrid materials [14, 15] caused added titaniumisopropoxide to precipitate out of the reaction mixture before it could react into the silicate network being formed. Hence, a procedure had

to be found that gently hydrolyzed the titaniumisopropoxide and would allow it to connect into the TEOS based glass network. A Chemically Controlled Condensation (CCC) method similar to that proposed by Schmidt [1-6] was developed to incorporate titaniumisopropoxide into PDMS/TEOS and PTMO/TEOS systems. The hybrid sol-gel systems incorporating endcapped oligomers were prepared in the following manner:

1. TEOS and PDMS or PTMO were added to a reaction vessel at ambient temperature in sufficient quantity to produce 10-20 grams of gelled material.
2. The mixture was diluted to ≃30 wt% reactants with a solvent blend of 3:1, IPA to THF. In the special case of PTMO(2900) containing hybrids the reaction mixture was heated to dissolve the polymer then allowed to cool before proceeding.
3. 1/2 mole glacial acetic acid per mole alkoxide function was added.
4. The reaction mixture was allowed to react overnight in a nitrogen atmosphere under constant stirring.
5. After 24 hours the desired amount of titaniumisopropoxide was introduced (at which point the reaction mixture turned yellow).
6. The reaction mixture was gently refluxed until either the yellow color faded or 2 hours expired.
7. The mixture was cast into Teflon coated glass petri dishes, covered and allowed to gel at ambient temperature (~22°C).

The multifunctional PTMO oligomers supplied by 3M were shipped in THF solution at various concentrations. For this reason, a slight alteration in the reaction procedure was required to utilize these oligomers. Hybrid silica-titania materials containing multifunctional PTMO oligomers were prepared in the following manner:

1. The multifunctional PTMO solution was weighed into a reaction vessel at ambient temperature in sufficient quantity to produce 10-20 grams of gelled material.
2. THF was added as necessary to dilute the PTMO solution to 34 wt% solids.

3. The appropriate amount of TEOS was added under stirring.
4. The reaction mixture was further diluted to ≃22 wt% reactants with IPA.
5. 1/2 mole glacial acetic acid per mole alkoxide function was added.
6. The reaction mixture was allowed to react overnight in a nitrogen atmosphere under constant stirring.
7. After 24 hours the desired amount of titaniumisopropoxide was introduced (at which point the reaction mixture turned yellow).
8. The reaction mixture was gently refluxed until either the yellow color faded or 2 hours expired.
9. The mixture was cast into Teflon coated glass petri dishes, covered and allowed to gel at ambient temperature (~22°C).

3.3.3 Hybrid Sol-Gel Materials: Metal Acetyl Acetonate Incorporation

A procedure was developed to use metal acetyl acetonates as sol-gel precursors. The starting raw materials used, $Al(acac)_3$, $Zr(acac)_4$ and $Zn(acac)_2$ were all air sensitive solids that required special handling and a unique procedure to allow incorporation into the silicate hybrid systems. The modified hybrid sol-gel procedure that follows was developed to meet these needs. The first step was to make a stable metal acetyl acetonate solution that could be stored and used at a later point in time. Such stable metal acetyl acetonate solutions were made in the following manner:

1. Prepurified N_2 gas was purged through a glovebag three times to achieve an inert atmosphere.
2. 10 grams of the desired metal acetyl acetonate was weighed into a clean dry roundbottom flask under inert atmosphere (i. e. in the glovebag).

3. 100 ml of dry ethanol was added under inert atmosphere to the vessel containing the metal acetyl acetonate.
4. The vessel was sealed with a rubber septum and removed from the glovebag.
5. 20 ml of a 0.1 N HCl stock solution was added by pipet under stirring (the solution was opened in air to carry out this step).
6. Concentrated 10 N HCl was added dropwise until the metal acetyl acetonate went completely into solution and the solution was clear with no observable suspended particles (~ 20-25 drops HCl were used).
7. The solution was sealed and stored until needed.

Table 4 on page 69 gives the concentrations of the three metal acetyl acetate solutions prepared in this manner. This procedure, though successful for metal acetyl acetonates, failed to produce clear solutions when applied to aluminum alkoxides; $Al(i\text{-}pr)_3$ and $Al(s\text{-}bu)_3$ did not dissolve using the above procedure regardless of the amount of added HCl.

Hybrid sol-gel materials were made using the metal acetyl acetonate solutions described above in conjunction with TEOS and functionalized PTMO oligomers. The amount of TEOS, PTMO and metal acetyl acetonate solution used to make hybrid materials was calculated to produce gelled materials with a molar ratio of components of: 21.48 moles silica (SiO_2) to 5.70 moles metal oxide (MO_n) to 1.00 moles multifunctional PTMO polymer. This particular molar ratio was chosen to allow comparison of the metal acetyl acetonate gels with those made using 15 weight percent $Ti(i\text{-}pr)_4$. The procedure used to make such hybrid sol-gel materials incorporating metal acetyl acetonates was as follows:

1. The multifunctional PTMO oligomer solution was weighed into a clean dry roundbottom flask in sufficient amount to produce 5-10 grams of gelled material.
2. The polymer solution was diluted to 34 wt% solids with THF under stirring.
3. TEOS was added in the correct amount.
4. The reaction mixture was further diluted to ≃22 wt% solids with IPA.
5. The appropriate amount of metal acetyl acetonate solution was added.

Table 4. Metal acetyl acetonate solutions

Metal acetyl acetonate	Mw	grams	ml of soln	concentration (mol/ml) X 10^4
$Al(acac)_3$	324.31	10.0	121	2.55
$Zn(acac)_2$	263.59	10.0	121	3.14
$Zr(acac)_4$	487.66	10.0	121	1.69

6. The reaction mixture was gently refluxed ~1/2 hr (except for zirconium containing reactions which were not heated due to the fast rate at which these systems gelled).
7. After refluxing (or mixing) the mixture was cast into Teflon coated petri dishes, covered and allowed to gel at ambient temperature (~22°C).
8. Once gelation occurred the covers were removed and the gels were allowed to air dry.

3.3.4 Extraction Experiments

A soxhlet apparatus with a 3 liter THF reservoir was employed to perform extraction experiments. Samples selected for extraction were dried to constant weight in vacuum at ~22°C then loaded into cellulose extraction thimbles which had also been dried to constant weight in vacuum. Cellulose thimbles containing ~1-3 grams of sol-gel material were then re-weighed and were placed into the soxhlet apparatus to be extracted for 48-72 hrs in refluxing THF. After extraction, the thimbles were removed, dried to constant weight in vacuum and weighed. To insure that any loss of material from the cellulose did not interfere with the extraction results, sol-gel residues were removed from the thimbles and both (residue and thimble) were weighed separately as well. Results were reported as weight percent of sample lost during the extraction process.

3.3.5 Swelling Experiments

Swelling experiments in THF were conducted on selected sol-gel materials that had been extracted first and dried to constant weight in vacuum. Single 0.3-0.7 gm pieces of these materials were loaded into separate covered beakers containing 250 ml of HPLC grade THF at ~20°C. After swelling for the desired amount of time (~30-380 hrs), samples were removed from the beakers, blotted dry and weighed. An effort was made to complete the blotting and

weighing procedure quickly in order to reduce the amount of weight lost through evaporation of THF. Results were reported as weight percent uptake of THF by the sample.

3.4 Characterization

Unless otherwise specified, all samples were characterized after having been allowed to gel and then dry open to the atmosphere. Sol-gel samples, after gelation and air drying, were stored in covered polystyrene petri dishes at room temperature (~22°C) until ready for testing. Gels were periodically tested to discover any aging effects that may have been taking place. The final dried films made by all of the given procedures ranged between 5 to 30 mils in thickness (1 mil = 2.54 X 10^{-2} mm).

3.4.1 Tensile Tests

Stress-strain experiments were carried out on an Instron Model 1122 tensile testing machine. Dumbbell samples 10.0mm X 2.9mm X 0.1-1.0mm in dimension were tested at an initial strain rate of 2mm/min. Engineering stress-strain curves were calculated from the measured force-time data obtained from the load to failure test. Except where otherwise specified, tensile properties reported represent average values obtained from the stress-strain data of at least five test specimens. Stress-strain curves plotted were digitized from the force-time data of individual test specimens which best represented the average for that sample population. Stress at break (or failure) was reported as the highest force reached during the test divided by the original cross-sectional area of the specimen. Strain to break was reported as the percent strain at which the specimen was observed to break. The elastic or Young's

Modulus was determined from the steepest portion of the stress-strain curve observed in the initial deformation region (~2-5% strain).

3.4.2 Dynamic Mechanical Analysis

Dynamic mechanical analysis (DMA) or dynamic mechanical spectra were obtained using an automated (IMASS) DDV-IIC Rheovibron Dynamic Viscoelastometer which operated in the tensile mode. Except where otherwise noted, specimens 3mm X 30mm X 0.1-1.0mm in dimension were tested at 11 Hz in the temperature range of -150°C to 220°C at a heating rate of 2°C/min. All plots of the storage modulus in the glassy region of the thermo-mechanical spectra were corrected to 9.1 on a log MPa scale to eliminate fluctuations due to calibration and/or nonuniformity in the sample dimensions. It should be recognized that relative ***not absolute*** values of modulus were used from the dynamic-mechanical spectra; only transitions in the storage modulus and tanδ (loss modulus/storage modulus) curves, on which the calibration correction had no effect, were of interest for analysis purposes.

3.4.3 NMR Spectroscopy

The solid state ^{29}Si NMR experiments were run on a modified Nicolet NT-200 spectrometer using a home-built 39.5 MHz silicon probe [89]. H_1 field strengths were typically 10-11 Gauss. Magic angle spinning, at rates of 1.8-2.5 kHz, employed a spinning system based on the design of Gay capable of spinning 8mm NMR tubes [90].

3.4.4 X-Ray Scattering

A Siemens kratky camera system was utilized for small angle x-ray scattering (SAXS) measurements in conjunction with an M. Braun position sensitive detector from Innovative Technology Inc. [91]. WAXS patterns were obtained from a Philips tabletop generator using a Warhus camera.

3.4.5 Raman Spectroscopy

These experiments were conducted on either a SPEX model 1403 double monochromator spectrometer with two 1800 grooves/mm planar holographic gratings [92] or an ISA double monochromator with two 1800 grooves/mm ruled gratings [93]. The detector, for both systems, was a cooled GaAs photodiode used for photon counting. The excitation source for both the SPEX and the ISA systems was, respectively, the 457.9 nm and the 514.5 nm radiation of an Ar^+ laser. The laser power at the sample was held at $\simeq$ 50 mW, the scattered radiation was collected using 90° geometry and the spectral resolution was $\simeq 3\ cm^{-1}$ during all scans. Solution spectra were obtained using ~5ml spectrosil quartz UV cells which had three polished optical windows. Solid samples cut from as cast films were held and positioned in the laser beam with a three direction (X-Y-Z) adjustable platform.

3.4.6 Scanning Electron Microscopy

A Cambridge Instruments Stereoscan 200 scanning electron microscope with a secondary electron detector was used to obtain micrographs of fracture surfaces. Fracture surfaces were prepared by breaking samples that had been cooled in liquid nitrogen (-176°C) for 15-25

minutes. Specimen surfaces were coated with a 150 Å layer of gold in a Surface Probe Inc. sputter-coater for contrast and painted with conducting silver to prevent charging.

3.4.7 Thermogravimetric Analysis

A DuPont Instruments model 951 thermogravimetric analyzer was used to obtain weight loss curves as a function of temperature. Selected sol-gel hybrid samples ~25mg in size were scanned in air from between ~35°C to either 450°C or 600°C (depending on the nature of the oligomer modifying component) at a heating rate of 10°C per minute [94].

CHAPTER IV

MODEL SOL-GEL COMPOUNDS

4.1 Introduction

New types of TEOS (tetraethylorthosilicate) based sol-gel materials have been made in recent years [1-20]. Of particular interest are the novel materials reported recently that incorporate polymeric/oligomeric components into silicate systems through the sol-gel process [14-20]. These materials show great potential commercially as well as scientifically because of their unique properties and hybrid nature; they have been deemed a new class of material somewhere between "pure inorganic" (ceramic) and "pure polymer". The properties that make these new materials interesting are, to a large degree, a result of the type of oxide structure and morphological texture formed during the sol-gel process. Both the oxide structure and the morphological features - hence also the physical properties of the final material - are governed by the overall degree of "reaction" or conversion attained by the sol-gel system.

The extent to which the hydrolysis and condensation reactions proceed determines the number of Si-O-Si links in the sol-gel material and, consequently, the oxide structure. Ideally, a four-functional metal alkoxide (four reactive sites per metal atom) such as TEOS reacts to

completion, forming a tetrahedrally bonded glass network. If either the hydrolysis or polycondensation reactions are incomplete, the glass network is not fully formed (i.e. tetrahedrally bonded SiO_2) and the final gelled materials contain unreacted alkoxy and/or hydroxy functions. Incomplete conversion, therefore, results in incomplete oxide formation which would effect the chemical properties as well as the mechanical strength of the gelled materials. The extent of completion of the overall sol-gel "reaction" or process is, therefore, an important quantity determining the structure/property behavior of all types of sol-gel materials.

The physical/mechanical properties as well as the structural/morphological features of modified sol-gel materials have been studied as a function of composition and reaction conditions [14, 15, 17-20]. These materials were found to be, generally, transparent and homogeneous with the polymer/oligomer modifying component well dispersed throughout the system. Further, the physical properties of the modified sol-gels were found to be significantly different from those of the pure modifying components [14-20]. In order to gain a better understanding of the properties of such "hybrid" or modified materials, in particular poly(dimethylsiloxane) (PDMS) and poly(tetramethylene oxide) (PTMO) modified materials, the gelling behavior of different silicon alkoxides and their mixtures have been studied independent of modifying components. This was done to allow the characteristics of pure oxide structures to be determined by eliminating contributions to physical properties arising from the polymeric/oligomeric modifiers.

In this chapter, the structure of the silicate components in sol-gel materials made from multifunctional silicon alkoxide precursors are probed. The multifunctional gels studied were made from materials listed in Table 2 on page 59 using the procedure outlined in section 3.3.1. These conditions, as mentioned, are identical to those used to produce the previously reported hybrid materials [14, 15, 17]. This was done in order to allow interpretation of the hybrid material behavior in terms of results garnered from unmodified alkoxide gels (assuming the alkoxide chemistry is independent of the modifying components). The main objectives are

to *identify* and *quantitate* the different types of silicate structures present in gelled alkoxide materials. Also, if possible, the observed physical properties of gels will be related to their composition and/or preparation conditions. The analytical techniques applied to achieve these goals were, primarily, solid state ^{29}Si NMR and Raman spectroscopy for which the experimental details are given in sections 3.4.3 and 3.4.5 respectively. Using these two techniques, the overall degree of conversion could be determined as well as which reaction, hydrolysis or condensation, limits the sol-gel process; also, the degree of reaction for each of the different silicon components could be calculated for the purposes of determining the final network "functionality". Dynamic mechanical spectroscopy and scanning electron microscopy were also applied as supplementary methods for characterizing gelled materials. The experimental details of DMA and SEM are given in sections 3.4.2 and 3.4.6.

4.2 Nomenclature

In the past, silicates have been qualitatively studied by solid state ^{29}Si NMR with Si-H cross-polarization and magic angle spinning [95-98]; more recently, crosslinked silicon polymers have also been qualitatively studied by these methods [75]. In the studies to be presented, solid state ^{29}Si NMR experiments, both single pulse (Fourier Transform or FT) and Si-H cross-polarization (CP), were run employing magic angle spinning (MAS) to obtain high resolution spectra. Lippmaa et al. have demonstrated for mineralogical samples that the isotropic chemical shifts observed in high resolution solid state ^{29}Si spectra are dependent on the degree of condensation of the silicate structures [95, 96, 97]. These researchers have also demonstrated that the isotropic ^{29}Si chemical shifts observed in the solid state correlate well with the chemical shifts observed in solution spectra for the same silicate structures. In their papers these authors developed a notation in which they labelled the various types of silicate structures using the symbol "Q" to represent any given silicon-oxygen tetrahedron

with an appropriate numeric superscript to indicate the number of other "Q" structures attached to the one in question [95, 96, 97]. A silicon-oxygen tetrahedron attached to four other silicon-oxygen tetrahedra - i.e. a "fully condensed" or "fully reacted" silicon species - would be labelled "Q^4"; likewise, a silicon-oxygen tetrahedra attached to only three other "Q" species would be "Q^3" and so on - see Figure 6 on page 79. In this manner Lippmaa et al. were able to describe/label all of the silicon species that they observed in the ^{29}Si NMR spectra of their mineralogical samples [95, 96, 97].

In this work, a modified form of Lippmaa's "Q" notation was adopted because of its inherent clarity and flexibility; the modifications, necessary to extend the notation to include our multifunctional systems, generated a notation identical to that of E. A. Williams [98]. The modifications are as follows for silicon based tetrahedra containing oxygen and organic "R" groups (R = methyl in our case): "Q" represents quaternary (four) oxygen tetrahedra, $Q=Si(O_{1/2})_4$, "T" represents "tri" oxygen one organic group tetrahedra, $T=Si(O_{1/2})_3R$, and "D" represents "di" oxygen two organic group tetrahedra, $D=Si(O_{1/2})_2R_2$. This modification scheme could be carried to the logical completion where "M" represents mono (one) oxygen three organic group tetrahedra, $M=SiO_{1/2}R_3$. However, since monofunctional alkoxides were not used to make any of the materials studied, the "M" notation is not necessary. The numeric superscript in the modified notation indicates the number of silicon-oxygen-organic tetrahedra (Q, T, D or M) attached to the tetrahedra in question. Figure 6 on page 79 schematically shows the different types of silicate species (structures) encountered in systems studied and the symbols used to designate those species. Henceforth the various silicate structures will be referred to by symbol according to the above notation scheme.

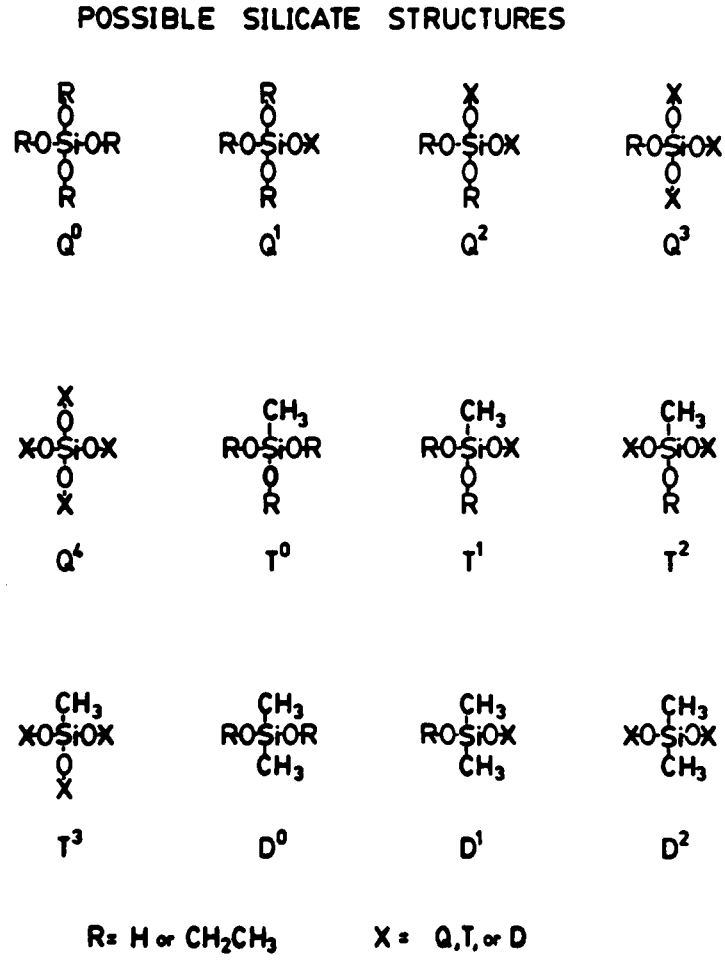

Figure 6. Possible silicate structures in mixed silicon alkoxide gels

4.3 Results and Discussion

4.3.1 Observed Properties of Multifunctional Silicate Gels

Figure 7 on page 81 is a compositional plot showing the systems studied, their gross physical features and the molar ratios of the three precursors used to make the materials. The nomenclature used to describe the materials is as follows: the letters 'D', 'M' and 'T' are abbreviations of DMDEOS, MTEOS and TEOS respectively whereas the numbers preceding these letters represent the mole percent of that particular component in the mixture. The label 37D/33M/30T would therefore represent a 37 mole percent DMDEOS, 33 mole percent MTEOS and 30 mole percent TEOS system. The distinctions between brittle gel, flexible gel and viscous liquid as well as turbid and clear gel in Figure 7 on page 81 are qualitative and are based primarily on visual and manual observations. Materials that could not be cut with a razor blade without shattering were considered brittle. Materials classified as flexible gels could be cut using a razor blade and/or a cutting die; specimens for dynamic mechanical study were successfully obtained in this manner. Additionally, pieces of the brittle materials shaken in a glass dish typically sound as though glass shards were being shaken; pieces of the more flexible materials, however, do not make this distinctive glass-like or "tinkling" sound when shaken in the same manner (a highly qualitative observation). Materials classified as viscous liquids were observed to be tacky/runny to the touch even after one year, therefore, it was concluded that they were ungelled (i.e. they did not form a self-supporting monolithic structure). Finally, the turbidity observed in some of the gelled materials was quite striking; these materials were white in appearance. This is most likely due to void structure on the micron (or larger) scale.

Figure 8 on page 83 shows the scanning electron micrographs taken of fracture surfaces from two different multifunctional gels: 23D/21M/56T and 0D/100M/0T (the notation on the

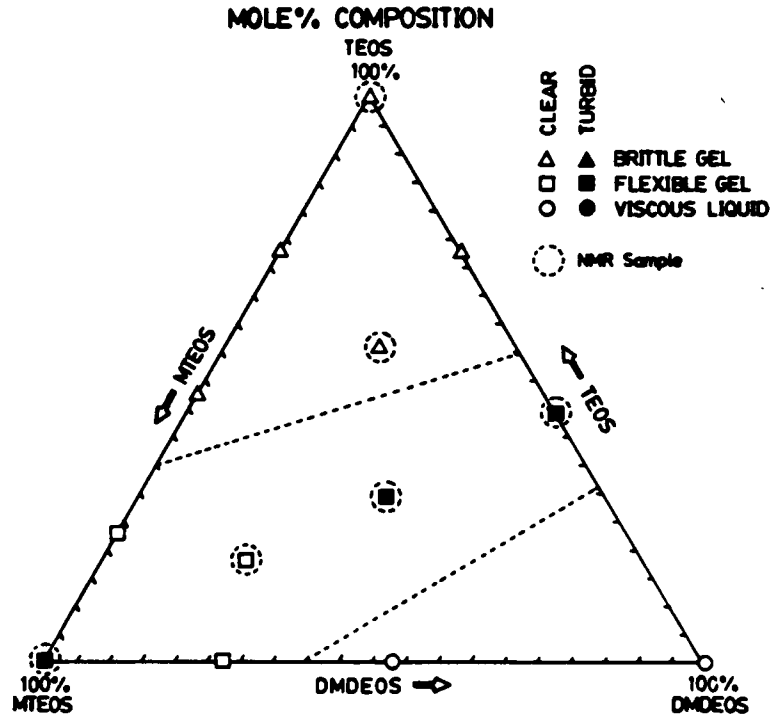

Figure 7. Mole percent composition plot of multifunctional gels studied

micrographs is in volume percent). The 23D/21M/56T gel is transparent and clear while the 0D/100M/0T gel is not transparent but white. At low magnifications (a-609X, b-593X) the fracture surface of the clear gel is textureless while the fracture surface of the turbid gel contains a textured structure. At higher magnifications (c-23,700X, d-24,300X) the difference between the two samples is more striking. The turbid material, 0D/100M/0T, is unmistakably porous while the clear material, 23D/21M/56T, though not completely featureless, is not. Further, pore diameters ≃20 nm are present in the high magnification micrograph of the 0D/100M/0T sample. Spherical scatterers ~20nm in diameter should scatter electro-magnetic radiation with a wavelength, $\lambda \simeq$ 400nm. Since visible light is between 380nm and 760nm, heterogeneous structure on the scale of 20nm should scatter visible light. Therefore, fluctuations in the refractive index arising from submicron voids within the 0D/100M/0T gel are, no doubt, the principle reason that pure MTEOS gels are not transparent. The observed void structure apparently forms during the drying/gelation process.

The dynamic mechanical spectra for two of the "flexible gels" (37D/33M/30T & 0D/100M/0T) are given in Figure 8 on page 83. These modulus-temperature spectra, the first ever presented for such materials (it is believed), show a storage modulus that slowly drops from ≃ 9 to 8.5 in the temperature range of ≃ -50 to 200°C and tanδ (ratio of loss to storage modulus) curves that display a small bimodal transition (at ≃ 0 & 60°C) superimposed on a very broad (≃ -100 to 130°C) weak transition (the final rise in the tanδ curves starting at ≃ 150°C could be due to thermal curing of the gel [17]). Though the features of these tanδ curves can not at present be explained completely, the existence of a transition at or below ≃ 20°C indicates a certain degree of molecular motion or mobility in these gels at room temperature. However, it is clear that these gels, though flexible at ambient temperature, can not be considered elastomeric materials in a conventional sense because of the high storage modulus they exhibit a room temperature (≃ 10^9 Pa as opposed to ≃ 10^6 Pa for conventional elastomers in their rubber plateau).

Figure 10 on page 86 shows the dynamic mechanical spectra of two trifunctional silicate gels made from different alkoxide precursors: MTMOS and MTEOS (both could be labelled as

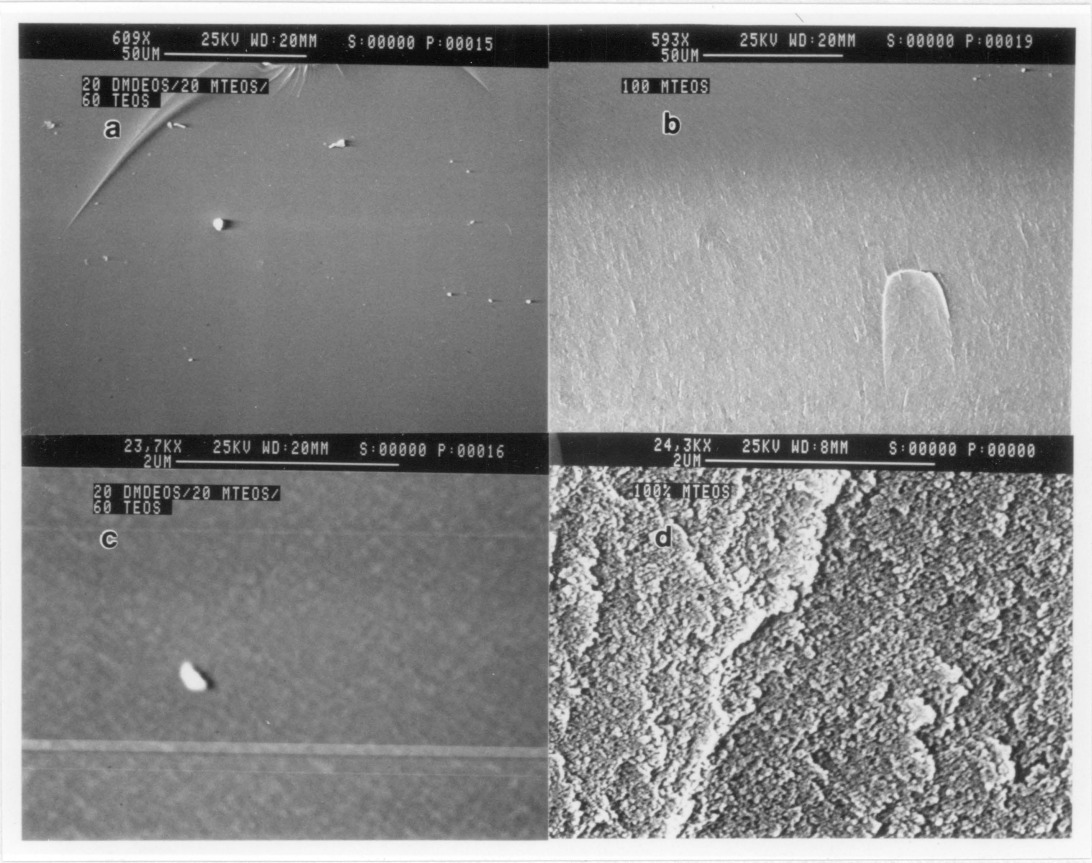

Figure 8. Scanning electron micrographs of multifunctional gels: a) 23D/21M/56T-magnified 609X, b) 0D/100M/0T-magnified 593X, c) 23D/21M/56T-magnified 23,700X, d) 0D/100M/0T-magnified 24,300X

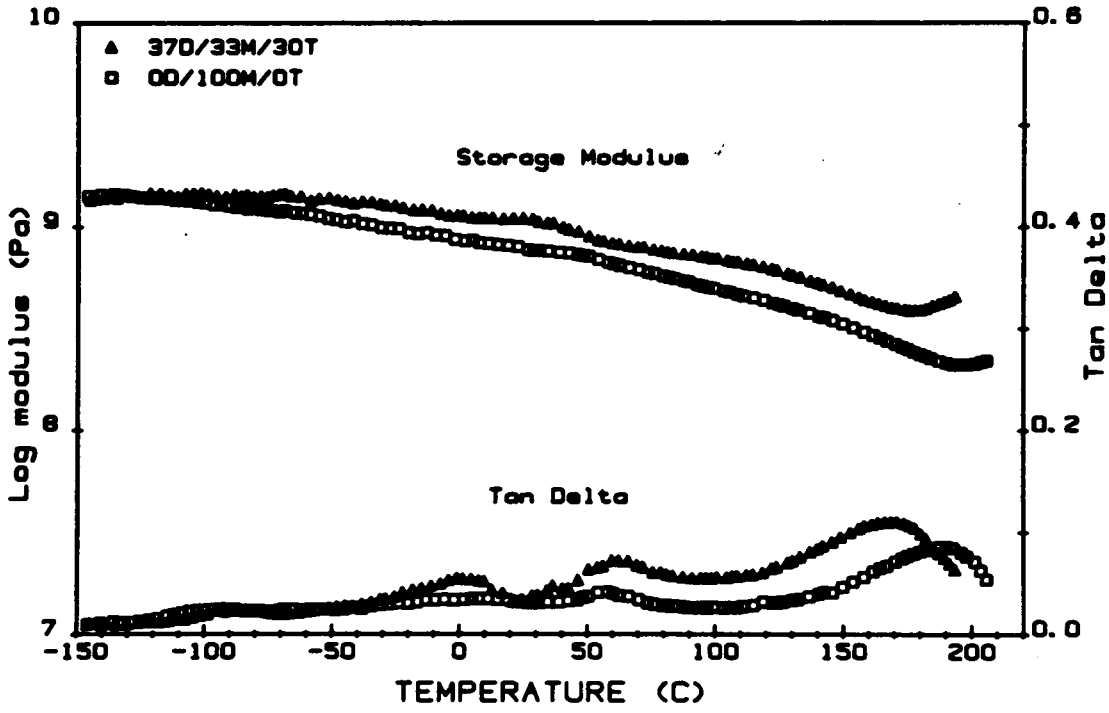

Figure 9. Dynamic mechanical spectra of multifunctional silicate gels: triangles-37D/33M/30T gel, squares-0D/100M/0T gel

0D/100M/0T gels therefore these two are distinguished by their precursor - unless specified otherwise, all gels are made using silicon ethoxides). These two gels were both made in the same manner, using 0.014 moles HCl per mole alkoxide group (for trifunctional alkoxides this would be equivalent to 0.042 moles HCl per mole alkoxide), and appear very simlilar in terms of their modulus-temperature and tanδ response. The MTEOS gel does display a somewhat lower modulus than the MTMOS gel at elevated temperatures ($\sim$140°C and higher) and an additional peak in the tanδ curve at $\simeq$60°C. These differences may be due to a slightly lower degree of conversion in the MTEOS gel as opposed to the MTMOS gel but could also be due to a difference in the motion of unreacted alkoxy functions: ethyl as opposed to methyl. However, for all practical purposes the differences observed in the dynamic mechanical spectra of the MTMOS and MTEOS gels in Figure 10 on page 86 are so small as to be insignificant.

Figure 11 on page 88 gives the dynamic mechanical spectra of three MTMOS gels made using different levels of HCl catalyst: 0.007 (squares), 0.014 (triangles) and 0.037 (crosses) moles of HCl per mole methoxide group. The mechanical spectra of the two gels made at higher catalyst content (0.014 & 0.037 moles HCl) are virtually identical except for the higher temperatures ($>$ 150°C) at which the 0.014 moles HCl gel displays a larger tanδ peak. It should be noted though, that the expanded tanδ scale exaggerates even slight differences in the ***magnitude*** of observed transitions. The dynamic mechanical spectrum of the 0.007 moles HCl MTMOS gel is fundamentally different from the other two. This gel displays a distinct transition in both the storage modulus and tanδ curves beginning at $\simeq$60°C that is not apparent in the spectra of the other gels. The storage modulus drops sharply from $\sim 10^{9}$Pa to $\sim 10^{8.6}$Pa then flattens; the storage moduli of the 0.014 and 0.037 moles HCl gels drops monotonically in this range. The sharp drop observed in the storage modulus curve of the 0.007 moles HCl gel is accompanied by a relatively large transition in the tanδ curve. Overall this behavior is very much like the dynamic mechanical behavior for an elastomeric system undergoing its glass transition though the transitions in the HCl MTMOS gel are much smaller and broader

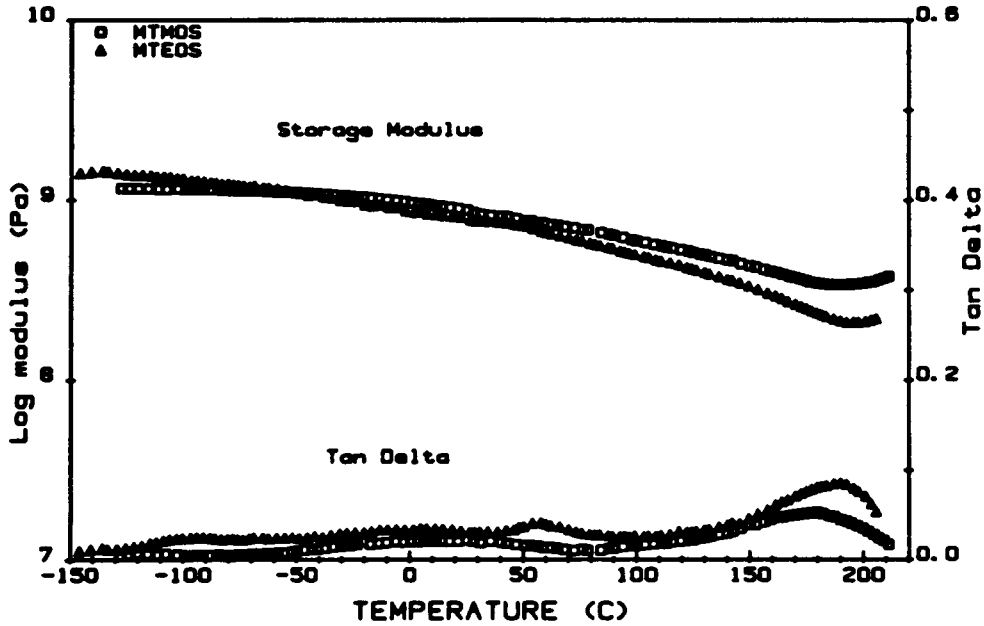

Figure 10. Dynamic mechanical spectra of MTMOS and MTEOS gels: squares-MTMOS based gel, triangles-MTEOS based gel

(less than 1/2 an order of magnitude as opposed to ~3 orders of magnitude change in the storage modulus).

In one regard, the observed differences in the dynamic mechanical spectra of the MTMOS gels in Figure 11 on page 88 are consistent with the thinking that HCl acts as a catalyst for the hydrolysis of ortho silicate esters. The low HCl MTMOS gel (0.007 moles HCl) can be viewed as a system that is not "fully" catalysed i. e. addition of more HCl will continue to accelerate the rate of hydrolysis reaction. The other two gels (0.014 & 0.037 moles HCl) are past the "saturation point" beyond which addition of HCl has no further ***catalytic*** effect. A change in the rate of hydrolysis, relative to condensation, brought about by a change in the amount of catalyst could alter the silicate structure formed. An alteration of the silicate structure in MTMOS gels made using different HCl concentrations is implied by the dynamic mechanical spectra given in Figure 11.

In order to be able to compare the properties of the final gels strictly on the basis of the average number of network links per silicon center (i. e. a mean field), the three different alkoxide components used to make the multifunctional mixed gels should not phase separate from each other during the sol-gel process. If ***large scale*** phase separation did occur, comparisons would not be as simple and would require that self condensation or exclusion of certain precursors be accounted for. It is reasonable to assume, however, that this is not the case; indirect experimental evidence to be presented shortly supports this assumption. Also, while the initial reactivities of the individual precursor species are undoubtedly different (the order being DMDEOS≥MTEOS > TEOS [74, 99]) the reactivities for successive sites (after one or more sites on a precursor species has reacted) can be assumed equivalent - at least on an "order of magnitude" scale. Then, since the various precursors contain more than one reactive site which react over a period of time, there is a high probability of different components interconnecting (or cross linking) making large scale phase separation in the mixtures during gelation unlikely. Therefore, differences in the properties of these gelled materials can simply be ascribed to the "functionality" of the system - where "functionality" refers to the number of bridging Si-O-Si bonds per silicon center.

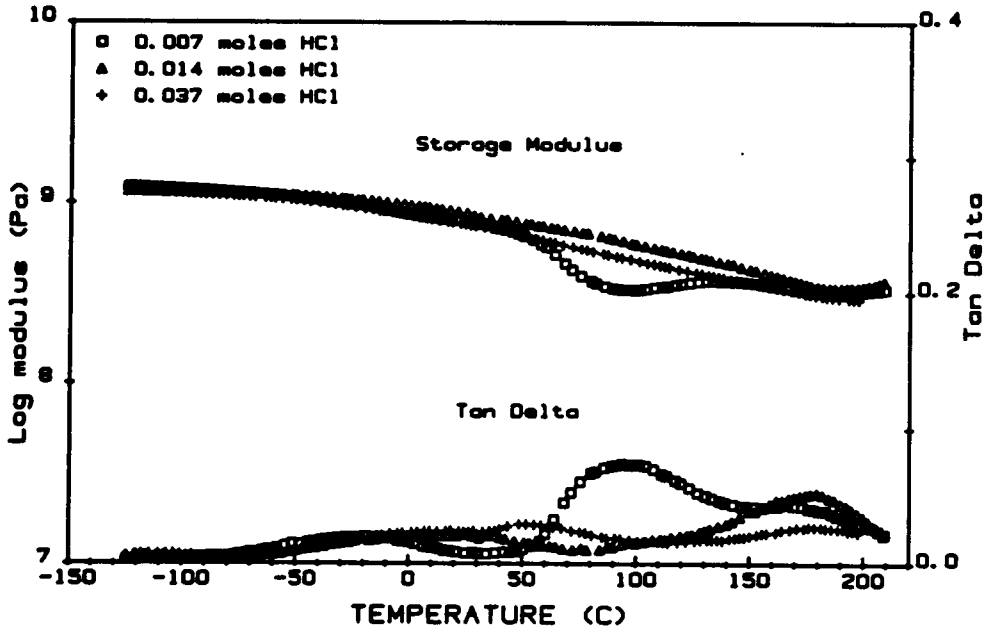

Figure 11. Dynamic mechanical spectra of MTMOS gels as a function of HCl content: squares-0.007 moles HCl/mole methoxide group, triangles-0.014 moles HCl/mole methoxide group, crosses-0.037 moles HCl/mole methoxide group

Using the terminology developed earlier, a Q^4 silicon center would be tetrafunctional whereas Q^3 and T^3 centers would be trifunctional and Q^2, T^2 and D^2 centers would be difunctional etc.. The potential limiting cases for our materials would be ***final*** systems consisting of all tetrafunctional, trifunctional or difunctional silicon centers. An all tetrafunctional material would be very brittle as compared to an all trifunctional material which would be less brittle. An all difunctional material would, in principle, be ungelled and therefore liquidlike since it could not even form a network structure. The overall functionality of a gel is, therefore, determined by ***two*** factors: the potential ***functionality*** of the precursor mix (overall functionality in the case of 100% reaction) ***and the degree of reaction*** attained by the components in the final gel.

4.3.2 Solid State Silicon NMR

Close examination of Figure 7 on page 81 reveals two "distinct" gelled regions. One in which the gels are flexible and one in which the gels are brittle. Samples were chosen from both regions for NMR analysis in order to observe the effects of functionality on the overall degree of reaction as well as to observe any possible changes in the number and/or type of silicate structures present in the differing materials. Two series of materials were selected for study: one in which the TEOS content was varied holding the DMDEOS : MTEOS ratio at roughly 1 : 1, and one in which the MTEOS content was varied holding the DMDEOS : TEOS ratio at roughly 1 : 1. The first series crosses the vitrified (brittle) gel/unvitrified (flexible) gel border while the second series follows the changes in composition for mixtures that produce flexible gels. Changes in the silicate structures formed as a result of changing mixture functionality and/or composition should be borne out in the NMR spectra of these two series. Unfortunately, the ungelled materials in Figure 7 on page 81 (53D/47M/0T & 100D/0M/OT) though potentially quite interesting, were not studied by solid state ^{29}Si NMR.

Table 5 on page 91 gives the isotropic chemical shift ranges observed for the ^{29}Si NMR resonances of various silicate structures. Included are values obtained for a wide range of materials, from naturally occurring substituted silicates [95, 96] to synthetic silica gels [100] and solid organo-silicon polymers [75, 97]. Also included in Table 5 on page 91, for reference, are the ^{29}Si CP and FT/MAS chemical shifts observed in this study for multifunctional sol-gel silicates. Lippmaa et al. assigned ^{29}Si chemical shifts to the different types of silicon-oxygen tetrahedra observed in the spectra of their substituted mineralogical silicates [95]. Assignments were made to ring structures of different sizes: cyclotetra Q^2 - 87.5 ppm, double three-rings Q^3 -90.4 ppm, double four-rings Q^3 -99.3 ppm and three-dimensional six-rings Q^4 -109.9 ppm. Other assignments were made for Q^2 single chain, -86.3 to -88.0 ppm, and Q^2 double chain, -86.8 ppm, linear silicate structures and for a Q^4 spiral structure, -107.4 ppm, observed in low quartz [95]. Beshah et al. observed a triplet at -104 ppm in the ^{29}Si CP/MAS spectra of their modified PDMS systems for which they tentatively assigned a "butterfly" or double closed loop structure to the - 105.2 ppm resonance and a single closed loop structure to the - 104.7 ppm resonance [75].

Figure 12 on page 93 and Figure 13 on page 94 show the ^{29}Si NMR spectra from the Fourier Transform or "single pulse" experiment with magic angle spinning (FT/MAS) while Figure 14 on page 95 and Figure 15 on page 96 show the cross polarization with magic angle spinning (CP/MAS) spectra of the six materials chosen for analysis (see Figure 7 on page 81). Figure 12 on page 93 and Figure 14 on page 95 show the ^{29}Si NMR spectra (FT/MAS and CP/MAS respectively) for a series of gels in which the functionality of the mixture (discussed later) was varied by changing the TEOS concentration holding the MTEOS : DMDEOS ratio relatively constant at $\simeq$ 1. Figure 13 on page 94 and Figure 15 on page 96 show the ^{29}Si NMR spectra (again, FT/MAS and CP/MAS respectively) for a series of gels in which the functionality was varied by changing the MTEOS concentration this time holding the TEOS : DMDEOS ratio at $\simeq$ 1. The first series of NMR samples were chosen in order to detect any effects of gel composition on the silicate structures observed in brittle samples as well as to detect any changes that may occur as a result of crossing the brittle gel/flexible gel compo-

Table 5. Silicon chemical shifts (-δppm*) for silicate structures

Q^4	Q^3	Q^2	Q^1	Q^0	T^3	T^2	D^2	D^1
107-110[e]	90-100[e]	83-88[e]	78-83[e]	66-74[e]	65-66[b]	55-56[b]	19[b]	12[d]
109.3[c]	99.8[c]	90.6[c]			55-66[d]	56[d]	19-23[d]	8-9[e]
99-110[d]	99[d]	89[d]			62-64[e]	53-57[e]	16-18[e]	
106-110[e]	98-101[e]	89[f]			61-64[f]	55-56[f]	13-18[f]	
105-108[f]	98-100[f]							

[a]taken from ref. 95
[b]taken from ref. 96
[c]taken from ref. 98
[d]taken from ref. 100
[e]FT/MAS data
[f]CP/MAS data
*relative to liquid TMS (tetramethylsilane)

sition borderline. The second series of NMR samples were chosen to detect any silicate structural changes in a homologous series of flexible gel compositions.

In both the FT/MAS and the CP/MAS ^{29}Si NMR spectra of the various gels, the different silicon centers are readily discernible due to the relatively large difference in chemical shifts caused by the substituents attached to the Si atoms. The 0D/0M/100T gel displays prominent Q^4 and Q^3 resonances with a hint of a Q^2 resonance. The 23D/21M/56T gel exhibits distinct Q^4 and Q^3 resonances with a hint of a Q^2 resonance for the TEOS component, a strong T^3 resonance with a weaker, diffuse T^2 resonance for the MTEOS component and essentially one D^2 resonance for the DMDEOS component. The spectra of the other gels in these four figures show the same structural features in the corresponding regions with only the intensities (and areas) observed varying as a function of composition. The series of gels in Figure 12 on page 93 and Figure 14 on page 95, for example, show the resonances in the TEOS region decreasing, relative to the resonances from the MTEOS and DMDEOS components, as the TEOS concentration is decreased. The series of gels in Figure 13 on page 94 and Figure 15 on page 96 show the same trend for the MTEOS resonances relative to the TEOS and DMDEOS resonances. In neither series does one observe any changes in the number of silicate structures observed for the three components as one changes the composition - except, of course, when one (or more) component(s) is (are) removed from the gel composition. This indicates that the composition of the mixture and the "potential functionality" (defined later) have little bearing on the type of silicate structures actually observed other than to dictate which species are possible; of course, if one or more of the precursor components is not present in the mixture, the corresponding NMR resonances will be absent in the spectra.

It is notable that in the ^{29}Si NMR spectra of all of the gels Q^1, T^1 or D^1 resonances are not present and only very small Q^2, and T^2 resonances are observed. This indicates that, within experimental limits, there are no dangling ends (Q^1, T^1,D^1) and not many linear segments (Q^2,T^2) - other than the D^2 - in the gelled systems. Further, since Q^0, T^0 or D^0 resonances also were not observed in either the FT/MAS or the CP/MAS ^{29}Si NMR spectra of any of the gels, one can conclude that unreacted precursors are not likely present as trapped

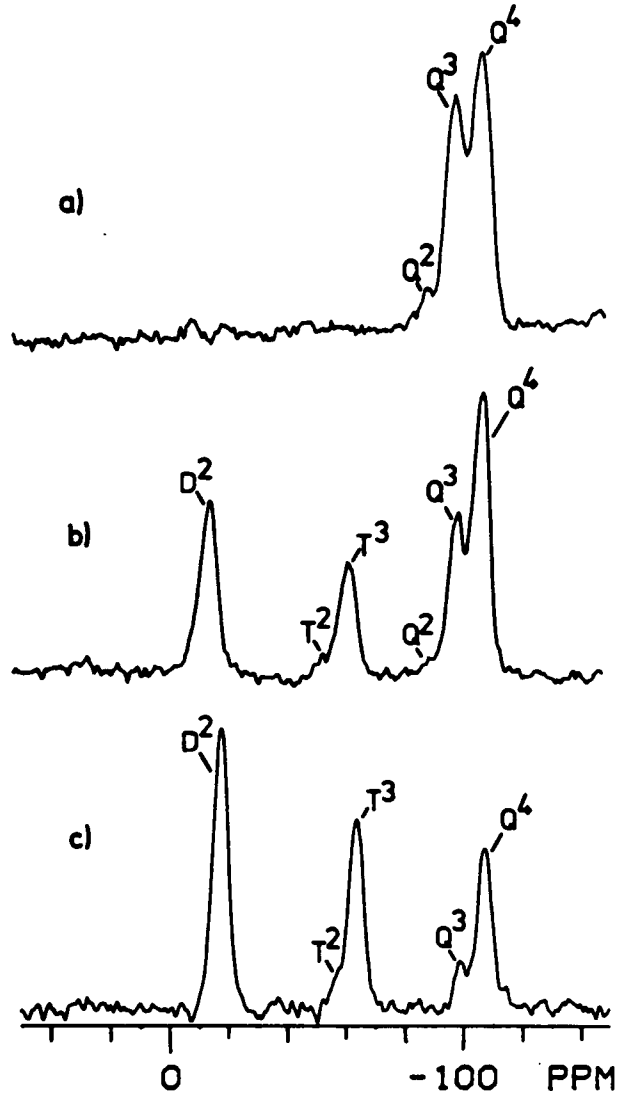

Figure 12. FT/MAS NMR spectra as a function of TEOS content: a) 0D/0M/100T gel, b) 23D/21M/56T gel, c) 37D/33M/30T gel

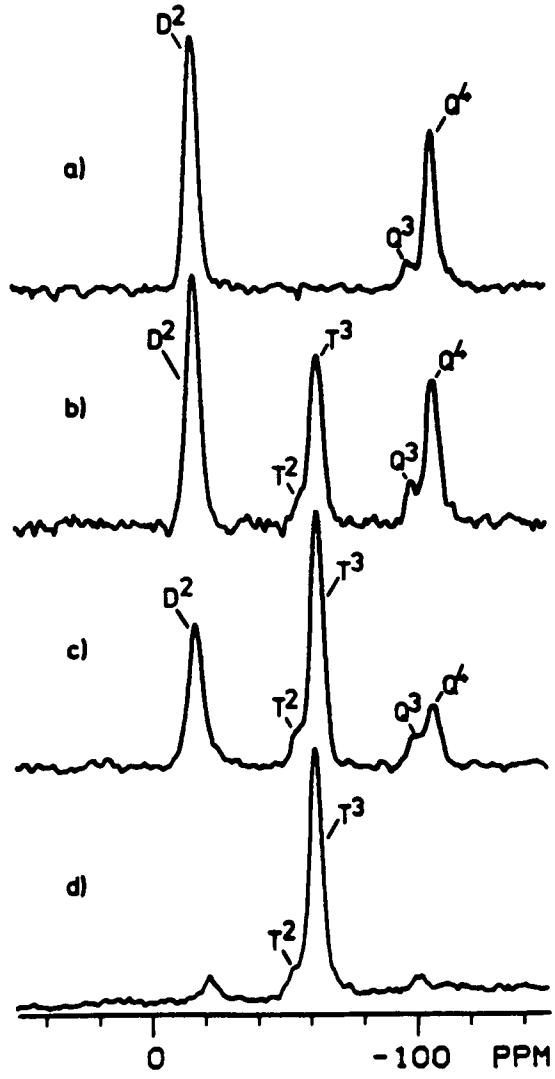

Figure 13. FT/MAS NMR spectra as a function of MTEOS content: a) 56D/0M/44T gel, b) 37D/33M/30T gel, c) 22D/60M/28T gel, d) 0D/100M/0T gel

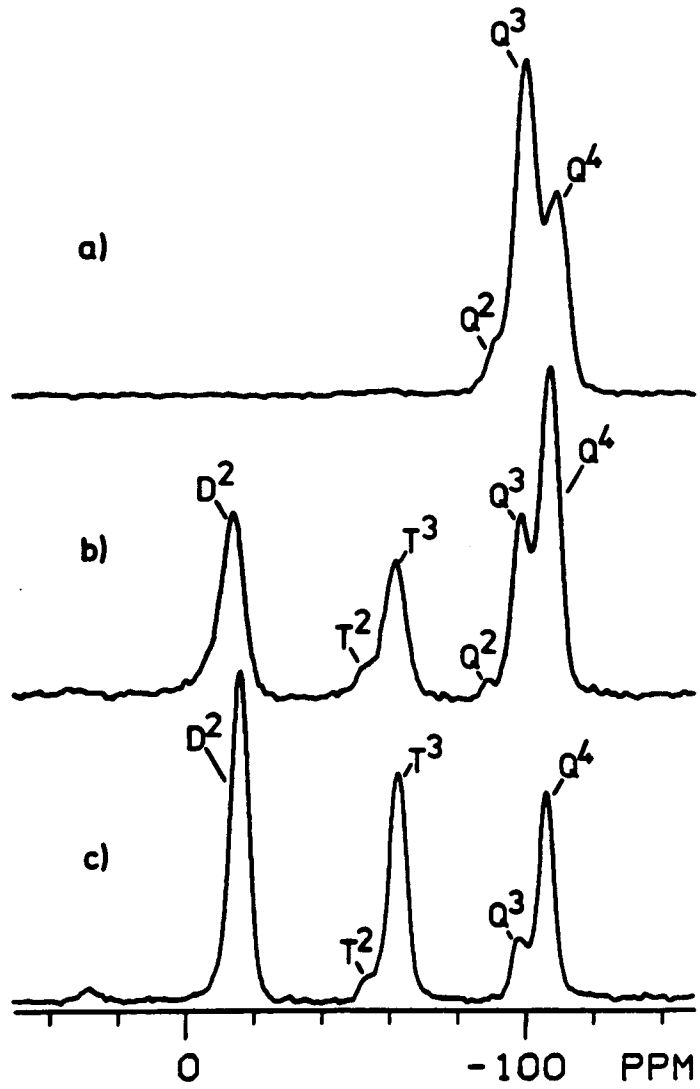

Figure 14. CP/MAS NMR spectra as a function of TEOS content: a) 0D/0M/100T gel, b) 23D/21M/56T gel, c) 37D/33M/30T gel

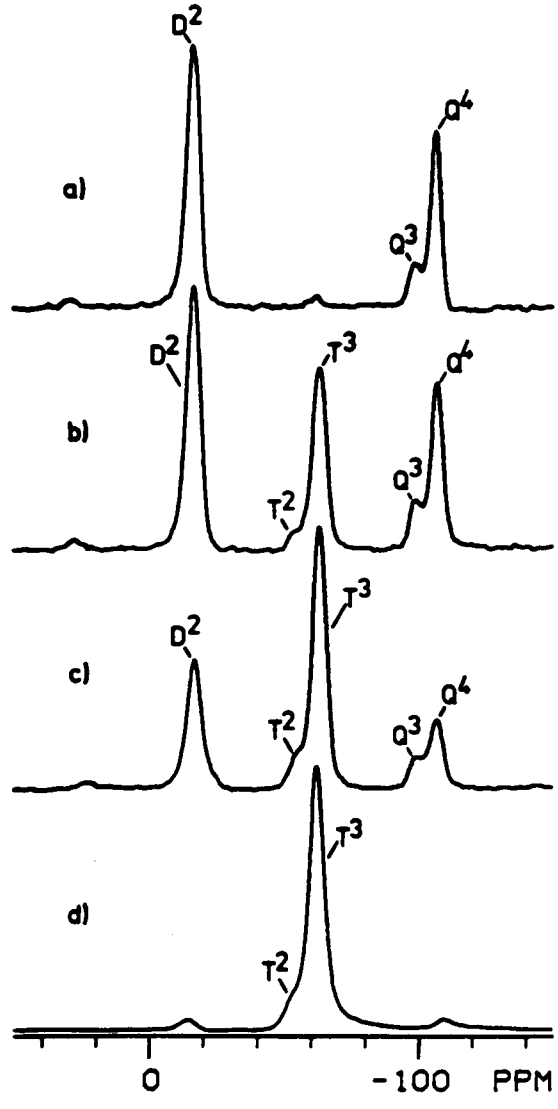

Figure 15. CP/MAS NMR spectra as a function of MTEOS content: a) 56D/0M/44T gel, b) 37D/33M/30T gel, c) 22D/60M/28T gel, d) 0D/100M/0T gel

species in the gel network; any unreacted precursors trapped in the gel network would have been present in the NMR spectra since these materials were ***not extracted*** prior to NMR analysis.

The measured ^{29}Si chemical shifts reported in Table 6 on page 98 allow assignment, at least in a tentative sense, of the observed Q^4 and Q^3 resonances based on prior literature assignments. With the exception of the Q^4 resonance in the 0D/0M/100T gel, which was displaced relative to the Q^4 resonances of the other gels, the resonances for a given silicate occurred at the same chemical shift regardless of the gelled system.

With the exception of the 0D/0M/100T gel, the ^{29}Si CP/MAS spectra match the FT/MAS spectra - for any given gel - both in detail and intensity of the peaks observed. The one notable exception, again, is the 0D/0M/100T gel for which the observed Q^4 peak in the FT/MAS spectrum (Figure 12 on page 93) is larger than the Q^3 peak whereas in the CP/MAS spectrum (Figure 14 on page 95) the reverse is the case. This has to do with the low cross polarization efficiency of the Q^4 species due to a lack of nearby protons to facilitate the transfer of polarization; an extremely poor cross polarization efficiency can result in resonances not appearing in a CP spectrum that are present in the FT spectrum of the same material. In our materials all of the resonances observed in the FT spectra are observed also in the corresponding CP spectra and the intensities are only affected for the Q^4 resonance in the 0D/0M/100T material. ***This is indirect evidence that large scale phase separation of Q^4 species does not occur in these materials since in order to be "seen" in CP spectra the Q^4 ^{29}Si atoms must be within approximately 10Å of a proton to facilitate polarization transfer*** [74]. CP contact time studies to be discussed shortly can produce Si-H polarization transfer constants which provide information on the local chemical environments in the different silicate structures.

In the FT experiment the observed peaks are inherently quantitative with respect to the amount of a given silicate species present in the sample - provided the delay time between pulses is at least three times longer than the T_1 of the slowest relaxing species. In the systems studied here the slowest relaxing species would be expected to be the Q^4 silicates in the

Table 6. Measured percentage of various silicate structures in gels

Sample	Peak	δ^*	$\%I^{FT}$	$\%A^{FT}$	$\%I^{CP}$	$\%A^{CP}$
0D/0M/100T	Q^4	-108	51.3	55.2	27.0	25.5
	Q^3	-99	41.7	39.8	62.3	63.2
	Q^2	-90	7.1	5.0	10.7	11.3
23D/21M/56T	Q^4	-108	37.3	38.5	38.4	35.5
	Q^3	-100	19.6	18.4	20.2	19.3
	Q^2	-89	0.0	0.0	1.3	0.7
	T^3	-64	13.7	12.0	15.6	15.4
	T^2	-60	5.3	4.9	3.4	4.1
	D^2	-16	24.1	26.2	21.1	24.9
56D/0M/44T	Q^4	-107	36.5	30.1	35.3	34.5
	Q^3	-99	8.8	8.8	6.3	6.0
	D^2	-18	54.7	61.0	58.4	59.5
37D/33M/30T	Q^4	-108	22.4	24.6	24.0	20.9
	Q^3	-100	6.7	5.1	7.2	7.0
	T^3	-64	26.9	25.0	26.2	26.6
	T^2	-57	4.8	4.4	3.0	2.9
	D^2	-18	39.2	40.9	39.6	42.5
22D/60M/18T	Q^4	-108	13.5	13.0	10.9	10.4
	Q^3	-100	5.9	6.3	6.6	8.1
	T^3	-64	50.9	48.3	49.0	46.3
	T^2	-56	5.9	6.1	6.5	6.7
	D^2	-18	23.9	26.4	27.0	28.5
0D/100M/0T	Q^4	-102	5.6	3.8	4.3	4.3
	T^3	-63	78.7	80.9	80.0	75.5
	T^2	-55	7.9	7.1	12.0	16.6
	D^2	-20	7.9	8.2	3.7	3.6

*ppm relative to liquid TMS (tetramethylsilane)

0D/0M/100T gels. These Q^4 Si centers have inherently fewer protons in their immediate vicinity (10Å or so) than do Si centers in gels that contain protons attached through covalently bonded methyl groups. Reducing the local proton concentration reduces the number and strength of Si-H dipolar interactions which, in turn, lowers the efficiency of the Q^4 Si spin-lattice relaxation. Si centers in "proton poor" environments would, therefore, be expected to have measured T_1s longer than those measured for Si centers in "proton rich" environments. In the extreme, the lack of protons can cause the Si T_1 to become inordinately long (in fused quartz, for example, a T_1 on the order of several of minutes is not unusual). In order to be able to meaningfully quantitate the FT/MAS spectra obtained for the various gels, determination of the T_1 for the Q^4 silicons in the 0D/0M/100T gels was necessary. A rigorous determination of the T_1 for the Q^4 silicates in the FT experiment was not practical, instead, Torchia's modification of the Freeman-Hill decay experiment [101] was conducted using CP/MAS. Figure 16 on page 100 shows the stacked plot of the CP/MAS spectra for the 0D/0M/100T gel collected using different delay times. In this experiment the T_1 is given as the time at which polarization reaches $1/e \simeq 35\%$ of its initial (equilibrium) value. Using this definition, T_1 for ***CP observable Q^4 species*** is on the order of 30-40 seconds. All FT/MAS spectra were, therefore, collected using at least 240 seconds delay between pulses. Based on the determined T_1 for the CP observable Q^4s, a 240 second delay between pulses is very conservative, taking into consideration that there may be CP invisible species with longer T_1 values.

Unlike the FT experiment, the CP experiment is not inherently quantitative. Since the different silicate species cross polarize with different efficiency (related to the local concentration of polarizable protons as inferred above), in order for a CP spectrum to be quantitative a cross-polarization "contact time" must be chosen so that all of the silicate species reach their equilibrium polarization before the FID (Free Induction Decay) is measured. Figure 17 on page 102 gives an example of the effect of contact time on the intensity of the different Si signals observed in a CP spectrum for a 23D/21M/56T gel. Figure 18 on page 103 gives a plot of the measured NMR intensity as a function of the contact time (in milliseconds) for the various Si species observed in the 23D/21M/56T gel (shown in the stacked plot in Figure 17 on

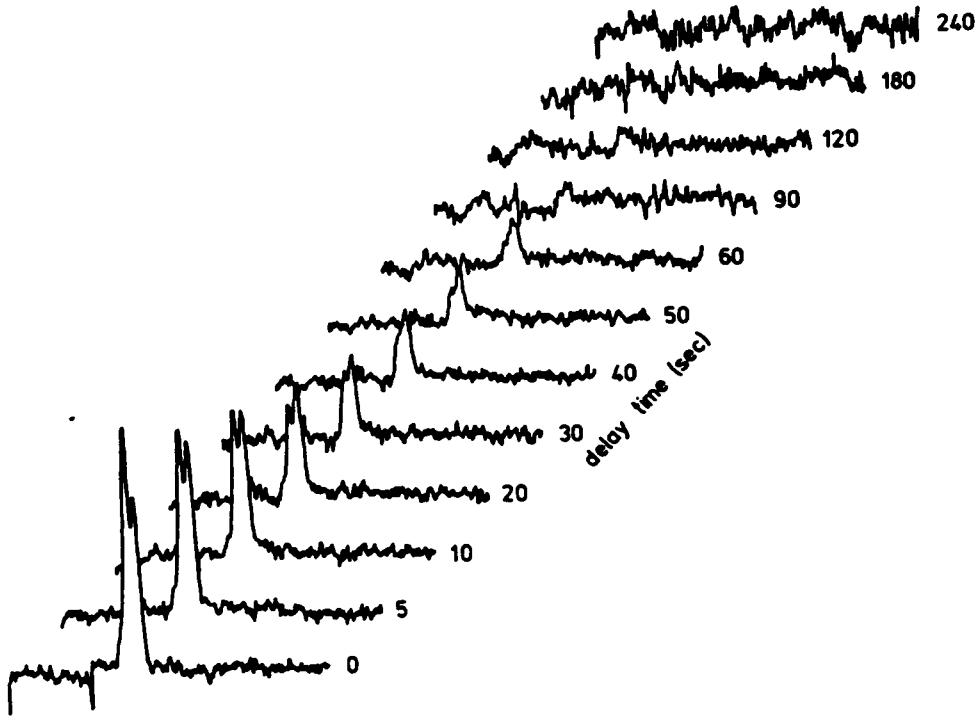

Figure 16. CP/MAS NMR spectra of a 0D/0M/100T gel as a function of delay time

page 102), and in the 0D/0M/100T gel. Notice that in the 23D/21M/56T gel at approximately 7 milliseconds contact time all of the observed resonances are at or near their maximum polarization; for this sample, a CP spectrum run using a 7 msec contact time could be quantitative provided the competition between T_{Si-H} and $T_{1\rho}$ processes is taken into account. However, for the 0D/0M/100T gel the resonance at -107 ppm, though close to being level, does not reach a maximum at any contact time up to the longest contact time of 20ms. Quantitation of a 0D/0M/100T gel based on a ^{29}Si CP/MAS NMR spectrum obtained using a 7 msec contact time would be (and is) inaccurate. Therefore, contact time studies were carried out on several materials to establish parameters for which cross polarization spectra would provide quantitative information.

Table 6 on page 98 gives the ^{29}Si resonance, δ (ppm), and the relative percentage of the various Si structures in the gelled materials as determined from both the FT/MAS and CP/MAS ^{29}Si NMR spectra. Calculations were made using line intensities, I^{FT} & I^{CP}, as well as peak areas, A^{FT} & A^{CP} from deconvoluted spectra. Figure 19 on page 104 gives an example of the deconvolution method employed in analyzing the ^{29}Si NMR spectra. This figure shows the FT/MAS NMR spectrum of a 0D/0M/100T gel: a) after Fourier transformation, b) after smoothing (simulated spectrum) and c) after deconvolution using a routine that adds generated Gaussian curves to fit the simulated spectrum.

The compiled NMR data in Table 6 on page 98 allow calculation of the composition as well as the functionality and degree of reaction of the various components in the final gelled materials. For a given gel mixture, one can use the relative percentages of the different silicate structures observed (from one of the four NMR techniques used for quantitation) to calculate the mole percent of a particular component contained in the final gel. This is simply the sum of the relative percentages (areas/intensities) of the ^{29}Si NMR resonances that arise from a given component; for the TEOS component the calculation would involve summing the percentages of the various "Q" structures observed, for the MTEOS the "T" structures and for the DMDEOS the "D" structures. Table 7 on page 106 gives the results of such calculations and was generated using the NMR data tabulated in Table 6 on page 98.

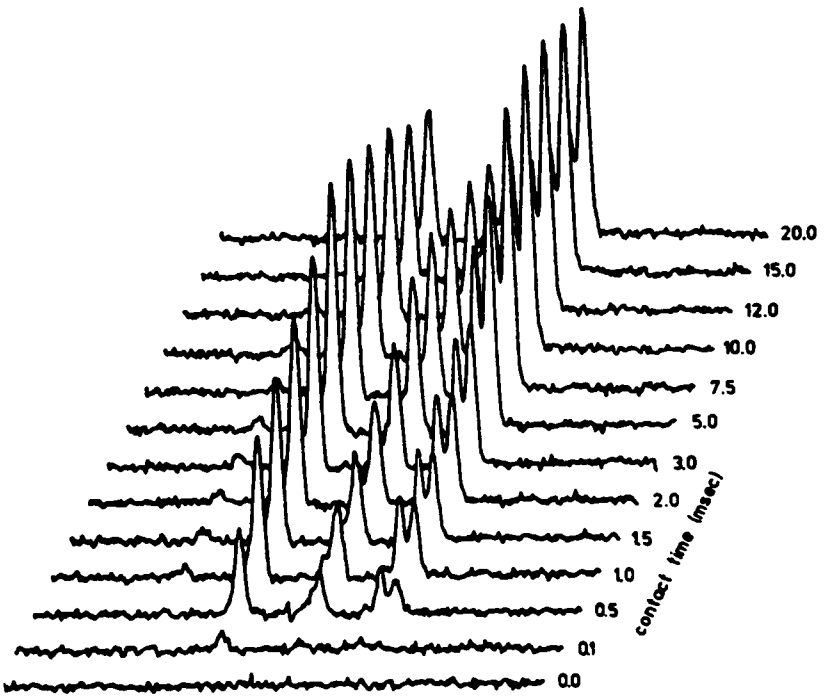

Figure 17. CP/MAS NMR spectra of a 23D/21M/56T gel as a function of contact time

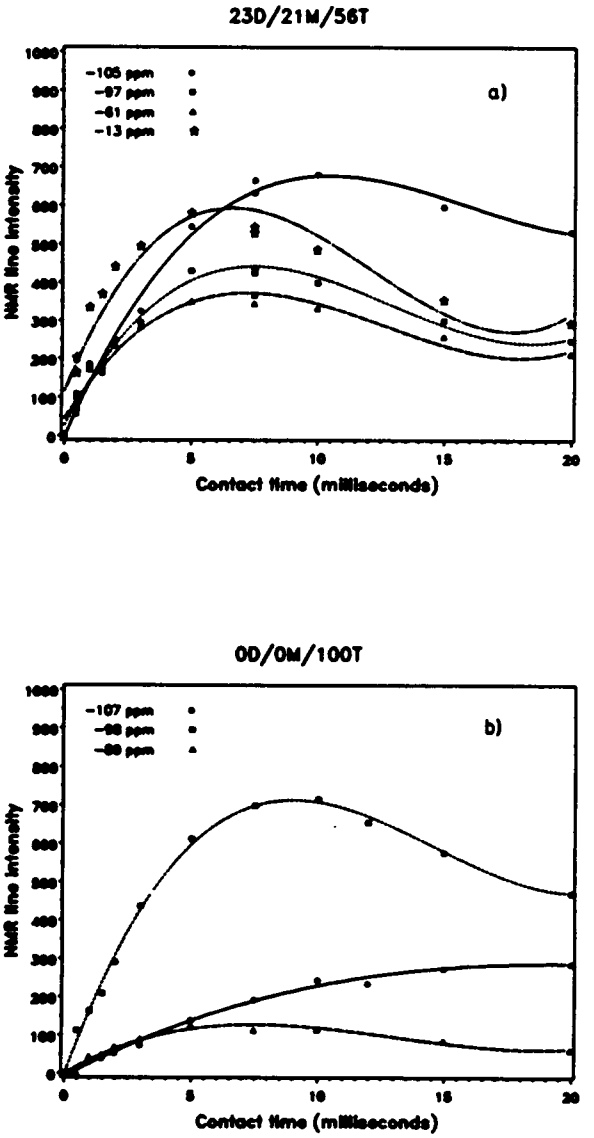

Figure 18. NMR peak intensity as a function of contact time: a) 23D/21M/56T gel, b) 0D/0M/100T gel

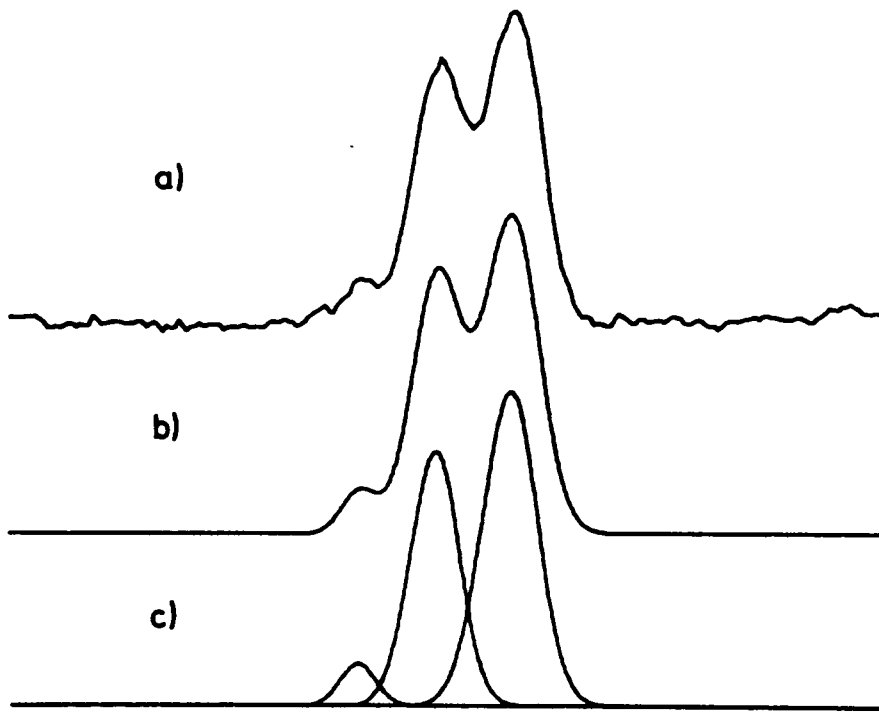

Figure 19. Sample deconvolution of an NMR spectrum: FT/MAS spectrum of a 0D/0M/100T gel: a) after Fourier transformation, b) aftcr smoothing (simulated spectrum), c) after deconvolution of the simulated spectrum

Table 7. Measured mole percent of the various silicate components in gels

Sample	Species	%Mix*	$\%I^{FT}$	$\%A^{FT}$	$\%I^{CP}$	$\%A^{CP}$
0D/0M/100T	D	0	0	0	0	0
	M	0	0	0	0	0
	T	100	100	100	100	100
23D/21M/56T	D	25	24	26	21	25
	M	18	19	17	19	20
	T	57	57	57	60	55
56D/0M/44T	D	56	55	61	58	59
	M	0	0	0	0	0
	T	44	45	39	42	41
37D/33M/30T	D	40	39	41	40	42
	M	29	32	29	29	30
	T	31	29	30	31	28
22D/60M/18T	D	27	24	26	27	29
	M	53	57	54	55	53
	T	20	19	19	18	18
0D/100M/0T	D	8	8	8	4	4
	M	88	86	88	92	92
	T	4	6	4	4	4

*corrected mole percent component in reaction mixture (correction based on MTEOS component containing 8% DMDEOS and 4% TEOS as impurities)

Table 7 on page 106 lists the relative percentages of the component species in the gelled mixtures, measured by the various NMR methods (%I^{FT},%A^{FT}, %I^{CP} & %A^{CP}), as well as the relative percentages of those component species in the original reaction mixture (%Mix). This facilitates direct comparison of the four quantitation methods used in this study. A comparison of the mole percent of D, M and T species in the original reaction mixtures to the percentages measured by NMR in the gelled materials demonstrates that all four NMR techniques are quantitative. The compositional data extracted from any of these techniques are quantitative to within, at least, ± 5%. The somewhat surprisingly good agreement between the "wet chemistry" and the solid state ^{29}Si NMR measurements (especially the CP/MAS) is virtually within the experimental error involved in pipeting the various components into the reaction mixtures (≃ ±2%). An important result from this close agreement is that all of the Q species in the mixtures can be accounted for in the NMR spectra - at least for gels other than 0D/0M/100T. This indicates that significant amounts of very long T_1 Q^4 species are not present in the gelled materials: further evidence of homogeneous mixing.

Also using the relative percentages of the different silicate structures (Table 6 on page 98) the degree of reaction, $DR_{comp/gel}$, for a given component and/or the gelled system as a whole can be calculated. This is accomplished by calculating the actual functionality, $AF_{comp/gel}$, and comparing it to the potential functionality, $PF_{comp/gel}$, of the component and/or gel system:

$$DR_{comp/gel} = \left(\frac{AF_{comp/gel}}{PF_{comp/gel}}\right) \bullet 100 \qquad (4.1)$$

where:

$$PF_{gel} = \sum_{i=1}^{\infty} \chi_i \bullet PF_{comp\ i} \qquad (4.2)$$

here χ_i is the mole fraction of component "i". Also:

$$AF_{gel} = \sum_{j=1}^{\infty} \chi_j \bullet RS_j \qquad (4.3)$$

here χ_j is the mole fraction of silicate structure "j" and RS_j is the number of fully reacted sites in silicate structure "j".

Table 8 on page 108 lists the potential and actual functionality calculated for the six gels studied by ^{29}Si NMR as well as the degree of reaction for the various individual silicate components. Using the calculated actual functionality (or potential functionality) as a measure, a comparison of the overall degree of reaction to the functionality of the gelled systems reveals a distinct trend. Materials with an actual functionality less than 3.00 exhibit a consistently high degree of reaction (≥96%) while those with an actual functionality greater than 3.00 show markedly lower degrees of reaction. This point is further evidenced when a comparison of the actual to the potential functionality is made. A plot of the actual functionality of the gelled materials as a function of the potential functionality of the systems given in Figure 20 on page 109 (see plot) clearly shows a deviation for the two gels of actual functionality greater than 3.00.

The lowering of the extent of reaction in the materials of functionality greater than 3.00 is undoubtedly related to their physical state. Recall that both the 23D/21M/56T and the 0D/0M/100T gels were observed to be brittle whereas the other gelled materials in Table 8 on page 108 were all observed to be flexible (see Figure 7 on page 81). Brittle materials are necessarily limited in the degree of reaction they can attain due to severe diffusional limitations brought on by vitrification; flexible materials, though gelled, retain a certain amount of mobility allowing the sol-gel reaction to reach a greater level of completion. This phenomenon can be explained in terms of the familiar time-temperature-transformation (TTT) effect observed for thermosetting resins [102]. Figure 21 on page 111 gives a typical time-temperature-transformation diagram for a thermosetting system (taken with permission from reference [102]). One also utilize this diagram to describe the features of a sol-gel reaction. The sol-gel system starts as a monomeric liquid mixture with a glass transition temperature,

Table 8. Degree of Reaction in Gelled Materials

Sample	Functionality		Degree of Reaction* (%)			
	Potential	Actual	DMDEOS	MTEOS	TEOS	Overall
56D/0M/44T	2.78	2.69	100.0	–	94.3	96.8
37D/33M/30T	2.89	2.79	100.0	95.0	95.7	96.6
22D/60M/18T	2.93	2.81	100.0	95.1	93.3	95.8
0D/100M/0T	2.95	2.88	–	97.8	–	97.8
23D/21M/56T	3.31	3.07	100.0	90.4	91.9	92.8
0D/0M/100T	4.00	3.50	–	–	87.4	87.4

*as determined by A^{FT} data

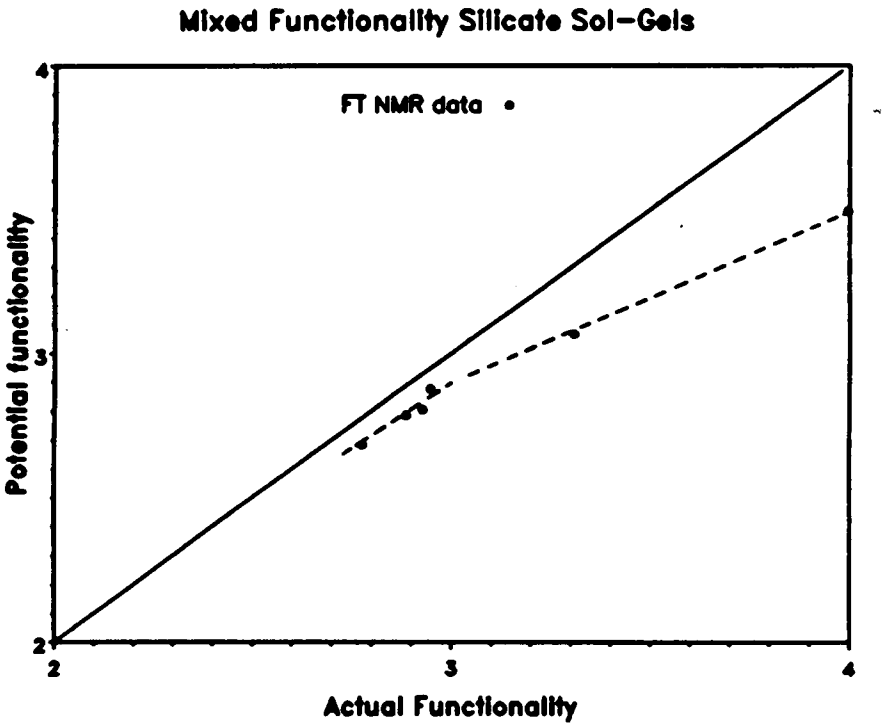

Figure 20. Plot of potential functionality vs actual functionality for silicate sol-gels

T_g, well below the temperature at which the cross-linking reaction takes place (in our case $\simeq$ 22°C). The T_g of the system steadily increases as the crosslinking reaction proceeds. In the case of the sol-gel materials presented here, the crosslinking reaction proceeds uninhibited until either the gel point is reached or the material vitrifies (in the later case the system is an ungelled glass - not relevant to our materials). At the gel point the crosslinking reaction is affected by diffusional restrictions in the transport of the reacting sites. However, the cross-linking reaction continues, albeit at a rate which is dependent on the sensitivity of the reaction to diffusional restrictions, until the T_g of the system rises past the temperature at which the gelation reaction takes place; the system then vitrifies. Once vitrified, the degree of reaction is essentially fixed since further reaction, without raising the temperature, is slow enough as to be practically nonexistent. Using this "TTT" reasoning, the data in Table 8 on page 108, Figure 7 on page 81 and Figure 20 on page 109 indicate that the multifunctional glass systems undergo the sol-gel reaction until they are either vitrified (which seems to occur as the actual functionality reaches 3.00) or until they have reached 96-99% completion.

Raman spectra to be presented indicate that, with the exception of the 0D/0M/100T gels, the unreacted sites are, within the limits of the Raman experiment, exclusively ethoxide rather than hydroxide functions. This is consistent with the concept of a severely diffusion limited reaction in the case of a vitrified gel. Hydroxyl or silanol functions formed in the nonvitrified (nonbrittle) gels have sufficient mobility to react; consequently, in time they all proceed to a very high level of completion ($\simeq$ 96-99%). In the two vitrified (brittle) gels studied, however, the diffusional restrictions on mobility essentially "freeze" unreacted hydroxyl (silanol) functions in the material matrix preventing them from reacting and thereby limiting the overall degree of reaction to $\lesssim$93%.

A by product of the ^{29}Si CP/MAS contact time studies is that the parameters governing the cross-polarization of the different silicate species can be determined. Table 9 on page 114 lists the Si-H polarization transfer relaxation time constant, T_{Si-H}, as well as the proton spin-lock relaxation (or decay) time constant, $T_{1\rho}^{H}$, and the contact time, t_{max}, at which the magnetization was observed to be maximized. These values were obtained from a double

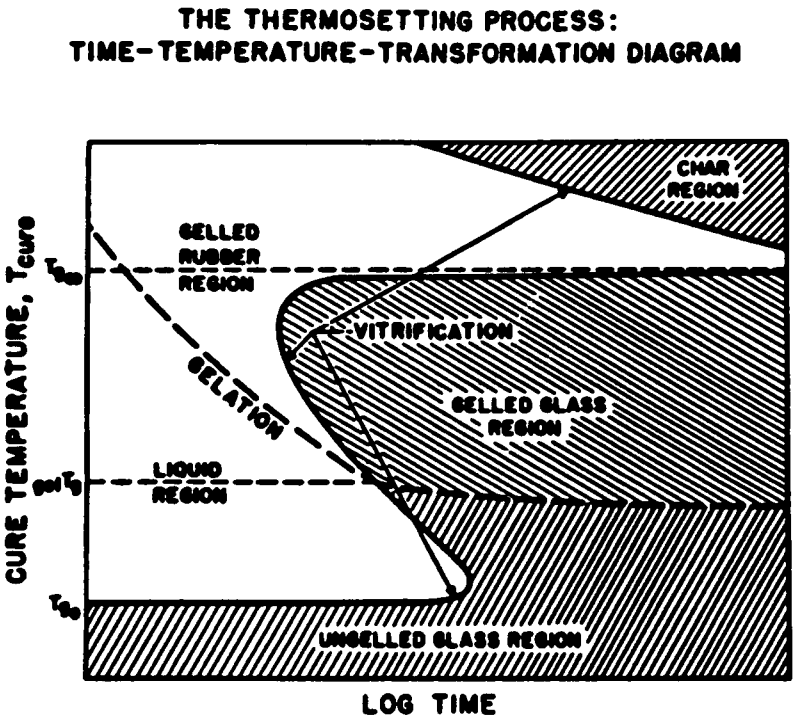

Figure 21. Time-Temperature-Transformation diagram (taken with permission from ref. 102)

exponential fit of the intensity as a function of contact time data for the curves in Figure 17 on page 102 [74]. The data in Table 9 on page 114 reflect the results of two different effects on the ability to cross-polarize a ^{29}Si nucleus. These effects, in an indirect way, are the result of local chemistry and system mobility - hence structure. It has already been mentioned that in order to cross-polarize efficiently, a silicon nucleus must have a proton within $\simeq$10Å [74]. The data shown in Table 9 on page 114 are consistent with this logic. Q^4 silicon centers should experience fewer and weaker Si-H dipolar interactions than their tri & difunctional counterparts (Q^3, T^3, Q^2 & D^2); their lack of directly bonded protons, should result in the Q^4 structures having the longest Si-H cross-polarization times (T_{Si-H}) and thus the longest proton spin-lock decay times when compared to the other structures ***in a given system***. The data bears this true. Conversely, the structures with the largest number of relatively close protons (Si-CH_3 vs Si-O-H or Si-O-CH_2CH_3) exhibit the shortest Si-H polarization transfer relaxations. In the 23D/21M/56T gel the D^2 structure with its two bonded methyl groups (six nearby protons) cross-polarizes quicker than the T^3 structure which contains only one bonded methyl group (three nearby protons). It should be noted, though, that the Q^3 structure, which has no directly bonded methyl groups, cross-polarizes almost as quickly as the T^3 structure. The implication is that the local chemical environment of the Q^3 centers contains protons which can provide the Si-H dipolar coupling not provided by directly bonded protons. In this fashion, data such as that in Table 9 on page 114 can be interpreted in terms of the local chemical composition. A consideration that has been tacitly ignored, however, is the effect of motional averaging on the Si-H dipolar vector, particularly on the average vector length $<r>$. Comparing the T_{Si-H} of two different silicon centers may reflect a difference in the motional averaging of the Si-H dipolar vector as well as differences in the local proton concentration. Greater motion could result in weaker Si-H dipolar coupling and longer T_{Si-H} relaxations. For example, internal rotation of CH_3 and/or overall motion of the network could increase the "residence" volume, $<r^3>$, and thereby decrease the average Si-H dipolar coupling. For this reason, caution must be exercised when cross-comparing different species and different gelled sys-

tems. Special regard must be given to compositional and structural differences to insure that any comparisons drawn are valid.

4.3.3 Raman Spectroscopy

In addition to NMR, Raman spectroscopy was investigated as a means to identify silicate structures and determine the extent of reaction attained in sol-gel materials. Previously, researchers have used Raman spectroscopy to follow changes in sol-gel derived materials as they are progressively heated from low temperatures (~25°C) to high temperatures (≥800°C) [80, 81, 82]. Other researchers have utilized Raman spectroscopy to identify silicate structures (or defects) present in sol-gel derived materials [78, 110-112]. The goals in this Raman work were to observe and attempt to quantitate changes in the spectra with respect to the extent of the overall reaction and to determine the type of chemical structures present in gelled materials. In this last regard, Raman spectroscopy was also employed to characterize the unreacted sites in silicate sol-gels. With these goals in mind, Raman spectra were obtained for a number of the same multifunctional sol-gel glasses used for NMR spectroscopy (section 4.3.2). Multifunctional gels made under different reaction conditions were also investigated using Raman spectroscopy. Specifically, gels made from MTMOS precursors were studied as a function of acid content and were compared to gels made from MTEOS (dynamic mechanical data presented in section 4.3.1).

The Raman spectra of a sol-gel material progresses through certain changes during the course of time as the crosslinking process proceeds. These changes are evidenced most clearly by spectra taken before and after gelation has occurred. The spectrum in Figure 22 on page 116 is for unreacted TEOS (tetraethoxysilane) glass precursor, for example, while the spectrum in Figure 23 on page 117 is for a 0D/0M/100T gel which had been vacuum dried. A comparison of these two spectra in the region from 0 cm^{-1} to 1600 cm^{-1} demonstrates the changes wrought by the gelation process. The majority of the unlabeled bands in Figure 22

Table 9. Si-H cross-polarization parameters

Sample	Peak	T_{Si-H} (msec)	$T_{1\rho}^{H}$(msec)	t_{max} (msec)	$I_{t_{max}}^{CP}$
0D/0M/100T	Q^4	9.8±0.2	103.0±6.0	25.7	298
	Q^3	5.8±0.1	15.4±0.4	9.1	688
	Q^2	3.4±0.0	16.2±0.6	6.9	118
23D/21M/56T	Q^4	5.1±0.1	30.0±0.0	11.0	651
	Q^3	3.6±0.0	17.0±0.3	7.1	421
	T^3	3.0±0.1	19.3±0.3	6.5	356
	D^2	2.0±0.0	18.2±0.2	4.9	569

on page 116 originate from the alkoxy function and disappear after hydrolysis and condensation have taken place (Figure 23 on page 117).

Fused quartz is an example of a "complete" glass network and was taken to represent the upper limit to the extent of reaction in the sol-gel process. Unreacted TEOS (Figure 22 on page 116), on the other hand, was taken to represent the lower limit to the extent of reaction in the sol-gel process. Given in Figure 24 on page 118 is the Raman spectrum for fused quartz (pure SiO_2). Comparison of the gelled TEOS spectrum (0D/0M/100T - Figure 23 on page 117) with that of fused quartz brings out many similarities but a few differences as well. The 0D/0M/100T gel displays four discernible peaks: a broad Si-O-Si bending peak at ~490 cm^{-1}, a weak Si-O-Si stretching peak at ~812 cm^{-1}, a broad Si-OH stretching peak at ~980 cm^{-1} and a weak C-H bending peak at ~1456 cm^{-1}. The fused quartz spectrum displays five "peaks": a broad Si-O-Si bending peak at ~429 cm^{-1} with a sharp shoulder at ~492 cm^{-1}, a relatively sharp Si-O-Si bending peak at ~603 cm^{-1}, a broad Si-O-Si stretching peak at ~800 cm^{-1} and two second order Si-O-Si bending peaks at ~1067 cm^{-1} and ~1200 cm^{-1}. The strong, broad Si-O-Si bending peak and relative lack of precursor peaks (see Figure 22 on page 116) suggests that the sol-gel process in the 0D/0M/100T gel has reached a high degree of completion. The presence of a Si-OH peak in the Raman spectrum also suggests that hydrolysis is not the limiting reaction in the sol-gel process, though the 0D/0M/100T gel is the exception rather than the rule.

It has been noted in the literature that TEOS based gels stored at room temperature develop a great deal of fluorescence with time due to a slow continuation of the sol-gel process [78, 80]. This was observed to be the case for 0D/0M/100T systems. These gels developed so much fluorescence over time that they had to be vacuum dried to remove some of the trapped reaction by-products (primarily ethanol) before any spectral features could be discerned. Even after drying, the spectra of the 0D/0M/100T gel given in Figure 23 on page 117 and Figure 26 on page 121 exhibit a strong fluorescent background (which explains the high level of noise observed). Figure 26 on page 121 shows the Raman spectrum of a vacuum dried 0D/0M/100T gel in the 2500-4000 cm^{-1} spectral region. In this spectrum, a broad band

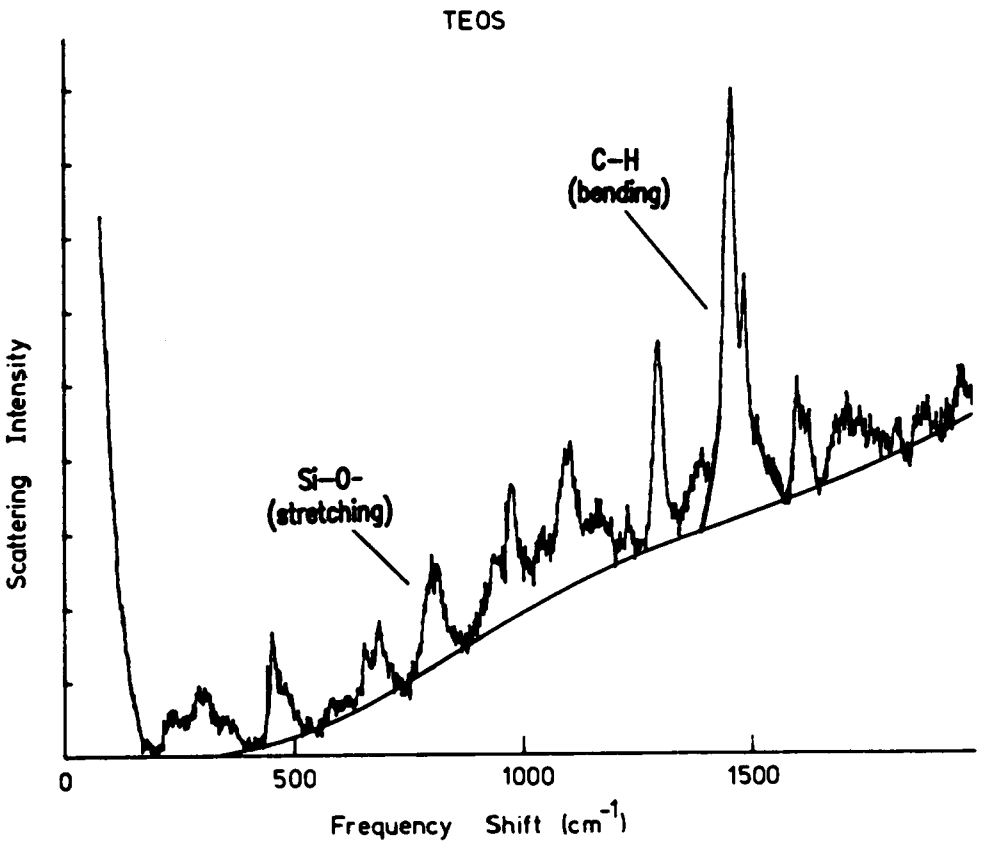

Figure 22. Raman spectrum of unreacted TEOS [92]

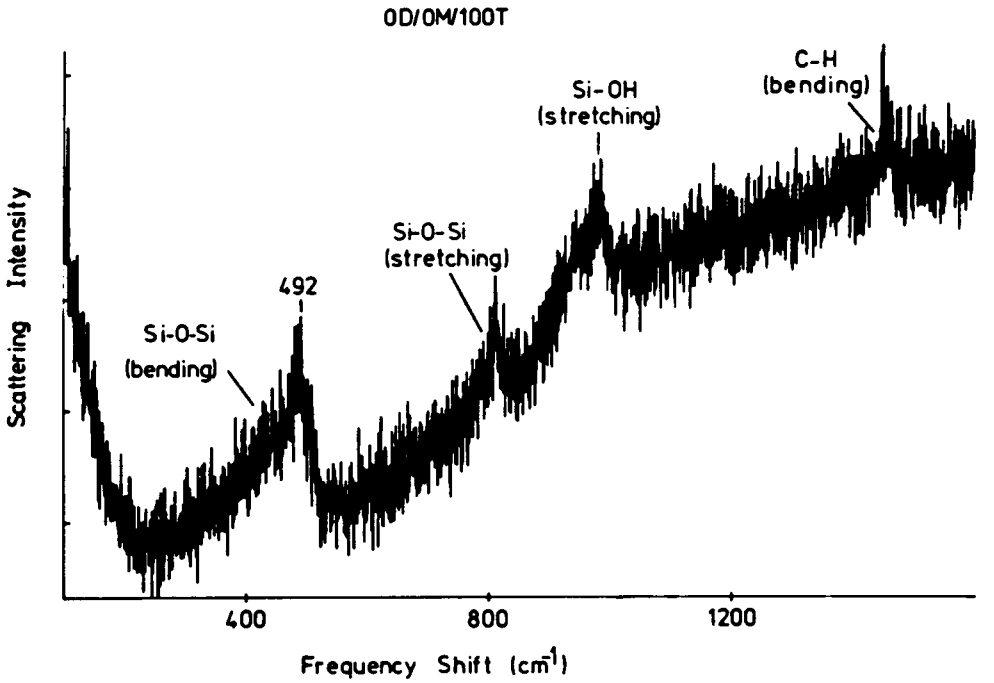

Figure 23. Raman spectrum of a 0D/0M/100T gel [93]

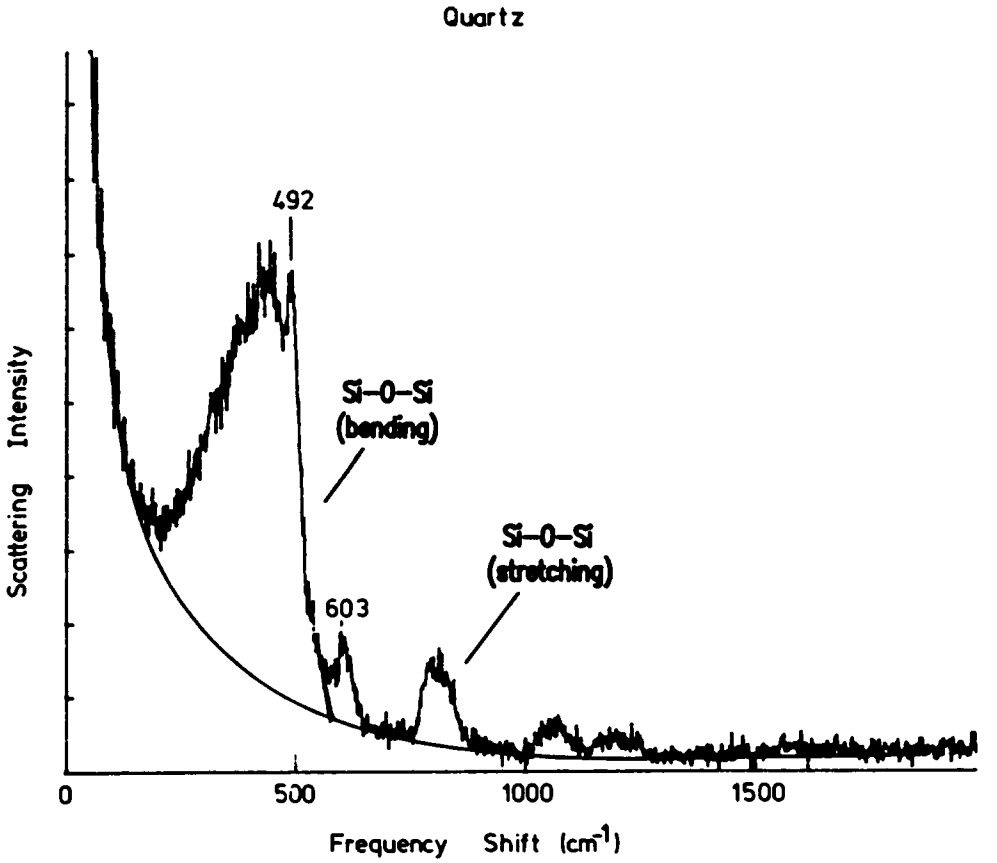

Figure 24. Raman spectrum of fused quartz [92]

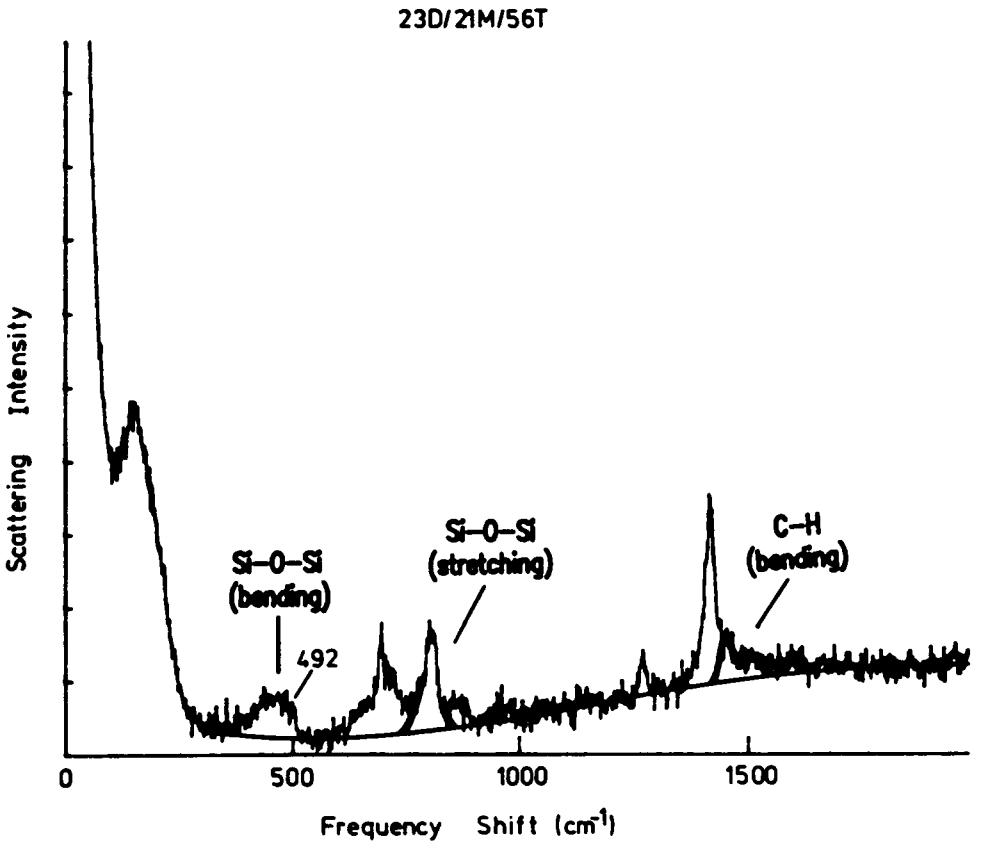

Figure 25. Raman spectrum of a 23D/21M/56T gel [92]

is observable in the 3200-3600 cm^{-1} region which is characteristic for the O-H stretching of a trapped alcohol. The Raman spectrum of a 23D/21M/56T gel contained in Figure 25 on page 119, however, is typical of those obtained for most of the multifunctional sol-gel compositions studied. These gels did not require vacuum drying prior to Raman analysis and generally exhibited very low background fluorescence. Also, compositions other than 0D/0M/100T did not exhibit Si-OH stretching bands in their Raman spectra; for these materials hydrolysis was the limiting reaction in the sol-gel process.

The key vibrational bands used in the quantitative analysis of the Raman spectra are listed in Table 10 on page 122 and are labelled in the figures. The Si-O stretching band at 800 cm^{-1} is observed in all spectra as would be expected; at various stages of the sol-gel process each silicon remains bound to four oxygen atoms though the chemical nature of the oxygens changes (ethoxy to hydroxy to silicate as the reaction proceeds). This vibrational band was, therefore, chosen as an internal standard to be used in quantifying the extent of reaction by Raman spectroscopy. Somewhat surprisingly, considering the change in the nature of the oxygen environment, the position of the Si-O stretching band does not shift during the reaction though it does broaden symmetrically as the material forms a three dimensional network.

Present in the TEOS precursor spectrum (Figure 22 on page 116) is a large C-H bending band occurring between 1460-1480 cm^{-1} which arises from the ethoxy groups bound to the silicon atoms. As the hydrolysis reaction progresses, these ethoxy groups disappear and are lost from the system as ethanol. A system in which complete hydrolysis has taken place would contain no ethoxy groups bound to silicon atoms and, therefore, would not exhibit a C-H bending band. Indeed, an ethoxy C-H bending vibration is not observed in the fused quartz spectrum (Figure 24 on page 118) however, a weak ethoxy C-H vibration is observed in the spectra of the 23D/21M/100T (Figure 25 on page 119) and the 0D/0M/100T (Figure 23 on page 117) gels. The presence of an ethoxy C-H vibration in the spectrum of a gelled material indicates that the hydrolysis did not go to completion; this means, in turn, that the polycondensation could not go to its theoretical completion. Note: ethoxy C-H vibrations should not be confused with C-H vibrations arising from methyl groups bound directly to

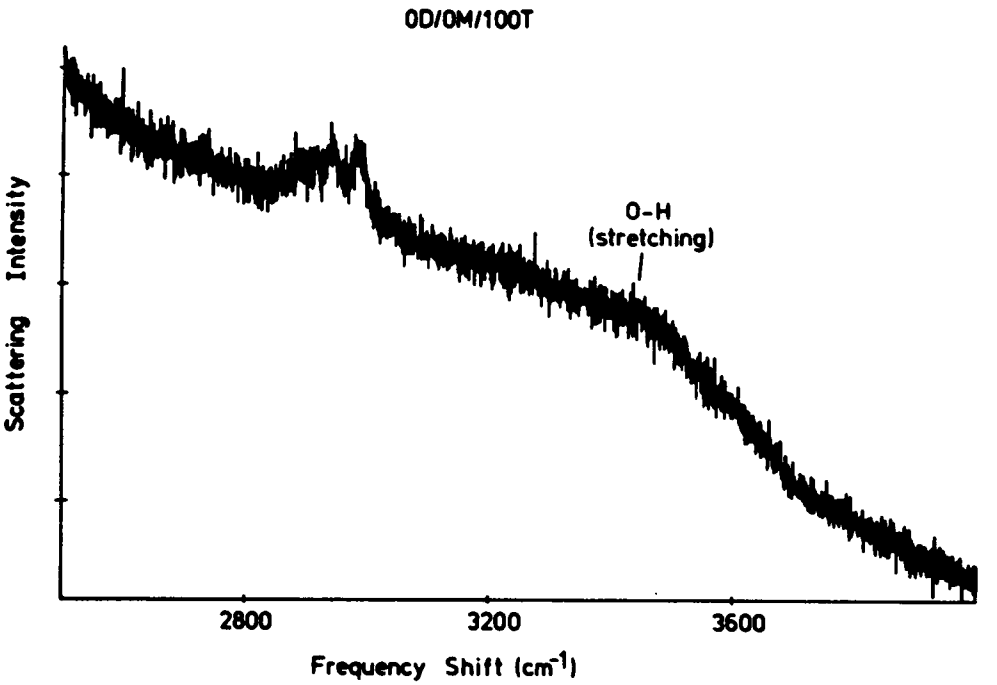

Figure 26. Raman spectrum of a 0D/0M/100T gel [93]

Table 10. Raman bands used for analysis

frequency $-\Delta\nu$ (cm^{-1})	structural group	type of vibration
460-492	Si-O-Si	network bending
800	Si-O-Si	symmetric stretching
980	Si-OH	stretching
1460-1485	C-H	bending
3220-3650	O-H	stretching

silicon atoms. The latter bands occur at 1420 cm^{-1} and are seen in materials containing $\equiv Si\text{-}CH_3$ functions such as MTEOS and DMDEOS. Furthermore, since Si-OH vibrations (~980 cm^{-1}) were not detected in the Raman spectra of gels other than 0D/0M/100T (for example see Figure 23 on page 117), the extent of the hydrolysis represents the extent of completion of the overall sol-gel process.

In order to quantify the extent of hydrolysis using Raman spectra an internal standard needed to be found that would be common to all of the spectra. To meet this requirement, a ratio of spectral bands was employed. This band ratio, R_1, was defined as the area of the C-H bending band arising from the alkoxide methyl functions (1460-1485 cm^{-1}) divided by the area of the Si-O stretching band arising from the silicate centers (800 cm^{-1}) or:

$$R_1 = \frac{\text{area of } (1460 - 1485\ cm^{-1})}{\text{area of } (800\ cm^{-1})} \tag{4.4}$$

For reference, the C-H bending bands and the Si-O-Si stretching bands in Figure 22 on page 116, Figure 25 on page 119 and Figure 24 on page 118 are labelled; the baselines and deconvolutions used to obtain the peak areas, by which these spectra were quantitated, are also shown. Fused quartz, pure SiO_2, was used as the 100% hydrolyzed reference while the unreacted TEOS precursor was used as a 0% hydrolyzed reference. Gels for which the degree of conversion is known from the ^{29}Si NMR could also be used as calibration points provided their degree of conversion is also equal to the degree of hydrolysis (i. e. no SiOH functions present). The 23D/21M/56T gel meets these conditions; the degree of conversion determined by ^{29}Si FT/MAS NMR is 92.8% (Table 8 on page 108).

The R_1 values obtained for SiO_2 (fused quartz), unreacted TEOS and the 23D/21M/100T gel are given in Table 11 on page 125; these values are also plotted in Figure 27 on page 126 as a function of percent hydrolysis. The relationship between R_1 and the percent hydrolysis demonstrated in Figure 27 on page 126 is, surprisingly, linear ($r = -0.9994$) albeit based on only 3 points (obtaining data points for low degrees of hydrolysis is extremely difficult, however, a "pseudo R_1" of 1.95 obtained for PDMS - $\simeq$ 50% hydrolyzed TEOS - ***qualitatively*** con-

firms the linear relationship between R_1 and percent hydrolysis). In principle, this "calibration curve" could be used to determine the degree of hydrolysis attained in silicon ethoxide sol-gel materials. Such was done for the 0D/0M/100T gel using the Raman spectra shown in Figure 23 on page 117 The R_1 measured for this gel (0.27) correlated to 95% hydrolysis according to the calibration curve in Figure 27 on page 126 The percent hydrolysis "determined" by Raman spectroscopy was higher for this gel than the degree of conversion determined from the NMR spectra (95% hydrolysis vs 87.4% conversion see Table 11 on page 125). This result indicates that for the 0D/0M/100T composition, condensation, not hydrolysis, is the limiting reaction in the sol-gel process. Recall that the Raman spectrum for the 0D/0M/100T gel exhibited a Si-OH band at ~980 cm^{-1}(Figure 23 on page 117) which supports the conclusion that the condensation of hydroxyl functions does not go to completion.

Raman spectra, in addition to degree of reaction, also provide information on the type of structure observed in sol-gel materials. As mentioned earlier, the nature of the Si-O stretching band (800 cm^{-1}) changes - broadens - as the network matures. Broadening also occurs, and is even more dramatic, in the Si-O-Si bending region of the Raman spectra as evidenced by the large broad peak observed for fused quartz ~250-500 cm^{-1} (Figure 24 on page 118). The 23D/21M/56T and 0D/0M/100T gels also display a broadened band at ~350-500 cm^{-1} (Figure 25 on page 119 and Figure 23 on page 117). The broadened Si-O-Si bending and stretching bands observed in these spectra gels are indicative of a three-dimensional silicate network, though one not as well formed as that in fused quartz (Figure 24 on page 118). Sharp bands at 492 cm^{-1} and 607 cm^{-1} were originally seen in quartz (fused silica) and were proposed to be the result of four-membered and three-membered siloxane ring "defect" structures by Galeener et al. [77]. Tallant et al. [78] using sol-gel derived materials confirmed Galeener's hypothesis of the origin of the 492 cm^{-1} and 607 cm^{-1} "defect" bands in quartz. Careful observation reveals that a sharp peak at 492 cm^{-1} can be resolved in the midst of the broad Si-O-Si bending region in the Raman spectra of fused quartz (Figure 24 on page 118), the 0D/0M/100T gel (Figure 23 on page 117). and even - with some imagination - in the 23D/21M/56T gel (Figure 25 on page 119).

Table 11. Measured R_1 and degree of hydrolysis for silicate sol-gels

sample	R_1	% hydr.	% conv.*
SiO_2†	0.0	100	–
23D/21M/56T†	0.44	92.8	92.8
PDMS†	1.94	50.0‡	–
TEOS†	3.98	0.00	–
0D/0M/100T	0.27	95	87.4

* determined by ^{29}Si FT/MAS NMR
† calibration standard
‡ equivalent to 50% hydrolyzed alkoxide

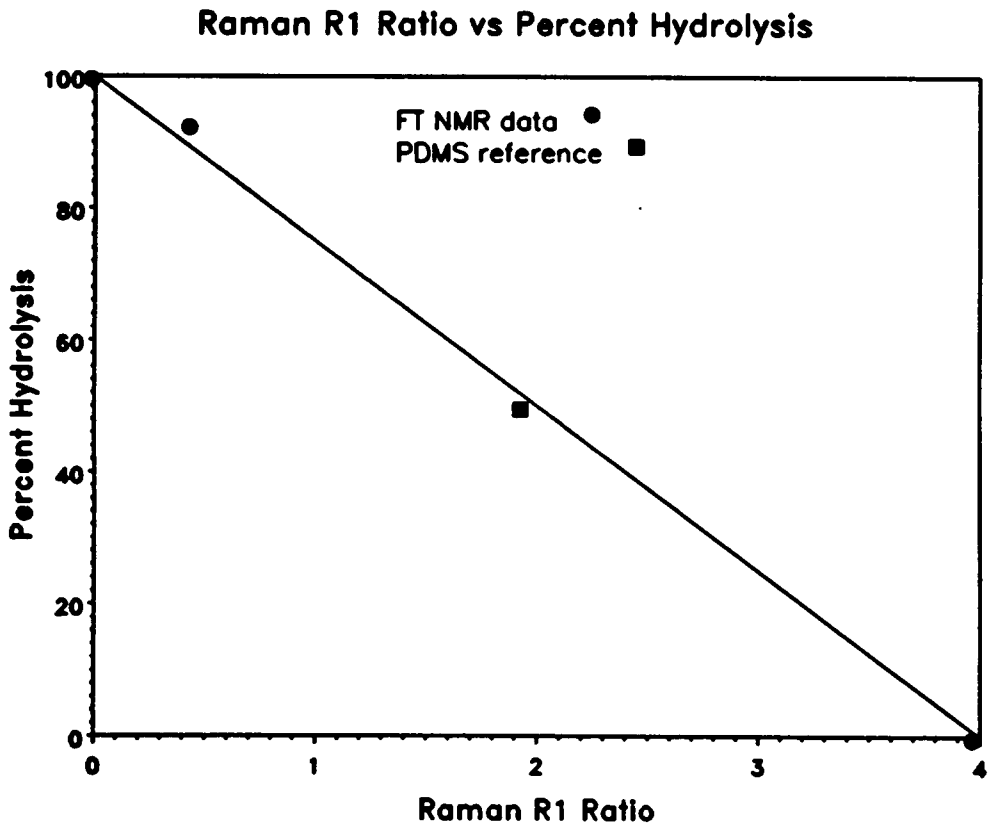

Figure 27. Raman R_1 vs Percent Hydrolysis

Figure 28 on page 128, Figure 29 on page 129 and Figure 30 on page 130 contain the Raman spectra of three different MTMOS gels made using different levels of HCl catalyst. These gels were made according to the procedure outlined in section 3.3.1 using 0.007, 0.014 and 0.037 moles of HCl per mole of alkoxide functional group. The same analytical method developed to quantitate the silicon ***ethoxide*** gels can be applied to the Raman spectra of these silicon ***methoxide*** gels. However, since a calibration curve such as that given in Figure 27 on page 126 was not developed for the methoxide system, only relative changes in the degree of hydrolysis can be obtained from the Raman spectra. Nonetheless, R_1' values (the prime here denoting a methoxy system) obtained from the spectra given decrease with increasing acid concentration: $R_1' = 0.29$, 0.19 and 0.15 for the 0.007, 0.014 and 0.037 mole HCl gels respectively. The decreasing value of R_1' indicates that the degree of hydrolysis increases with increasing acid content. The differences in R_1', though, are not great, the largest is that between the 0.007 mole HCl gel and the 0.014 mole HCl gel. This result is not a great surprise. Since HCl is postulated to act as a catalyst during the sol-gel process, a large change in the degree of hydrolysis would not be expected for these gels; catalysts are supposed to effect the kinetics but not the equilibrium of the reactions in which they are used. Differences in the solution pH, however, can effect the equilibria which could be the reason a small difference in degree of hydrolysis is observed.

Though the degree of hydrolysis does not change drastically, there are unique spectral changes observed as a function of acid in the MTMOS gels. In particular, there is a sharp peak at $\simeq$ 396 cm^{-1} that increases in intensity relative to the broader Si-O-Si bending band at $\simeq$ 460 cm^{-1}. The 396 cm^{-1} peak is barely discernible in the spectrum of the 0.007 mole HCl gel (Figure 28 on page 128), but becomes stronger in the 0.014 mole HCl gel (Figure 29 on page 129) and towers over the 496 cm^{-1} peak in the 0.037 mole HCl gel (Figure 30 on page 130). At the same time the 395 cm^{-1} peak is growing, the 742 cm^{-1} Si-CH_3 stretching peak changes from a broad band to a well defined doublet while the Si-CH_3 bending band in the 154-196 cm^{-1} region also becomes a well defined doublet. No correlation is observed, however, between the relative size of the Si-CH_3 bands and the HCl concentration.

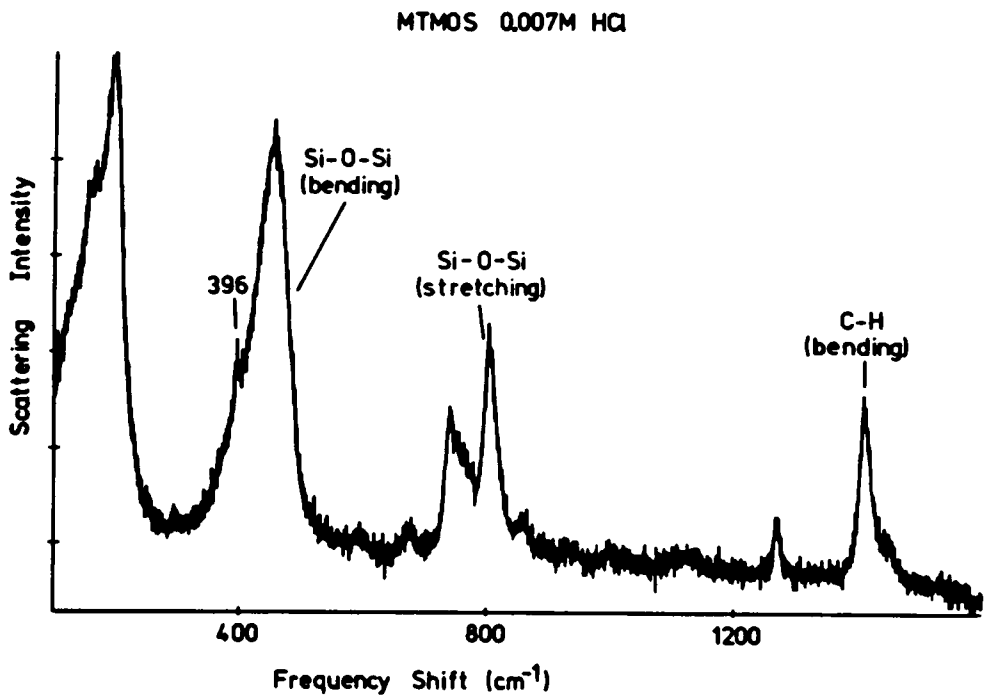

Figure 28. Raman spectrum of MTMOS gel (0.007 moles HCl)

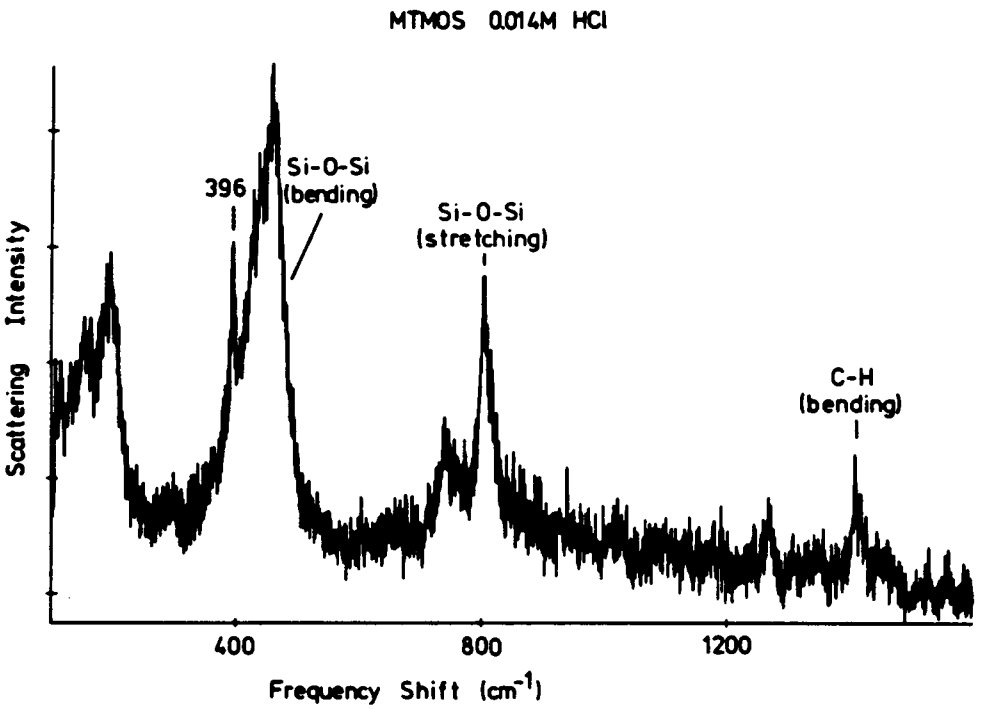

Figure 29. Raman spectrum of MTMOS gel (0.014 moles HCl)

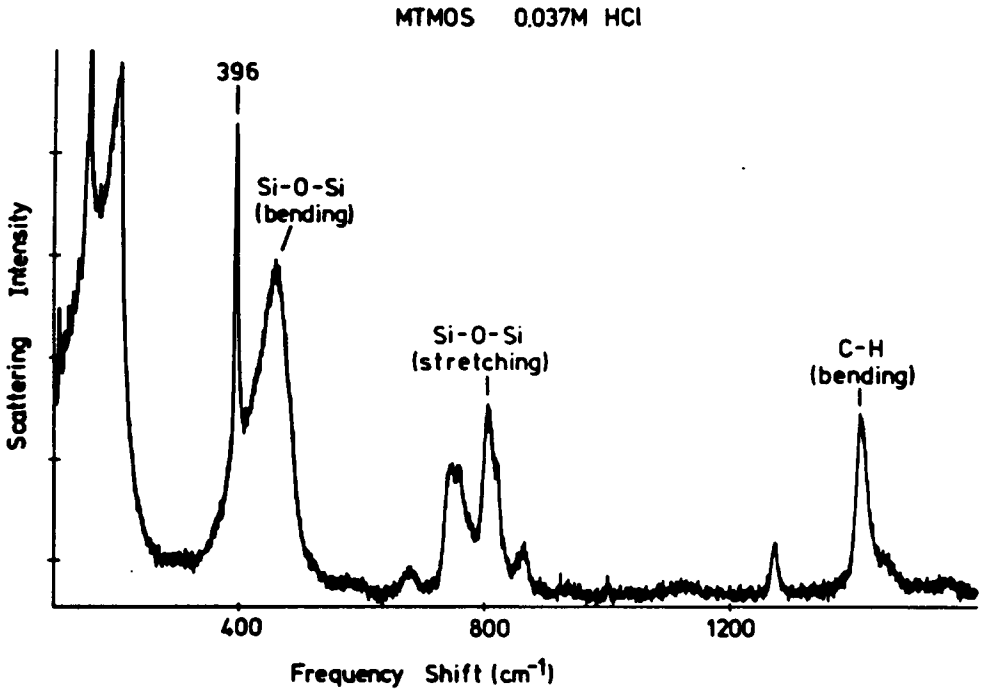

Figure 30. Raman spectrum of MTMOS gel (0.037 moles HCl)

The change in the sharp peak at 396 cm^{-1} can be correlated directly to the acid concentration which, in turn, coincides with changes observed in the dynamic mechanical spectra of MTMOS sol-gels. Figure 11 on page 88 contains the dynamic mechanical spectra of these same MTMOS gels for which Raman spectra have been given. Both the storage modulus and the tanδ curves display a dramatic difference between the 0.007 moles HCl gel and the 0.014 and 0.037 moles HCl gels as was pointed out earlier in this chapter (discussed in detail in section 4.3.1). The later two gels are very similar on the other hand, their storage modulus curves being virtually superimposable on one another. The spectral feature that distinguishes the 0.007 moles HCl gel from the other two is the absence of a strong distinct peak at 396 cm^{-1}. The nature of this Raman band and the structural feature that gives rise to it appears to have a great bearing on the dynamic mechanical behavior of the final gelled material. Both of the higher acid content gels (0.014 & 0.037 moles HCl) display very distinct peaks at 396 cm^{-1} in their Raman spectra. At least in a qualitative sense, changes observed in the Raman spectra of gels made under different conditions can be related to changes in the mechanical properties.

The exact nature of the structure giving rise to the 396 cm^{-1} peaks is not known though it could be due to five membered (or larger) silicate rings. While it is generally held that the weak depolarized bands in the Si-O-Si bending region of the Raman spectra of silica are due to network structure [76-82, 110-112], some specific spectral assignments have been made. In addition to the 492 & 602 cm^{-1} "defect" bands discussed earlier, other Raman bending bands have been attributed to ringlike silicate structures. The 430 cm^{-1} peak, for example, has been attributed to five membered silicate rings [78]. Five membered (and larger) ring structure would develop as part of the network forming process and could, reasonably, be involked to explain the 396 cm^{-1} peaks observed in the Raman spectra of the high acid MTMOS gels.

4.3.4 Gelation Threshold

In light of the high overall degree of reaction observed for the flexible gels, the gelation borderline observed in Figure 7 on page 81 can not be explained by "standard" gelation theories. Simple percolation theory, a stochastic approach which has been successfully applied to explain gelation and the changes in properties accompanying gelation [103, 104, 105], does not predict (ignoring site-bond percolation) the observed gelation borderline in Figure 7 on page 81; the "classical" Flory-Stockmayer theory of gelation [26, 107, 108] fails in this respect also. For a pure TEOS system, which has a potential functionality (PF) of four, bond percolation on a three dimensional diamond lattice predicts a critical degree of reaction for gelation to be 39% [103]. Flory-Stockmayer (FS) gelation theory (unmodified) predicts the critical degree of reaction to be [26, 107, 108]:

$$P_c = \frac{1}{(f-1)} \tag{4.5}$$

where "f" is the average functionality of the reacting system (potential functionality); for a four functional system such as TEOS this predicts the critical degree of reaction to be 33%. The final extent of reaction in the pure TEOS system is considerably higher than either predicted critical extent of reaction for gelation, P_c , and the system is observed to gel. However, whether gelation occurs at P_c = 33% or 39% or at some other value remains uncertain. It is observed, though, that a 53D/47M/0T composition does not gel. The potential functionality (PF) for this ungelled composition is calculated, according to eq. 4.2, to be 2.47. Substituting this value for "f" in eq. 4.5 gives a predicted critical degree of reaction P_c = 68%. Using an empirical relation to obtain the approximate value predicted by bond percolation [103]:

$$P_c = \frac{1.45}{z} \tag{4.6}$$

where "z" is the coordination number which is equal to "PF", the predicted bond percolation threshold is even lower than that predicted by FS theory being: P_c = 59%. Considering the consistently high degrees of reaction observed for compositions in the flexible region of Figure 7 on page 81(~96-98% - see Table 7 on page 106), it is reasonable to assume that the two ungelled compositions reacted to a similar degree of completion. Clearly, then, neither bond percolation or the Flory-Stockmayer theory of gelation predict that the 53D/47M/0T mixture would remain ungelled.

A strong possible explanation of this "non-gelling behavior" is the formation of cyclic silicates during the sol-gel process. Such cyclics could conceivably reach a high degree of reaction prior to gelling (provided the cyclics remained separate i. e. unconnected). The Flory-Stockmayer gelation theory being based on a Bethe lattice does not account for the formation of cyclic structures, a recognized limitation [107], and would in such a case predict critical degrees of reaction lower than those observed. Later work by Stockmayer and others accounted for the formation of cyclic structures [108, 109]. Although the evidence for cyclic silicate structures in the gelled compositions is not definitive (based on a rough correlation of chemical shifts with those observed and assigned by Lippmaa et al. for cyclic silicates observed in mineralogical samples [95] and Raman spectra presented), the presence of non-connected silicate "macro-cycles" or "gelled particles" would explain how a system such as the 53D/47M/0T composition does not gel yet could have a high degree of reaction.

4.4 Conclusions

In the systems studied, using conditions established for synthesising PDMS containing hybrid sol-gel materials [14, 15, 17], HCl appears to act as a catalyst for hydrolysis. The amount of acid added beyond a minimum level did not effect the degree of reaction to a sig-

nificant degree but did effect the type of silicate structure formed as evidenced by the dynamic mechanical behavior and Raman spectroscopy.

The different silicate structures formed during a sol-gel reaction can be distinctly observed using solid state ^{29}Si NMR. Furthermore, both the FT/MAS and the CP/MAS techniques can be quantitated meaningfully provided they are conducted under the appropriate experimental conditions. Such experiments demonstrated that, within the limits of the techniques, unreacted precursors and dangling ends are not present in the gelled materials; few linear segments are present in these materials. Raman spectroscopy provides a means for determining the degree of hydrolysis and for characterizing the unreacted sites and silicate structures formed.

Silicon alkoxide components in nonvitrified (flexible) gels were found to react to $\simeq$ 96-98 % completion, with hydrolysis being the limiting reaction, regardless of the individual component and despite differences in reactivities. Also, the overall degree of reaction in the nonvitrified gels is very high ($\simeq$ 96-98%) and approximately constant regardless of mixture composition or functionality. The overall degree of reaction in the vitrified (brittle) gels, on the other hand, falls from $\simeq$ 93 % at the brittle/flexible border to 87 % for pure TEOS. Pure TEOS gels are not hydrolysis limited; unreacted silanol groups are present in the gels. This can be attributed to a time-temperature-transformation (TTT) behavior where diffusion limitations brought on by vitrification prevent even the highly reactive Si-OH groups from condensing fully.

CHAPTER V

PDMS MODIFIED SILICATE SOL-GEL COMPOUNDS CONTAINING TITANIA

5.1 Introduction

Within the last two years it has been demonstrated that PDMS oligomers can be successfully incorporated into a TEOS based network via the sol-gel process [14, 15]. Since that time, hybrid materials of this sort have been studied extensively to determine their structure-property behavior [17, 20]. Several experimental parameters have been reviewed during the course of these structure-property studies including: the amount of acid (HCl) used to catalyze the sol-gel process, the amount of water added and the loading of TEOS relative to the modifying component [14, 15, 17, 20]. In light of this work, the incorporation of a metal oxide other than silica appeared to be a new and fundamentally different method through which to impart unique properties to the modified sol-gel materials. In particular, based on previously published literature results [3, 4], the incorporation of titania (TiO_2) into PDMS/TEOS systems promised a material with higher refractive index and greater mechanical strength than previ-

ously achieved. Primarily for these reasons, studies of the structure-property effects of titanium incorporation on modified silicate sol-gel materials were undertaken.

While incorporation of metal atoms into silicate networks via the sol-gel process is not new [22, 24, 31, 32], incorporation of metal atoms into organically modified TEOS based glasses is [3, 4, 16]. Only recently, Parkhurst et al. reported the thermal properties (DSC) of PDMS/TEOS based materials incorporating titaniumethoxide and titaniumbutoxide [16]. Schmidt and co-workers also incorporated titania into their ORMOSIL systems but did not report any detailed structure-property behavior other than scratch resistance and/or refractive index [3, 4]. Both of these groups developed techniques whereby they were able to incorporate titania and still produce monolithic materials (see Chapter II section 2.5 for review of these techniques); this is not a trivial accomplishment. After careful deliberation and a certain amount of trial and error, a Chemically Controlled Condensation (CCC) method distinct from that proposed by Schmidt [5] was developed to incorporate titaniumisopropoxide into PDMS/TEOS sol-gel systems. The exact procedure developed to make the hybrid titania-silica-PDMS materials studied in this chapter is detailed in Chapter III section 3.3.2.

5.2 Nomenclature

Primarily three compositions of titania-silica-PDMS were prepared to study the effects of titanium incorporation on modified sol-gel materials. By convention [14, 15], the different gel compositions have been identified by the initial weight percent of each reactant used to make the gels. In terms of the starting weight percentages, the three compositions of interest are : 6 wt% $Ti(i\text{-}pr)_4$: 44 wt% TEOS : 50 wt% PDMS(1700), 15 wt% $Ti(i\text{-}pr)_4$: 35 wt% TEOS : 50 wt% PDMS(1700) and 30 wt% $Ti(i\text{-}pr)_4$: 20 wt% TEOS : 50 wt% PDMS(1700). Hereafter (including the chapters to follow), hybrid sol-gel compositions will be referred to in terms of the starting weight percentages of only the titaniumisopropoxide (or equivalent) and the specific oligomer

used to make the material. For example, 6Ti-50PDMS(1700) identifies a gel made starting with 6 wt% titaniumisopropoxide, 50 wt% 1700Mw PDMS and 44 wt% TEOS. The actual weight percentages of titaniumisopropoxide, TEOS and PDMS(1700) used to make the three different compositions discussed above as well as a 56Ti-39PDMS(1700) hybrid sol-gel material are tabulated in Table 12 on page 138. Also presented in Table 12 on page 138 are the final weight percentages of titania, silica and PDMS(1700) (calculated based on complete conversion) and the mole percent of each of these components contained in the hybrid gels prepared. Molar concentrations involving the silanol terminated PDMS modifying component have been calculated in terms of the repeat segment, $-(CH_3)_2Si-O-$, and ignore the effect of the hydroxy terminated chain ends on the molecular weight.

The reason for calculating the molar concentration of the PDMS(1700) component in terms of the repeat unit was to give an accurate appraisal of the molecular composition of the material matrix. Molar concentrations based on the molecular weight of the polymer would give the misleading impression that PDMS is a minor component in the final gel. For example, molar concentrations calculated in terms of the polymer molecular weight, 1700 amu, as opposed to the molecular weight of the repeat segment, 74.15 amu, show that the 6Ti-50PDMS(1700) gel contains 11.2 mole percent PDMS(1700), 80.4 mole percent TEOS and 8.4 mole percent titaniumisopropoxide. These mole percent values give the false impression that the inorganic oxide is the continuous phase of the material matrix and, further, that the titanium component is almost as prevalent as the PDMS(1700) component. In actuality, PDMS comprises 77.6 weight percent of the final material and titania only 2.7 weight percent (assuming 100% conversion). The mole percent calculations based on the PDMS repeat segment more accurately reflect the final weight percent of the components in a fully reacted gel. Again, using the 6Ti-50PDMS(1700) gel as an example, the mole percent reactants: 2.4% $Ti(l\text{-}pr)_4$, 23.2% TEOS, 74.4% $-(CH_3)_2Si-O-$, are quite close to the final weight percent oxides: 2.7% TiO_2, 19.7% SiO_2, 77.6% PDMS(1700). After a review of Table 12 on page 138 it is apparent that the mole percent concentration of the reactants for all of the compositions matches the theoretical weight percent relatively well. Another reason, albeit a minor one, for calcu-

Table 12. Starting composition and theoretical gel composition of hybrid sol-gels

sample	quantity	$Ti(i\text{-}pr)_4/TiO_2$	$TEOS/SiO_2$	$-(CH_3)_2Si\text{-}O-$*
6Ti-50PDMS(1700)	initial wt%	6.1	43.9	50.0
	final wt%†	2.7	19.7	77.6
	mole %	2.4	23.2	74.4
15Ti-50PDMS(1700)	initial wt%	14.6	35.4	50.0
	final wt%†	6.5	15.8	77.7
	mole %	5.7	19.0	75.3
30Ti-50PDMS(1700)	initial wt%	30.2	19.8	50.0
	final wt%†	12.7	11.8	75.5
	mole %	12.2	10.9	77.0
56Ti-39PDMS(1700)	initial wt%	55.5	5.7	38.9
	final wt%†	27.8	2.8	69.4
	mole %	26.1	3.6	70.3

*PDMS repeat segment, Mw = 74.15
†assuming 100% conversion

lating the molar concentration of PDMS(1700) in terms of the repeat unit relates to a problem common to macromolecules. The PDMS(1700) oligomer is polydisperse, the molecular weight expressed is an average value, whereas the repeat unit molecular weight can be precisely determined. Therefore, molar concentrations based on the molecular weight of the repeat unit are more accurate than those based on an average molecular weight (Mw) of the polymer since they are unaffected by the PDMS polydispersity. The fact that the molecular weight of a silanol chain end is only one atomic mass unit heavier than the repeat unit makes any errors incurred by ignoring chain ends in the molar calculations of the repeat unit concentration insignificantly small.

5.3 Results and Discussion

5.3.1 Observed Properties

All four of the titanium containing PDMS(1700) hybrid sol-gel compositions listed in Table 12 on page 138 were observed to produce single monoliths possessing limited flexibility. Generally, the deep yellow color of the reaction mixture caused by the addition of titaniumisopropoxide was observed to fade after approximately 1/2 hour of gentle refluxing. However, though the films obtained were all transparent, the addition of titanium did impart a yellowish-orange color to the samples. This yellow color, it has been speculated, is caused by the presence of octahedral titanium acetate complexes in the gels [86]. Titanium acetyl acetonates, for example, are octahedral complexes and are deep yellow in appearance [86]. As such, the yellow color should be (and is) observed to be a function of the titanium loading. The 6Ti-50PDMS(1700) material is only faintly yellow while the 56Ti-39PDMS(1700) material is unmistakably yellow in appearance, though still transparent.

The pure PDMS/TEOS materials reported earlier [14, 15] showed relatively poor physical-mechanical properties. For example, under ambient conditions using a draw rate of 2mm/min a 48% TEOS 52% 1700 Mw PDMS sample made using 0.045 moles of HCl catalyst (herafter referred to as 48TEOS-52PDMS(1700)0.045) had an initial modulus $\simeq$12 MPa, a stress at break app.1 MPa and a 9% elongation at break [17]. Incorporation of titanium, it was hoped, would increase the observed stress at break and initial modulus of the PDMS modified materials by strengthening the TEOS based network. The titaniumisopropoxide, it was thought, might drive the mixed alkoxide network to a higher degree of conversion than attainable for the pure silicon alkoxide sol-gels. Comparable PDMS(1700) modified sol-gel materials incorporating 6, 15 and 30 wt% $Ti(i\text{-}pr)_4$ proved to be stiffer in a qualitative sense than the 48TEOS-52PDMS(1700)0.045 material but very brittle; tensile test specimens were impossible to obtain from the titanium containing materials. However, the stiffness qualitatively observed on incorporation of titanium could be interpreted as an indication of an increased modulus.

5.3.2 Dynamic Mechanical Behavior

Though "dumbbell" tensile test specimens could not be easily obtained from the titanium containing PDMS modified TEOS materials, specimens for dynamic mechanical analysis were able to be prepared. The sample films had sufficient flexibility so that narrow strips could be cut (using a razor blade) and mounted in the dynamic mechanical tester. This flexibility, though limited, indicates that the titanium hybrid material may have some useful applications. Figure 31 on page 142 compares the storage modulus and Figure 32 on page 143 the tanδ curves of the 48TEOS-52PDMS(1700)0.045 material (triangles) mentioned previously [17] with those of 6Ti-50PDMS(1700) (diamonds) and 30Ti-50PDMS(1700) (squares). Comparing the storage modulus curves first (Figure 31 on page 142) one immediately notes that the 48TEOS-52PDMS(1700)0.045 material exhibits a decrease of 1.5 orders of magnitude in the storage modulus after a very broad glass transition ending at $\simeq$40°C. On the other hand, both

the 6Ti-50PDMS(1700) and the 30Ti-50PDMS(1700) materials exhibit a decrease in the storage modulus of only one order of magnitude. Furthermore, the magnitude of the storage modulus of the titanium containing materials is essentially the same for all three compositions: 6, 15 and 30 weight percent titaniumisopropoxide (for clarity only data for 6Ti-50PDMS(1700) and 30Ti-50PDMS(1700) are shown in Figure 31 on page 142). The storage modulus data lends credence to the hypothesis that the incorporation of titanium drives the TEOS based network to a higher degree of completion.

The corresponding tanδ curves, given in Figure 32 on page 143, also show differences between the 6Ti-50PDMS(1700), the 30Ti-50PDMS(1700) and the 48TEOS-52PDMS(1700)0.045 materials. The gel made with only PDMS(1700) and TEOS, X=0 wt%. titaniumisopropoxide (triangles in Figure 32 on page 143), displays a broad "bimodal" tanδ behavior with peaks at ~-100°C and ~-50°C. The tanδ transition for this material eventually decreases to near zero after ~70°C. The 6Ti-50PDMS(1700) material (diamonds in Figure 32 on page 143) is quite different in that it displays one sharp tanδ transition at -110°C which slowly decreases to zero at ~20°C. The 15Ti-50PDMS(1700) and 30Ti-50PDMS(1700) (squares Figure 32 on page 143) materials exhibit tanδ curves that are qualitatively the same though, in the interest of clarity, only the latter curve is shown. Both curves contain broad bimodal transitions with peaks at ~-100°C and ~-80°C. These "bimodal" tanδ transitions are similar to, though not as broad as, that observed for the 48TEOS-52PDMS(1700)0.045 material. However, unlike the 48TEOS-52PDMS(1700)0.045 material, the tanδ transition for samples containing 15 and 30 weight percent $Ti(i\text{-}pr)_4$ does not approach zero after ~70°C but, rather, increases giving rise to a second extremely broad transition between 50°C and 200°C. Furthermore, these tanδ transitions observed above ~50°C for the 6Ti-50PDMS(1700) and 30Ti-50PDMS(1700) materials are not accompanied by any change in the storage modulus (see Figure 31 on page 142 for storage modulus curves).

A complete explanation is not yet available but the tanδ transitions observed in the PDMS modified materials are believed to be due to the oligomers undergoing the glass transition temperature, T_g. The observed shifting to higher temperatures and broadening of the glass

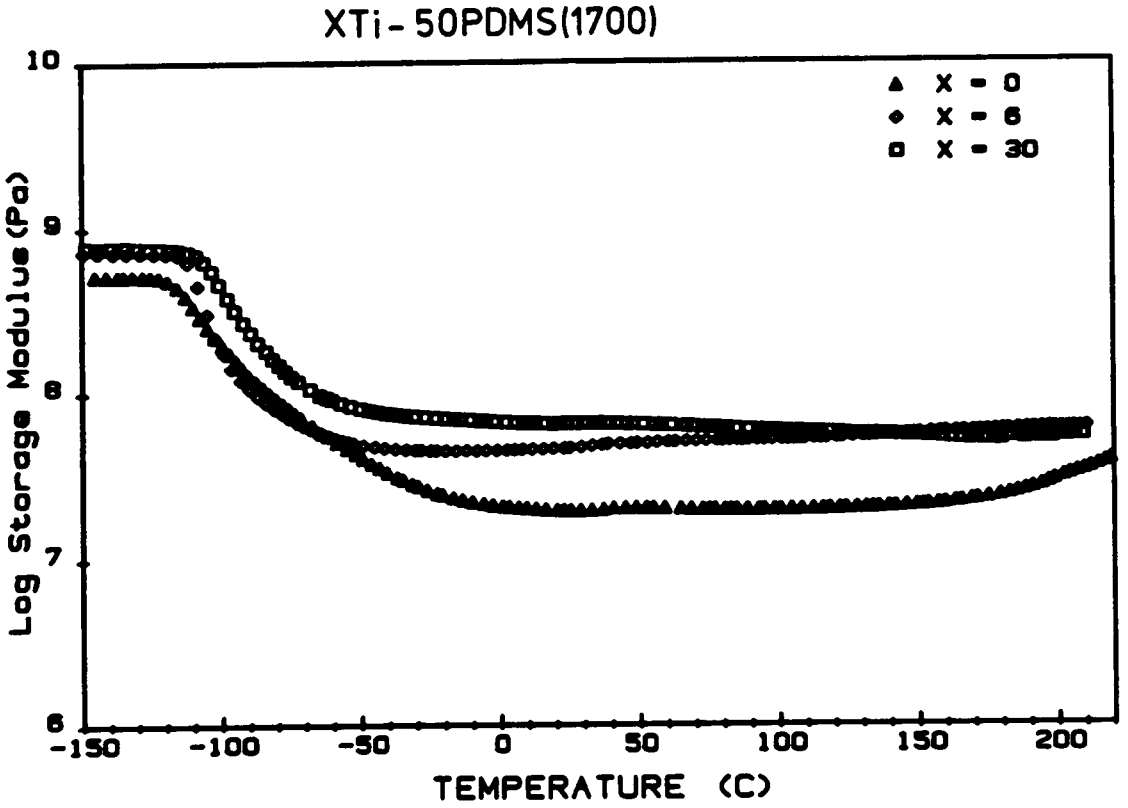

Figure 31. Storage modulus curves of PDMS modified TEOS based sol-gels as a function of titanium content: triangles-0 wt% $Ti(i\text{-}pr)_4$, diamonds-6 wt% $Ti(i\text{-}pr)_4$, squares-30 wt% $Ti(i\text{-}pr)_4$

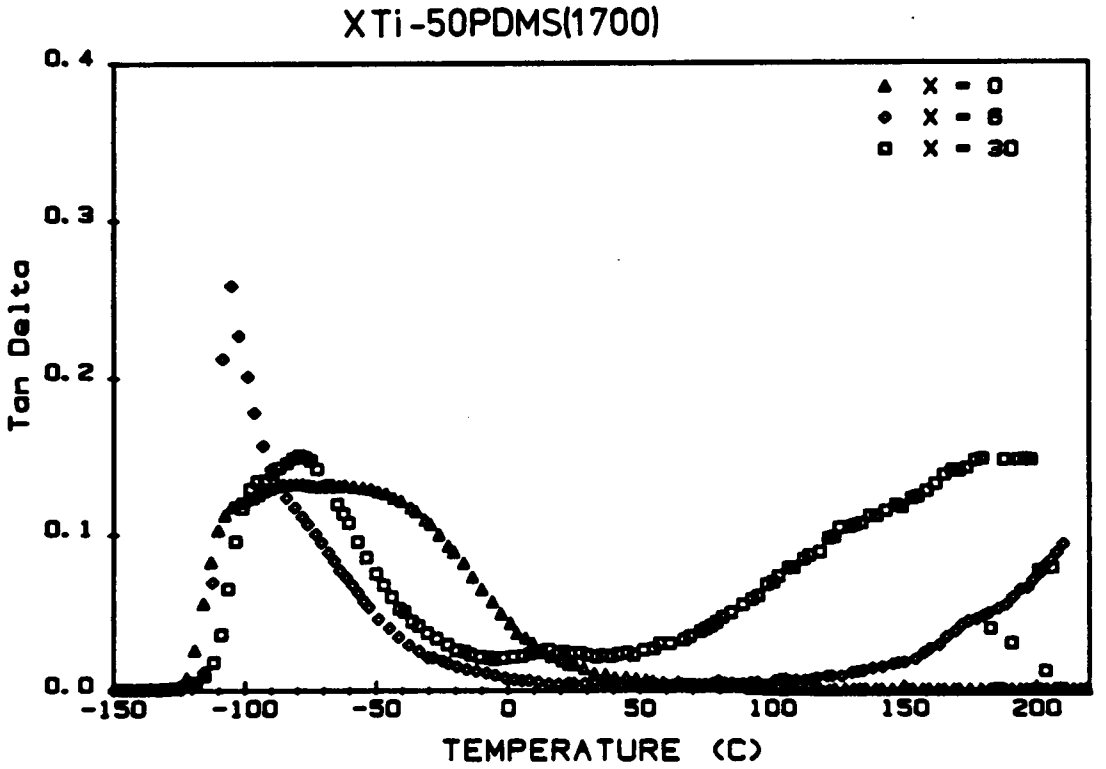

Figure 32. Tanδ curves of PDMS modified TEOS based sol-gels as a function of titanium content: triangles-0 wt% $Ti(i\text{-}pr)_4$, diamonds-6 wt% $Ti(i\text{-}pr)_4$, squares-30 wt% $Ti(i\text{-}pr)_4$

transitions relative to that of the pure PDMS oligomers (≃-120°C) are the result, it is believed, of the physico-chemical environment of the oligomer chains in the glass network. This shifting of the T_g strongly indicates that the oligomers are well, but not necessarily uniformly, dispersed throughout the material "matrix" [14, 15, 17]. The two distinct transitions observed in the titanium containing tanδ curves for both of the PDMS(1700) gels indicate that at least two types of physical-chemical environments exist for the oligomer chains in these materials. The incorporation of titanium into TEOS-PDMS(1700) sol-gel materials results in an ***apparent shifting*** of the oligomer T_g to lower temperatures accompanied by an increase in a second higher temperature (50°C or greater) oligomer transition. In terms of a "two environment" model, the higher tanδ transition would correlate to an area in which the oligomer chains are sterically hindered or "encapsulated" by the inorganic glass based network whereas the lower transition (closer to the T_g of pure oligomer) would correlate to a less hindered "oligomer-rich" area [18]. If such were the case, titanium incorporation could increase the level of steric hindrance or "encapsulation" by driving the overall system to a higher degree of reaction. This would explain the tanδ curves in Figure 32 on page 143. The PDMS(1700) chains undergoing the glass transition at ≃-50°C in the 48TEOS-52PDMS(1700)0.045 material undergo the glass transition at higher temperatures in the titanium containing materials. Further, the PDMS(1700) chains undergoing T_g at temperatures above 50°C in the titanium containing materials would be missing in the low temperature end of the dynamic mechanical spectrum. This could be the cause of the ***apparent shift*** to lower temperatures observed in the first tanδ peak of the 6Ti-50PDMS(1700) and 30Ti-PDMS(1700) materials.

5.3.3 Extraction and Swelling Behavior

The PDMS(1700) oligomer used to modify the sol-gel systems studied was hydroxy terminated (or silanol terminated - see Chapter III section 3.2.2 for details concerning the PDMS(1700) oligomer). As such, barring any side reactions, the oligomer has only two func-

tional groups with which to tie into the silicate network formed during the sol-gel process. Additionally, since the functional ends are already Si-OH, the oligomer does not have to hydrolyze before it can undergo condensation reactions with the silicate precursors ***or with itself***. Should any one of the two functions fail to connect into the SiO_2 network, the final sol-gel material would contain "dangling" PDMS(1700) chains. If neither of the two ends connects, the final gel would contain "loose" PDMS(1700) chains and/or cyclic materials that, in principle, could be removed by solvent extraction. Both situations, if they exist to any great degree, would be expected to influence the mechanical properties of the hybrid sol-gel material. Loose or dangling chains would not be be able to contribute to the mechanical integrity of the material but could, at best, function as a type of toughening agent for the surrounding material matrix.

Extraction and swelling techniques provide information regarding the nature of the material matrix. Solvent extraction is the method of choice to determine the amount of non-connected or "trapped" oligomer in the hybrid sol-gels. On the other hand, differences in the network structure, specifically the crosslink density of compositionally similar materials, are evidenced by changes in the amount of solvent uptake measured in the swelling experiment. Swelling data, then, compliment extraction data when both are obtained for the same materials. Table 13 on page 146 contains the results of such extraction and swelling experiments performed on three titanium containing compositions of PDMS(1700) modified sol-gel materials. These experiments were carried out in THF according to the procedures outlined in Chapter III sections 3.3.4 and 3.3.5. For comparative purposes, extraction and swelling experiments were carried out on a number of PDMS(1700) modified TEOS based sol-gel materials as well. These materials, the original "CERAMERs", were graciously supplied by Dr. Hao-Hsin Huang of VPI and SU and have been studied in detail elsewhere [14, 15, 20]. It should be noted that all materials had been allowed to gel and dry thoroughly (>1 year) prior to the extraction which should eliminate any possibility of an aging effect clouding the comparisons between different materials.

Table 13. Extraction and swelling behavior of PDMS(1700) modified sol-gels in THF

sample	age*	extraction wt% loss	swelling wt% uptake†
48TEOS-52PDMS(1700)0.022‡	> 1yr	3.2	18
48TEOS-52PDMS(1700)0.045‡	> 1yr	3.4	44
48TEOS-52PDMS(1700)0.111‡	> 1yr	14.2	24
60TEOS-40PDMS(1700)0.022‡	> 1yr	2.2	--
60TEOS-40PDMS(1700)0.111‡	> 1yr	1.2	44
6Ti-50PDMS(1700)	> 1yr	3.5	--
15Ti-50PDMS(1700)	> 1yr	3.6	38
30Ti-50PDMS(1700)	> 1yr	3.3	47

*elapsed time between gelation and extraction (stored at room temperature)
†measured after 30 hours in THF at 20±2°C
‡samples graciously supplied by Dr. Hao-Hsin Huang (these materials have been discussed in detail elsewhere [14, 15, 20])

The amount of material extracted from the various gels tested ranged between 1.2 and 3.6 weight percent, with the exception of the 48TEOS-52PDMS(1700)0.111 gel for which 14.2 weight percent of the material was extracted (more than likely an experimental anomaly). Surprisingly, there exists no notable correlation between the extraction data and the different compositions tested other than a ~30% decrease in the percentage of extractable material in the 60TEOS-40PDMS gels relative to the others. The titanium containing gels show a similar amount of extractable materials as those without titanium, especially when they are compared to the 48TEOS-52PDMS(1700) gels. This result indicates that, within the limits of the extraction experiment, both the titanium containing PDMS(1700) and the 48TEOS-52PDMS(1700) sol-gels are crosslinked to a similarly high degree despite the differences in composition and preparation scheme.

As a whole, the extraction data obtained indicate that the material matrix of PDMS(1700) modified sol-gel materials contain little or no non-connected oligomers in the "as gelled" state (with the proviso that the extraction conditions used would have removed these species had they existed). This is somewhat remarkable when it is considered that in the titanium materials well over 70 wt% of the final material matrix is PDMS; furthermore, in the 48TEOS-52PDMS(1700) compositions the final PDMS content is ~80 wt% and in the 60TEOS-40PDMS(1700) compositions it is ~70wt% [20] (these calculations are based on 100% conversion of the sol-gel process). The extraction data implies that TEOS based crosslinks formed during the sol-gel process connect virtually all of the PDMS oligomers to the material matrix (though one end of the chains could still be disconnected). Carried one step further, the extraction data indicate a high degree of dispersion of the crosslinking component (TEOS) in the material matrix and a relatively high degree of conversion of the sol-gel process.

A quick calculation demonstrates that, based on the observed extraction results, the degree of conversion in the aged PDMS(1700) sol-gel systems must be relatively high. If one assumes, arbitrarily, that the overall extent of conversion is only 80% (NMR data presented in Chapter IV and to be presented in this chapter prove this to be a conservative estimate), and that all sites react to equal degrees of completion (if anything, the silanol PDMS sites

should react to a higher degree of completion than the ethoxy TEOS sites), one would estimate that 20% of the PDMS chains would contain at least one unreacted (non-connected) end and that 20% of these chains would, in turn, be completely unreacted (non-connected). Under these assumptions, then, a minimum of 4 wt% of the PDMS component should be extractable from the sol-gel hybrids. A 48TEOS-52PDMS(1700) composition gel would, therefore, be expected to lose 3.2 wt% ***from just the unreacted chains in the PDMS component***. This crude estimate does not include the chain extended dimers, trimers, et c., PDMS based cyclics or unreacted TEOS which would also undoubtedly exist at 80% conversion. The presence of such cyclics or unreacted ortho silicate esters would only serve to increase the expected estimate. The predicted weight loss, as calculated, is on the order of the observed values but the measured weight loss values undoubtedly contain contributions from residual solvent trapped in the original gels. Based on the considerations presented, the extraction data obtained for the PDMS hybrid sol-gels are indicative of at least 80% conversion.

The swelling data obtained for the different PDMS(1700) modified materials varied a substantial amount (see Table 13 on page 146), especially that obtained for the "CERAMER" materials provided by Dr. Huang. It is highly probable, though, that the large variations observed were due to experimental difficulties rather than real differences in the samples. The swelling experiments for these materials were generally carried out on two or three large pieces of film that, during the course of swelling in THF, cracked and were difficult to handle (this is interesting in itself). Having to remove from the solvent, blot dry and weigh two or three fragile pieces of gel increased the time during which THF could evaporate from the swollen material thereby increasing the uncertainty in the weight uptake measurement. Two samples, 6Ti-50PDMS(1700) and 60TEOS-40PDMS(1700)0.022, cracked so severely during the swelling experiment that no data were obtainable at all. All samples, it is interesting to note, cracked on air drying subsequent to the swelling experiment. The swelling data presented, especially when viewed in light of the extraction results, indicates that the various PDMS modified sol-gel hybrid materials studied are all similar in their degree of crosslinking.

Only one notable difference was observed in the extraction and/or swelling results of the different gels tested and this was due to the level of TEOS loading. No significant differences were observed between the other gels eventhough the titanium containing materials were made using an entirely different synthetic scheme than the TEOS-PDMS(1700) materials which were, in turn, made using three different acid concentrations. Further, the relatively small amount of material extracted from these samples (~1 to ~4 wt%) indicates that there are few, if any, trapped PDMS(1700) oligomer chains or cyclic PDMS molecules in the hybrid materials (the fact that the various gelled materials swell to between 20 and 50 weight percent in 20°C THF adds confidence that Soxhlet extraction in THF is sufficiently rigorous to remove any trapped oligomer species present).

5.3.4 Thermo-gravimetric Analysis

Thermo-gravimetric analysis was carried out on selected titanium containing PDMS modified materials. These experiments were conducted to determine the amount of volatiles contained in the gelled materials as well as to determine the heat stability of the hybrid systems as a function of titanium content. Three different titanium compositions were tested in air at a 10°C per minute heating rate according to the procedure outlined in Chapter III section 3.4.7. Figure 33 on page 150 gives the weight percent versus temperature curves obtained for the gels: (a) 6Ti-50PDMS(1700), (b) 30Ti-50PDMS(1700) and (c) 56Ti-39PDMS(1700). These curves demonstrate significant differences in thermal behavior for different loadings of titania and contain three regions of interest: 0-250°C, 250-500°C and 500-600°C. In the 0-250°C volatiles trapped in the material matrix are removed while between 250°C and 500°C any number of events can take place including completion of the sol-gel process [47], and/or hydrolytic oxidation of the PDMS oligomer (it is possible that the PDMS may depolymerize in the presence of residual acid at lower temperatures). In the 250-500°C temperature regime crystallization of the TiO_2 component is also possible [50, 61] but would not be expected to

appear as a weight loss. Finally, in the 500-600°C range oxidative degradation of the PDMS is likely to occur if it has not already done so.

Comparing the different titanium content gels in the low temperature regime (0-250°C) gives rise to a mild surprise. As the titanium content is increased from 6 to 30 to 56 weight percent the observed weight loss increases from ~2.6 wt% to ~4.4 wt% to ~6.2 wt% respectively. At first glance, this is contrary to what is expected. The higher titanium content materials have been speculated to react to a higher degree of completion than their TEOS-PDMS counterparts; consequently, one would expect these materials to exhibit successively lower weight loss in the 0-250°C range as the titanium loading is increased due to fewer unreacted sites being present. However, considering that the weight loss in this temperature regime is due to loss of trapped volatiles and bound organics, the observed results are not so surprising. As the titanium loading is increased the possibility of forming octahedral titanium acetate complexes increases [86]. Such titanium acetate complexes in the material matrix could account for the observed increase in the level of bound organics lost in the 0-250°C region of the thermo-gravimetric data presented in Figure 33.

In the "intermediate" temperature regime, the shape of the thermo-gravimetric curves given in Figure 33 are similar for the different titanium materials. In the 250-450°C region all three compositions display sigmoidal shaped curves with a drop between "plateaus" that corresponds to a weight loss of ≃12 wt%. However, the onset of the sigmoidal shaped curve (the first steep increase in weight loss) shifts to lower temperatures as the titanium loading is increased. The observed onset temperature progresses from ≃375°C for the 6Ti-50PDMS(1700) gel to ≃325°C for the 30Ti-50PDMS(1700) gel and finally to ≃275°C for the 56Ti-39PDMS(1700) gel. Increased titanium loading apparently serves to promote whatever event occurs in the 200-400°C region thereby causing the shift to lower temperatures (almost as if the titanium lowers the "activation energy" of the event). Beyond ~400°C, the 30Ti-50PDMS(1700) and the 56Ti-39PDMS(1700) gels show a gradual weight loss of approximately 7%; at 600°C the amount of material remaining from these gels was observed to be 76 wt% and 74 wt% respectively. The 6Ti-50PDMS(1700) material, however, shows a dramatic

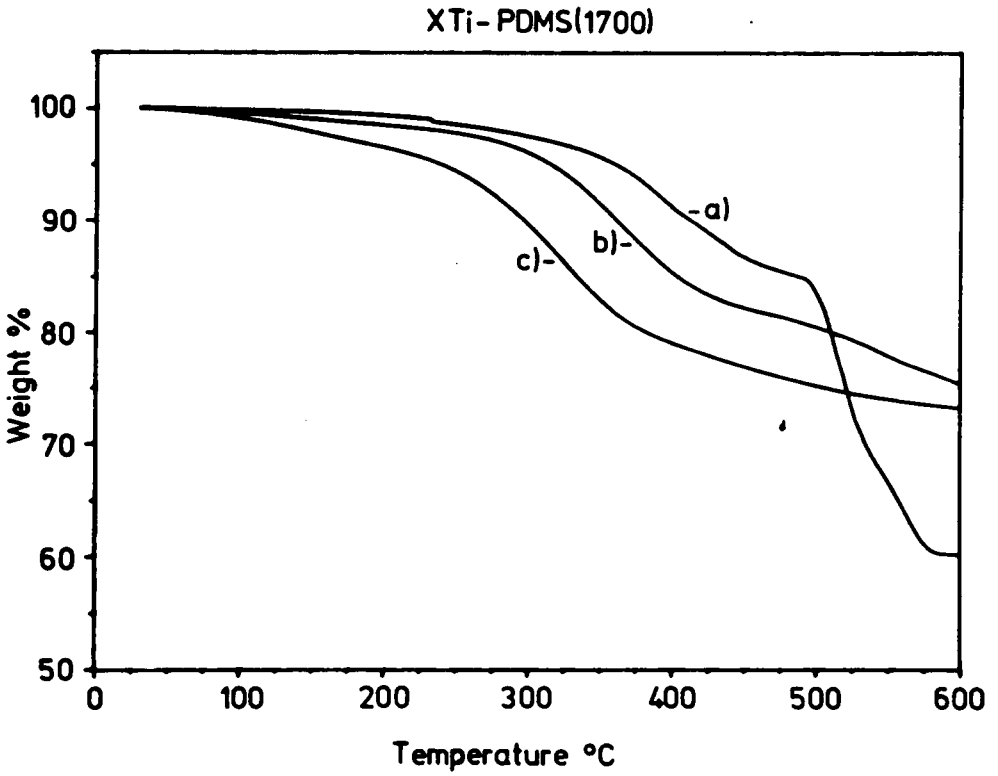

Figure 33. Thermo-gravimetric analysis of titanium containing PDMS(1700) sol-gel materials: a) 6Ti-50PDMS(1700), b) 30Ti-50PDMS(1700), c) 56Ti-39PDMS(1700)

weight loss of 25 wt% occurring at 500°C. A similar weight loss occurring at 400°C in the thermo-gravimetric experiment has been observed for the degradation of neat PDMS polymer [113]. More than likely, the dramatic weight loss observed for the 6Ti-50PDMS(1700) material at 500°C corresponds to the degradation of whatever PDMS structures survived to that temperature; the reason that the same dramatic weight loss is not observed for the 30Ti-PDMS(1700) and 56Ti-39PDMS(1700) gels in that temperature range may relate to inherent differences in the composition and/or structure of those materials.

Figure 34 on page 153 shows the thermo-gravimetric traces of a 6Ti-50PDMS(1700) gel before (a) and after (b) the swelling experiment. The two curves are virtually superimposable except for the final residual content which differs by ≃4.4 wt%, the swollen material retaining the higher percentage of its original weight. Recall that the extraction experiment conducted on the 6Ti-50PDMS(1700) removed only 3.5 wt% of the material. The TGA results in Figure 34 on page 153 indicate that the 3.5 wt% extracted material was insignificant in terms of the material composition. Further, the swelling experiment, which proved to be harsh enough to destroy the material integrity (the 6Ti-50PDMS(1700) material cracked severely during swelling), also did not significantly alter the material. If either of the two "wet" experiments had altered the composition of the gelled materials, or if significant amounts of trapped species were removed, the TGA curves would not match. For example, had a significant portion of PDMS been removed from the material by either the extraction or the swelling process, the weight loss due to PDMS degradation (at the higher temperatures) for that sample would have constituted a smaller percentage than for the non-extracted non-swollen sample. A similar argument can be put forth to explain why little or no unreacted TEOS component was removed by the extraction and swelling procedures.

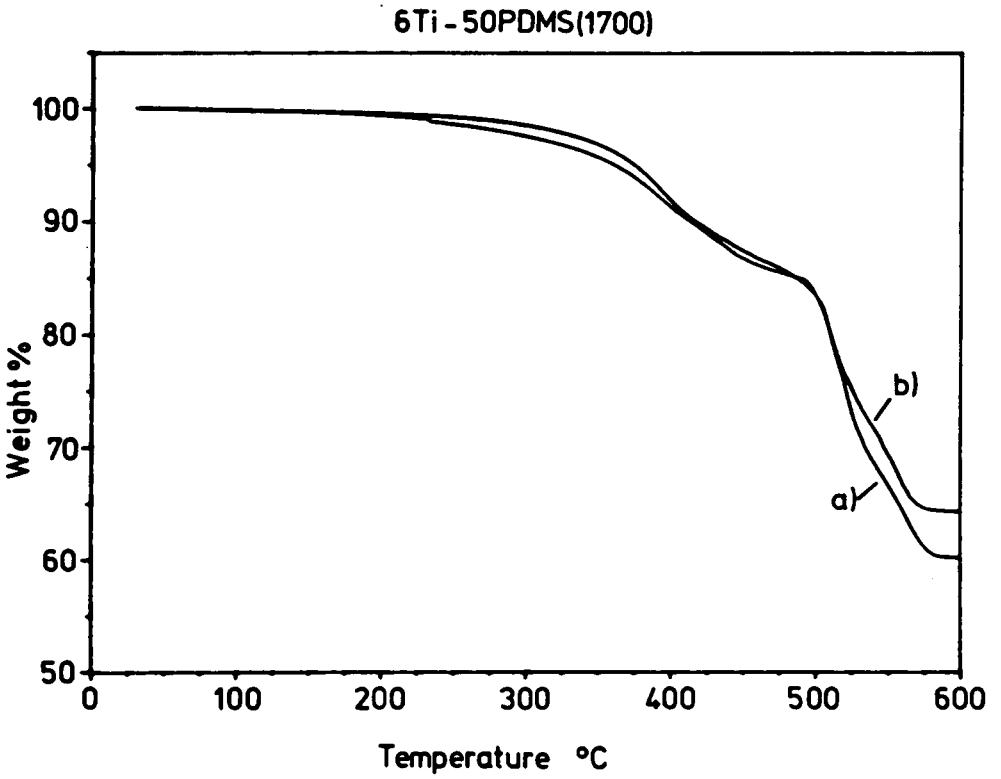

Figure 34. Thermo-gravimetric analysis of 6Ti-50PDMS(1700) gel before and after swelling in THF: a) before swelling, b) after swelling

5.3.7 Solid State NMR

The NMR techniques used in Chapter IV to study multifunctional silicate sol-gels were also applied to certain PDMS containing hybrid sol-gel materials. Solid state ^{29}Si FT/MAS and CP/MAS NMR were performed to determine the degree of reaction of the TEOS component and to observe the type of silicate structures formed (as was the case for the multifunctional sol-gels). Figure 35 on page 155 gives the FT/MAS NMR spectra obtained for three typical gels studied: (a) 48TEOS-52PDMS(1700)0.022, (b) 6Ti-50PDMS(1700), (c) 30Ti-50PDMS(1700). All three of these spectra are dominated by a large sharp resonance observed in the D^2 region (13-20 ppm). The resonances observed in the "Q" region of the ^{29}Si NMR spectra (~-78 to -110ppm) are, for the most part, quite small. This is especially true for the spectra of the two titanium containing gels in Figure 35 on page 155 which represent the sum of 1024 (b) and 384 (c) collected scans using a delay of 60 seconds between pulses (in light of the the results in Chapter IV, this is undoubtedly too short a delay time). The ill-resolved Q^3 peaks in these spectra do not allow for accurate quantitation, but they do indicate that the Q^4 (or "fully reacted" SiO_2) species are the dominant structure arising from the TEOS component. This, in turn, indicates a high degree of conversion of the TEOS component. The FT/MAS spectrum for the 48TEOS-52PDMS(1700)0.022 gel, on the other hand, represents the sum of 480 scans using a delay of 120 seconds between pulses and is better resolved than the other two spectra in Figure 35 on page 155. The Q^3 resonance in this spectrum is sufficiently well resolved to allow quantitation with some degree of confidence. Based on the integrated peaks from the FT/MAS spectrum given in Figure 35 on page 155, using a Gaussian deconvolution detailed in the previous chapter, the degree of conversion for the TEOS component in the 48TEOS-52PDMS(1700)0.022 gel was determined to be 94%.

Unlike the multifunctional silicate sol-gels quantified in Chapter IV, the hybrid sol-gels are not predominantly silicate in composition. The PDMS(1700) modified hybrid materials contain on the order of ~25 wt% or less SiO_2 species which is why the NMR spectra are dominated

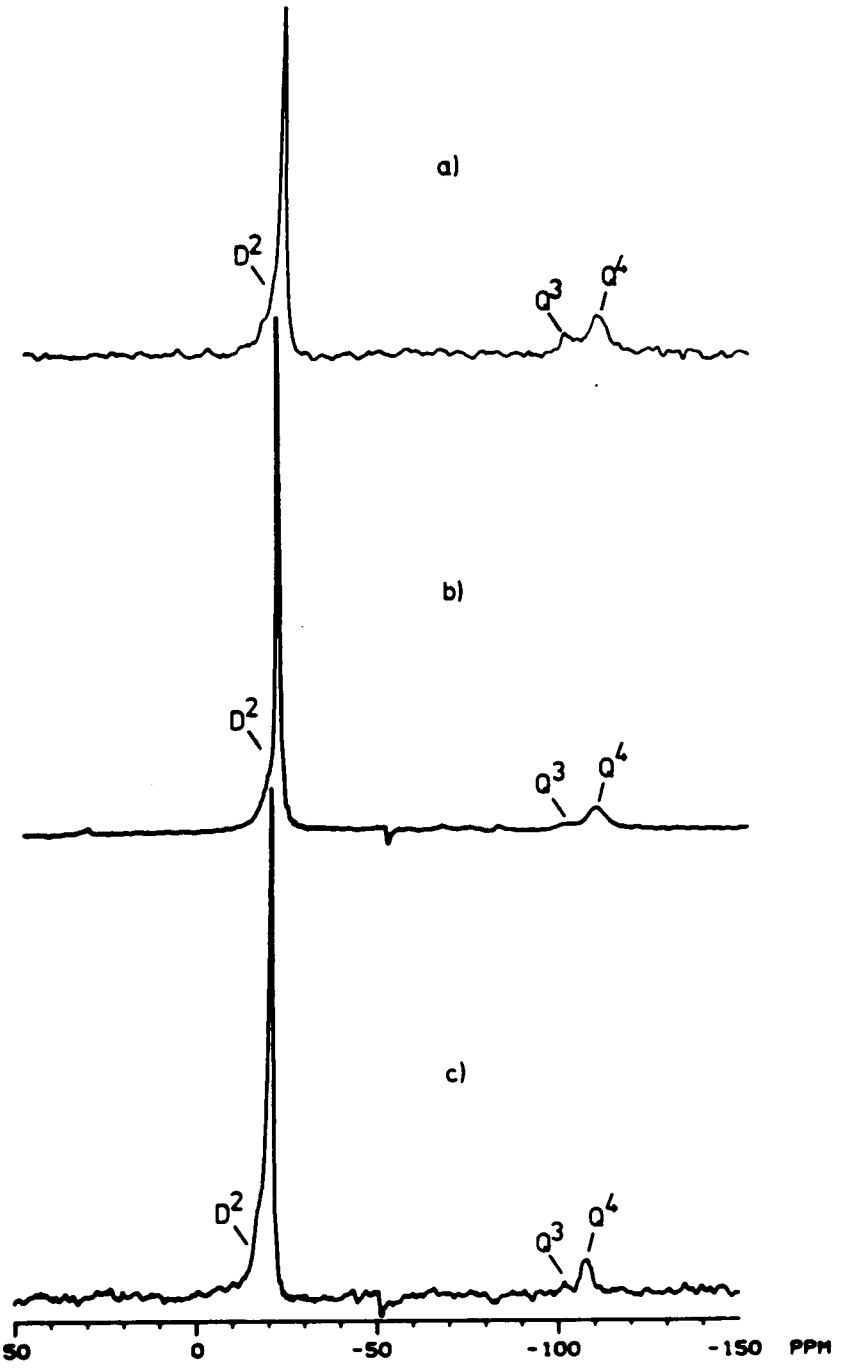

Figure 35. FT/MAS spectra of PDMS modified sol-gels as a function of titanium content: a) 48TEOS-52PDMS(1700)0.022 b) 6Ti-50PDMS(1700) c) 30Ti-50PDMS(1700)

by the PDMS(1700) component. As titanium is incorporated into the sol-gel systems, displacing TEOS in the process, the amount of "Q" silicates in the gels is reduced further exacerbating the problem of spectral resolution. In any case, the large amount of spectrometer time required to obtain the marginal FT/MAS spectrum given in Figure 35 (a), ~16 hours (120 seconds delay between scans multiplied by 480 scans), make this technique impractical for studying the silicate structures of a large number of hybrid sol-gel materials. The CP/MAS technique, however, if properly optimized may prove to be the method by which to obtain such information: especially in light of the quantitative results obtained for the multifunctional sol-gels in Chapter IV. Figure 36 on page 157 compares the FT/MAS spectrum (a) to the CP/MAS spectrum (b) obtained for the 6Ti-50PDMS(1700) gel. The improvement over the FT/MAS spectrum in the resolution of the Q^4 and Q^3 peaks is readily apparent in the CP/MAS spectrum. Furthermore, the FT/MAS spectrum (a) required a full 17 hours of spectrometer time to collect while the CP/MAS spectrum (b) required only 3/4 hour. Such preliminary results have been quite encouraging. As a consequence, additional solid state NMR studies on hybrid sol-gel materials are pending awaiting the optimization of the CP/MAS experiment.

5.3.6 *Raman Spectroscopy*

Raman spectroscopy was also carried out on a number of hybrid PDMS(1700) modified silicate sol-gel materials. Given in Figure 37 on page 158 is the Raman spectrum obtained for a typical PDMS modified sol-gel (in this case 48TEOS-52PDMS(1700)0.05). Many of the same features observed in the Raman spectra of the multifunctional gels presented in Chapter IV are also observed in the spectra of the hybrid PDMS(1700) modified gels. The C-H bending vibration arising from unreacted ethoxy methyl groups at ~1450 cm^{-1}, the Si-O-Si stretching vibration at ~800 cm^{-1}, as well as the Si-O-Si bending vibration at 492 cm^{-1} are readily observed. However, additional vibrational bands arising from the PDMS(1700) component are

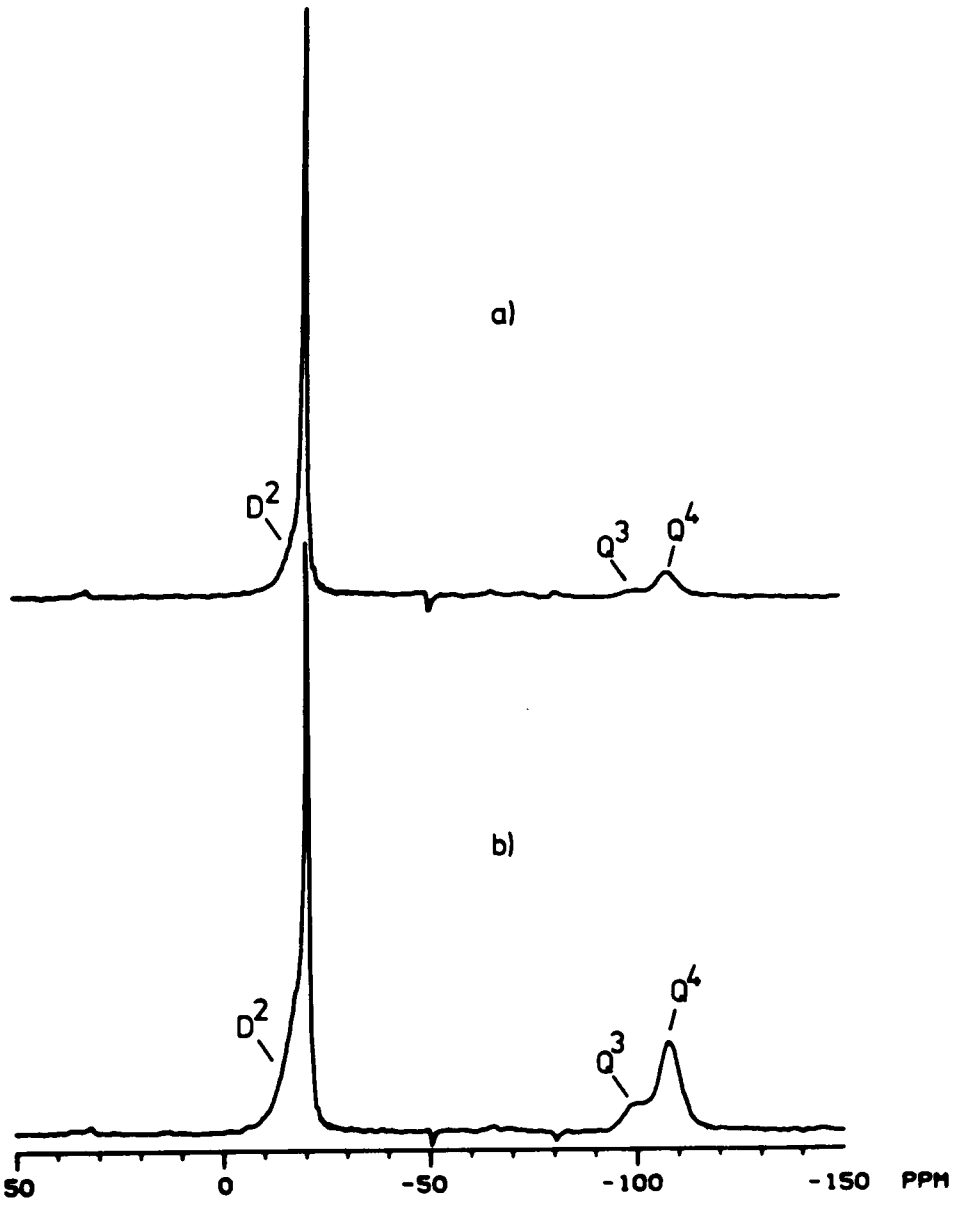

Figure 36. FT/MAS and CP/MAS NMR spectra of 6Ti-50PDMS(1700): a) FT/MAS spectrum, b) CP/MAS spectrum

also present in the Raman spectra of the modified hybrid materials. Figure 38 on page 159 gives the Raman spectrum obtained for the pure PDMS(1700) silanol terminated oligomer for reference. PDMS vibrational bands are seen in a number of regions, C-H bending at ~1420 cm^{-1}, Si-O-Si stretching at ~795 cm^{-1}, $Si-CH_3$ stretching at ~723 cm^{-1}, Si-O-Si bending at 492 cm^{-1} (due to D4 siloxane rings) and $Si-CH_3$ bending at 155 & 210 cm^{-1}.

Because of interference from PDMS bands in the 800 cm^{-1} region, the method developed in Chapter IV to quantitate the Raman spectra could not be used to quantitate the degree of hydrolysis in the hybrid PDMS(1700) modified sol-gels studied except in a qualitative fashion. However, despite interference from the PDMS(1700) bands, useful information can be obtained from the Raman spectra of the hybrid materials. Though no quantitative measurement can be reasonably made, the C-H bending vibration at ~1460 cm^{-1} observed in the spectra of the hybrid materials indicates that the hydrolysis reaction does not go to completion. Furthermore, since Si-OH bands are not detected at 980 cm^{-1}, hydrolysis is observed to be the limiting reaction in the overall sol-gel process. Structural information can be obtained from the Raman spectra as well. The presence of a sharp Si-O-Si bending band at 492 cm^{-1} in all of the hybrid spectra (see Figure 36 on page 157) is indicative of D4 silicate ring structures. The D4 vibrational band is also seen in the spectra of the silanol terminated PDMS(1700) oligomer (Figure 38 on page 159) but is small in comparison to the Si-O-Si stretching band. However, in the hybrid spectra the 492 cm^{-1} vibration dominates the spectrum (Figure 37) much in the same way the 492 cm^{-1} vibration does in the spectrum of pure PDMS cyclic D4 tetramer which is given in Figure 39 on page 162. This result strongly hints that perhaps some of the PDMS oligomer rearranges during the sol-gel process to form the cyclic D4 tetramer; also possible, is the formation of 4 membered cyclic rings by the TEOS component. Recall that 492 cm^{-1} peaks were observed in the Raman spectra of fused quartz (Figure 24 on page 118) and pure TEOS gels (Figure 23 on page 117).

The Raman spectra of titanium containing PDMS modified sol-gels resemble those of the non-titanium containing gels presented. Figure 40 on page 163 gives the Raman spectrum of the 56Ti-39PDMS(1700) gel which displays a prominent 492 cm^{-1} peak and all of the other

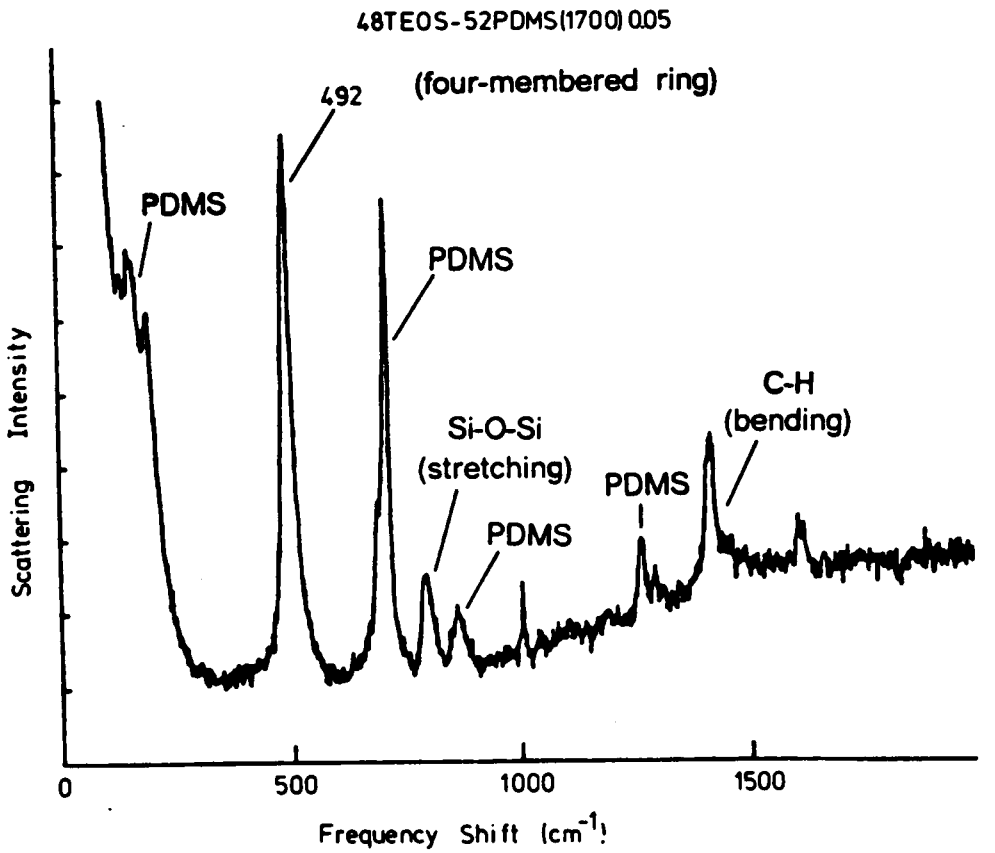

Figure 37. Raman spectrum [92] of a 48TEOS-52PDMS(1700)0.05 gel

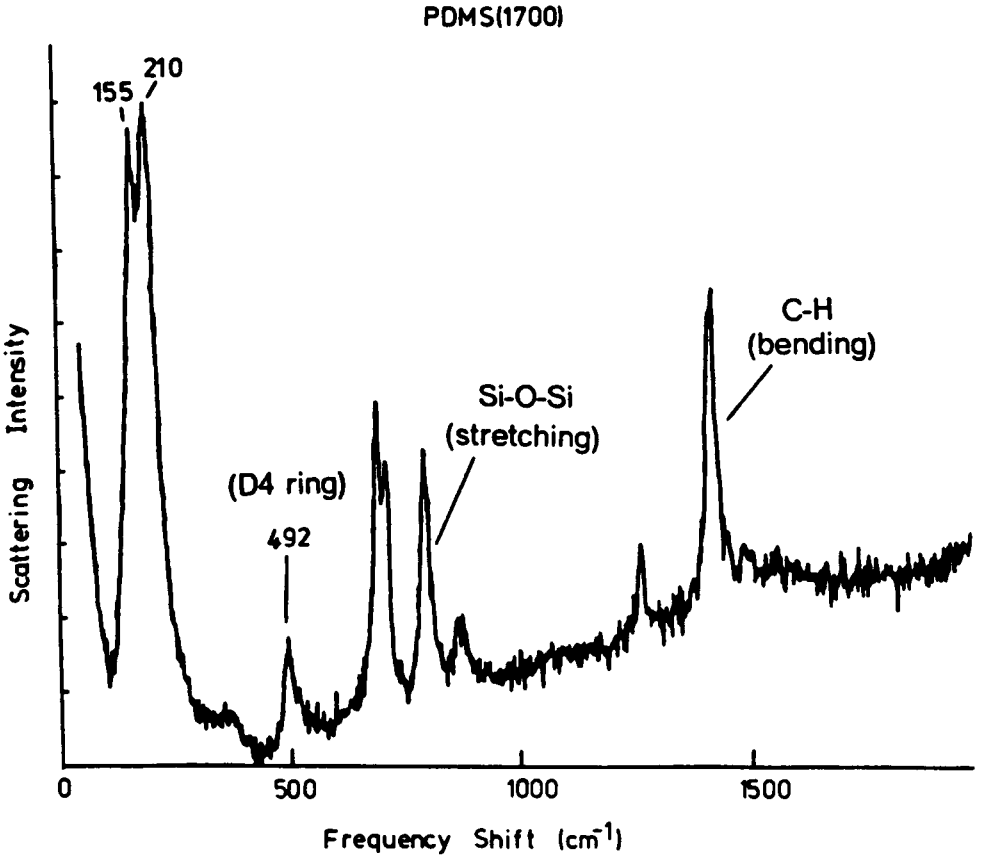

Figure 38. Raman spectrum [92] of silanol terminated PDMS(1700)

bands observed for the TEOS-PDMS(1700) hybrid sol-gels though not as well resolved. There is also a slight peak distinguishable at ~950 cm^{-1} which is attributed to tetrahedrally coordinated Ti^{+} atoms [50]. The major differences observed in the spectra of titanium incorporated materials are much weaker scattering peaks and higher noise levels. At present, the spectra indicate no great structural differences are brought about by titanium incorporation.

5.3.7 SAXS

Figure 41 on page 164 shows the SAXS profiles obtained for two $Ti(i\text{-}pr)_4$ containing gels: 15Ti-50PDMS(1700) and 30Ti-50PDMS(1700). The profile obtained for the 15 wt% $Ti(i\text{-}pr)_4$ material resembles those obtained for 0 wt% CERAMER materials [17, 20]; no distinct peaks were observed in their scattering profiles either. However, the 30 wt% $Ti(i\text{-}pr)_4$ gel displays a marked increase in the observed scattering intensity at low angles. This is an indication of large scale electron density fluctuations within the material which is usually the result of phase separation. The inverse of the scattering vector s gives an idea of the correlation distance between regions of similar electron density, consequently, s^{-1} provides a measure of the scale of the phase separation. The scattering measured for the 30Ti-50PDMS(1700) gel as a function of the angular variable s is still increasing at the lower limit of the SAXS curve; no distinct "peak" is observable. Using the low limit as a guide, though, the electron density flutuation is on the order of 35nm or 350Å.

5.4 Conclusions

A new procedure has been developed by which titaniumisopropoxide can be successfully incorporated into the sol-gel systems previously used to make the PDMS modified TEOS

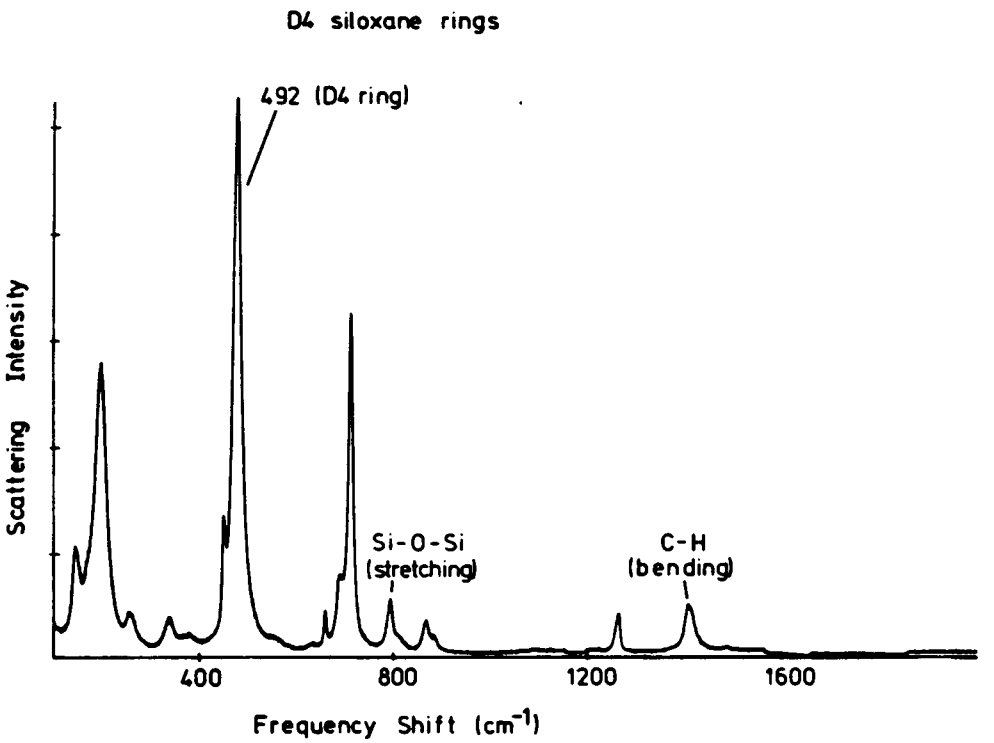

Figure 39. Raman spectrum [93] of D4 siloxane rings

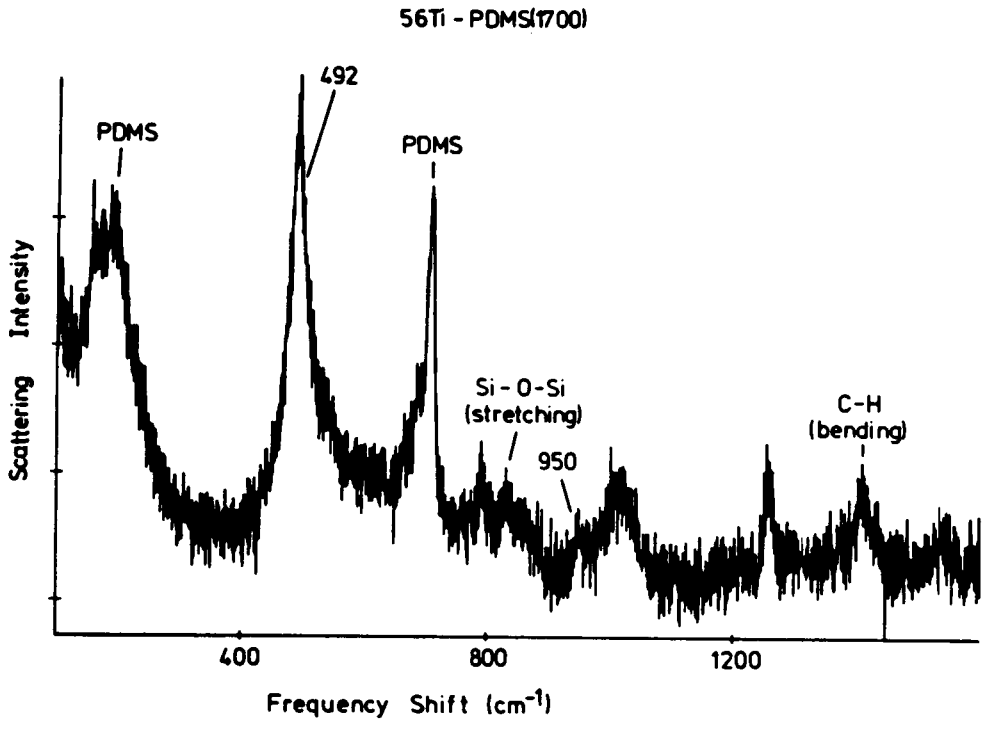

Figure 40. Raman spectrum [93] of a 56Ti-PDMS(1700) gel

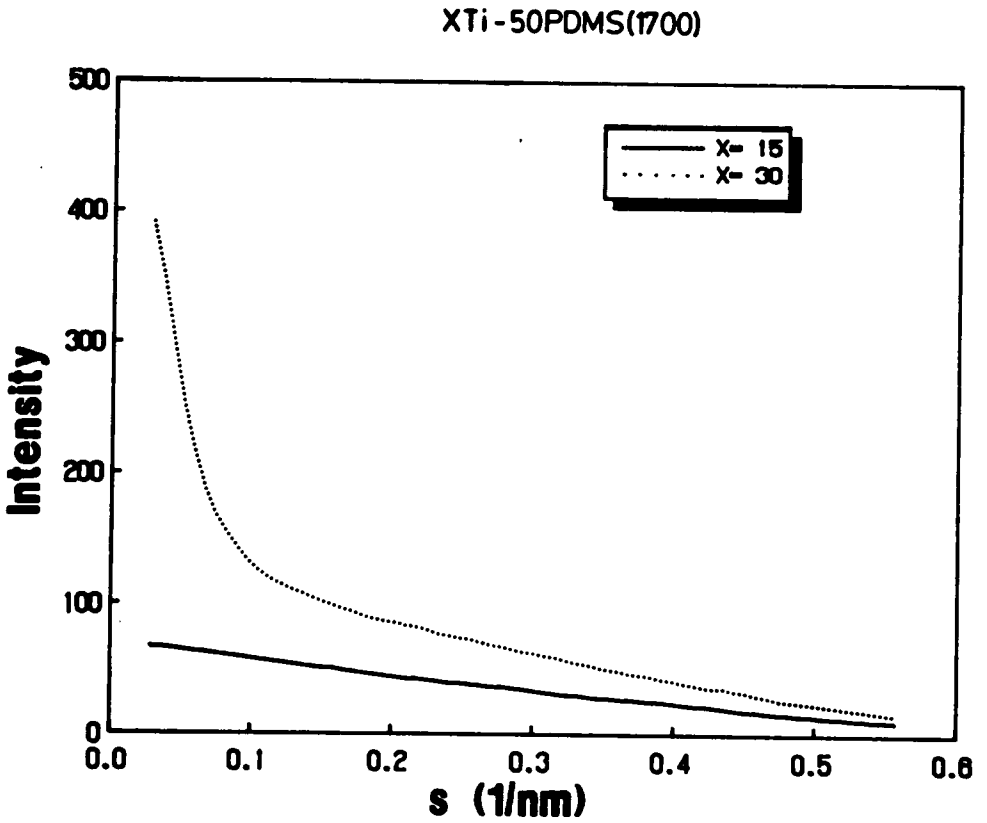

Figure 41. SAXS profiles of XTi-50PDMS(1700) sol-gel materials

based "CERAMER" materials [14, 15]. Gelled films incorporating titanium are monolithic and transparent but yellow in color. The intensity of the observed yellow color is roughly proportional to the amount of titanium incorporated and is, most likely, due to octahedral titanium acetate complexes formed in the gels.

In addition to the optical properties, the physical properties of the titanium containing PDMS modified sol-gel materials are distinctly different from prior CERAMER systems. The storage modulus in titanium containing materials, in the dynamic mechanical spectra, decreases only one order of magnitude after T_g whereas in non-titanium containing materials the storage modulus exhibits a greater decrease. The tanδ curves, also demonstrate unique behavior in displaying an additional transition at temperatures above ~50°C. Thermogravimetric data for these materials demonstrate that the materials in the dynamic mechanical analysis curves do not undergo any further reaction during their first run from -150°C to 220°C (essentially no weight loss is observed by TGA in this region). The second high temperature tanδ transition observed in the dynamic mechanical must, therefore, relate to molecular motion. Unlike the optical and dynamic mechanical properties, titanium incorporation was not observed to effect the extraction and swelling properties of the PDMS modified hybrid sol-gels. Furthermore, extraction and swelling data as well as the limited amount of NMR data available indicate that the titanium containing materials probably do not react to an appreciably higher degree of conversion than the non-titanium PDMS(1700) modified sol-gels (which reach, in one case, 94% conversion). Differences in the dynamic mechanical properties on the incorporation of titanium must, therefore, lie in the nature of the titania component within the gel matrix. SAXS profiles for 30Ti-50PDMS(1700) materials along with the observed dynamic mechanical behavior suggest that perhaps a separate phase is formed. Phase separation may account for the bimodal tanδ curves observed in the dynamic mechanical spectra of $Ti(i\text{-}pr)_4$ containing materials. In principle vibrational spectroscopy (specifically Raman) could establish the nature of the titania component and determine whether it exists as some sort of separate phase or whether it is integrated into the silica network. The Raman spectra obtained for titanium components at this point in time, however, are not sufficiently well re-

solved to permit such determinations due to the high background noise levels and weak scattering peaks observed.

CHAPTER VI

PTMO MODIFIED SILICATE SOL-GEL COMPOUNDS CONTAINING TITANIA

6.1 Introduction

In the last chapter a procedure was developed that allowed $Ti(i\text{-}pr)_4$ to be successfully incorporated into a hybrid PDMS modified TEOS based network system via the sol-gel process. Materials made by this procedure were monolithic, crack-free gels and demonstrated unique optical and dynamic-mechanical properties. The $Ti(i\text{-}pr)_4$ containing materials were, in certain respects, distinctly different from their pure PDMS-TEOS counterparts: they were yellow in color, though still transparent, and showed a high temperature transition in the tanδ curves of their dynamic mechanical spectra. In terms of their mechanical performance, though, the $Ti(i\text{-}pr)_4$ incorporated PDMS modified sol-gels in general were quite disappointing. These materials proved to be quite brittle in nature with only limited flexibility.

The poor mechanical properties observed in the hybrid materials can, to a degree, be attributed to limitations brought about by the nature of the modifying oligomer. Recall that the PDMS(1700) oligomer used was silanol terminated and as such could only link into the forming

silicate network at the chain ends with a total of two links. Also, polydimethylsiloxanes, in general, are not known for high strength; to exacerbate this problem, there exists the possibility of the siloxane chain unzipping during the sol-gel reaction [114] which would further reduce the mechanical performance of the final materials. Primarily for these reasons, new oligomer/polymer systems were sought to incorporate into the sol-gel scheme. It should be mentioned, though, that the first generation of oligomer modified sol-gel materials made with silanol terminated PDMS were successful in many respects. These materials demonstrated the feasibility of oligomer modification of inorganic oxides and are the base upon which the hybrid sol-gel work conducted here is founded.

Endcapped and multifunctional PTMO oligomers and polymers supplied by Dr. James Carlson of the 3M corporation provided the opportunity to incorporate a modifying component that could connect to the silicate structure at several points (at least 6 possible - see Chapter III). These new PTMO modifiers made it possible to observe not only the effects of titanium incorporation on the mechanical properties of a hybrid sol-gel, but also the effect of using a non-compatible oligomer on the material matrix formed by the sol-gel process. This latter effect has been examined in detail elsewhere [18, 20] and will be mentioned only in passing where relevant. Of interest in this chapter, in particular, are the effects of $Ti(i\text{-}pr)_4$ incorporation on the mechanical structure and properties of various PTMO-TEOS sol-gel systems.

6.2 Nomenclature

The nomenclature used in this chapter to identify the various gel compositions studied will follow the example established in the previous chapter. Only the starting weight percent of $Ti(i\text{-}pr)_4$ and the oligomer used will be cited, the remaining balance of the gel composition in all cases, except where otherwise specified, consists of TEOS. The various PTMO oligomers used will be identified by either their molecular weight if they are endcapped or the

number of triethoxy silane groups on the polymer backbone if they are multifunctional. The characteristics of the PTMO oligomers and the various alkoxide precursors used are detailed in Chapter III as well as the nomenclature used to identify these materials. The gelled materials studied in this chapter were prepared according to the procedures outlined in Chapter III section 3.3.2.

The Ti-PTMO modified gel compositions prepared for study are listed in Table 14 and Table 15 on page 170. Specifically, Table 14 contains the gel compositions of the hybrid sol-gels made using linear or endcapped PTMO oligomers while Table 15 contains the compositions of the hybrid gels made using chain extended or multifunctional PTMO polymers. As was the case for the Ti-PDMS(1700) materials, the different Ti-PTMO gel compositions are given in terms of starting and final weight percentages of the three components used. The mole percent composition in terms of the oligomer repeat unit, however, is not given. Unlike the PDMS(1700) oligomer for which a break-down in terms of the repeat unit is logical and straight forward, the PTMO oligomers can not be meaningfully described in terms of a simple repeat unit due to the chemistry of the endcaps (see Chapter III). Therefore, only the starting weight percent, the final weight percent (for 100% conversion) and the molar ratio of components, $Ti(i\text{-}pr)_4$: TEOS : PTMO(oligomer/polymer), are given in the two tables.

The starting compositions listed in Table 14 and Table 15 hint that the oxide and organic components in the various gelled materials should be co-continuous. However, the final compositions demonstrate that Ti-PTMO hybrid gels, like the Ti-PDMS(1700) hybrid gels discussed in Chapter V, are predominantly polymeric (oligomeric) in composition. The dramatic reduction of the oxide components in the composition of the final materials, as opposed to the composition of the reaction mixture, is a direct result of the the hydrolysis and gelation process. Alkoxy functions constitute a significant portion of the original alkoxide; when they are removed, as the result of hydrolysis and condensation, the metal component loses a considerable percentage of its mass. For example, the TEOS precursor has a molecular mass of 208.3 amu while fully hydrolyzed and condensed TEOS, or SiO_2, has a molecular mass of only 60.09 amu. The fully completed sol-gel process results in a 71.2 percent weight loss for the

Table 14. Starting and final gel compositions for Ti containing endcapped PTMO modified sol-gel materials

sample	quantity	$Ti(i\text{-}pr)_4/TiO_2$	$TEOS/SiO_2$*	oligomer
0Ti-47PTMO(2000)	initial wt%	0.0	52.8	47.2
	final wt%†	0.0	24.5	75.5
	molar ratio	0.0	10.8	1.0
15Ti-50PTMO(2000)	initial wt%	15.1	34.9	50.0
	final wt%†	6.3	19.5	74.2
	molar ratio	2.1	8.7	1.0
30Ti-50PTMO(2000)	initial wt%	30.0	20.2	49.8
	final wt%†	13.4	13.7	72.9
	molar ratio	4.6	6.2	1.0
0Ti-50PTMO(2900)	initial wt%	0.0	50.0	50.0
	final wt%†	0.0	24.5	75.5
	molar ratio	0.0	15.7	1.0
15Ti-50PTMO(2900)	initial wt%	15.0	35.0	50.0
	final wt%†	6.1	18.2	75.8
	molar ratio	3.1	11.8	1.0
30Ti-50PTMO(2900)	initial wt%	30.0	20.0	50.0
	final wt%†	12.7	11.8	75.5
	molar ratio	6.1	7.6	1.0

*final SiO_2 wt% and molar ratio includes contribution from triethoxy groups from the PTMO oligomer

†based on 100% conversion of the sol-gel process

Table 15. Starting and final gel compositions for Ti containing multifunctional PTMO modified sol-gel materials

sample	quantity	$Ti(i\text{-}pr)_4/TiO_2$	$TEOS/SiO_2$*	polymer
15Ti-50PTMO(2)	initial wt%	15.0	35.0	50.0
	final wt%°	6.7	18.9	74.4
	molar ratio	6.4	23.9	1.0
30Ti-48PTMO(2)	initial wt%	30.4	22.1	47.5
	final wt%†	13.6	11.9	74.5
	molar ratio	12.9	15.0	1.0
15Ti-50PTMO(3)	initial wt%	15.0	35.0	50.0
	final wt%†	6.7	18.9	74.4
	molar ratio	5.8	21.8	1.0
30Ti-50PTMO(3)	initial wt%	30.0	20.0	50.0
	final wt%†	13.6	11.9	74.5
	molar ratio	11.8	13.8	1.0
15Ti-52PTMO(4)	initial wt%	15.0	33.5	51.5
	final wt%†	6.3	18.0	75.7
	molar ratio	5.7	21.4	1.0
30Ti-52PTMO(4)	initial wt%	30.5	18.1	51.6
	finalwt%†	13.3	10.9	75.8
	molar ratio	11.6	13.5	1.0
15Ti-53PTMO(5)	initial wt%	15.0	31.6	53.4
	final wt%†	6.5	17.8	75.7
	molar ratio	5.7	21.4	1.0
30Ti-53PTMO(5)	initial wt%	30.3	16.5	53.2
	final wt%†	13.0	11.4	75.7
	molar ratio	11.6	13.5	1.0

*final SiO_2 wt% and molar ratio includes contribution from triethoxy groups from the PTMO oligomer

†based on 100% conversion of the sol-gel process

TEOS component. Similarly, the Ti component goes from a mass of 284.26 amu ($Ti(i\text{-}pr)_4$) to 79.90 amu (TiO_2): a weight loss of 71.9%. A consequence of this weight loss is that the metal oxides become minority components in the final gel composition. Therefore, the predominance of the oligomeric/polymeric component in the final gel can be attributed to the large mass lost by the alkoxide components as a result of the sol-gel process.

6.3 Ti Containing Linear PTMO Systems

The gelled Ti-PTMO films were generally transparent though the addition of titanium did impart the same yellowish color to the samples that was observed in the Ti-PDMS(1700) hybrid sol-gels. The yellow color observed in all of the Ti-PTMO materials, like the Ti-PDMS(1700) materials, can be explained in terms of octahedral titanium complexes present in the gels. Unlike the Ti-PDMS(1700) materials, Ti-PTMO were quite flexible and specimens for all mechanical tests were easily obtained.

6.3.1 Mechanical Properties

Figure 42 on page 173 and Figure 43 on page 174 show the dynamic mechanical spectra of Ti-PTMO(2000) sol-gels as a function of titanium incorporation. Figure 42 shows the storage modulus curves while Figure 43 shows the tanδ curves. Comparing the storage moduli first, one notices similarities and differences between the PDMS(1700) and PTMO(2000) modified materials. The storage modulus for both of the Ti containing PTMO(2000) materials are similar and display a noticeably higher "rubbery plateau" above the T_g when compared to the storage modulus curve for a 50TEOS-PTMO(2000)0.04 gel (data for the 50TEOS-50PTMO(2000)0.04 material was taken from ref. [20]). As was the case for the PDMS(1700) sol-gel systems,

$Ti(i\text{-}pr)_4$ incorporation into PTMO(2000) modified sol-gel systems reduces the change in the storage modulus above the observed transition from two to one order of magnitude. Unlike the PDMS(1700) hybrids, the PTMO(2000) hybrids ***all*** show a distinct, partially reversible increase in the storage modulus at temperatures above 100°C. This rise in the storage modulus at high temperatures can be partially attributed to a continuation or "thermal curing" of the sol-gel reaction (specifically, condensation) [18]. The titanium containing materials in Figure 42, though, exhibit a smaller increase in the storage modulus above 100°C than does the TEOS-PTMO(2000) material. Taken together, the higher modulus observed in the "rubbery plateau" and smaller rise in modulus at high temperatures indicate that the titanium containing sol-gel materials may have reached a higher degree of conversion than comparable PTMO modified materials without titanium.

Comparison of the tan δ curves also brings out differences between the sol-gel materials that do and do not have titania incorporated into their structure. The 50TEOS-50PTMO(2000)0.04 material in Figure 43 displays a prominent tanδ transition centered at 0°C with a shoulder at ~50°C. On the other hand, both the 15Ti-50PTMO(2000) and the 30Ti-50PTMO(2000) materials display a "weaker" tanδ transition centered at -30°C with a second broad tanδ transition centered at 50°C and continuing beyond 100°C.

These tanδ transitions, observed in the dynamic mechanical spectra of PTMO(2000) modified sol-gel materials, are believed to be due to the oligomers undergoing the glass transition temperature, T_g. The two distinct transitions observed in the tanδ curves for the Ti-PTMO(2000) systems indicate that at least two types of physico-chemical environments exist for the oligomer chains in these materials. As was observed for the PDMS(1700) modified hybrid systems, the incorporation of titanium into the PTMO(2000) modified materials also results in an ***apparent shifting*** of the oligomer T_g to lower temperatures accompanied by an increase in a second higher temperature (50°C or greater) oligomer transition. Again, in terms of a "two environment" model, the higher PTMO transition would correlate to an area in which the oligomer chains are sterically hindered or "encapsulated" by the inorganic glass based network whereas the lower transition (closer to the T_g of pure oligomer) would correlate to a

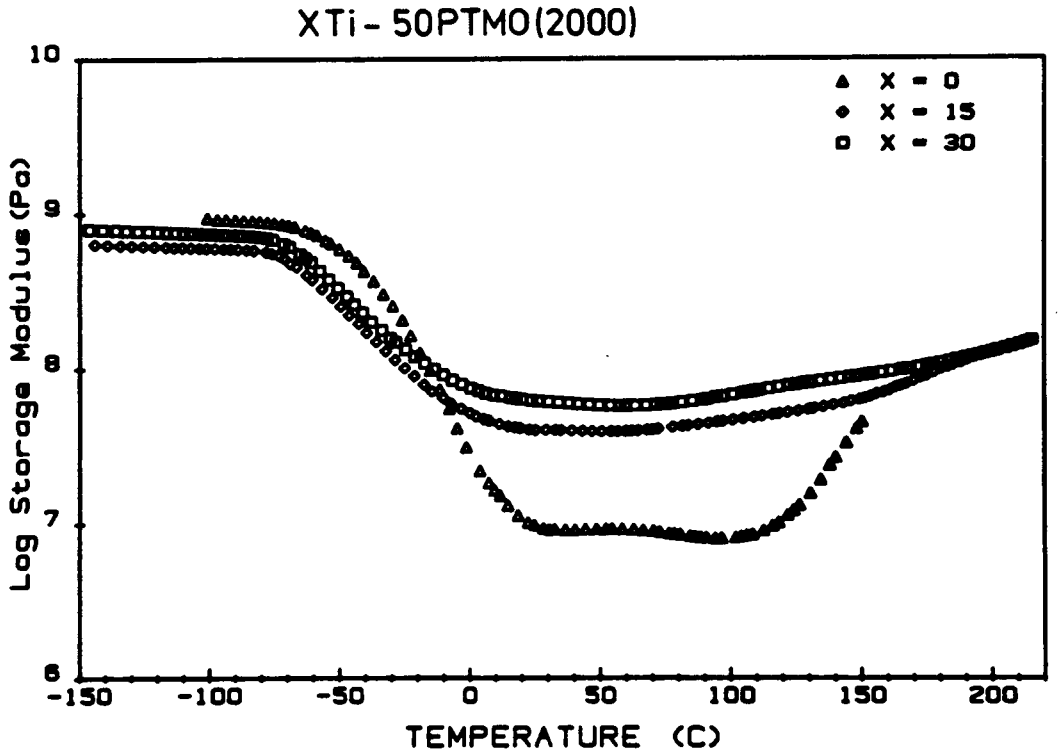

Figure 42. Storage modulus curves of Ti containing PTMO(2000) modified sol-gel materials: (triangles) 50TEOS-50PTMO(2000)0.04 [20], (diamonds) 15Ti-50PTMO(2000), (squares) 30Ti-50PTMO(2000)

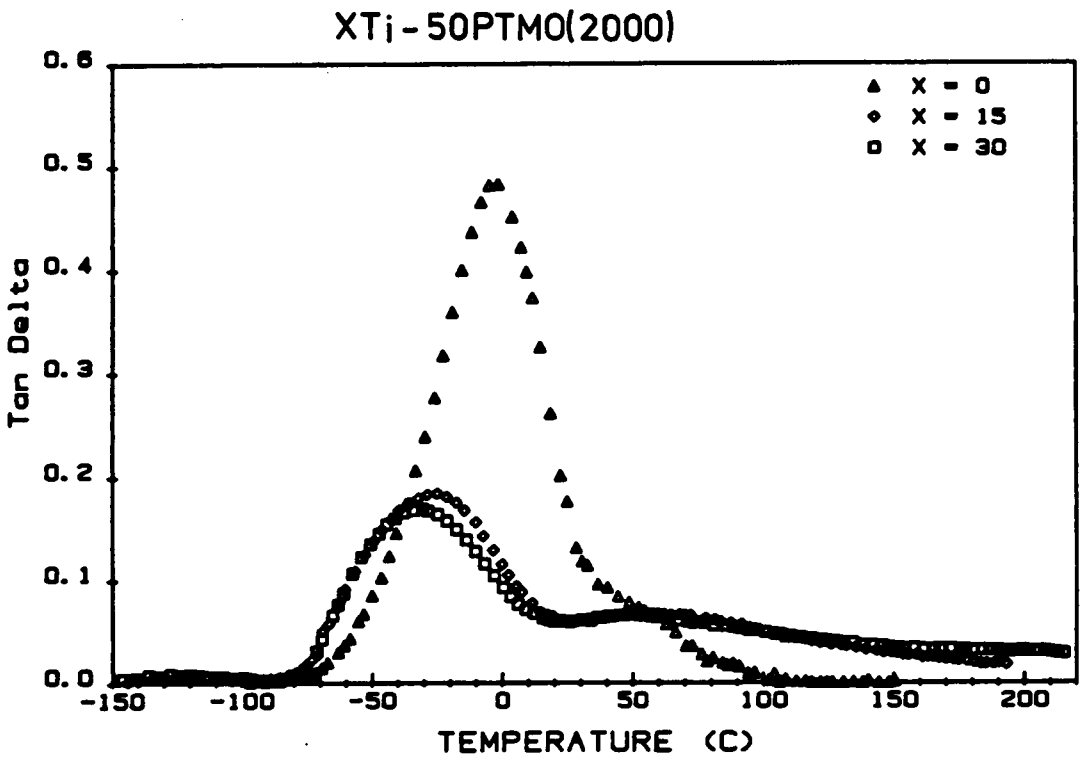

Figure 43. Tanδ curves of Ti containing PTMO(2000) modified sol-gel materials: (triangles) 50TEOS - 50PTMO(2000)0.04 [20], (diamonds) 15Ti - 50PTMO(2000), (squares) 30Ti - 50PTMO(2000)

less hindered "oligomer-rich" area [18]. If such were the case, titanium incorporation could be argued to increase the level of steric hindrance or "encapsulation" by driving the overall system to a higher degree of reaction. This would explain the tan δ curves in that the chains undergoing their glass transition at 0°C in the 50TEOS-50PTMO(2000)0.04 material would undergo their glass transition at higher temperatures in the Ti-PTMO(2000) materials (see Figure 43). Further, the "unencapsulated" chains with T_g at $\simeq$0°C would be missing in the Ti-PTMO(2000) materials thus causing the ***apparent shift*** in the first tanδ peak to lower temperatures.

Figure 44 shows the effect of titanium incorporation on the the stress-strain curves of the hybrid Ti-PTMO(2000) sol-gel materials. As was qualitatively observed for the PDMS(1700) materials, the incorporation of titanium into the PTMO(2000) materials "toughens" the material in that the initial (or Young's) modulus, the ultimate stress and the elongation at break are observed to increase (note that in this figure the 0 wt% $Ti(i\text{-}pr)_4$ gel was made using the modified CCC procedure outlined in Chapter III section 3.3.2). As $Ti(i\text{-}pr)_4$ is introduced, the stress-strain curves (Figure 44) progress from being featureless and somewhat "Hookian" (A), to showing some curvature (B), to almost showing a yield point (C). The most notable change in the stress-strain curves occurs between the 0Ti-47PTMO(2000) (A) and the 15Ti-50PTMO(2000) (B) gels. The modulus increases sharply, as does the elongation at break and ultimate stress, on the incorporation of 15 wt% $Ti(i\text{-}pr)_4$. The changes between the 15Ti-50PTMO(2000) (B) gels and the 30Ti-50PTMO(2000) (C) gels are not as dramatic. The initial modulus does increase notably, but the ultimate stress is virtually unchanged and the elongation at break actually decreases slightly as the $Ti(i\text{-}pr)_4$ content is increased to 30 wt%.

Figure 45 on page 178 and Figure 46 on page 179 contain the dynamic mechanical spectra of a 0Ti-47PTMO(2000) with a 30Ti-50PTMO(2000) gel included for comparison. The storage modulus curve observed for the 0Ti-47PTMO(2000) gel (Figure 45 on page 178 - triangles) sharply drops ~1.5 orders of magnitude at ~-70°C (which is close to the observed T_g for pure PTMO oligomers) then rises only to fall again (probably due to crystallization and melting of the PTMO) to its low value, at 0°C, of 2 orders of magnitude below the glassy

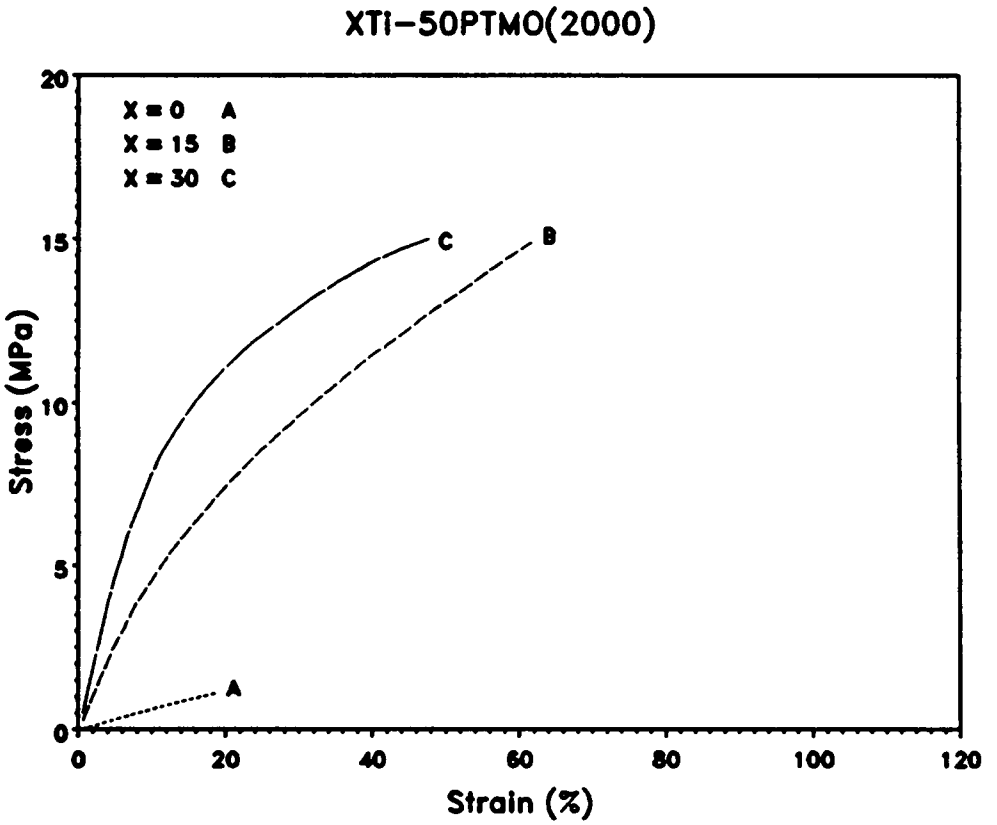

Figure 44. Stress-strain curves of Ti containing PTMO(2000) modified sol-gel materials: (A) 0Ti-PTMO(2000), (B) 15Ti-PTMO(2000), (C) 30Ti-PTMO(2000)

modulus value. The storage modulus then increases parallel to but below that of the 30Ti-50PTMO(2000) material (squares) out to 150°C. The tanδ curve for the 0Ti-47PTMO(2000) material (Figure 46 on page 179 - triangles) displays a prominent, sharp transition centered at ≃-65° (the peak of which is only ~30°C wide) that is quite close to the -80°C value expected for the pure PTMO oligomer. Overlapping this sharp peak is a broader tandδ transition that drops to 0.0 after ≃10°C unlike any of the other hybrid PTMO materials (see Figure 43 on page 174). The storage modulus curves in Figure 45 demonstrates that the 0Ti-47PTMO(2000) material (triangles) is not only different in behavior from the $Ti(i\text{-}pr)_4$ containing gels, but also distinctly different from the 50TEOS-50PTMO(2000) gels. The tanδ curves in Figure 46 on page 179 confirm this conclusion.

Table 16 on page 180 lists the tensile stress-strain properties for a series of hybrid Ti-PTMO(2000) materials made using different levels of $Ti(i\text{-}pr)_4$ in the starting reaction mixture. As a reference to allow comparison with PTMO(2000) hybrid sol-gel materials made using the "standard CERAMER" procedure, tensile data for a 50TEOS-PTMO(2000)0.04 gel [18, 20] have been included. The relative age of the samples at the time of the tensile tests are also noted in Table 16 in terms of the number of days the gel was stored at ~22°C after gelation. The tensile stress-strain properties do change with the passage of time, particularly the so-called "ultimate properties" (elongation and stress at break), suggesting that there may be some kind of "aging" process occurring after gelation. Perhaps a slow continuation of the hydrolysis and condensation reactions is taking place. However, if one follows the initial modulus as the gauge of crosslink density, hence degree of conversion, the tensile data do not indicate major changes in the gels if stored for at least 15 days. A systematic study is needed, though, before aging effects can be adequately assessed.

Comparing the mechanical properties of the materials in Table 16, one first observes a somewhat lower stress at break, a lower elongation at break, and a higher initial modulus for the 0Ti-PTMO(2000) material made using the modified CCC reaction scheme (see Chapter III section 3.3.2 for procedure) as opposed to the "standard" HCl catalyzed procedure used to make the 50TEOS-50PTMO(2000) [18, 20]. The difference between the two materials is be-

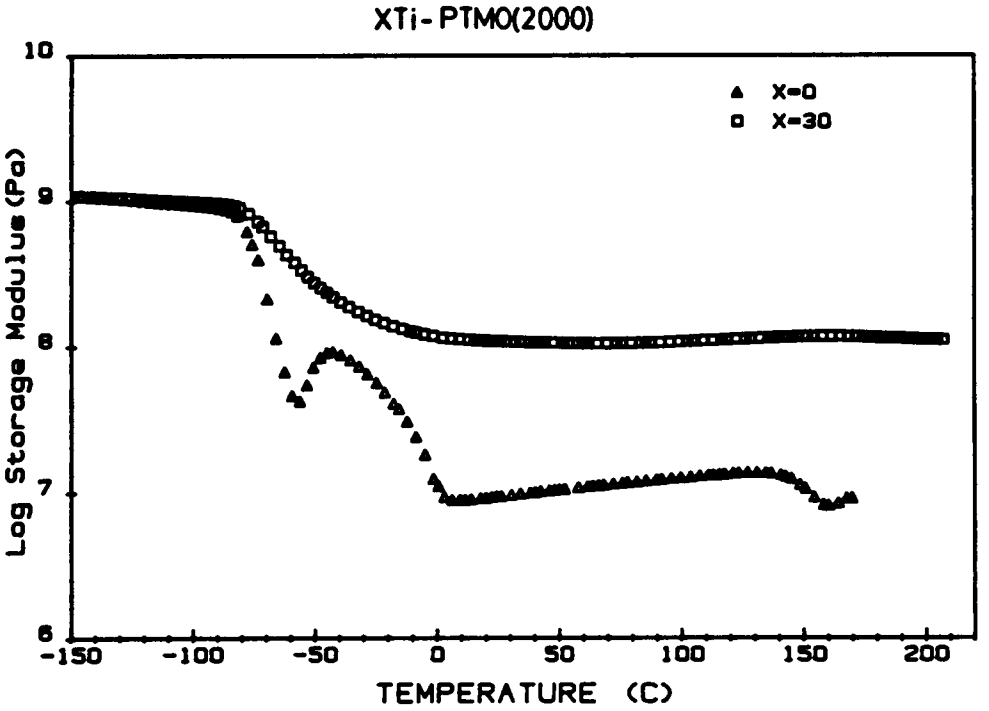

Figure 45. Storage modulus curves of 0Ti-47PTMO(2000) and 30Ti-50PTMO(2000) modified sol-gel materials: (triangles) 0Ti-47PTMO(2000), (squares) 30Ti-50PTMO(2000)

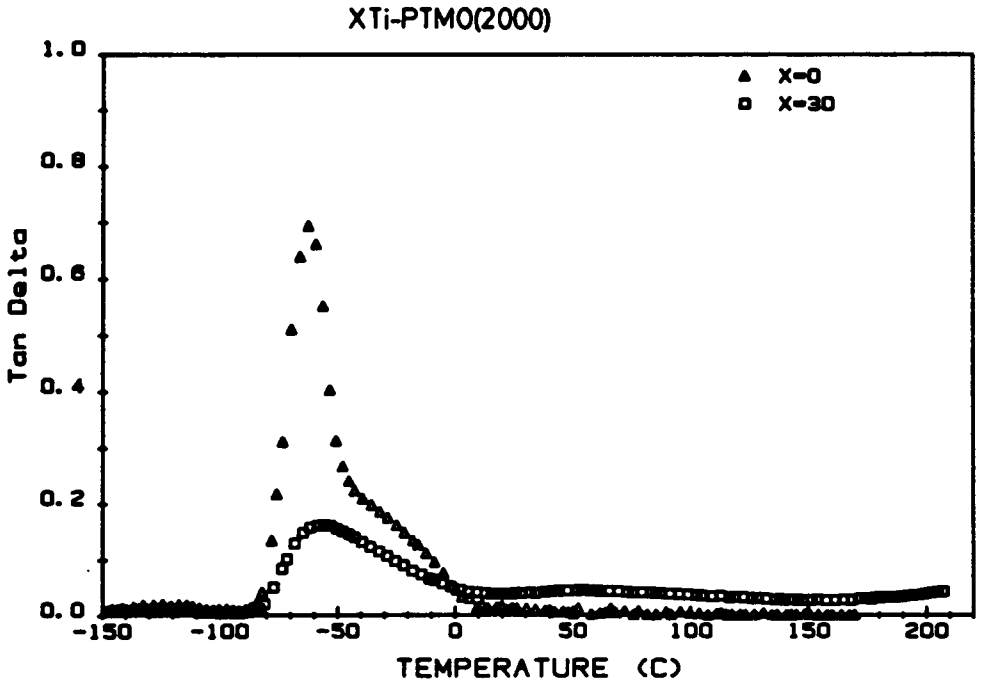

Figure 46. Tanδ curves of 0Ti-47PTMO(2000) and 30Ti-50PTMO(2000) modified sol-gel materials: (triangles) 0Ti-47PTMO(2000), (squares) 30Ti-50PTMO(2000)

Table 16. Tensile properties of Ti containing PTMO(2000) modified sol-gel materials

sample	days at 22°C	elongation at break (%)	ultimate strength (MPa)	Young's modulus (MPa)
50TEOS-50PTMO(2000)0.04*	--	104±13	1.6±0.7	2.4±0.6
0Ti-47PTMO(2000)†	14	17±5	1.0±0.2	6.9±0.5
15Ti-50PTMO(2000)	6	135±33	11±2	22±2
15Ti-50PTMO(2000)†	107	68±13	15.2&pm1.6	54.3±3.9
30Ti-50PTMO(2000)	26	57±10	10.9±0.9	67.0±0.2
30Ti-50PTMO(2000)‡	15	61±14	12.0±0.2	71±10
30Ti-50PTMO(2000)†‡	131	50.3±2.3	15.8±0.3	77±13

*data from reference [20]
†sample shown in Figure 44 on page 176
‡turbid samples (different reaction batch)

lieved to be due to the nature of the network formed under the different reaction conditions. The material made using the modified reaction scheme could be argued to have a more completely developed network because of the higher initial modulus and lower elongation at break. It should be noted, though, that the values of ultimate stress and initial modulus for both materials are of the same order of magnitude. Therefore, the differences between the network structures formed by the two reaction schemes are viewed as rather small in significance. The addition of titanium to the system, however, introduces drastic changes in the hybrid network structure as is evidenced primarily by the much larger observed values for stress at break and initial modulus. The addition of 15wt% $Ti(i\text{-}pr)_4$ to the reaction mixture results in an increase in the ultimate stress of greater than an order of magnitude, a three-fold increase in the elongation at break and almost an order of magnitude increase in the initial modulus as compared to the 0Ti-47PTMO(2000) gel. The upward trend in the mechanical properties, however, is continued only for the initial modulus which increases by approximately 50% (from $\simeq$54 to$\simeq$77 MPa) when the $Ti(i\text{-}pr)_4$ content is further increased from 15 to 30wt%. The comparable (in age) 30Ti-50PTMO(2000) material showed a slight decrease in elongation at break as compared to the 15Ti-50PTMO(2000) material ($\sim$50% vs $\sim$68%) while the ultimate stress remained approximately the same ($\simeq$15 MPa). The initial modulus value for the 30Ti-50PTMO(2000) material is over one order of magnitude greater than observed for either the 0Ti-47PTMO(2000) or the 50TEOS-50PTMO(2000)0.04 material. Obviously the addition of $Ti(i\text{-}pr)_4$ is strongly influencing the final gel structure in these hybrid materials.

It has been reported that Ti catalyzes the polycondensation reaction in the sol-gel scheme [4, 5]. This has been observed to be the case. The 0Ti-47PTMO(2000) composition took several days to gel after casting unlike the $Ti(i\text{-}pr)_4$ containing compositions which all gelled within one day. A catalytic effect could explain the large changes in the mechanical properties observed on initial addition of $Ti(i\text{-}pr)_4$ (see Figure 44 or Figure 45). In the presence of a condensation catalyst, the network forming step-growth polymerization might be "less hindered" by vitrification. In other words, since the energy barrier for condensation is lowered by the catalyst, neighboring silanol functions condense more readily in the presence

of a catalyst. Therefore, since vitrification limits the diffusion process (reactive groups come in contact less often), the extent of the condensation reaction for catalyzed systems (materials containing Ti) could go to higher degrees of conversion than that of uncatalyzed systems. A "tighter" better developed oxide network would, logically, result in higher moduli, ultimate stress and lower elongations to break. Also, since the titanium acts as a catalyst, the initial addition would have the greatest effect on the reaction; further addition, however, may not be as effective in changing the structure and, hence, the mechanical properties of the overall material. In short, initial addition of titanium would be expected to produce the largest change in the structure and, therefore, the mechanical properties while further addition of titanium would result in less significant changes. Again, this model, though attractive in explaining the observed mechanical behavior, is still highly speculative and needs to be substantiated or disproven by structural analysis and determination of the extent of reaction of the titanium containing materials.

6.3.4 Morphology

Unlike the PDMS(1700) modified sol-gel systems which do not exhibit peaks in their SAXS profiles [17], PTMO(2000) modified sol-gel systems exhibit peaks in their SAXS profiles. The peaks observed in the scattering profiles indicate that a certain degree of microphase separation exists in these materials [18, 20]. Furthermore, the estimated "d spacing" or "correlation length" between the two phases, approximated by taking the inverse of the scattering vector s at which the SAXS peaks were centered, was on the order of 10nm. The SAXS profiles of 50TEOS-50PTMO(2000) sol-gel materials display a broad peak in the plot of smeared intensity vs the scattering vector, s ($s = 2 \sin \theta/\lambda$ where λ is the wavelength and θ is 1/2 the radial scattering angle) [20].

The distinctly lower glass transition temperatures observed in the tanδ curves of Ti-50PTMO(2000) hybrids as opposed to the pure TEOS-PTMO hybrids (Figure 43) are indic-

ative of structural differences brought on by titanium incorporation. Since the glass transition is lowered in the $Ti(i\text{-}pr)_4$ containing materials, closer to the transition temperature of the pure PTMO material, it could be argued that the titanium containing gels are less homogeneously mixed: i.e. there are PTMO rich "phases" in the titanium containing systems which would give rise to a T_g nearer to that of the pure PTMO oligomer. Such a difference in phase separation should be discernible in the SAXS profiles of the hybrid materials, especially since the two potential phases, PTMO and SiO_2, are chemically dissimilar (which should give rise to an observable electron density contrast).

Figure 47 on page 185 shows the SAXS profiles of the Ti-PTMO(2000) sol-gel materials as a function of $Ti(i\text{-}pr)_4$ content (the 0% Ti data taken from ref. [20] is for a 50TEOS-50PTMO(2000)0.04. gel). The increase in the scattering intensity observed as $Ti(i\text{-}pr)_4$ is incorporated into the materials can be explained in terms of an increase in the relative electron density difference between the network "phase" and the polymer "phase". This is expected due to the inherent electron density difference between SiO_2 and TiO_2 and, possibly, a higher degree of completion of the metal-oxide network in the Ti containing materials. The result, therefore, would be a greater difference in electron density between the Ti containing phase and the "PTMO rich" phase and hence higher scattering intensity. The most notable feature of Figure 47 is that the SAXS peaks for all of the materials are centered at the same value of s: $s \simeq 0.11\ nm^{-1}$. The SAXS peak at $s \simeq 0.11 nm^{-1}$ implies a correlation length of 9.1 nm between phases of the same electron density in the sample [18, 20]. The fact that all of the materials in Figure 47 show SAXS peaks at nearly this same value, $s \simeq 0.11 nm^{-1}$, indicates that the general character of the microphase separation is the same in all of the materials, i.e., $Ti(i\text{-}pr)_4$ incorporation does not appear to change the structural features of the sol-gel material in the ~10nm size range. Additionally, the HCl catalyzed procedure produces a structurally similar material to that made by the CCC procedure provided $Ti(i\text{-}pr)_4$ is added (the SAXS profile of 0Ti-47PTMO(2000) contains a peak at $s \simeq 0.9 nm^{-1}$ - data not shown). Increasing the titania content of the hybrid sol-gel material must result in "subtler" changes in structure.

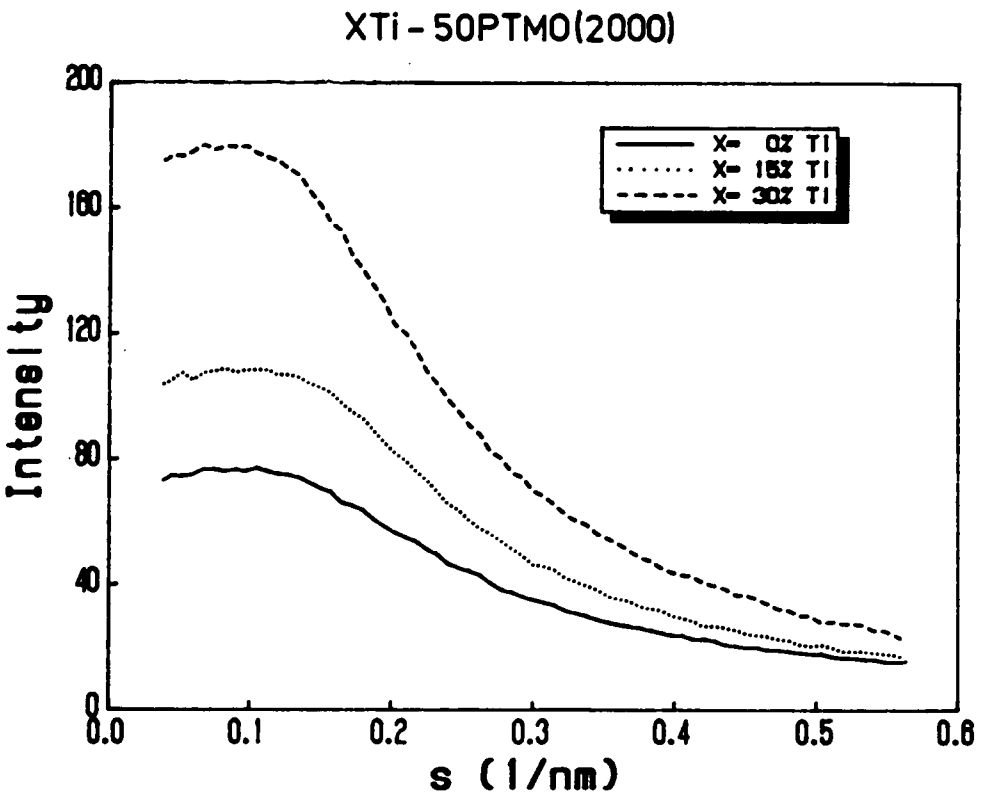

Figure 47. SAXS profiles of Ti containing PTMO(2000) modified sol-gel materials

PTMO(2000) in its pure state can crystallize as can the higher molecular weight PTMO(2900). The potential for crystallization brings concerns about the analysis of the low temperature end (≤0°C) of the dynamic mechanical spectrum. Crystalline PTMO oligomers could exist below those temperatures which would interfere with the interpretation of the thermo-mechanical spectra of the PTMO modified sol-gel materials. The presence of crystalline components generally lessen the magnitude of the storage modulus drop and mask the T_g transition in the tanδ curve as well (see Figure 48 on page 187 for example of this behavior). At the melting point, however, a sharp drop in the storage modulus should be observed accompanied by a rise in the tanδ curve (as the crystals melt, mechanical energy is "lost" hence the rise in tanδ). This type of behavior is displayed in the -50 to 0°C region of the storage modulus curve of the 0Ti-47PTMO(2000) gel (Figure 45), it can also be seen in the 0 to 25°C region of the dynamic mechanical spectrum of the 0Ti-50PTMO(2900) gel given in Figure 48 on page 187. In this figure, the dynamic mechanical behavior of a 0Ti-50PTMO(2900) gel (aged 34 days) is compared to that of a 30Ti-50PTMO(2900) gel (aged 204 days) to demonstrate the dramatic change brought about by incorporation of $Ti(i\text{-}pr)_4$. In the 0Ti-47PTMO(2000) sol-gel material the PTMO component melted below room temperature (based on storage modulus given in Figure 45 on page 178). Therefore, the PTMO(2000) in the sol-gel matrix had to crystallize while between the T_g (~-80°C) and the melting temperature (~0°C) as evidenced in the storage modulus (triangles) presented earlier in Figure 45. The comparable 0Ti-50PTMO(2900) material, however, does not melt until ~25° as evidenced by the storage modulus curve (triangles) given in Figure 48 on page 187. The higher melting temperature, relative to the PTMO(2000) material, allowed the use of WAXS at room temperature (~22°C) to determine whether or not crystalline PTMO(2900) was present in sol-gel materials.

Figure 49 on page 188 contains the WAXS patterns obtained for the two materials shown in Figure 48. The pattern for the 0 wt% $Ti(i\text{-}pr)_4$ material (a) shows two sharp crystalline rings along with an amorphous halo while the pattern for the 30 wt% $Ti(i\text{-}pr)_4$ (b) only displays an amorphous halo. This is clear proof that the 0Ti-PTMO(2900) sol-gel material is crystalline and

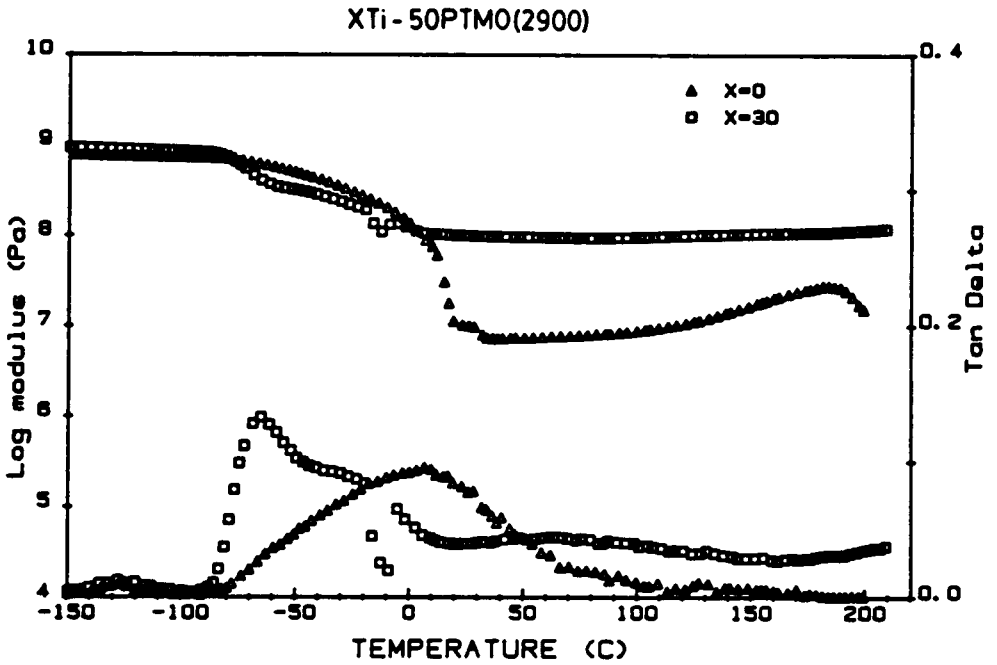

Figure 48. Dynamic-mechanical spectra of 0Ti-50PTMO(2900) and 30Ti-50PTMO(2900) sol-gel materials: (triangles) 0Ti-50PTMO(2900), (squares) 30Ti-50PTMO(2900)

is structurally different than the $Ti(i\text{-}pr)_4$ containing materials. The long time required for the 0 wt% $Ti(i\text{-}pr)_4$ compositions to gel must allow these systems to phase separate into larger more homogeneous domains that would, in turn, allow the PTMO oligomers to crystallize. Indeed, the SAXS profile (not shown) of the 0Ti-47PTMO(2000) gel is shifted to a lower value of s. This, in turn, indicates a larger correlation distance which translates into larger or better phase separated domains as compared to the $Ti(i\text{-}pr)_4$ containing materials or those made using the "standard" CERAMER procedure.

Ti-PTMO(2000) and Ti-PTMO(2900) hybrid sol-gel materials afforded a unique opportunity to observe morphological changes in the light scattering size regime ($\simeq 10^{-5} - 10^{-3}$cm). Though the majority of the hybrid PTMO gel compositions prepared were transparent with only a slightly yellowish color, a number of the 30 wt% $Ti(i\text{-}pr)_4$ gels were observed to be turbid. In particular, the 30Ti-50PTMO(2900) materials all were turbid while the 30Ti-50PTMO(2000) materials were found to form turbid or clear gels depending on when they were first exposed to the open atmosphere. Clear gels were formed when the 30Ti-50PTMO(2000) mixtures were left covered for a prolonged period after gelling ($\simeq$ 1 week or more), otherwise the gels were all observed to be turbid. The tensile properties stress-strain properties, in particular the initial modulus, of the turbid gels were slightly higher than for the clear gels (see Table 16 on page 180) As was the case for the multifunctional materials presented in Chapter IV, turbidity in the PTMO hybrid materials was suspected to be caused by morphological structures large enough to scatter visible light. Specimens from clear and turbid films were therefore prepared for study by SEM according to the procedures outlined in Chapter III section 3.4.6 in hope of correlating turbidity with observed structures (if any are observed).

Figure 50 on page 190 contains the scanning electron micrographs obtained for two 30Ti-50PTMO(2000) gels, one turbid (a) & (c) the other clear (b) & (d). Micrographs (a) and (b) are of the undisturbed surfaces of the respective gelled films. Micrograph (a) of the turbid gel shows unmistakable structures on the order of 2-3μ while micrograph (b) of the clear gel shows no distinct structure on this size scale. The surface structure observed for the turbid gel, (a), is definitely in the size range to be able to scatter visible light and could, therefore,

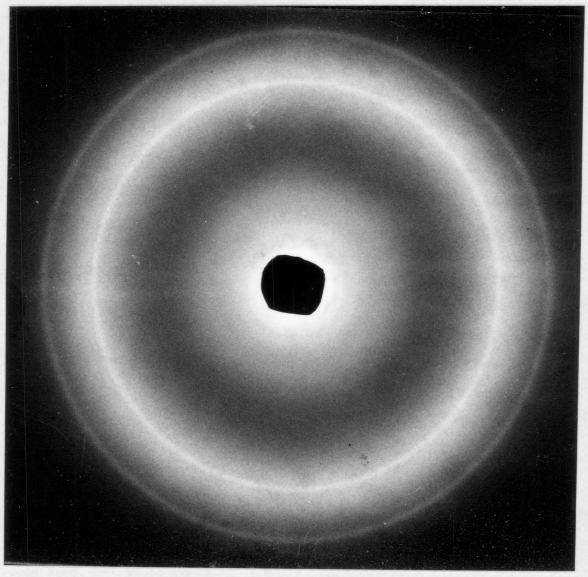

a)

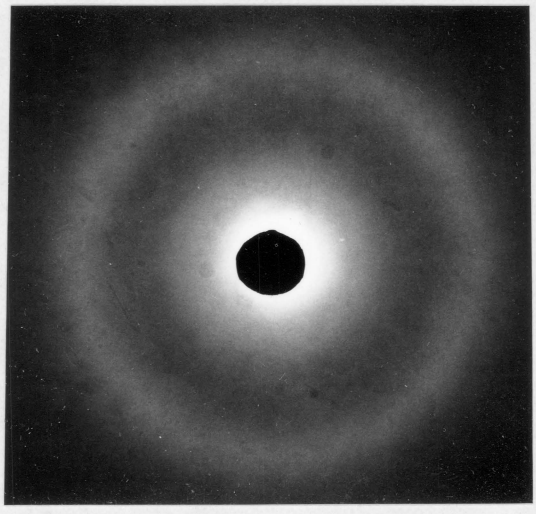

b)

Figure 49. WAXS patterns of 0Ti-50PTMO(2900) and 30Ti-50PTMO(2900): (a) 0Ti-50PTMO(2900), (b) 30Ti-50PTMO(2900)

be the origin of the turbidity of the sample. The relatively featureless surface observed for the clear gel, (b), is in keeping with expectations; clear gels should not display structures capable of scattering visible light. Low magnification (173X & 174X) micrographs of the fracture surfaces for these same gels are also given in Figure 50 on page 190: (c) a 30Ti-50PTMO(2000) turbid gel and (d) a 30Ti-PTMO(2000) clear gel. Both of the fracture surfaces in these micrographs contain at least some evidence of ductile failure but the micrograph of the turbid gel, (c), contains some type of spherical structures as well. Higher magnifications of the fracture surfaces need to be examined, however, in order to be able to discern the nature of the apparent spherical structures in micrograph (c).

Figure 51 contains the micrographs obtained of the fracture surfaces of two clear and two turbid gel compositions: (a) 30Ti-50PTMO(2000) turbid, (b) 30Ti-50PTMO(2000) clear, (c) 30Ti-50PTMO(2900) turbid and (d) 15Ti-50PTMO(2000) clear. These micrographs simultaneously show the fracture surfaces at relatively low magnification, 240-247X, and at higher magnification (8 times higher) with a "zoom" view of the highlighted area in the low magnification shot. The higher "zoom" magnification in Figure 51 allows better resolution of the microstructure while the low magnification portion gives a perspective of the fracture surface as a whole. Samples (a) and (b) correlate to the samples in Figure 50. Samples (c) and (d) are included to illustrate the generality of the structural effects observed in the 30Ti-50PTMO(2000) gels. Observed in both the low and high magnification micrographs of the two turbid gels, (a) & (c), are unmistakable sphere-like microstructures that seem to be interconnected; these structures are noticeably absent from the micrographs of the two clear gels (b) and (d). The presence or absence of these features is even more evident at higher magnifications. Figure 52 on page 193 contains micrographs for the same four fracture surfaces given in Figure 51 but at magnifications of 3,950-4,190X. The higher magnification in Figure 52 on page 193 allows the sphere-like structures observed in the turbid gels to be measured. Using the 10μ bar at the top of each micrograph as a reference, the sphere-like structures observed in micrographs (a) and (c) were determined to be 2-3μ in size. The size measured for the bulk microstructure matches that measured for the surface structures ob-

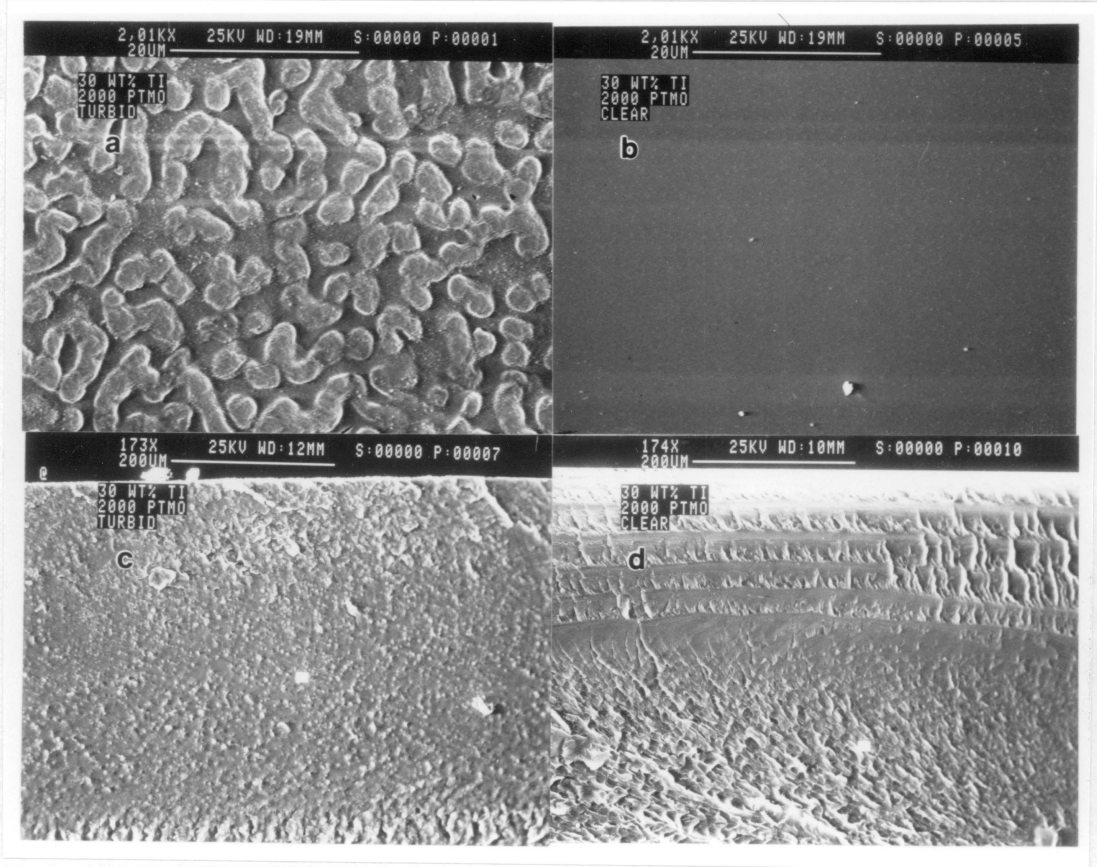

Figure 50. Scanning electron micrographs of clear and turbid 30Ti-PTMO(2900) sol-gel films: (a) turbid 30Ti-PTMO(2000), mag. = 2,010X, (b) clear 30Ti-PTMO(2000), mag. = 2,010X, (c) turbid 30Ti-PTMO(2000), mag. = 173X, (d) clear 30Ti-PTMO(2000), mag. = 174X

served in micrograph (a) of the 30Ti-50PTMO(2000) gel given in Figure 50. Moreover, the interconnected nature of the superstructure observed in the fracture surfaces of the bulk indicate strongly that the bulk microstructures are the same as those observed on the surface of the turbid PTMO(2000) gel.

Interconnected sphere-like microstructures, such as those observed in the scanning electron micrographs presented, are undoubtedly the cause of the turbidity observed in certain gelled materials. These structures could also be the reason the turbid gels have a slightly but significantly higher modulus and ultimate stress than the clear gels (see data for 30Ti-50PTMO(2000) gels in Table 16 on page 180). The formation of this microstructure correlates to either the $Ti(i\text{-}pr)_4$ loading and/or the drying process; gels containing 15 wt% $Ti(i\text{-}pr)_4$ were clear and their micrographs did not contain any sphere-like microstructure. On the other hand, 30 wt% $Ti(i\text{-}pr)_4$ gels made with PTMO(2900) were always turbid while the gels made with PTMO(2000) were not always turbid but could be clear when allowed to "age" in a covered container after gelation. In any case, the sphere-like microstructure was always observed in the micrographs of the turbid samples studied but was always missing in the micrographs of clear materials. Furthermore, the sphere-like microstructure appeared interconnected and permeated the entire sample being present in the bulk as well as the surface.

Extraction and swelling experiments carried out on three Ti-PTMO(2900) sol-gel materials show no distictions between the turbid and non-turbid gels except in the case of the 0Ti-50PTMO(2900) material which, as expected, behaved differently than either the 15Ti-50PTMO(2900) or the 30Ti-50PTMO(2900) materials. Table 17 on page 195 contains the results of the extraction and swelling experiments carried out on the hybrid PTMO(2900) sol-gel materials according to the procedures outlined in Chapter III sections 3.3.4 and 3.3.5. Both of the $Ti(i\text{-}pr)_4$ containing gels showed a significantly lower amount of extracted materials (0.5 & 1.4 wt% vs 6.1 wt%) as well as displaying lower levels of solvent uptake (92 & 86 wt% vs 114 wt%). The lowered level of extractable material would be consistent with a higher degree of conversion expected for the Ti containing gels while the lower level of solvent uptake would indicate a higher degree of crosslinking further emphasizing this point.

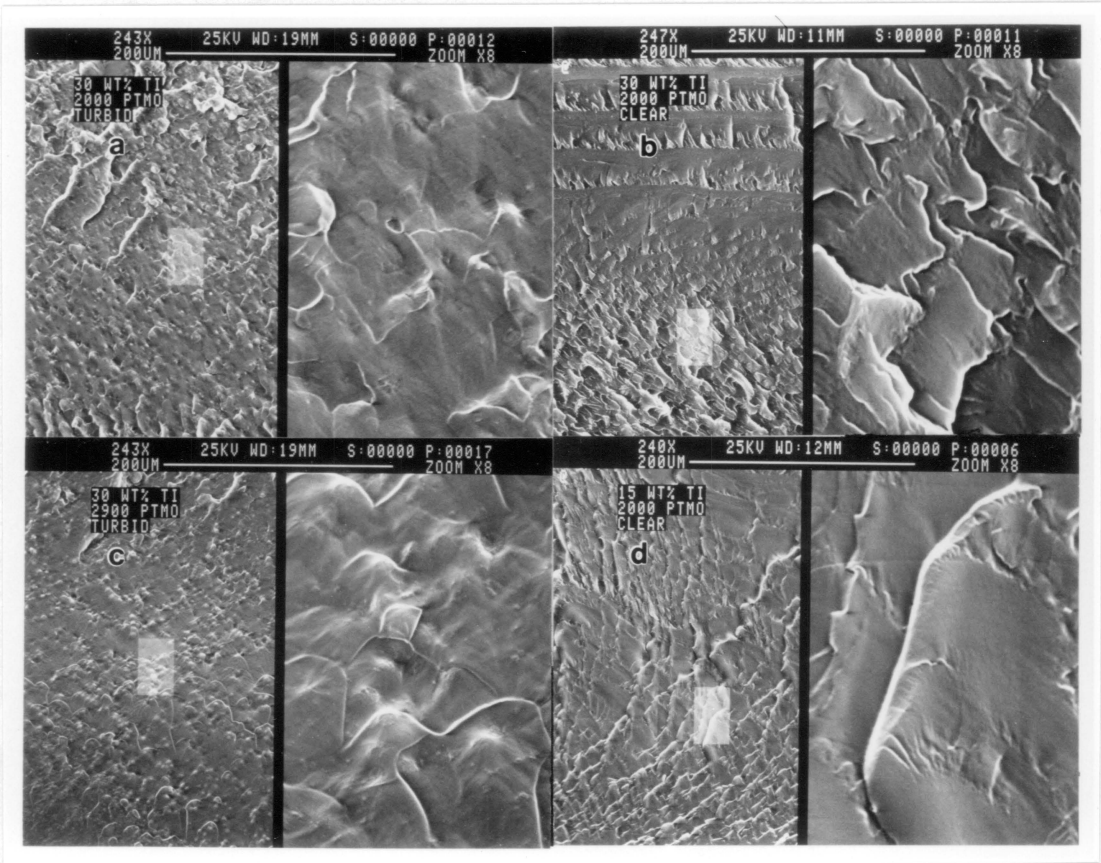

Figure 51. Scanning electron micrographs of clear and turbid Ti containing PTMO modified sol-gel films: (a) turbid 30Ti-PTMO(2000), mag.=243X & 1,944X, (b) clear 30Ti-PTMO(2000), mag.=247X & 1976X, (c) turbid 30Ti-PTMO(2900), mag.=243X & 1944X, (d) clear 15Ti-PTMO(2000),mag.=240X & 1920X

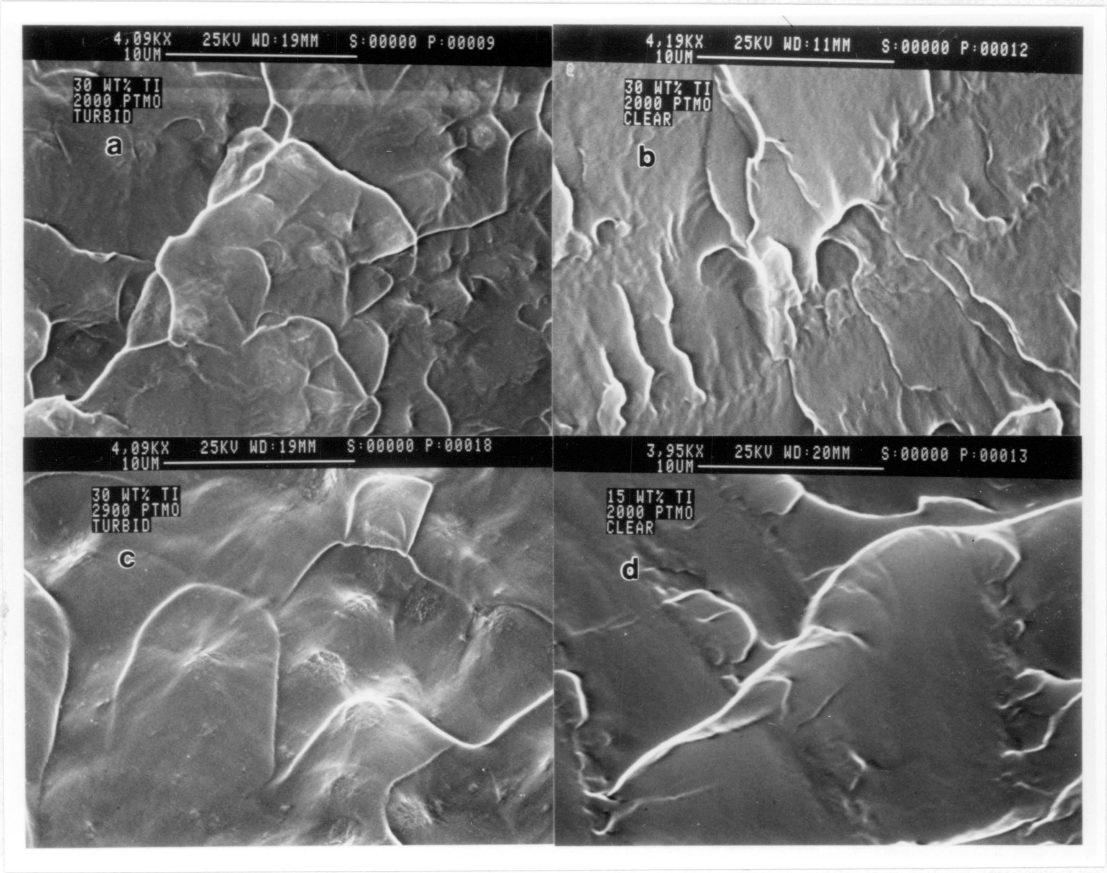

Figure 52. Scanning electron micrographs of clear and turbid Ti containing PTMO modified sol-gel films: (a) turbid 30Ti-PTMO(2000), mag. = 4,090X, (b) clear 30Ti-PTMO(2000), mag. = 4,190X, (c) turbid 30Ti-PTMO(2900), mag. = 4,090X, (d) clear 15Ti-PTMO(2000), mag. = 3,950X

Table 17. Extraction and swelling behavior of Ti containing PTMO(2900) modified sol-gel materials in THF

sample	age*	extraction wt% loss	swelling wt% uptake†
0Ti-50PTMO(2900)	>6Mo	6.1	114
15Ti-50PTMO(2900)	>6Mo	1.4	86
30Ti-50PTMO(2900)	>6Mo	0.5	92

*elapsed time between gelation and extraction (stored at ~22°C)
†measured after 60 hours in THF at 20±2°C

6.3.5 *Aging Effects on Properties*

TEOS-PDMS(1700) hybrid sol-gel materials have demonstrated long time stability under ambient conditions [17]. However, unlike the TEOS-PDMS materials, TEOS-PTMO sol-gel materials change with time after gelation (note: data presented for comparison, up to this point, are for samples of similar age). Long-term aging (over several weeks) of TEOS-PTMO materials under ambient conditions has been shown to result in an increase in the observed initial modulus and stress at break of as much as 700% and 100% respectively with a corresponding tenfold decrease in the observed elongation at break [18, 20].

The dramatic long-term aging observed in materials made using an HCl catalyst and a given quantity of water does not seem to be as significant in the Ti-PTMO(2000) materials presented to date. The limited stress-strain data obtained for the 30Ti-50PTMO(2000) gels indicate that at least after 15 days at ~22°C no changes in mechanical properties are observed (recall Table 16). Moreover, using initial modulus as the primary indicator, stress-strain obtained data for the 15Ti-50PTMO(2000) gels implies that the largest observed changes in the mechanical properties occurs during the first two weeks after gelation. The aging phenomenon seems to be more dramatic for materials without titanium as opposed to those with titanium incorporated into the TEOS based network.

Table 18 on page 197 contains mechanical data obtained for 15Ti-50PTMO(2900) and 30Ti-50PTMO(2900) sol-gels as a function of time at ~22°C after gelation. The 15Ti-50PTMO(2900) material 4 days after gelation has reached ~43% of the initial modulus value observed for samples aged 60 days. After 6 days the 15Ti-50PTMO(2900) composition has reached its full potential in terms of the so-called "ultimate properties" (ultimate stress and ultimate elongation) but is still at ~43% of the initial modulus observed for mature samples. After 13 days at 22°C the 15 wt% $Ti(i\text{-}pr)_4$ containing gels have attained 57% of their potential initial modulus while the ultimate properties have begun to erode, the elongation at break shrinking most noticeably. After 20 days at 22°C the gels have "finished aging"; no

further major changes are observed in the mechanical properties on aging to 60 days. The corresponding 30Ti-50PTMO(2900) gels show much the same behavior as a function of time, the stress-strain data in Table 18 on page 197 illustrates this point. After three days the 30 wt% $Ti(i\text{-}pr)_4$ containing sol-gels have reached ~30% of their potential initial modulus, after 7 days ~75%. The ultimate stress, in the meantime, continues to increase between 3 and 30 days, going from ~6 to ~14 MPa while the ultimate strain remains relatively constant at ~110%. Aging the 30Ti-50PTMO(2900) gels from 30 to 105 days at 22°C produces no significant changes in the initial modulus but does result in a decay of the ultimate properties: ultimate stress decreases slightly from .~14 to ~14 MPa and the ultimate strain decreases dramatically from ~110 to ~58%.

Figure 53 on page 198 contains representative stress-strain curves for the 30Ti-50PTMO(2900) gels listed in Table 18. It is interesting to note that the nature of the stress-strain curves does not change as a function of age though the initial modulus and ultimate stress and strain do. All four curves given in Figure 53 show a relatively steep initial modulus that gently bends over to give another linear region which extends to the break point. The greatest difference is observed on aging the samples from 3 to 7 days. After 33 days at ~22°C the initial stress-strain behavior of the 30Ti-50PTMO(2900) materials is established; continued aging effects only the ultimate properties (also demonstrated by the data in Table 18).

The initial modulus of network materials is well known to be a function of the crosslink density: higher crosslink densities translate into higher values of initial modulus. Furthermore, since the sol-gel process is actually a crosslinking process and since initial modulus of the $Ti(i\text{-}pr)_4$ containing PTMO modified materials increases for a short period of time after gelation, "initial aging" effects observed during the first two weeks after gelation can be attributed to a continuation of the sol-gel process. Such an aging process would not be expected to change the nature of the microphase separation in the hybrid materials, the correlation distance in the SAXS experiment should remain unchanged. Rather, a post-gel continuation of the sol-gel process would be expected to increase the density of the inorganic oxides hence

Table 18. Tensile properties of Ti containing PTMO(2900) modified sol-gel materials

sample	days at 22°C	elongation at break (%)	ultimate strength (MPa)	Young's modulus (MPa)
15Ti-50PTMO(2900)	4	70±20	6.1±0.9	23±2
15Ti-50PTMO(2900)	6	130±10	13.7±0.8	23.4±0.8
15Ti-50PTMO(2900)	13	88±3	12.5±0.8	30±3
15Ti-50PTMO(2900)	20	60±7	11.8±1.0	54±6
15Ti-50PTMO(2900	60	49±6	11.7±1.0	52±2
30Ti-50PTMO(2900)	3	108±18	5.8±0.4	20.4±0.8
30Ti-50PTMO(2900)	7	113±4	10.8±0.3	49±4
30Ti-50PTMO(2900)	33	109±6	14.1±0.4	65±2
30Ti-50PTMO(2900)	105	58±5	12.7±0.6	64±8

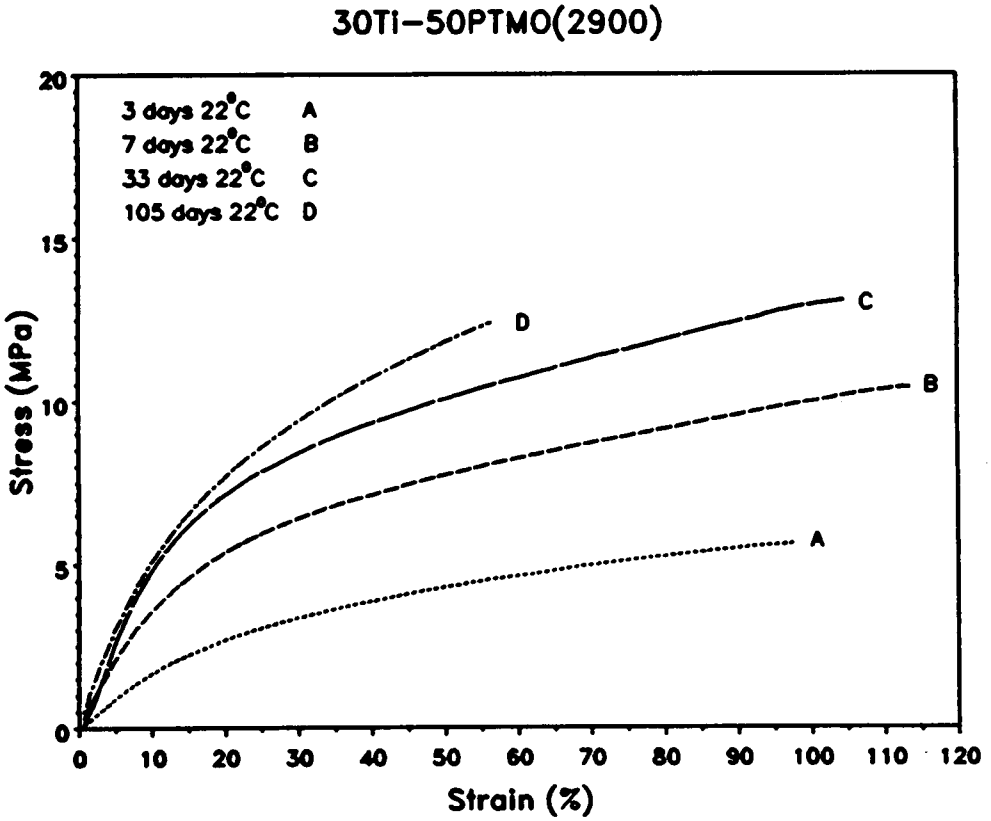

Figure 53. Stress-strain curves of Ti containing PTMO(2900) modified sol-gel materials vs age: aged at ~22°C after casting for: (A) 3 days, (B) 7days, (C) 33 days, (D) 105 days

increase the electron density of these components. An increase in the electron density of one component in a two phase system should, in turn, be observed as an increase in the measured scattering intensity of the SAXS experiment: i. e. a higher intensity peak in the SAXS profile of an aged sample relative to a fresh gel. Such and increase in scattering intensity has been observed for TEOS-PTMO systems [18, 20] and is borne out in Figure 54 for the 30Ti-50PTMO(2900) materials aged in the time period of interest (first two weeks after gelation). The 17 day sample in Figure 54 shows a higher scattering intensity but the same correlation distance as its younger 5 day counterpart.

The changes observed at long times (~100 days) for the ultimate properties of the PTMO modified sol-gels are most likely due to depolymerization of the PTMO polymer. Ultimate properties are very sensitive to minor defects in the material matrix. Any flaws contained in the structure of a material will cause the observed stress at break and strain at break to decrease relative to a comparable material with a flawless structure. Since the ultimate properties of the PTMO hybrid sol-gels were observed to decay with time, this would indicate that flaws or defects are formed in the material matrix with age. This explanation seems to be most plausible, especially in light of the fact that PTMO polymers are susceptible to depolymerization [115] and no stabilizers were added to our materials; the PTMO used was pure. The overall aging "phenomenon" as observed for PTMO(2000) and PTMO(2900) containing sol-gel materials is, more than likely, a post gelation continuation of the sol-gel process coupled with depolymerization of the oligomers occurring at long times.

6.4 Ti Containing Multifunctional PTMO Systems

Ti containing multifunctional PTMO modified sol-gel materials were prepared according to the procedure detailed in Chapter III section 3.3.2. The $Ti(i\text{-}pr)_4$ containing multifunctional PTMO sol-gel systems gelled within one day and formed films that were monolithic. As has

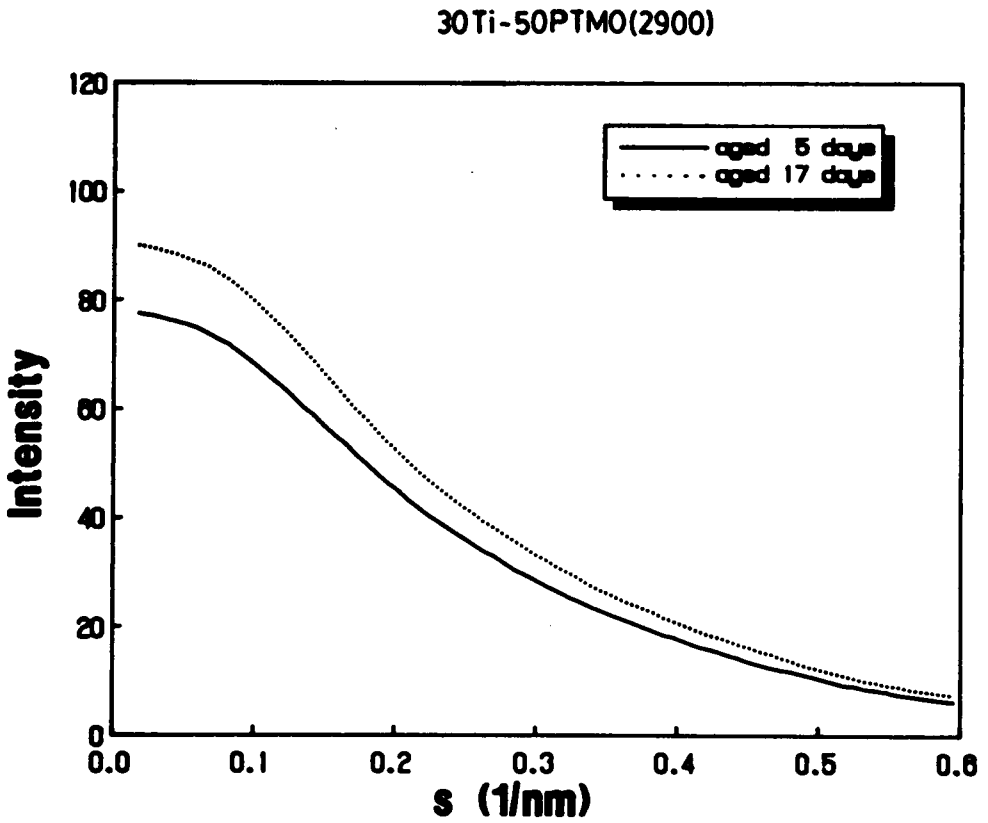

Figure 54. SAXS profiles of 30Ti-50PTMO(2900) sol-gels aged at ~22°C for 5 and 17 days

been observed for all materials incorporating $Ti(i\text{-}pr)_4$, the multifunctional PTMO materials were yellow in color. The 15 wt% $Ti(i\text{-}pr)_4$ compositions were transparent but the 30 wt% $Ti(i\text{-}pr)_4$ compositions were generally opaque. The starting reaction mixture and final gel compositions of the multifunctional hybrid materials are given earlier in Table 15. Since the multifunctional PTMO polymers are of similar molecular weight, Mn~5575-5763 (see Table 2 on page 59), the hybrid gels formed from these materials made it possible to observe the effects of branching on a number of physical properties. Detailed studies of the effect of acid, water, and TEOS loading on multifunctional PTMO hybrids have been reported elsewhere [20]; in this section, the mechanical properties and the gelling behavior of Ti containing multifunctional PTMO systems will be reported.

6.4.1 Mechanical Properties

Figure 55 on page 203 and Figure 56 on page 204 show the stress-strain curves of hybrid sol-gels made using 15 and 30 wt% $Ti(i\text{-}pr)_4$ and each of the four different multifunctional PTMO polymers: (A) PTMO(5), (B) PTMO(4), (C) PTMO(3) and (D) PTMO(2). The curves given in these two figures are for well aged samples so that the differences observed are due to the modifying polymer and not the relative age of the material.

The stress-strain curves of the 15 wt% $Ti(i\text{-}pr)_4$ composition gels in Figure 55 exhibit a similar steep initial slope (indicating a high Young's modulus) and, with the possible exception of the linear PTMO(2) gel, they all display a yield point before ~6% strain at a yield stress of ~18-23 MPa. A case could be made that the PTMO(2) gel also displays yielding behavior because of the sharp bend observed in the stress-strain curve at ~6% and ~19MPa. Nonetheless, the four materials are remarkably similar in their tensile behavior below 25% strain despite significant differences in the number of crosslinkable sites per polymer chain. Ignoring the ultimate properties (they may be influenced by oxidation of the PTMO polymer), at greater than 50% strain the differences in the observed stress levels for the four gels falls as

expected; namely, the material with the highest number of crosslinkable triethoxysilane functions, PTMO(5), displays the greatest stress level and the next highest material, PTMO(4), finally exceeds the stress level of the two lower functionality gels: PTMO(3) and PTMO(2). Excluding the PTMO(4) gel, the stresses observed at any given strain in Figure 55 are in concert with the number of functional sites on the polymer chain.

Figure 56 gives the stress-strain curves corresponding to the 30 wt% $Ti(i\text{-}pr)_4$ composition gels. Unlike the 15 wt% $Ti(i\text{-}pr)_4$ gels, which were all similar in the early stages of the tensile experiment, the 30 wt% $Ti(i\text{-}pr)_4$ materials fall into two distinct groups. One group, PTMO(3) and PTMO(2), display similar initial slopes with both curves bending at ~5-10% strain (~8-12 MPa) without showing a true yield point. The other group, PTMO(5) and PTMO(4), display steeper initial slopes and show distinct yield points at ~5% strain at stress levels of 23-25 MPa. Both sets of curves continue increasing monotonically after the "yielding" region. A comparison of the the stress levels observed for the different gels at any given strain falls as expected. The highest "crosslinkable" material, PTMO(5), exhibits the highest stress levels followed, in order, by PTMO(4), PTMO(3) and finally PTMO(2). This result is intuitively satisfying although the large change in the stress levels between the PTMO(2)&(3) gels and the PTMO(4)&(5) gels is surprising and, at this point, unexplainable.

Figure 57 on page 205 gives the SAXS profiles of the 30 wt% $Ti(i\text{-}pr)_4$ gels shown in Figure 56 on page 204. Like the stress-strain curves, the SAXS profiles show the materials to fall into two distinct groups: PTMO(4)&(5) and PTMO(2)&(3). The peaks in the profiles become broadened and shift to lower values of s (smaller correlation distance) as the number of functional sites per chain is increased. It has been demonstrated, for TEOS-PTMO sol-gel systems, that the molecular weight of the modifying oligomer/polymer chain controls the correlation distance observed in the SAXS profiles of the hybrid materials [20]. Therefore, the shift to lower s values going from PTMO(2) to PTMO(5) is expected since the molecular weight between crosslinks shrinks as more crosslink sites are added to the chain. Furthermore, since the crosslink sites are added in a "random" fashion (see Figure 5 on page 63 for schematic), the molecular weight between crosslinks is disperse, or broadened, thereby causing

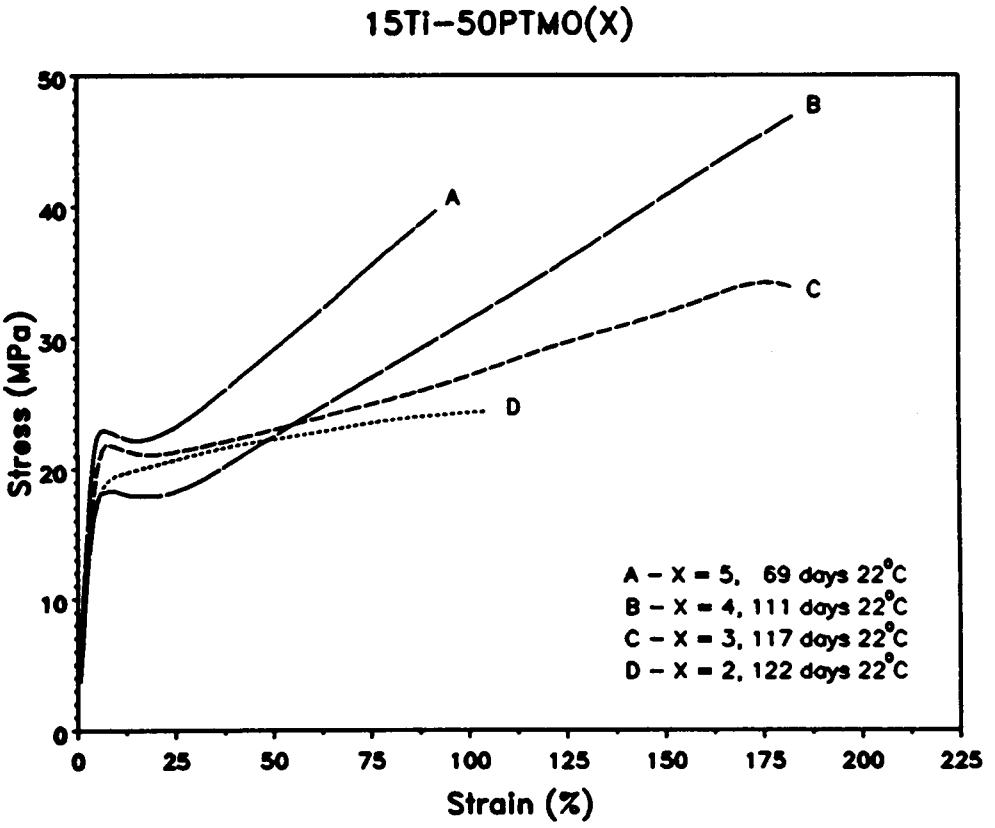

Figure 55. Stress-strain curves of 15Ti-PTMO(X) sol-gel materials: (A) X=5, (B) X=4, (C) X=3, (D) X=2

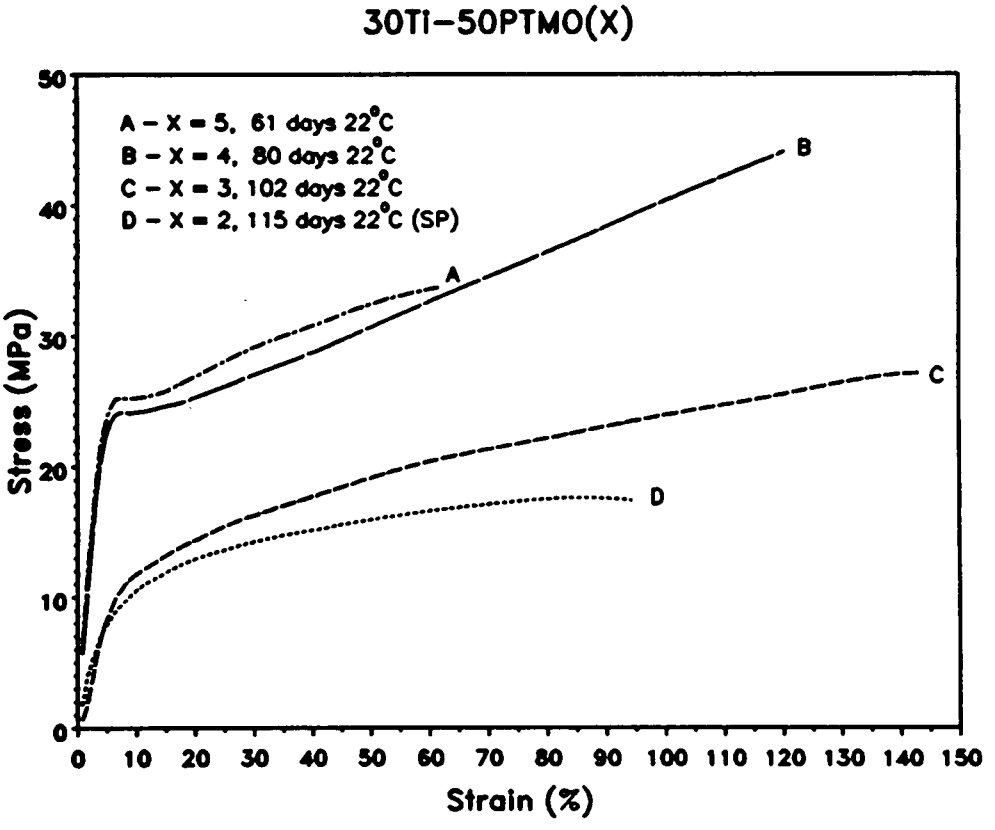

Figure 56. Stress-strain curves of 30Ti-PTMO(X) sol-gel materials: (A) X=5, (B) X=4, (C) X=3, (D) X=2

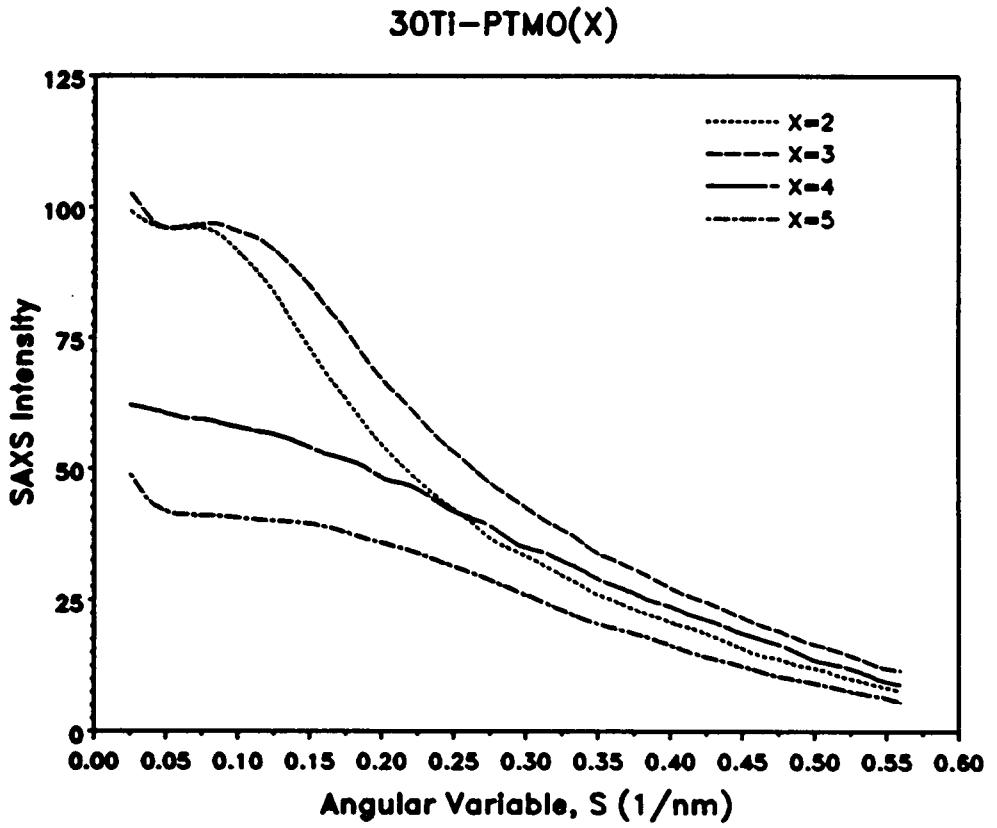

Figure 57. SAXS profiles of 30Ti-PTMO(X) sol-gel materials

the correlation distance between similar phases to also be disperse. Since the gels are all of similar chemical composition and are assumed to have reacted to the same degree of conversion, the difference in the observed scattering intensity between the PTMO(2)&(3) and PTMO(4)&(5) gels (Figure 57 on page 205) relates to the degree of phase separation in the two sets of materials. The higher scattering intensity observed for the 30Ti-PTMO(2)&(3) gels indicates that they are phase separated to a higher extent than the 30Ti-PTMO(4)&(5) gels: i. e. the 30Ti-PTMO(4)&(5) gels are more homogeneous than the 30Ti-PTMO(2)&(3) gels.

The SAXS data provides an explanation for the mechanical behavior observed in Figure 56. The continuous phase in the hybrid PTMO(X) materials, as for the other hybrid sol-gel materials, is the polymeric component. As such, the degree to which the inorganic oxide is dispersed throughout the material matrix will affect the mechanical behavior. Well dispersed oxide crosslinks would result in a stiff network by preventing relatively soft "PTMO-rich" phases from forming. A stiff material matrix with a well dispersed inorganic oxide crosslink would explain the high initial modulus and yielding behavior exhibited by the 30Ti-PTMO(4)&(5) gels in Figure 56 (or all of the gels in Figure 55 for that matter). The phase separated 30Ti-PTMO(2)&(3) materials undoubtedly contain soft "PTMO-rich" regions which would explain why they behave more like two-phase thermoplastic elastomers (low stresses and no yielding behavior) than do the other Ti-PTMO(X) materials.

6.4.2 Aging Effects on Properties

The mechanical data presented for the PTMO(X) hybrid materials (Figure 55 & Figure 56) was collected from aged samples to allow cross-comparison of materials independent of any aging effects. In this section aging effects on the mechanical behavior will be examined for each Ti-PTMO(X) composition. Specifically, the initial modulus and the dynamic mechanical behavior (when available) will be correlated to the age of various samples. Changes in the ultimate properties, stress at break and strain to break, with time will be tacitly

ignored as they are probably due to polymer depolymerization which is not of prime interest here.

Figure 58 contains the stress-strain curves for a 15Ti-50PTMO(2) sol-gel aged at ~22°C for 6 (C), 76(B) and 122 (A) days before testing. The curve for the 6 day old sample, (C), resembles that of a "lightly crosslinked" elastomer network; a low initial slope (Young's modulus) that gradually turns, beginning at ~6% strain and ~2 MPa stress, into a long flat almost horizontal plateau region where large strains are observed for small increases in stress. This type of stress-strain profile is consistent with that expected for an "immature" network formed by the gelled but incompletely reacted PTMO(2) system. After 76 days at ~22°C the material has changed significantly, the stress-strain curve (B) exhibits a steep initial slope (high Young's modulus) and a distinct yield point at ~6% strain and ~18 MPa stress. Past the yield point the stress increases almost monotonically with the strain until failure. Sample aged 122 days (A) before mechanical testing demonstrate essentially the same stress-strain behavior as those aged for 76 days (B) (see Figure 58), except for the ultimate properties which, undoubtedly, reflect the effects of PTMO depolymerization.

The dynamic mechanical spectra of 15Ti-50PTMO(2) gels aged for 6 (triangles) and 122 (squares) days at ~22°C are given in Figure 59 on page 210. The specimen that had been aged for 6 days prior to testing (triangles) demonstrates a drop in the storage modulus slightly greater than 1 order of magnitude that begins at roughly -60°C and bottoms out at ≃50°C; the corresponding tanδ curve contains a broad transition beginning at approximately -60°C that extends past 200°C. with a peak at ≃10°C. The sample that had been aged 122 days at ~22°C prior to testing (squares) displays a gradual drop of less than one order of magnitude in the storage modulus beginning at ~20°C. The tanδ curve for this specimen (squares in Figure 59 on page 210) displays a broad transition centered at ≃70°C that extends (asymmetrically) from ~ -30°C to 200+°C (note that the high end superimposes on the tanδ curve of the 6 day old sample).

Comparing the two sets of dynamic mechanical data reveals certain interesting differences. At room temperature (~22°) the 122 day old 15Ti-50PTMO(2) gel is vitrified whereas

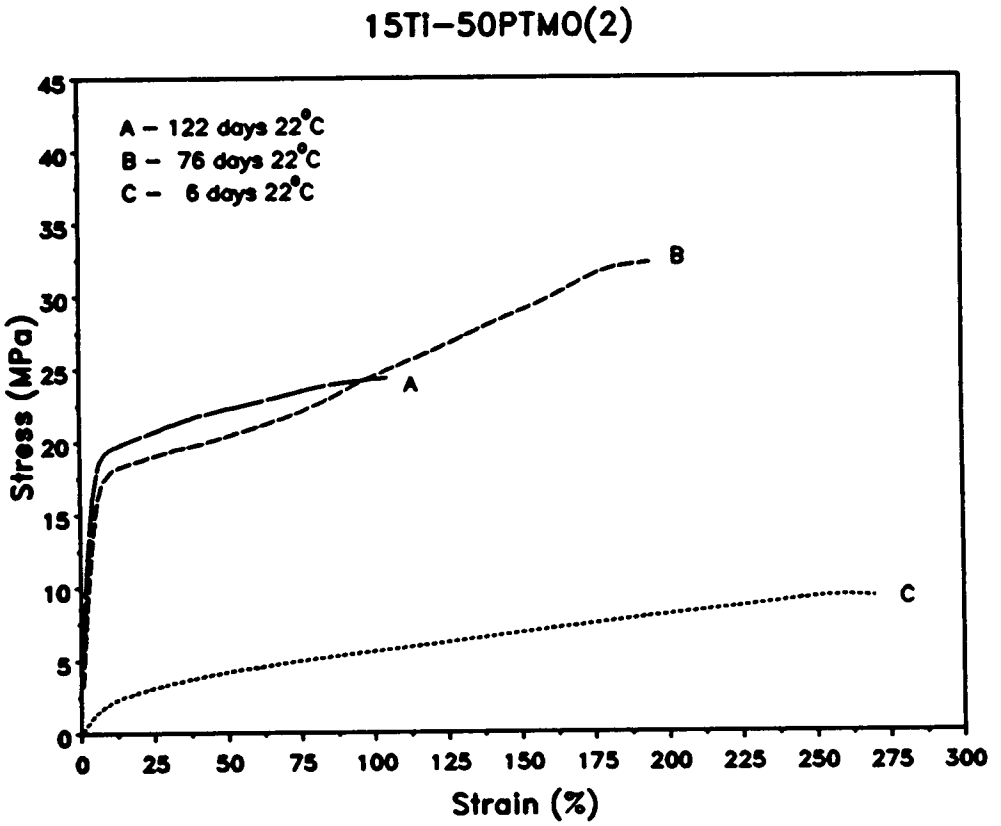

Figure 58. Stress-strain curves for 15Ti-50PTMO(2) gels vs age at ~22°C

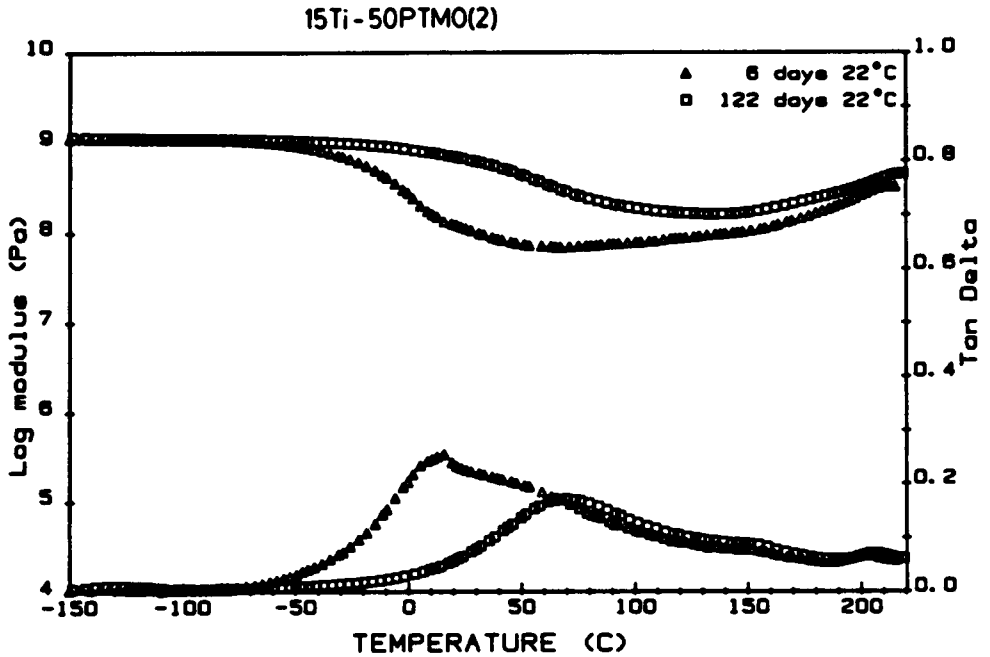

Figure 59. Dynamic mechanical spectra of 15Ti-50PTMO(2) gels vs age at ~22°C: (triangles) aged 6 days at ~22°C, (squares) aged 122 days at ~22°C

the 6 day old gel is past its glass transition temperature, T_g, as evidenced by the storage modulus curves. These differences are reflected in the stress-strain curves given in Figure 58 which were collected at 22±2°C. The 6 day old 15T-50PTMO(2) sample (C) behaves as an elastomer while the 122 day old 15Ti-50PTMO(2) sample behaves in the manner expected for a glassy material (i. e. high Young's modulus accompanied by yielding).

Figure 60 on page 212 contains the stress-strain curves for 30Ti-48PTMO(2) gels made by two slightly different procedures. The curves labelled "SP", or "standard procedure", are for gels made in exactly the same manner as all of the previously discussed gels. The curves labelled "LP", or "long procedure", are for gels that were made by refluxing the reaction mixture for 3 hours after the addition of the $Ti(i\text{-}pr)_4$ rather than the usual 1/2-2 hours ***or until the yellow color of the reaction mixture fades*** (this usually occurred within minutes after refluxing). Both of the LP gels, (D) and (E), display elastomeric behavior showing no yield point or "bend" in their stress-strain curves at all. The LP gels are clearly different from even the 14 day old SP gel (C) which not only exhibits a higher initial modulus but a distinct bend in the stress-strain curve at approximately 12% elongation and 6-8 MPa stress (see Figure 60). The additional time under refluxing undoubtedly allowed the inorganic oxide components in the LP gels to react to a higher degree prior to casting which may have allowed these systems to phase separate to a higher extent than those made by the normal, or "standard procedure" (SP). A higher degree of phase separation would explain the significant differences observed in the tensile behavior observed in Figure 60 on page 212 for the LP versus the SP materials; SAXS profiles, given in Figure 61 on page 213, substantiate this explanation. The SP gel displays a similar SAXS profile as was observed for other PTMO materials (see Figure 57 on page 205). The LP gel, however, displays a sharp increase in scattering at very low angles indicating both a high degreee of phase separation and large domains (implied by the large correlation distance) are present in these gels (a similar SAX profile was observed for the 30Ti-50PDMS(1700) material - see Figure 41 on page 164).

Concentrating on the SP gels in Figure 60, one notices that the shape of the stress-strain curve observed for the 14 day old 30Ti-48PTMO(2) gel (C) displays the same features as ob-

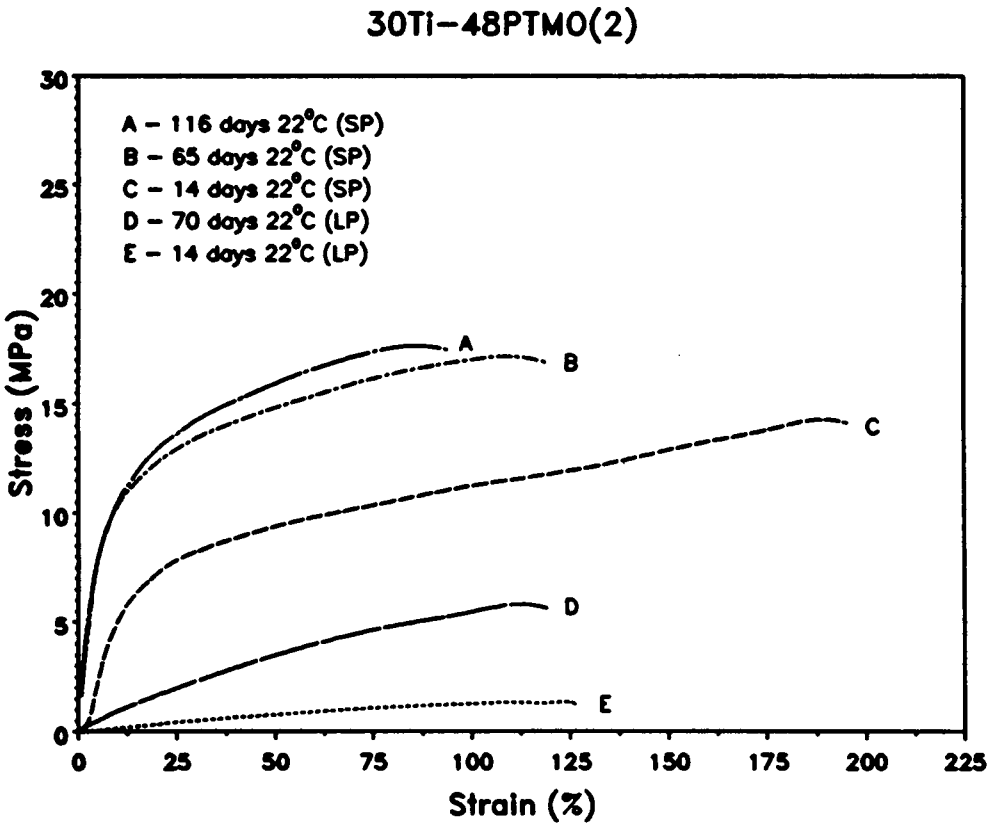

Figure 60. Stress-strain curves for 30Ti-48PTMO(2) gels vs age at ~22°C: SP = standard procedure, LP = long procedure (refluxed 3 hours after $Ti(i\text{-}pr)_4$ addition

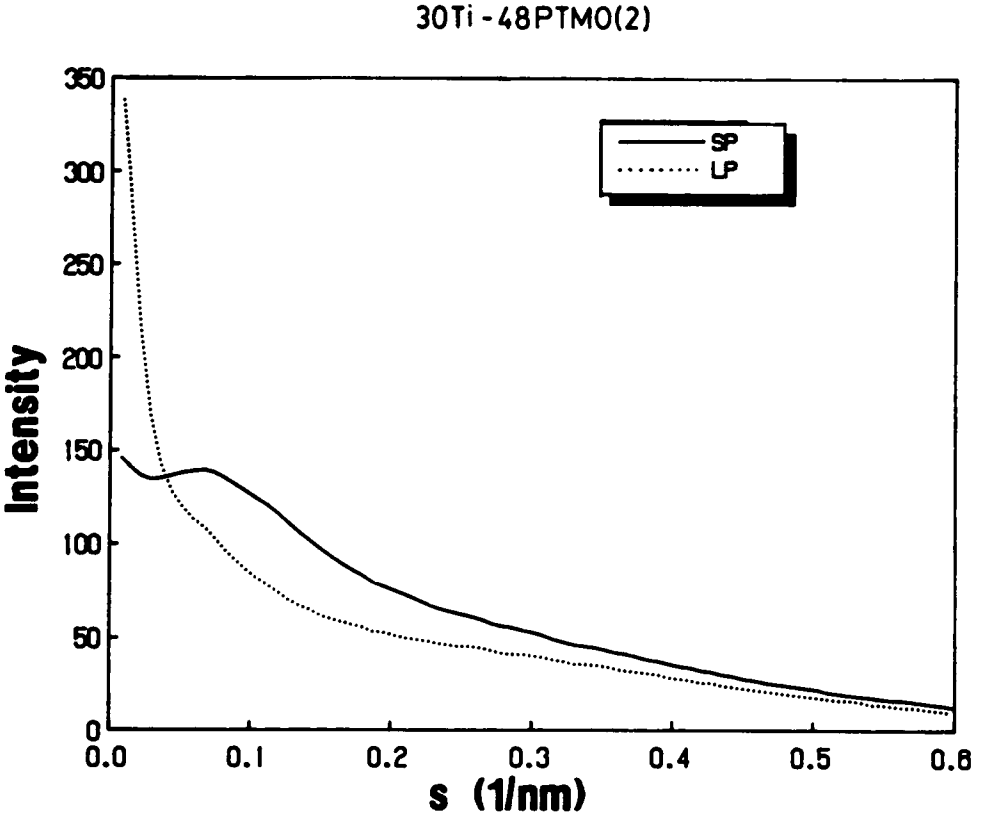

Figure 61. SAXS profiles of 30Ti-48PTMO(2) gels made by two different procedures: SP = standard procedure, LP = long procedure (3 hr reflux after $Ti(i\text{-}pr)_4$ addition

served for the older 65 (B) and 116 (A) day gels. Allowing the samples to age from 14 days (C) to 65 days (B), results in an increase of the initial slope and stress level at the bend or "quasi-yield" point in the stress-strain curve. Aging the samples past 65 days at ~22°C, however, has no further effect on the tensile properties as evidenced by curves (A) and (B) in Figure 60.

Based on the dynamic mechanical evidence used to explain the tensile behavior of the 15Ti-50PTMO(2) gels, the dynamic mechanical behavior of the of 30T0-48PTMO(2) SP gels aged at ~22°C for long times (65 days or longer) would be expected to show a T_g occurring at or slightly above 20°C. Indeed, the dynamic mechanical spectrum given in Figure 62 on page 215 for a 30Ti-48PTMO(2) SP gel aged at ~22°C for 140 days (triangles) displays a glass transition at ≃20°C (using the inflection point of the storage modulus transition). Though the actually begins at ~ -50°C in the tanδ curve, the majority of T_g peak occurs at temperatures above 20°C; The T_g peak in the tanδ curve is centered at 50°C. The fact that the majority of the oligomer chains in aged 30Ti-48PTMO(2) SP gels undergo the glass transition above 20°C indicates that this material is at least partially vitrified during the tensile test (which are conducted at ~22°C). A partially vitrified system, in turn, would be expected to exhibit a relatively steep initial stress-strain curves such as those observed for aged specimens recall Figure 60.

Figure 62 on page 215 compares the dynamic mechanical spectra of an aged 30Ti-48PTMO(2) sample that has been strained to 50% elongation with a comparable sample that has not been strained (both samples were aged 140 days at ~22°C prior to straining and/or testing by DMA). The stress-strain curves for the unstrained specimen would correspond to curves (A) or (B) given earlier in Figure 60. To strain such a gel to 50% elongation would take the material well past the bend or "yield point" observed in the stress-strain curves and should result in structural change. Yet, these samples physically are observed to relax back to their original dimensions within a few hours (6 hours or less). The dynamic mechanical spectrum of the strained sample (after it had been allowed to relax for 6 hours) in Figure 62 on page 215 is virtually identical to that of the unstrained sample. The modulus at

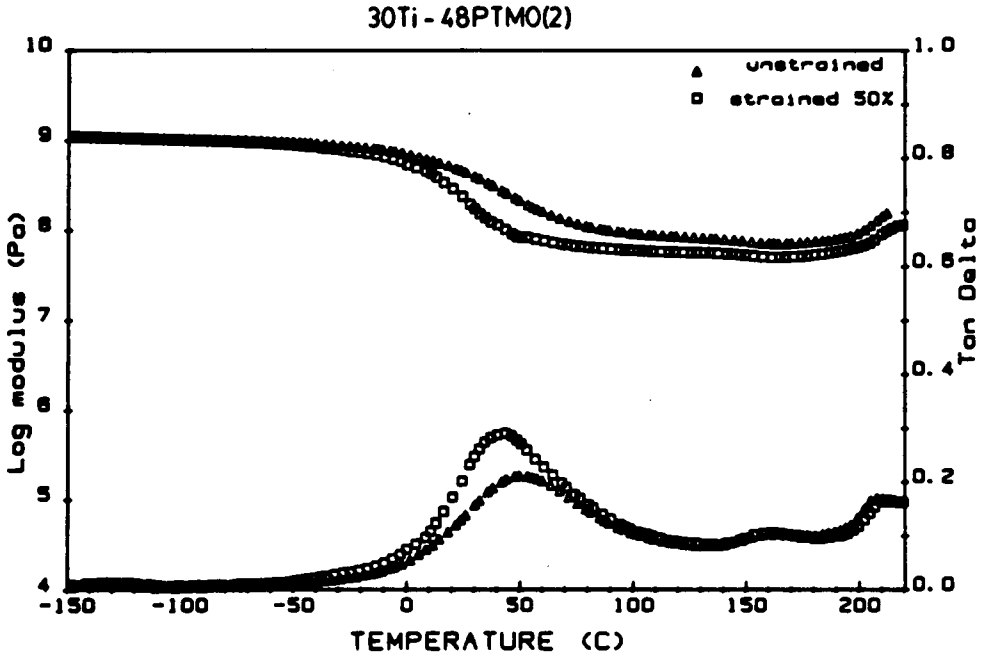

Figure 62. DMA spectra of a 30Ti-48PTMO(2) gel before and after straining to 50% elongation: (triangles) 140 days at ~22°C, unstrained, (squares) 140 days at ~22°C, strained to 50% elongation

room temperature is observed to be lower in the strained sample which must be due to structural damage caused by the mechanical deformation. However, straining to 50% elongation did not result in any major changes in the nature of the material. Data not presented show this to be a general effect. For example, a fresh (12 day old) 30Ti-53PTMO(5) gel displayed the ***exact same*** storage modulus and tanδ curves before and after deformation to 86% elongation (the sample was allowed to relax for 12 hours after deformation before the second DMA was run).

Figure 63 on page 217 contains the stress-strain curves for the 15Ti-50PTMO(3) gel composition as a function of time aged at ~22°C while Figure 64 on page 218 contains corresponding the stress-strain curves for the 30Ti-50PTMO(3) composition. Both figures contain data obtained for samples that had been annealed at 170°C for 24 hours in vacuum prior to testing. In much the same fashion as was observed for the PTMO(2) gels, the stress-strain curves for the PTMO(3) gels change as a function of time at 22°C. The curves in Figure 64 on page 218 demonstrate this change, the initial slope increases with time while the bend observed in early samples, (B) and (C), becomes a distinct yield point after 117 days (A). The apparent inversion of curves (B) and (C) in Figure 63 on page 217 is surprising and difficult to explain but may be due to differences in the gel batches from which test specimens were taken. The same general trend is observed for the 30Ti-50PTMO(3) gels in Figure 64 on page 218 though even after 102 days at ~22°C these gels do not exhibit a clear yield point. In both gel systems, annealing at 170°C for 24 hours in vacuum prior to testing was found to stiffen the material (see curve (D) in both Figure 63 on page 217 and Figure 64 on page 218). Curve (E) in Figure 63 was obtained from a 180 day old gel that was tested at 80$\pm$1°C in an environmental chamber to determine whether or not the glass transition observed in the dynamic mechanical spectra accurately reflects the tensile behavior (it does); this data will be discussed shortly.

Figure 65 on page 219 gives the dynamic mechanical spectra for 30Ti-50PTMO(3) gels stored a short time, 6 days (triangles), and a long time, 103 days (squares), after gelation at ~22°C. Also given in this figure is the spectrum for a gel that had been annealed for 24 hours

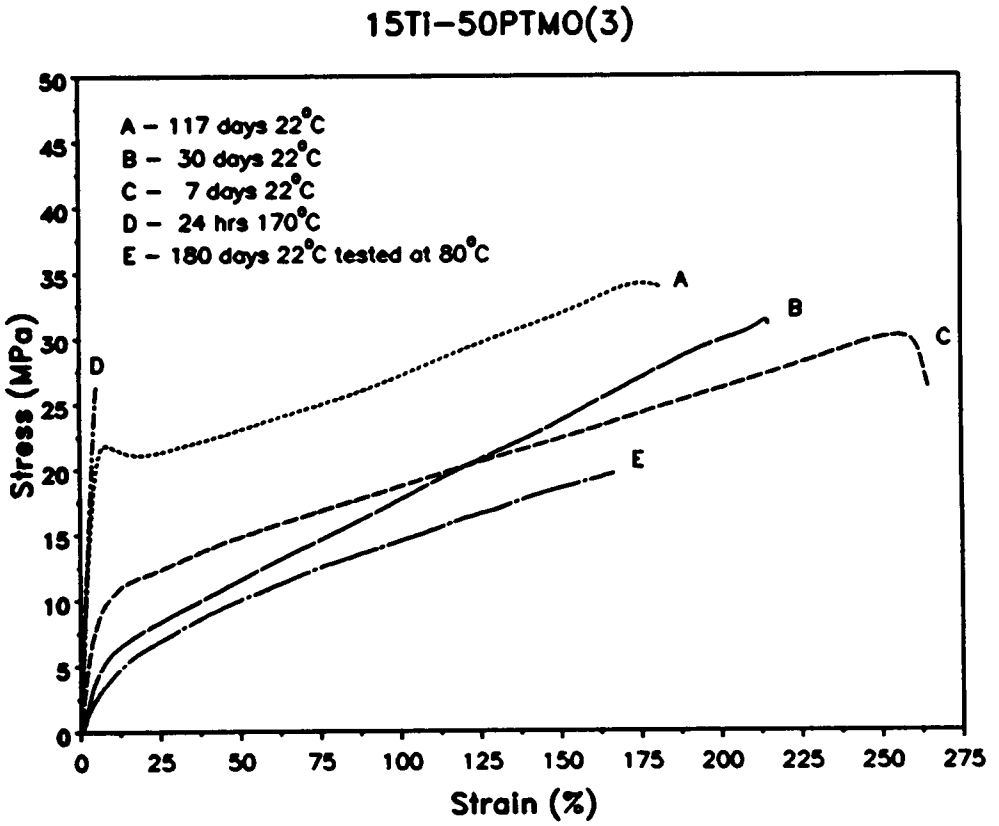

Figure 63. Stress-strain curves for 15Ti-50PTMO(3) gels vs age at ~22°C

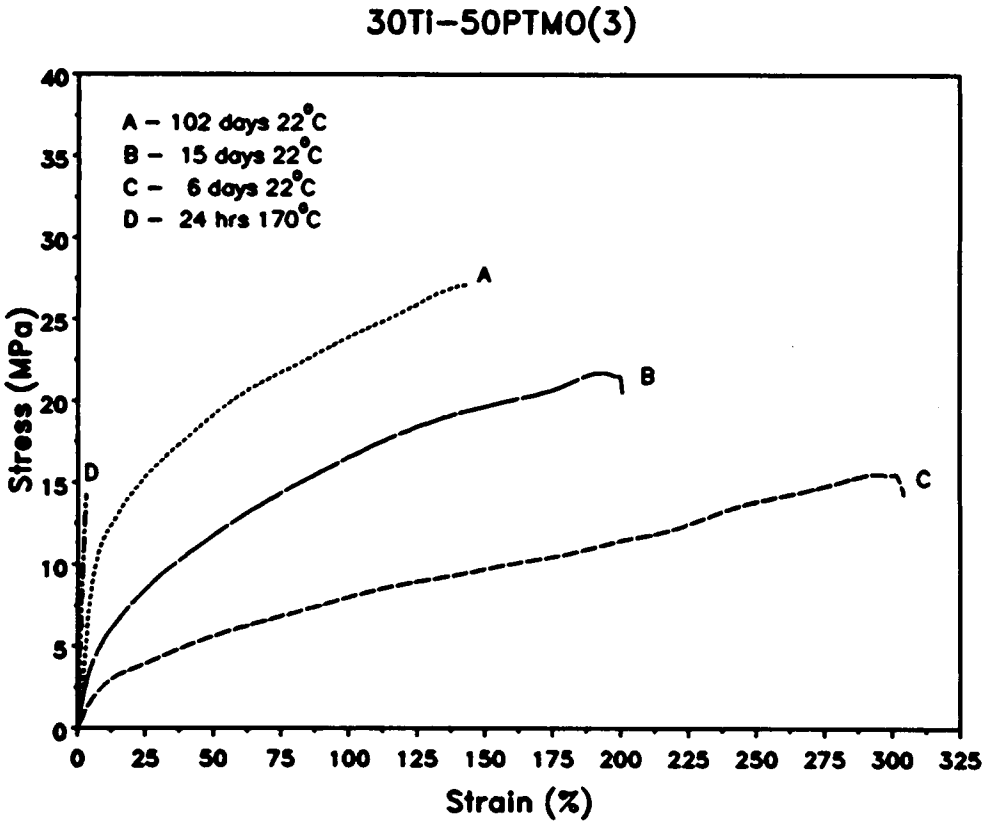

Figure 64. Stress-strain curves for 30Ti-50PTMO(3) gels vs age at ~22°C

at 170°C in vacuum (diamonds). The curves in Figure 65 on page 219 correspond to curves (A), (C) and (D) in Figure 64 on page 218 allowing comparisons to be made between the dynamic mechanical and tensile data. The tanδ and the storage modulus behavior of the 6 day old gel (triangles) both show that at 22°C some of the PTMO(3) chains have undergone the glass transition. The 6 day old gel at 22°C has a certain degree of molecular mobility, for this reason and is not as stiff as the 103 day old gel (squares) or the gel annealed at 170°C (diamonds). These last two gels are closer to being fully vitrified at 22°C as evidenced by their storage modulus and tanδ curves in Figure 65. This correlates well with the observed increase in the initial slope of the stress-strain curves of the 102 day old gel (A) and the 170°C annealed gel (D) in Figure 64 on page 218.

Figure 66 on page 221 and Figure 67 on page 222 contain the stress-strain curves as a function of time at ~22°C for the 15Ti-52PTMO(4) and the 30Ti-52PTMO(4) gels respectively. Also shown, but to be discussed later, is the stress-strain curve obtained for a 122 day old 15Ti-52PTMO(4) gel that was tested at 80±1°C. The curves in these two figures exhibit the same aging effects observed for the lower functionality PTMO gels. The 7 day old samples in both of the figures display curves typical of elastomeric materials (a well worn phrase at this point) while the samples after 60 and 80 days respectively show distinct yielding in their tensile behavior at ~22° The 15 wt% Ti(i-pr)$_4$ composition gels exhibit yielding and a high initial slope after 60 days (possibly sooner). The 30 wt% Ti9i-pr)$_4$ composition gels, while showing a high initial slope after 32 days, do not exhibit a distinct yield point in their stress-strain curves until they have been aged 80 days at ~22°C. However, curve (A) in Figure 67 on page 222 is the first example of a true yield point observed for a 30 wt% Ti(i-pr)$_4$ composition gel.

As was done for certain previous gels, dynamic mechanical spectra were obtained for 30Ti-52PTMO(4) gels that corresponded in age to the tensile experiments in order to allow cross-comparison of the results. Figure 68 on page 223 contains the results of these efforts showing the dynamic mechanical spectra for two samples: 6 days at ~22°C and 80 days at ~22°C. The shifting of the glass transition of the PTMO component is quite apparent in both

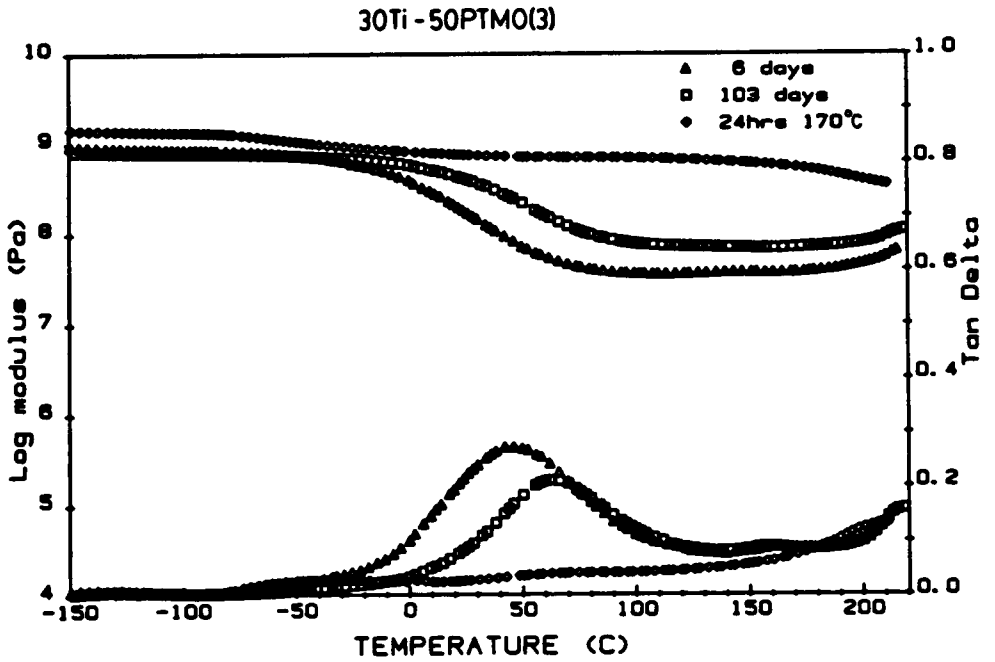

Figure 65. Dynamic mechanical spectra for 30Ti-50PTMO(3) gels: (triangles) 6 days at ~22°C, (squares) 103 days at ~22°C, (diamonds) 24 hours at 170°C in vacuum

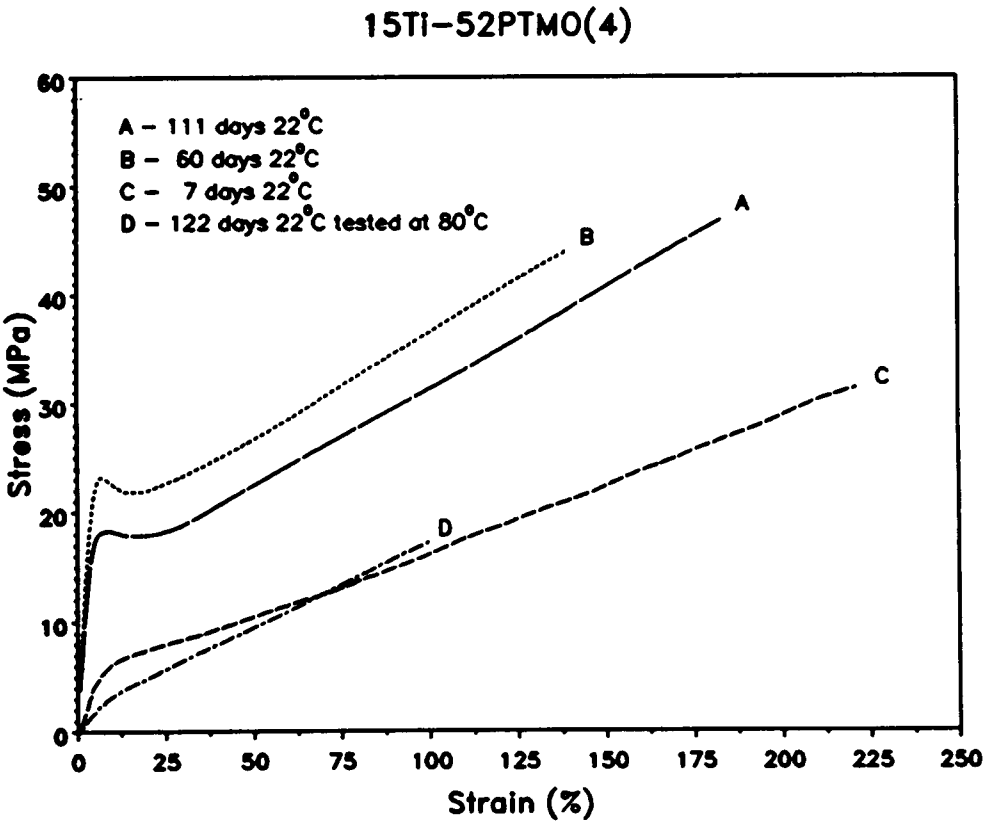

Figure 66. Stress-strain curves for 15Ti-52PTMO(4) gels vs age at ~22°C

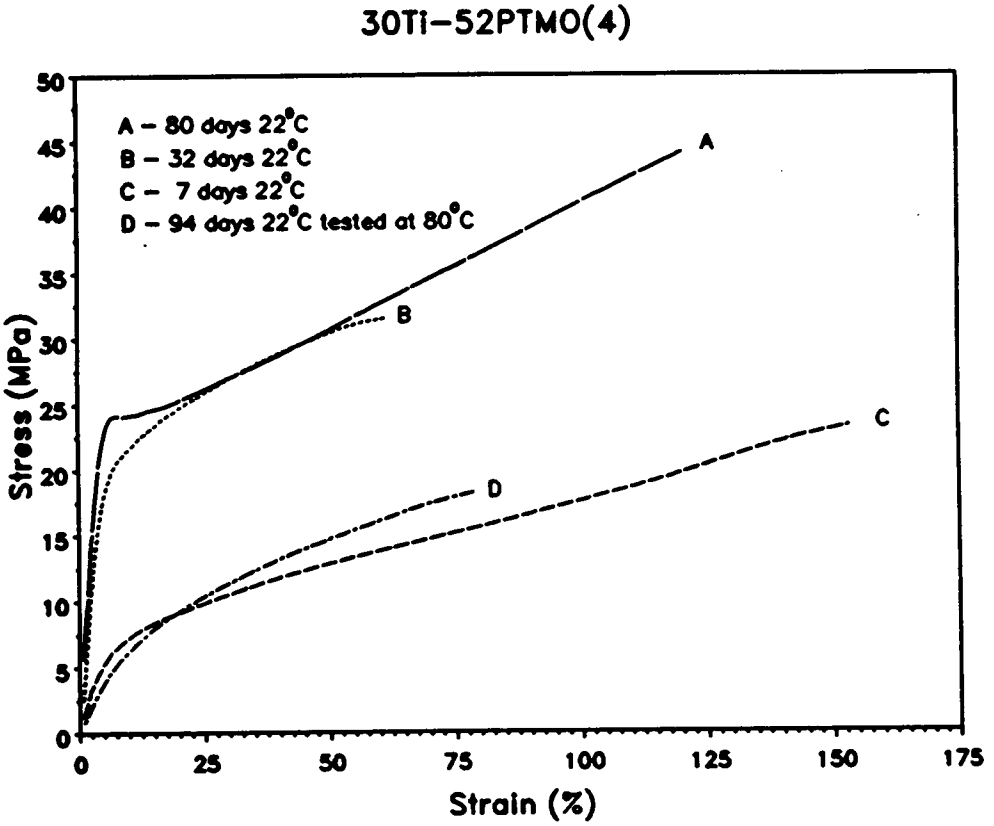

Figure 67. Stress-strain curves for 30Ti-52PTMO(4) gels vs age at ~22°C

the storage modulus and the tanδ curves. The storage modulus has dropped substantially by 20°C in the thermomechanical spectrum of the 7 day old gel (triangles). A significant portion of the transition in the tanδ curve has also been passed at this temperature indicating that a certain amount of molecular motion exists at 20°C. A result of the shifting brought about by aging the samples is that the 80 day old gel (squares) still displays a glassy storage modulus at ~20°; only a slight "tail portion" of the tanδ transition has been surpassed indicating that there is little molecular motion in this material at 20°C. Again, as for two previous materials, the dynamic mechanical spectra of the 30Ti-52PTMO(4) gels in Figure 68 explain the stress-strain curves given in Figure 67 on page 222. This is yet one more piece of evidence that the physical state of the polymeric component determines the tensile behavior of the hybrid gels.

Figure 69 on page 225 contains not only the stress-strain curves as a function of time, but also of annealing temperature for gels of the composition: 15Ti-53PTMO(5). Figure 70 on page 226 contains the same set of stress-strain curves for gels of the composition: 30Ti-53PTMO(5). The the aging effects on the curves shown in both figures are consistent with those observed for the stress-strain curves of PTMO(2), PTMO(3), and PTMO(4) gels. Generally, the initial slope of the stress-strain curves increases dramatically in the first three weeks after gelation. The nature of the curves changes during this time also going from elastomeric to "glassy" as evidenced by the yielding behavior in gels aged past 21 days at ~22°C.

The dynamic mechanical spectra given in Figure 71 on page 227 and Figure 72 on page 228 correspond directly with the stress-strain curves given in Figure 69 and Figure 70 for gels aged at ~22°C. The storage modulus curves and the tanδ curves for both the 15 wt% and 30 wt% Ti(i-pr)$_4$ composition gels show a broad glass transition that shifts to higher temperatures with time. Both sets of spectra indicate that after $\simeq$21-22 days the shifting of the glass transition (or the aging process) is essentially complete. The shifting of the glass transition, therefore, is probably due to a post gel continuation of the sol-gel process as was speculated to occur in the PTMO(2000) and PTMO(2900) hybrid gels.

Further analysis of the dynamic mechanical spectra provides insight regarding the nature of the stress-strain curves for similarly aged gels. The tanδ transition observed for the 7 day

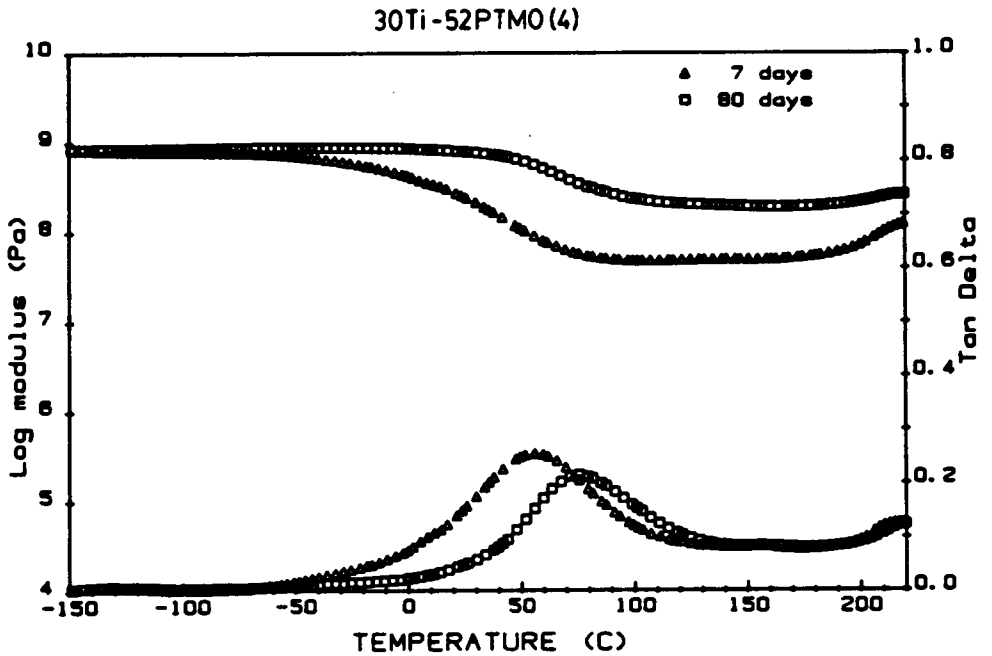

Figure 68. Dynamic mechanical spectra for 30Ti-52PTMO(4) gels vs age at ~22°C: (triangles) 7 days at ~22°C, (squares) 80 days at ~22°C

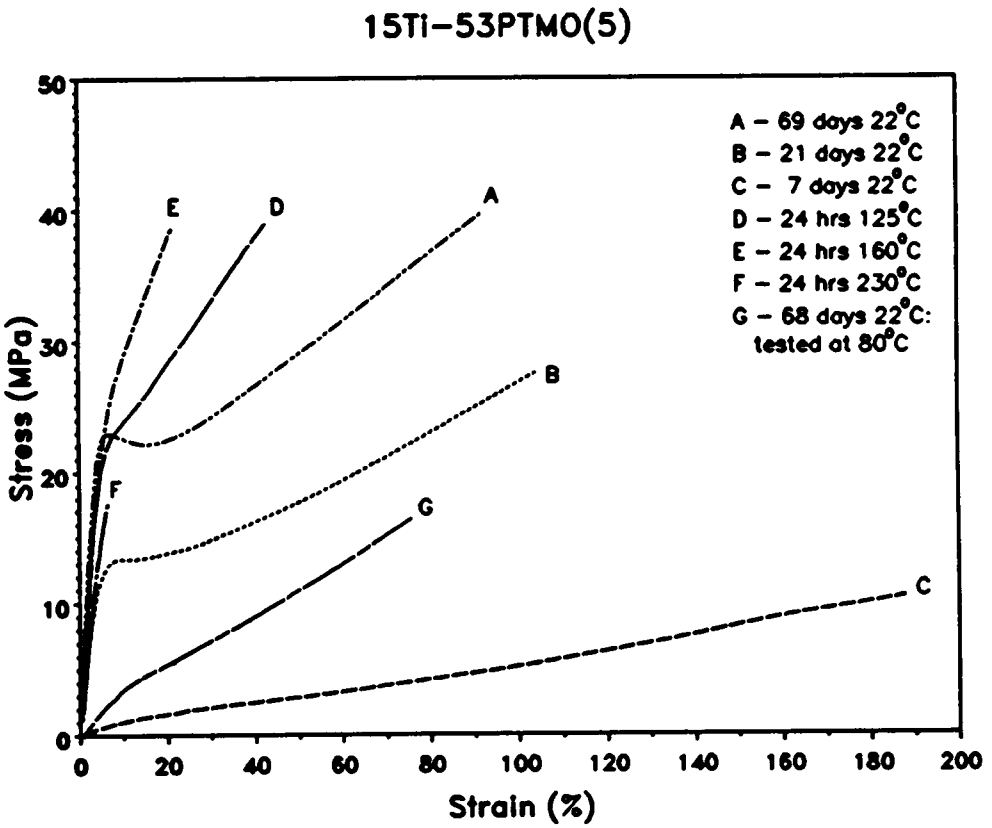

Figure 69. Stress-strain curves for 15Ti-53PTMO(5) gels vs age at ~22°C

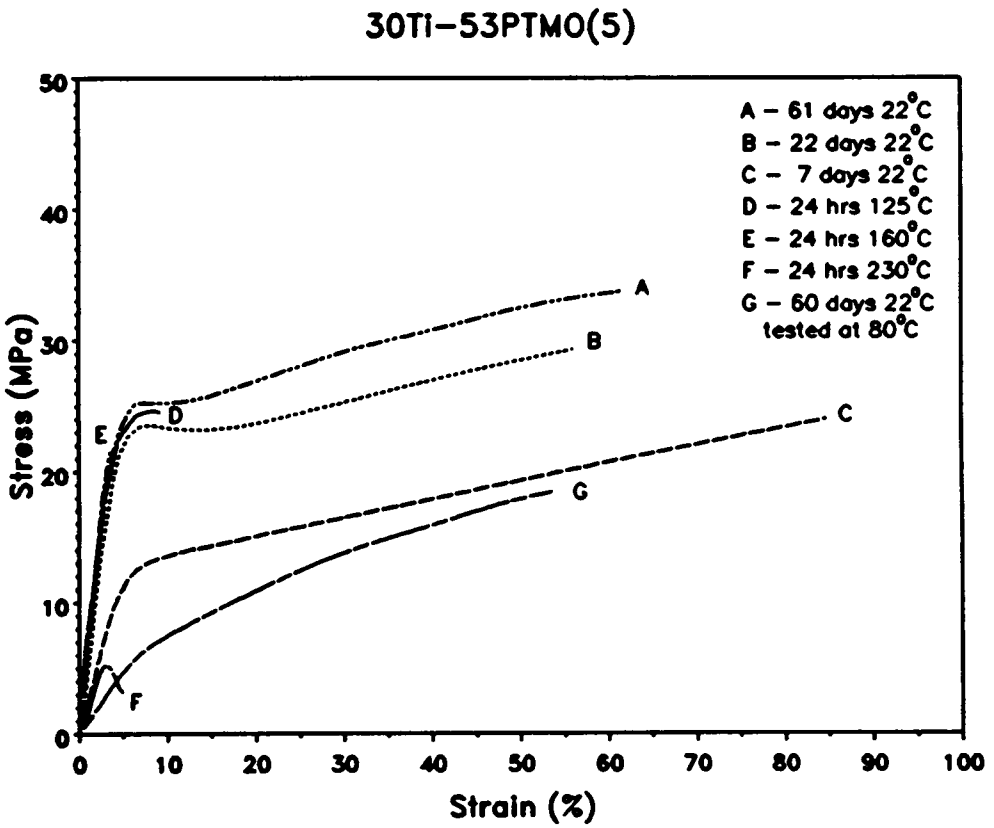

Figure 70. Stress-strain curves for 30Ti-53PTMO(5) gels vs age at ~22°C

old 15Ti-53PTMO(5) gel (triangles in Figure 71 on page 227) is centered at ~30°C while the corresponding minimum in the storage modulus occurs at ~50°C. In the 7 day old 15 wt% $Ti(i\text{-}pr)_4$ gel at 20°C there is, relatively speaking, a higher amount of molecular motion as compared to the 7 day old 30Ti-53PTMO(5) gel (triangles in Figure 72 on page 228). The center of the glass transition for the 6 day old 30 wt% $Ti(i\text{-}pr)_4$ gel has already shifted to ~60°C while the minimum in its storage modulus curve occurs at ~70°C. Furthermore, the storage modulus in the 7 day 15Ti-53PTMO(5) gel drops 1.5 orders of magnitude while that in the corresponding 6 day old 30Ti-53PTMO(5) gel drops less than one order of magnitude. Taken together, these results indicate that the 6 day old 30Ti-53PTMO(5) gel has reacted to a higher degree of completion than its 7 day old 15Ti-53PTMO(5) counterpart. This is corroborated by the stress-strain curves of these two materials. The curve for the 30Ti-53PTMO(5) gel displays a relatively steep initial slope and the beginnings of a yield point (curve (C) in Figure 70 on page 226) whereas the 15Ti-53PTMO(5) gel displays low-strength, flat, featureless curve (curve (C) in Figure 69). The same sort of analysis applied to the dynamic mechanical spectra of the gels aged for longer times faithfully "predicts" the tensile stress-strain behavior.

It has been suggested, in this chapter, that the tensile properties observed for the hybrid materials reflect the state of the polymeric component. Should this actually be the case, tensile tests conducted on vitrified materials at sufficiently elevated temperatures would "bring back" the elastomeric type response observed for gels tested at 22°C before they vitrified. The vitrified materials for which dynamic mechanical spectra were available all displayed broad glass transitions in the tanδ curves that were centered at $\simeq$ 80°C. At 20°C, however, these materials were in the low "tail" region of the glass transition and were speculated to be, therefore, mostly vitrified. Vitrification, in turn, was the explanation given for the observed yielding behavior in the tensile stress-strain curves. Tensile tests conducted at 80°C were carried out on a number of vitrified materials that showed distinct yield points in their 22°C stress-strain curves. These materials were: 15Ti-50PTMO(3), 15Ti-48PTMO(4), 15Ti-53PTMO(5) and 30Ti-53PTMO(5). Earlier figures (Figure 69, Figure 70, Figure 66 and Figure 63), provided the stress-strain curves of these aged gels tested at 80$\pm$1°C. The results

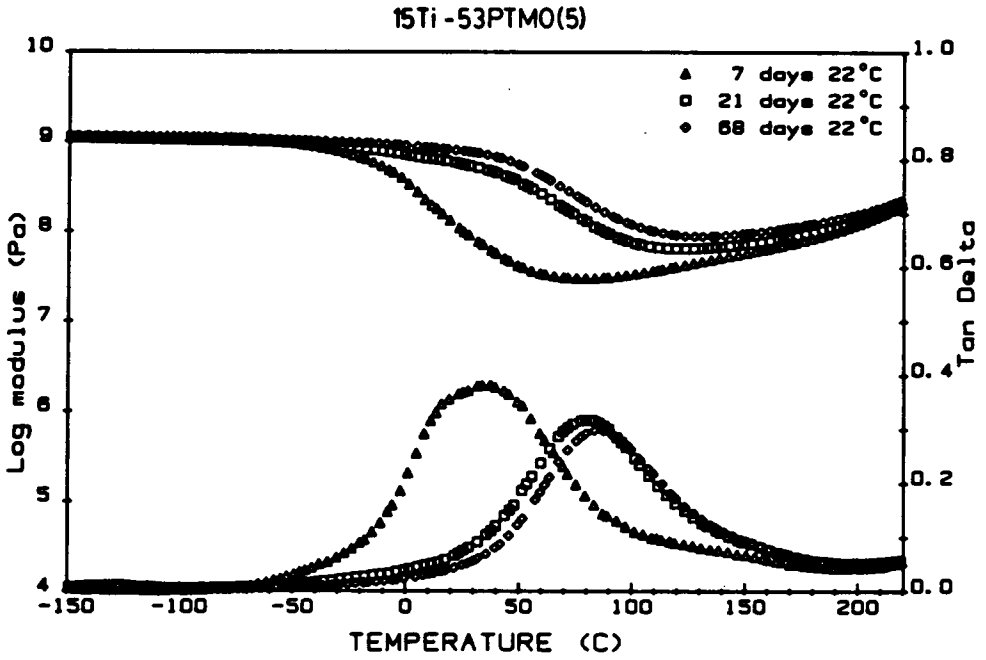

Figure 71. Dynamic mechanical spectra for 15Ti-53PTMO(5) gels vs age at ~22°C: (triangles) 7 days at ~22°C, (squares) 21 days at ~22°C, (diamonds) 68 days at ~22°C

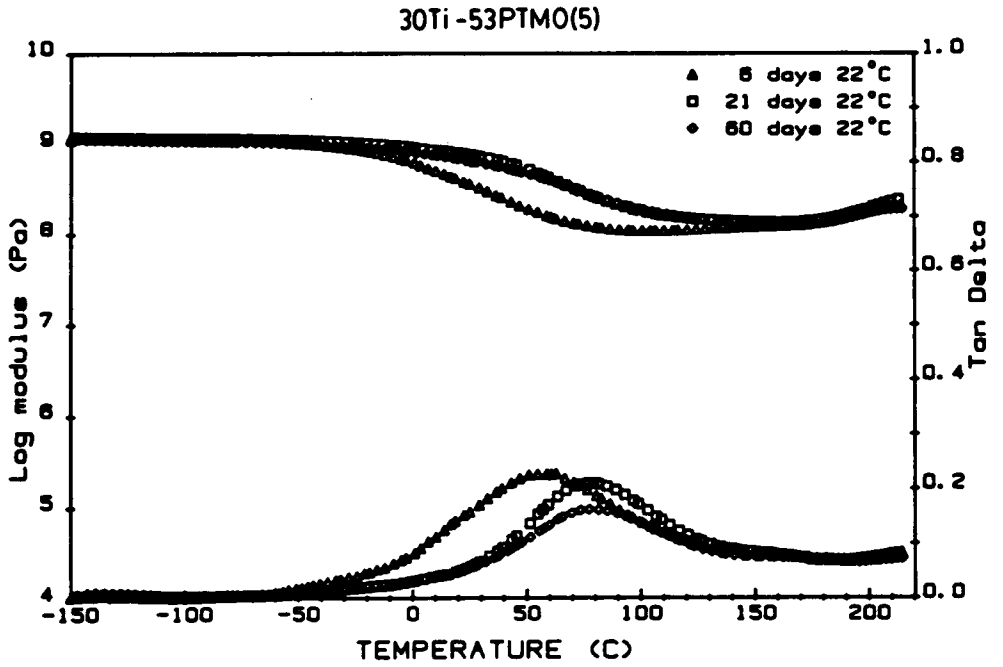

Figure 72. Dynamic mechanical spectra for 30Ti-53PTMO(5) gels vs age at ~22°C: (triangles) 6 days at ~22°C, (squares) 21 days at ~22°C, (diamonds) 60 days at ~22°C

are clear in each case. Samples tested at or above the T_g of the polymeric component showed elastomeric stress-strain behavior while samples tested below the T_g exhibit glassy behavior (as already shown numerous times).

Studying the tanδ curves in Figure 71 and Figure 72 shows that the glass transition stops shifting after the majority of the transition has shifted ~22°C (ambient temperature). Whether this indicates that the sol-gel or aging process is complete at this point can not be determined from this information alone. If the shifting of the glass transition were stopped by vitrification then heating the samples to temperatures above the glass transition should allow the "aging process" to continue. To determine if this was the case, annealing studies were undertaken. Samples were allowed to age for 6-7 days at ~22°C before they were annealed at 125±2°C, 160±2°C or 230°C for 24 hours under vacuum. The annealing curves shown in Figure 69 and Figure 70 demonstrate that the samples do undergo further change as a consequence of heat treatment but, again, the stress-strain curves by themselves are not very informative. The dynamic mechanical spectra of the same annealed samples for which stress-strain curves are shown are given in Figure 73 on page 231 and Figure 74 on page 232. As a reference, the spectra for non-annealed samples are included.

Heating the samples to 125°C for 24 hours shifts the glass transition observed in the dynamic mechanical spectra to higher temperatures as was expected (triangles in both Figure 73 and Figure 74). The temperature to which the transitions were shifted (based on the center of the tanδ peak from the curves given in Figure 73 and Figure 74) was ≃90°C for both compositions though the 30Ti-53PTMO(5) gel displays a bimodal transition which gives a second "peak" at ≃150°C. The centers of these shifted tanδ peaks correspond to those observed for samples which had been aged for long times at ~22°C (see Figure 71 on page 227 and Figure 72 on page 228). The storage modulus curves for the 125°C annealed gels also resemble those observed for the corresponding aged gels. Figure 73and Figure 74 also show that samples annealed at 160°C do not show a "shift" in the glass transition but do display stronger secondary peaks at higher temperatures (~180°C). The storage modulus curves for the 160°C annealed samples show hardly any drop in magnitude on passing through the glass

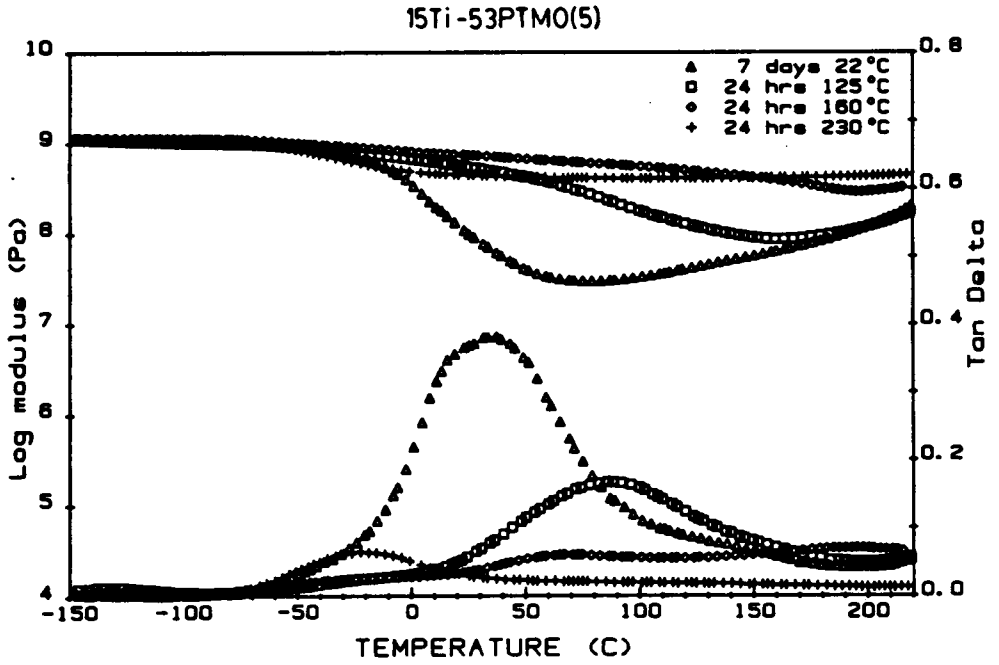

Figure 73. Dynamic mechanical spectra for annealed 15Ti-53PTMO(5) gels: (triangles) 7 days at ~22°C, (squares) 24 hours at 125°C, (diamonds) 24 hours at 160°C, (crosses) 24 hours at 230°C

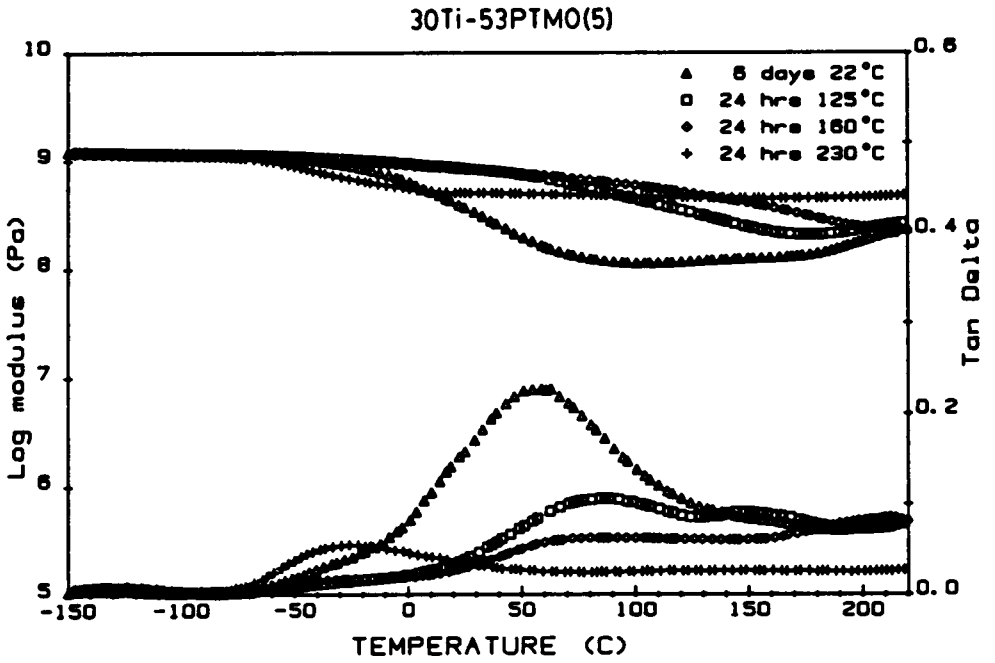

Figure 74. Dynamic mechanical spectra for annealed 30Ti-53PTMO(5) gels: (triangles) 6 days at ~22°C, (squares) 24 hours at 125°C, (diamonds) 24 hours at 160°C, (crosses) 24 hours at 230°C

transition which indicates that the amount of molecular motion in these samples must be small. The stress-strain behavior observed for these materials corroborate this finding. The dynamic mechanical spectra for samples annealed at 230°C show serious evidence of polymer degradation. The tanδ transition at the higher temperatures all but disappears for these gels being replaced by a low temperature peak centered at $\simeq$ -30°C which extends as far down as -70°C. This low temperature transition observed in the tanδ spectra of the 230°C annealed gels is suspected to be due to PTMO(5) fragments and is reflected in not only the storage modulus curves but the stress-strain curves as well (see curve (F) in both Figure 69 and Figure 70). Potentially, depolymerization of the PTMO could be a serious problem for any annealed specimens especially since the PTMO polymers used were not stabilized in any way. The samples annealed at 230°C undoubtedly degraded, this was obvious from the decay in mechanical properties. The loss of elongation observed for the samples annealed at 160°C and 125°C could also be due to a certain amount of PTMO degradation as well though the Young's modulus (listed in Table 20 on page 235) and dynamic mechanical spectra do not indicate so. As a whole, the annealing experiments demonstrate that the aging effect can be accelerated but that overall degree of conversion reached can not be appreciably higher than that observed in samples sufficiently aged at ~22°C. Had the degree of conversion been appreciably raised by annealing at elevated temperatures, the glass transition of the hybrid materials would have shifted to higher temperatures than observed for well aged samples.

Table 19 on page 234 and Table 20 on page 235 contain the compiled stress-strain data obtained for the Ti containing multifunctional PTMO gels as a function of age at ~22°C and, in some cases, annealing temperature. These data confirm what has already been discussed in a qualitative fashion from the representative stress-strain curves presented. An overview of these tables demonstrates that the Young's modulus increases with age changing an order of magnitude when the the corresponding stress-strain curve begins to show signs of a yield point. Furthermore, the large change in Young's modulus also corresponds to the point at which the dynamic mechanical spectra indicate vitrification is occurring. The ultimate properties, on the other hand, generally decay for samples aged over long periods of time (~60

days). This is especially true for the observed elongation at break which generally drops 50% or more. The large drop off in elongation at break is even more dramatic for samples that had been annealed at elevated temperatures which is in line with the assumption that the decay in ultimate properties is the result of PTMO depolymerization.

Figure 75 on page 236 shows a normalized plot of the Young's modulus measured for the various Ti containing PTMO(X) sol-gels made. The modulus values were for the various gels were normalized by assuming the oldest gels had reached 100% of their full modulus, then taking the log of the modulus at any given time and dividing it by the log of the modulus measured for the oldest gel. The data for the various gels all fall (within reason) on the same curve (see Figure 75 on page 236) which indicates that the gels all age at the same relative rate. This implies that the mechanism for aging must be independent of the oligomer which is consistent with the concept that aging occurs as a continuation of the sol-gel process after initial gelation has occurred.

Extraction studies were carried out on the different gels to determine whether or not any material was removable. Also, swelling experiments were conducted to determine the susceptibility of the hybrid material to solvent uptake and to gain a qualitative understanding of the crosslink density in the network. The extraction and swelling experiments were both conducted using THF according to the procedures outlined in Chapter III sections 3.3.4 and 3.3.5. Table 21 on page 238 gives the results of these experiments.

The extraction data in Table 21 on page 238 do not correlate to the number of functional groups attached to the PTMO polymer. Surprisingly, these data all fall on the same curve when plotted against the time aged at ~22° prior to extraction. Figure 76 on page 239 shows this plot. The fact that all of the various gels fall on this plot is somewhat remarkable but further reinforces the concept that aging occurs independent of the modifying polymer - aging must be the result of the alkoxide components in the gels. However, the swelling behavior, i. e. the crosslink density, does correlate to the number of functional groups on the PTMO polymer. A plot of the wt% THF uptake vs number of triethoxysilane functional groups is given in Figure 77 on page 240 The relationship between the amount of swelling and the number

Table 19. Tensile properties of Ti containing multifunctional PTMO modified sol-gel materials (part 1)

sample	days at 22°C	elongation at break (%)	ultimate strength (MPa)	Young's modulus (MPa)
15Ti-50PTMO(2)	6	270±45	9±2	30±9
15Ti-50PTMO(2)	76	204±15	34±2	422±26
15Ti-50PTMO(2)	122	104±10	25±0.6	565±55
30Ti-48PTMO(2)[a]	14	130±11	1.3±0.1	2.0±0.1
30Ti-48PTMO(2)[a]	70	125±9	5.6±0.4	11±1.6
30Ti-48PTMO(2)	14	180±20	13±1	84±8
30Ti-48PTMO(2)	65	121±11	17±0.6	218±20
30Ti-48PTMO(2)	116	104±20	17±0.7	234±29
15Ti-50PTMO(3)	7	237±24	31±4	110±20
15Ti-50PTMO(3)	30	270±37	32±2	194±27
15Ti-50PTMO(3)	117	206±25	37±5	557±29
15Ti-50PTMO(3)	180[b]	186±14	19±1	51±6
15Ti-50PTMO(3)	27[c]	4±1	23±5	590±13
30Ti-50PTMO(3)	6	290±20	15±1	40±15
30Ti-50PTMO(3)	15	190±13	21±2	106±12
30Ti-50PTMO(3)	102	134±18	26±2	259±35
30Ti-50PTMO(3)	12[c]	3±1	12±4	520±60

a- refluxed 3 hrs after addition of titaniumisopropoxide prior to casting
b-strained to break at 80±1°C
c-annealed 24 hrs in vacuum at 170±2°C
d-annealed 24 hrs in vacuum at 125±2°C
e-annealed 24 hrs in vacuum at 160±2°C
f-annealed 24 hrs in vacuum at 230±2°C (PTMO is probably degrading)

Table 20. Tensile properties of Ti containing multifunctional PTMO modified sol-gel materials (part 2)

sample	days at 22°C	elongation at break (%)	ultimate strength (MPa)	Young's modulus (MPa)
15Ti-52PTMO(4)	7	215±19	30±2	99±13
15Ti-52PTMO(4)	60	129±17	40±4	527±55
15Ti-52PTMO(4)	111	180±7	46±2	567±28
15Ti-52PTMO(4)	122[b]	102±10	18±2	36±6
30Ti-52PTMO(4)	7	157±13	23±2	140±20
30Ti-52PTMO(4)	32	68±16	33±4	589±52
30Ti-52PTMO(4)	80	120±19	43±5	685±42
30Ti-52PTMO(4)	94[b]	82±10	19±1	80±13
15Ti-53PTMO(5)	7	185±17	10±2	12±5
15Ti-53PTMO(5)	21	109±14	29±3	360±24
15Ti-53PTMO(5)	21[g]	95±19	28±6	370±51
15Ti-53PTMO(5)	69	84±10	36±4	650±70
15Ti-53PTMO(5)	68[b]	73±3	15±2	35±4
15Ti-53PTMO(5)	7[d]	42±5	39±2	568±49
15Ti-53PTMO(5)	7[e]	19±3	37±2	610±30
15Ti-53PTMO(5)	7[f]	4±3	10±6	350±17
30Ti-53PTMO(5)	7	92±17	24±4	308±47
30Ti-53PTMO(5)	22	59±4	30±0.4	630±49
30Ti-53PTMO(5)	61	55±16	34±4	757±45
30Ti-53PTMO(5)	60[b]	54±4	18.4±0.6	83±10
30Ti-53PTMO(5)	7[d]	12±6	27±6	740±65
30Ti-53PTMO(5)	7[e]	5±1.5	24±4	733±41
30Ti-53PTMO(5)	7[f]	5±0.6	4±1	297±33

a- refluxed 3 hrs after addition of titaniumisopropoxide prior to casting
b-strained to break at 80±1°C
c-annealed 24 hrs in vacuum at 170±2°C
d-annealed 24 hrs in vacuum at 125±2°C
e-annealed 24 hrs in vacuum at 160±2°C
f-annealed 24 hrs in vacuum at 230±2°C (PTMO is probably degrading)
g-extracted in THF after 21 days (8.7 wt% removed); aged 265 days at 22°C

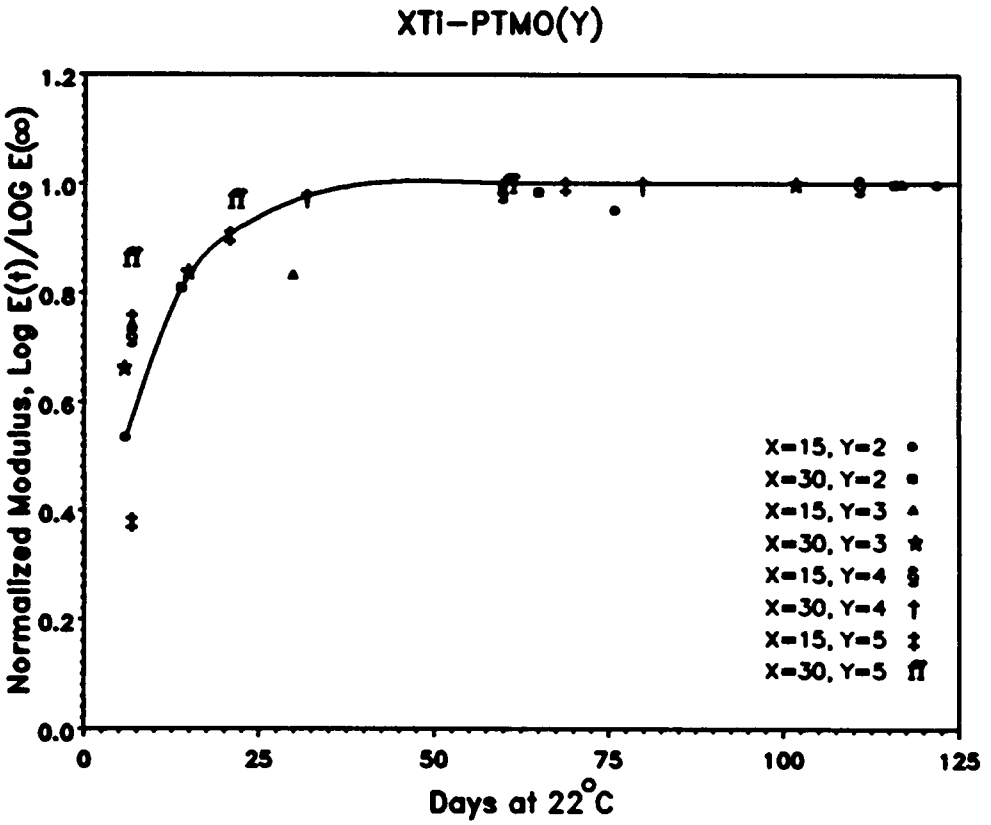

Figure 75. Normalized Young's modulus of Ti containing PTMO(Y) sol-gels vs age at ~22°C

Table 21. Extraction and swelling behavior of Ti containing multifunctional PTMO modified sol-gel materials in THF

sample	age*	extraction wt% loss	swelling wt% uptake†
15Ti-50PTMO(2)	6 wks	5.0	157
30Ti-48PTMO(2)	4 wks	8.6	168
15Ti-50PTMO(3)	12 wks	1.3	132
30Ti-50PTMO(3)	8 wks	3.2	136
15Ti-52PTMO(4)	4 wks	1.3	137
30Ti-52PTMO(4)	2 wks	10.2	113
15Ti-53PTMO(5)	3 wks	8.7	108
30Ti-53PTMO(5)	11 days	13.7	90

*elapsed time between gelation and extraction (stored at room temperature)
†after 60 hours in 22°C THF

of functional groups is approximately linear and appears to be independent of the $Ti(i\text{-}pr)_4$ loading.

Figure 78 on page 242 demonstrates the effects of extraction on the dynamic mechanical properties of the hybrid Ti containing sol-gels. This set of dynamic mechanical data is representative of several other runs on extracted and non-extracted materials. In all cases the results are the same: no significant change is brought about by extraction although as much as 10.2 wt% of the material was extracted (as was the case for the extracted material in Figure 78). The same can be said for the effect on the stress-strain curves as shown in Figure 79 on page 243 for a 30Ti-48PTMO(2) material (data given in Table 20 on page 235). The tensile properties before and after extraction are virtually identical. It is interesting to note, however, that even after aging the gels 244+ days at ~22°C ***after extraction***, the ultimate properties are the same as for a 21 day old gel prior to extraction (Table 20 on page 235). Moreover, the 21 day old gel aged an additional 48 days (to 69 days) shows a noticeable decrease in ultimate properties. This observation. though circumstantial, is evidence that solvent and trapped organics, such as acetic acid, in "as gelled" materials contribute to the observed decline in mechanical properties with time; extracted materials, from which these solvents and organics have been removed, prove relatively stable with time at ~22°C.

6.5 Discussion of the Aging Phenomenon

In a network forming process, as gelation occurs, the weight average molecular weight of the growing molecules become infinitely large. As a result, the viscosity of the system increases drastically at the gel point. The high viscosity after gelation considerably decelerates the crosslinking process through diffusion limitation of the chemical reaction. However, chemical crosslinking does not necessarily stop after gelation; the chemical reaction can continue towards completion, albeit at a slower rate. Hence, given sufficient time, a network

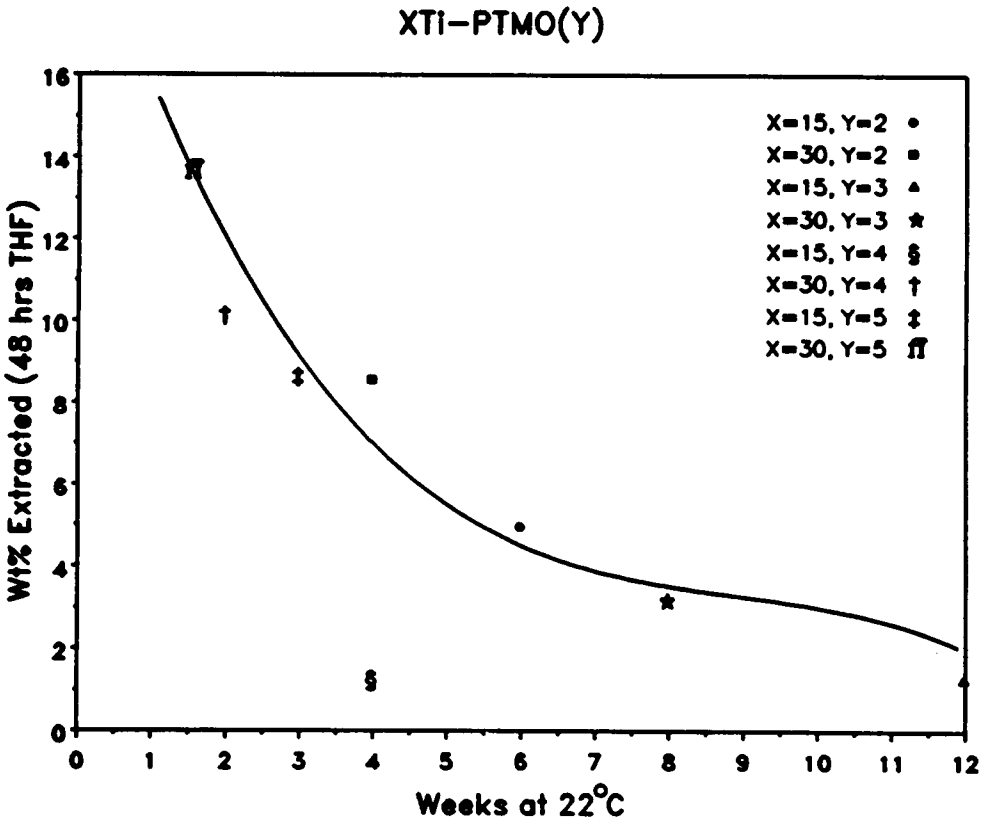

Figure 76. Wt% extracted from Ti containing PTMO(Y) sol-gels vs age at ~22°C

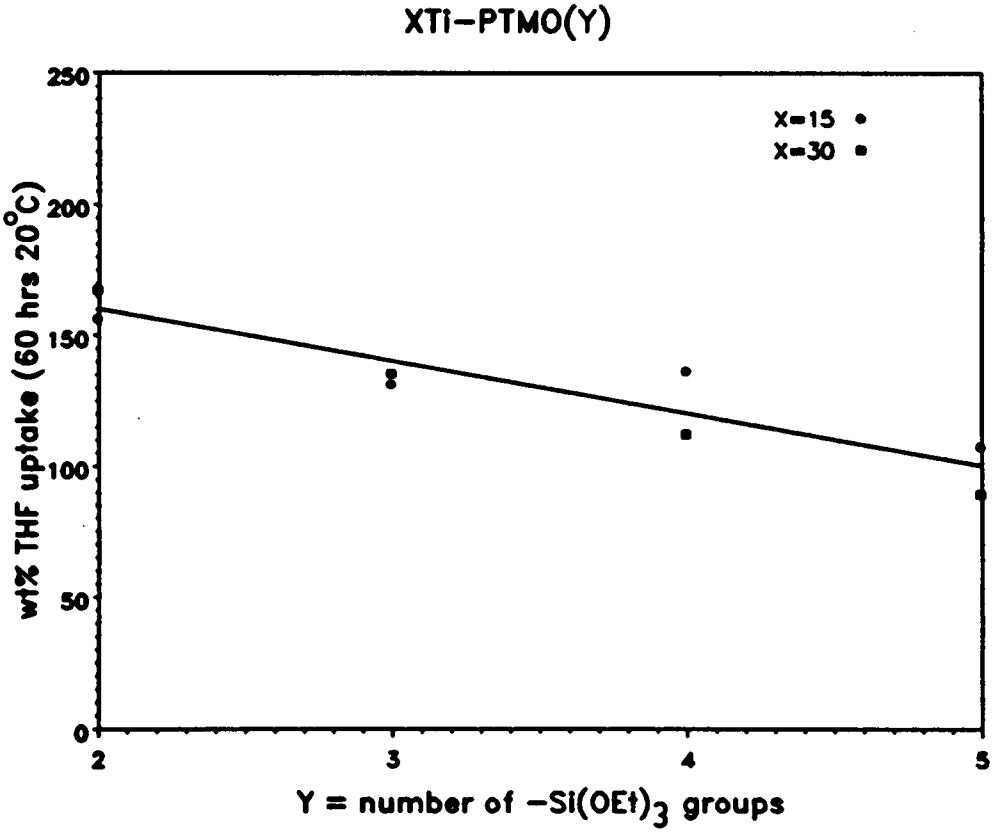

Figure 77. Wt% THF uptake at ~20°C vs number of triethoxysilane functional groups

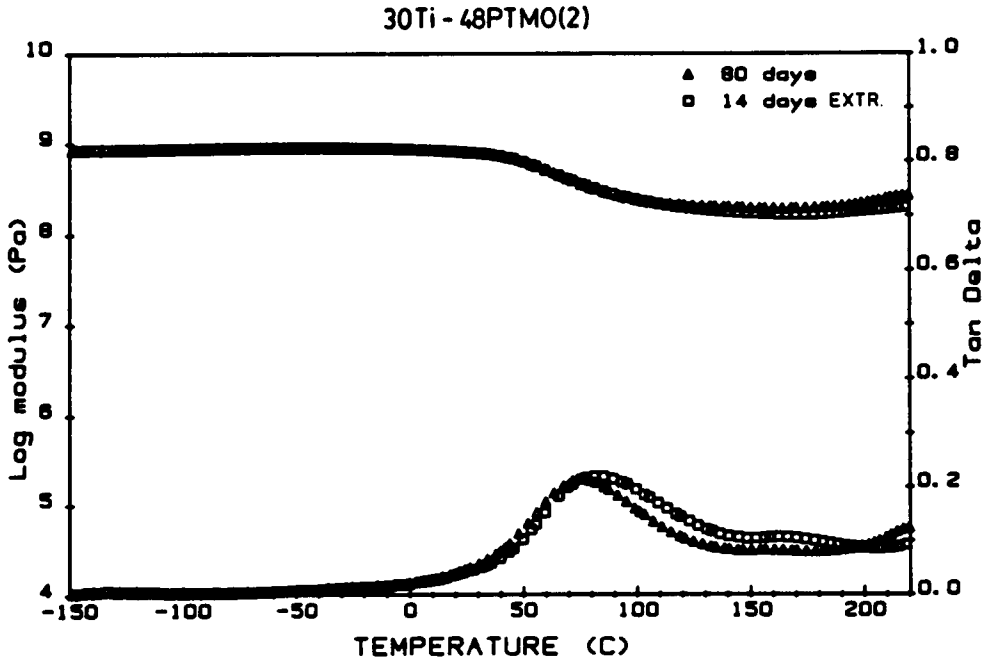

Figure 78. Dynamic mechanical spectra of 30Ti-50PTMO(2) gels before and after extraction in THF: (triangles) aged 80 days at ~22°C, (squares) aged 14 days at ~22°C then extracted in THF

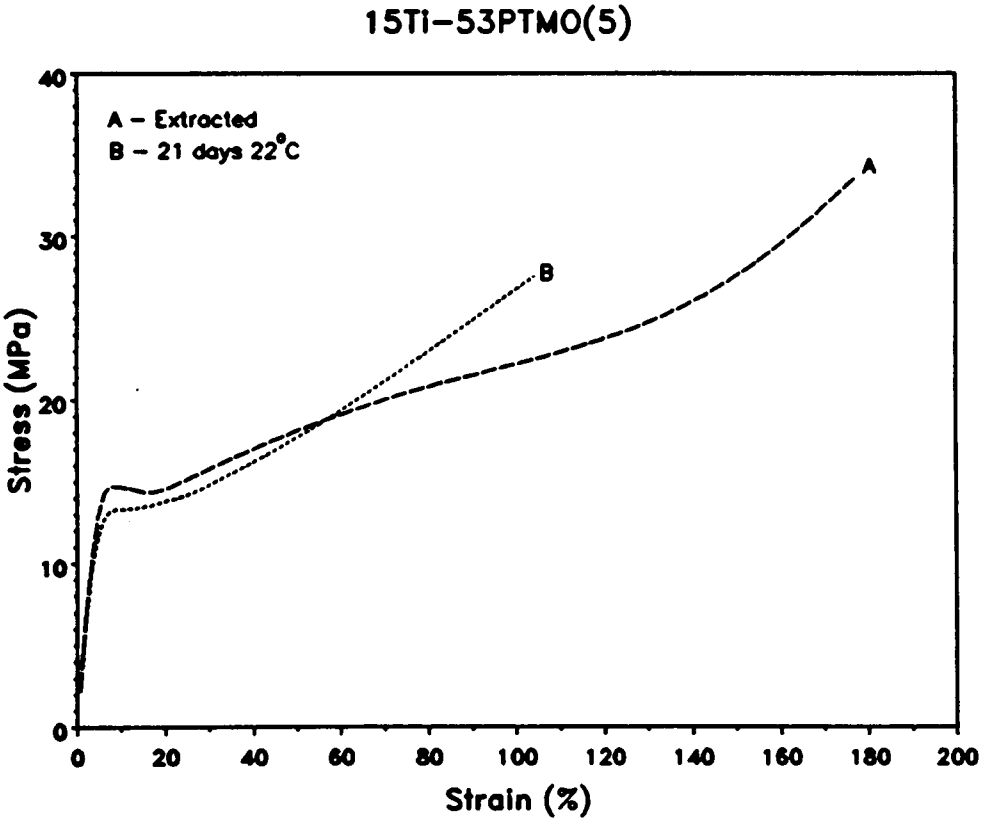

Figure 79. Stress-strain curves of 15Ti-53PTMO(5) before and after extraction in THF

forming system can continue to crosslink after gelation until all reactive sites are spent or vitrification occurs quenching mobility. Though vitrification, like gelation, does not necessarily terminate the chemical crosslinking, the diffusion limitation is so great that additional reaction in a vitrified material can be, generally, ignored. Once vitrified, large scale molecular motions are not possible in the system; reactive sites can no longer come together with any great frequency and the chemical crosslinking reaction is effectively quenched. Therefore, a slow continuation of the crosslinking reaction after gelation is what will be referred to as aging or "initial aging". Should vitrification happen to occur before gelation, aging, as defined, would not be expected to take place to any considerable degree.

Since aging happens in the time period between gelation and vitrification, the aging process is governed primarily by two factors: the ***extent of reaction*** required for gelation (if this is very high little aging can take place) and the ***molecular mobility*** (diffusion) in the gel. The first factor is determined by the average functionality of the system in question and is independent of polymer properties as predicted by Flory [26]. The second factor, molecular mobility in the gel, varies with the chemistry of the system and generally increases as the curing or aging temperature is raised above the glass transition temperature of the system. Molecular mobility would also increase as the size of the "moving species" decreases. The lack of long term aging effects on the properties of TEOS-PDMS(1700) systems presented in earlier publications [17] can be attributed to a combination of these two factors. The difunctional PDMS oligomers lower the average functionality of the system thereby raising the extent of reaction required for gelation; this limits the amount of aging possible since the system is closer to complete reaction when it reaches the gel point. Secondly, the low glass transition temperature of the PDMS(1700) species (~ -120°C) affords a certain degree of oligomer mobility in materials gelled at ambient temperature. This mobility, in turn, would allow the PDMS systems to "age" quickly; i. e. the sol-gel reaction would reach its limiting degree of completion in several hours or days instead of several weeks. In the multifunctional PTMO containing systems, however, the aging process at ambient temperature should be more substantial than in the difunctional PDMS containing systems due to the following: a

higher average functionality in the system and lower oligomer mobility in gelled materials (as evidenced by glass transition temperatures that approach and exceed ambient temperature). The higher PTMO functionality results in gelation of the PTMO hybrid systems at a lower extent of reaction as compared to the PDMS hybrid systems. Therefore, more reactive sites are available for potential aging in the gelled PTMO systems than in the gelled PDMS systems. Furthermore, the higher glass transition temperatures observed in gelled PTMO materials indicates considerable diffusion limitation (low oligomer mobility), which causes the chemical aging process to proceed slowly. Hence, the time period between gelation and vitrification increases and aging becomes significant with time.

Using the initial modulus as the primary gauge of aging one observes that the most drastic changes occur in the first few days after gelation (as might be expected). The ***initial*** effect of the aging process on the titanium containing materials is to increase the Young's modulus by an order of magnitude or more as well as increase the measured stress at break and elongation to break. The room temperature aging process in the titanium containing PTMO materials, in terms of the Young's modulus, though, is finished after thirty to fifty days (see Table 18 on page 197 & Figure 75 on page 236). However, further aging results in a drastic decrease in the measured elongation at break and a slight decrease in the measured stress at break. During the discussion of the data presented in this chapter this effect was attributed to the potential depolymerization of the PTMO polymers. The reason for this speculation is that PTMO or poly(tetrahydrofuran) can undergo a depolymerization to form the cyclic five-membered THF monomer which is quite thermally stable [115]. This process is well known for polyethers and is especially favorable for systems that revert to stable five or six-membered rings (such as PTMO); such systems display low ceiling temperatures. Furthermore, the unzipping effect is known to be greatly enhanced in the presence of acid for poly(methylene oxide). As such, since the functionalized PTMO oligomers used in the sol-gel schemes were not stabilized and the gelled materials undoubtedly contained residual acid, a certain degree of PTMO depolimerization would be expected at very long times (~100 days) even at room temperature.

Annealing gelled samples at elevated temperatures has been found to accelerate the "aging process" for the multifunctional PTMO gels as is expected in view of the "TTT" behavior displayed. Comparing the mechanical spectra as well as the stress-strain curves of annealed and virgin - unannealed - materials supports this conclusion (see Figure 69 on page 225 and Figure 73 on page 231). Most notably, the storage modulus in annealed samples does not drop as severely after the glass transition as in virgin samples. Also, the storage modulus remains level i. e., no upturn is observed at the end of the spectrum. The annealed storage modulus corresponds to the level observed at the end of the scan of a virgin material (after the upturn). Furthermore, the glass transition regions are almost identical, the only difference being a lower intensity observed for the T_g of the annealed specimen (no doubt a result of the higher storage modulus). Annealing has been observed to accelerate the decay of the ultimate properties in the multifunctional PTMO sol-gels (stblref refid=6g.). Again, this is to be expected if the loss in properties is due to depolymerization of the PTMO.

6.6 Conclusions

Titaniumisopropoxide, which is known to have a fast rate of condensation, has been successfully incorporated into functionalized PTMO modified silicate sol-gel systems. This has been accomplished by employing the reaction procedure developed in Chapter V to make titania containing PDMS sol-gels. The resulting materials are yellow or orange in color but usually transparent. The exceptions being the 30 wt% $Ti(i\text{-}pr)_4$ gels which, on occasion, are turbid and display spherical microstructures ~2-3μ in size. The multifunctional PTMO gels demonstrate, further, that the 30 wt% $Ti(i\text{-}pr)_4$ gels are unique from the 15 wt% $Ti(i\text{-}pr)_4$ compositions.

The observed mechanical properties change significantly on the addition of titanium. The measured Young's modulus increases while the ultimate stress also appears to increase with

respect to the pure TEOS-PTMO(2000)&(2900) hybrid systems (the ultimate properties for aged samples may not be strictly comparable, though, due to complications arising from potential long term depolymerization of PTMO). These differences may be due to a tighter network structure brought on by the titanium component. Glass transition temperatures observed in dynamic mechanical spectra of PTMO(2000) systems indicate that the phase separation may be enhanced for $Ti(i\text{-}pr)_4$ containing systems as opposed to those without. The Intensity of the observed scattering in the SAXS profiles of PTMO modified sol-gels are increased on $Ti(i\text{-}pr)_4$ addition. However, the correlation distance, taken from the SAXS peak, indicates that the phase separation is the same for both types of materials. Slightly altering the reaction procedure, though, has been demonstrated to change the correlation distance measured by SAXS for a 30Ti-48PTMO(2) composition.

Aging is significant in both the linear and multifunctional PTMO modified $Ti(i\text{-}pr)_4$ containing sol-gel systems. Similar to the multifunctional silicate glasses reported in Chapter IV, aging in the hybrid PTMO systems is initially due to further reaction of the alkoxide species. This results in an increase of the Young's modulus resulting from a higher crosslink density. However, the extremely high Young's modulus observed for many of the aged multifunctional Ti-PTMO gels is simply the result of a vitrified polymeric component in the hybrid material rather additional crosslinks. The high moduli observed after aging is clearly a function of the state of the polymer. Increased restrictions on the chain ends from further crosslinking is, undoubtedly, the reason the PTMO chains vitrify at ~22°C; reduced mobility forced on the chains by the tied ends requires that more thermal energy be put into the system to generate the backbone motion associated with the glass transition, hence a higher T_g is observed for the restricted chains.

The PTMO containing sol-gels suffer from a long term loss of elongation due to a second type of "aging": polymer depolymerization. However, no change is observed, as a function of time, in the correlation length shown by SAXS profiles of a PTMO(2900) material. This result indicates that there is no change in the gross structure of the material matrix with time.

CHAPTER VII

MODIFIED OXIDE SOL-GEL MATERIALS

7.1 Introduction

The basic sol-gel scheme employed to make hybrid materials allows for two fundamentally different types of modifications: the oligomer/polymer component can be modified and/or the oxide component(s) can be modified. Since the effects incurred by changing the oligomer component have been studied in detail elsewhere [19, 20], the studies undertaken in this work focused on, primarily, exploring the contributions of the oxide component to the properties of sol-gel materials. The following chapter will ***introduce*** the newest developments in this direction. Two different types of oxide modifications will be presented in this chapter: "structural modification" of the silicate component and substitution of the titania component in previous hybrid compositions by alumina, zirconia and zinc oxide. PTMO(5) will be used as the polymer modifying component for all of these new hybrid systems; the compositions will all be based on the 15Ti-53PTMO(5) gel studied in Chapter VI. This "standard" has been chosen to provide a relatively well characterized reference with which to compare the new materials.

7.2 Nomenclature

The nomenclature used to identify the new oxide modified materials to be presented is based on the standard composition: 15Ti-53PTMO(5). Materials that have been made using MTEOS or DMDEOS instead of TEOS will include an additional symbol, either an 'M' or a 'D' respectively, to signify the substitution. The metal substituted oxides will simply contain the traditional chemical symbols that represent the metal used. For example, 15Al-53PTMO(5) identifies a gel in which alumina has been substituted for titania. Furthermore, since only one source for each metal was used, the nomenclature, at present, need not distinguish the type of precursor (i. e. alkoxide or acetylacetonate) used to incorporate the metal in question. Although in this chapter, the substituted metals all originated from acetylacetonate precursors (except for the 15Ti-53PTMO(5) material used for comparison). Unlike past chapters, the nomenclature used here will not accurately reflect the true starting composition of the gels; these are given, along with the final composition in terms of silicate metal oxide and polymer, in Table 22 on page 250. The initial wt% values in Table 22 underscore the differences between the various reagents used to modify the sol-gel derived oxide. The starting compositions for these new materials were calculated to approach, as closely as possible, the molar ratio of the components that constitute the reference material: 15Ti-53PTMO(5) (also given in Table 22). The nomenclature used was chosen, therefore, to reinforce the similarities between the modified oxide gels and the "standard" 15Ti-53PTMO(5) gel. Though the starting compositions and some of the final weight percent compositions vary, the ***molar compositions*** of the gels are generally quite consistent and close to the chosen reference.

Table 22. Starting and final composition of hybrid oxide sol-gel materials

sample	quantity	metal oxide	silicate	PTMO(5)
15Ti-53PTMO(5)	initial wt%	15.0	31.6	53.4
	final wt%	6.5	17.8*	75.7
	molar ratio	5.7	21.4*	1.0
15Ti-32M-53PTMO(5)	initial wt%	16.2	26.5	57.3
	final wt%	6.1	16.9*	77.0
	molar ratio	5.7	19.9*	1.0
15Ti-32D-53PTMO(5)	initial wt%	16.5	24.8	58.7
	final wt%	5.9	19.2*	74.9
	molar ratio	5.7	21.4*	1.0
15Al-53PTMO(5)	initial wt%	16.8	31.0	52.2
	final wt%	7.7	16.9*	75.4
	molar ratio	5.7	21.5*	1.0
15Zn-53PTMO(5)	initial wt%	14.1	32.0	53.9
	final wt%	6.1	17.2*	76.7
	molar ratio	5.7	21.5*	1.0
15Zr-53PTMO(5)	initial wt%	23.3	28.6	48.1
	final wt%	9.1	16.5*	74.3
	molar ratio	5.7	21.5*	1.0

*includes contribution from triethoxysilane groups on polymer
†based on 100% conversion

7.3 Results and Discussion

3.1 Modified Silicates: MTEOS & DMDEOS incorporation

MTEOS and DMDEOS were chosen as substitutes for the TEOS component in 15Ti-53PTMO(5) composition gels to observe the effects of oxide functionality on the material structure (discussed at length in Chapter IV for pure sol-gel oxides). These effects are expected to be two-fold: 1) increased homogeneity and 2) decreased crosslink density. The methyl substituents on the MTEOS and DMDEOS silicate components should be more compatible with the aliphatic portions of the PTMO(5) polymer. Improved compatibility would promote better phase mixing between the silicate ester and the polymer modifier. Consequently, sol-gel materials higher in homogeneity should be produced by using methyl substituted silicate esters as opposed to using tetraethylorthosilicate (TEOS). A more homogeneous material, in turn, should display a higher modulus and greater strength than its phase separated counterpart (based on the discussion in Chapter VI). On the other hand, the methyl substituents, though improving compatibility, reduce the number of reactive sites on the silicate components. This deleterious effect limits the number of potential crosslinks; each methyl substituent displaces one potential crosslink site. The greater the amount of TEOS replaced by MTEOS or DMDEOS in the reaction mixture, the lower the potential crosslink density in the oxide component of the final gel. In the extreme, for full DMDEOS substitution, the silicate component can only form linear connections; a network formed in such a case would probably be the result of the multifunctional polymer crosslinking with itself (which most likely occurs regardless of the silicate component - see the discussion on the aging effect in Chapter VI). The TiO_2 component in the gel, it is noted, also forms crosslinks but because of its low relative concentration, ~7 wt%, the number of crosslinks contributed would be expected to be small.

Two gel compositions were made as preliminary materials to observe the gross effects of either complete substitution of MTEOS or DMDEOS. These materials, listed in Table 22, were made according to the procedures outlined in Chapter III section 3.3.2. Both compositions formed clear monolithic gelled films on the same relative timescale as the TEOS compositions.

Figure 80 on page 253 contains the stress-strain curves obtained for three comparably aged gels of different silicate composition: (A) 100% DMDEOS aged 7 days at ~22°C, (B) 100% TEOS (reference) aged 7 days at ~22°C and (C) 100% MTEOS aged 6 days at ~22°C. Remarkably, the DMDEOS gel (15Ti-32D-53PTMO(5)) shows qualitatively the same tensile behavior as the TEOS gel (15Ti-53PTMO(5) or 15Ti-32T-53PTMO(5)). At the same relative age, the MTEOS gel shows a surprisingly low flat stress-strain curve relative to that observed for either the DMDEOS or TEOS gel. This result is very puzzling; that the DMDEOS and TEOS gels but not the MTEOS gels would be similar was not expected. Figure 81 on page 254 contains the stress-strain curves of the 15Ti-32M-53PTMO(5) gel for two different aging times. After 21 days at ~22°C this gel, which displayed poor mechanical properties after 6 days (curve B), shows a relatively high modulus and the yield behavior commonly seen for aged 15Ti-53PTMO(5) gels in Chapter VI. Table 23 on page 255 lists the mechanical behavior measured from the tensile strain to break test. After 7 days at ~22°C the mechanical properties of the 15Ti-32D-53PTMO(5) gels are at least equivalent to if not better than those of the corresponding 15Ti-53PTMO(5) gels. On the other hand, as was qualitatively seen in the stress strain curves, the 15Ti-32M-53PTMO(5) gels after 6 days at ~22°C are clearly inferior in strength to both the TEOS and the DMDEOS substituted gels. However, after 21 days at ~22°C the 15Ti-32M-53PTMO(5) gels display an increase of greater than one order of magnitude in the measured Young's modulus. The mechanical properties of the MTEOS substituted material after 21 days begin to approach that of the corresponding 15Ti-53PTMO(5) material.

The changes observed in the stress-strain behavior of the 15Ti-32M-53PTMO(5) gel with time, especially the emergence of a yield point, indicate the same sort of aging phenomenon occurs as was previously observed for the hybrid TEOS based oxide materials. The dynamic

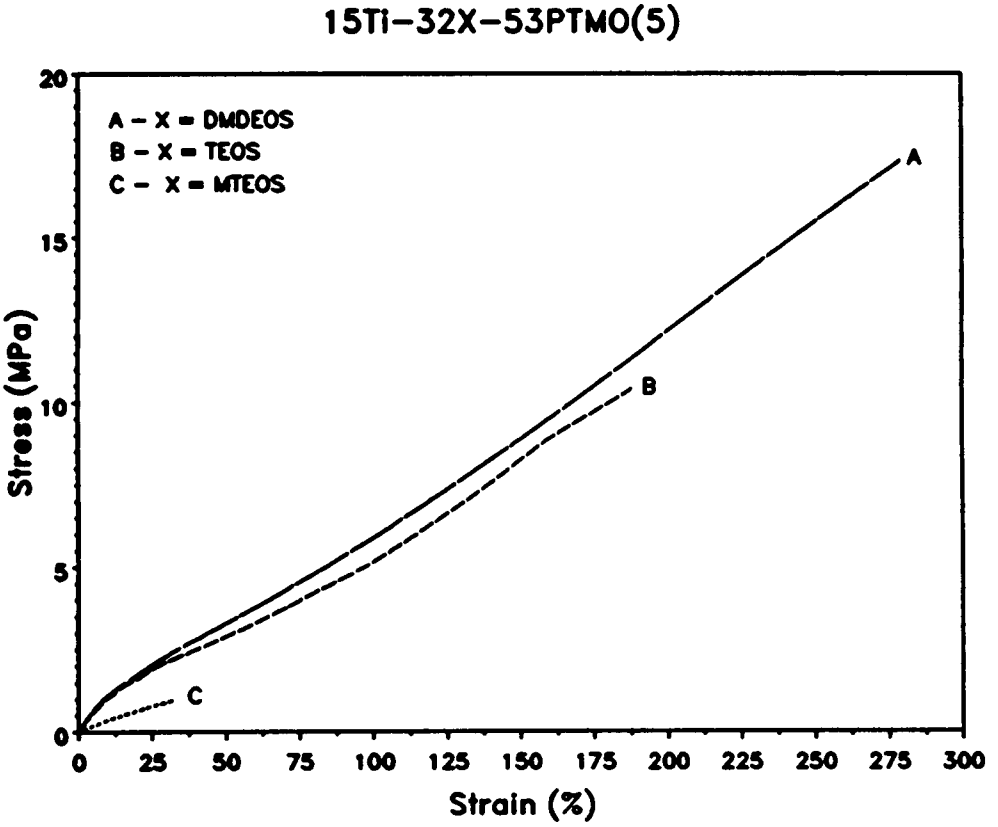

Figure 80. Stress-strain curves of 15Ti-32X-53PTMO(5) gels

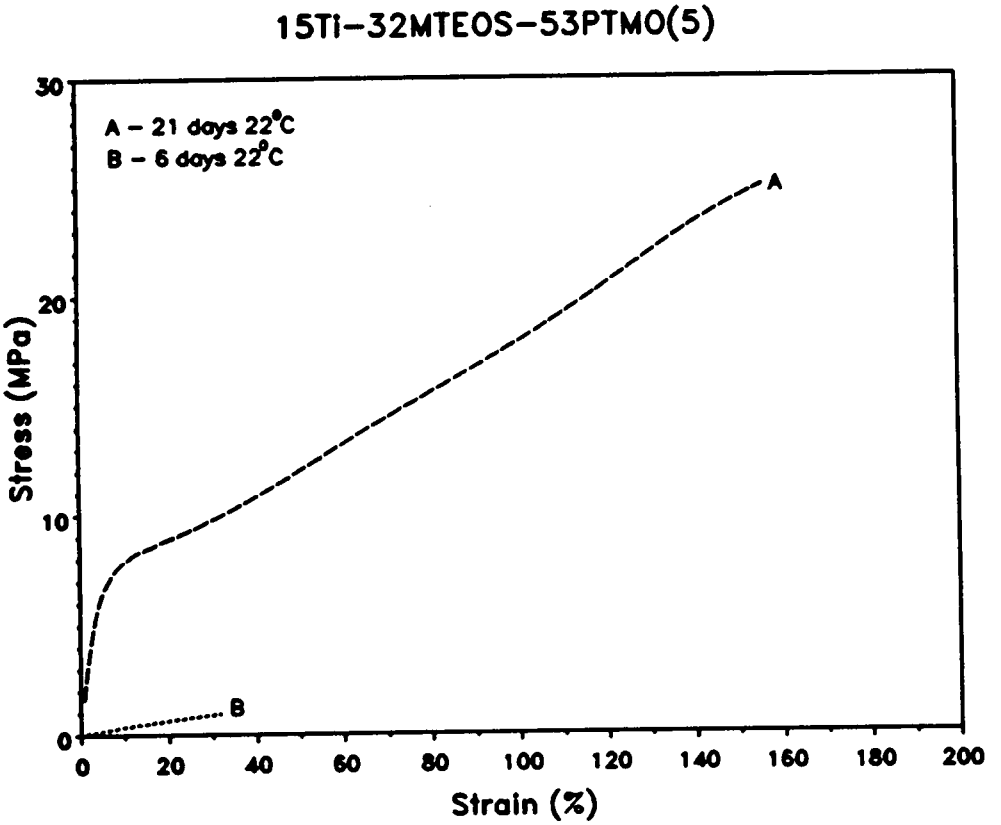

Figure 81. Stress-strain curves of 15Ti-32M-53PTMO(5) gels

Table 23. Mechanical properties of MTEOS and DMDEOS modified sol-gel materials

sample	days at 22°C	elongation at break (%)	ultimate strength (MPa)	Young's modulus (MPa)
15Ti-53PTMO(5)	7	185±17	10±2	12±5
15Ti-53PTMO(5)	21	109±14	29±3	360±24
15Ti-32M-53PTMO(5)	6	62±22	1.5±0.4	3.3±0.9
15Ti-32M-53PTMO(5)	20	172±13	25.5±3.0	183±21
15Ti-32D-53PTMO(5)	7	282±31	17.8±2.6	13.8±4.2

mechanical spectra given in Figure 82 confirm this suspicion for the 15Ti-32M-53PTMO(5) material. After 6 days at ~22°C (triangles) the tanδ curve displays a large broad glass transition that is centered at $\simeq$ -30°C but approaches zero at ~10°C. The corresponding storage modulus curve, at 0°C, has dropped more than two orders of magnitude; the 6 day old 15Ti-32M-53PTMO(5) gel is well into its rubbery plateau region above 0°C. At room temperature (~22°C) this material would be expected to display a low Young's modulus in the tensile strain to break test. After 20 days, both the tanδ curve and the storage modulus curve indicate that the material at 20°C is glassy in nature (which, as in Chapter VI, explains the yielding behavior observed in the stress-strain curves of this gel). The dynamic mechanical spectra in Figure 83 on page 258, comparing the 6 day old sample (triangle) to one that had been annealed in the dynamic mechanical instrument at 100°C for $\simeq$ 1 hour (squares), demonstrate that the aging effect can be accelerated - witness the shift to higher temperatures of the glass transition.

Figure 84 on page 260 contains the corresponding dynamic mechanical curves obtained for a 15Ti-32D-53PTMO(5) sample aged at ~22°C for 7 days (triangles) along with the curves for samples annealed at 150°C (squares) and 200°C (crosses) in the dynamic mechanical instrument (heated at 2°C/min to the annealing temperature then slow-cooled to ambient conditions). The 7 day old specimen displays a prominent tandδ transition centered at ~30°C. The storage modulus curve for this sample at 20°C is undergoing the glass transition but is still, relatively speaking, higher than that observed for the 6 day old 15Ti-32M-53PTMO(5) sample at the same temperature - this correlates with the observed stress-strain behavior for the same two gels (see Figure 80). The observed shifting of the glass transition with annealing indicates that this material, like the MTEOS and TEOS materials, can become vitrified at room temperature (~22°C). Again, this result is somewhat surprising. The shifted tanδ curves observed in Figure 84 for the annealed specimens suggests that the lowered functionality of the added DMDEOS silicate, contrary to expected, does not prevent the material from vitrifying. Since the DMDEOS is only difunctional, the crosslinking that results in the

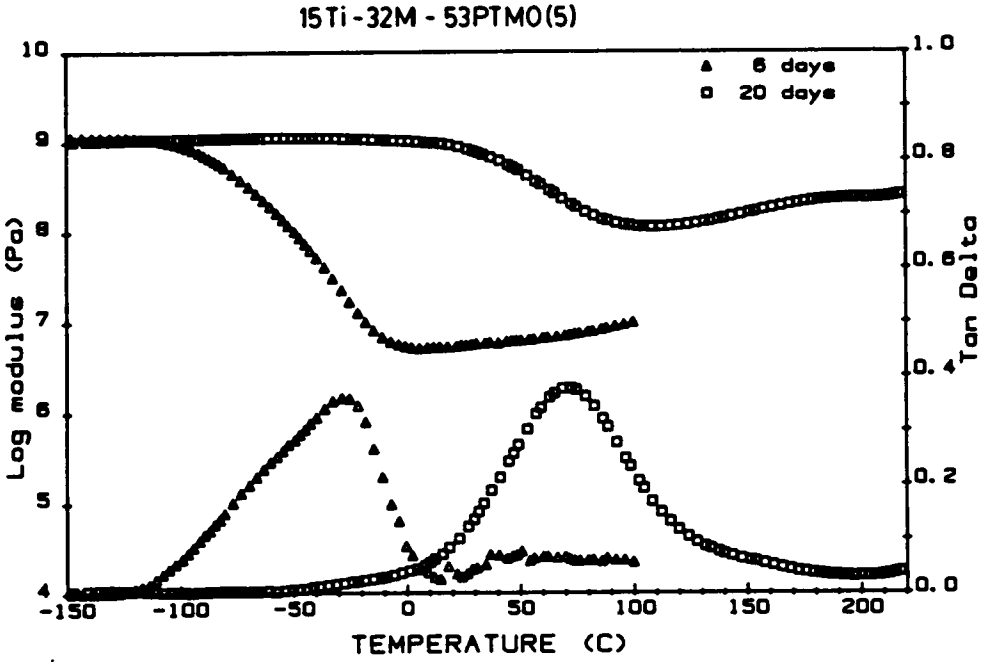

Figure 82. Dynamic mechanical spectra of 15Ti-32M-53PTMO(5) gels vs age: (triangles) 6 days ~22°C, (squares) 20 days ~22°C

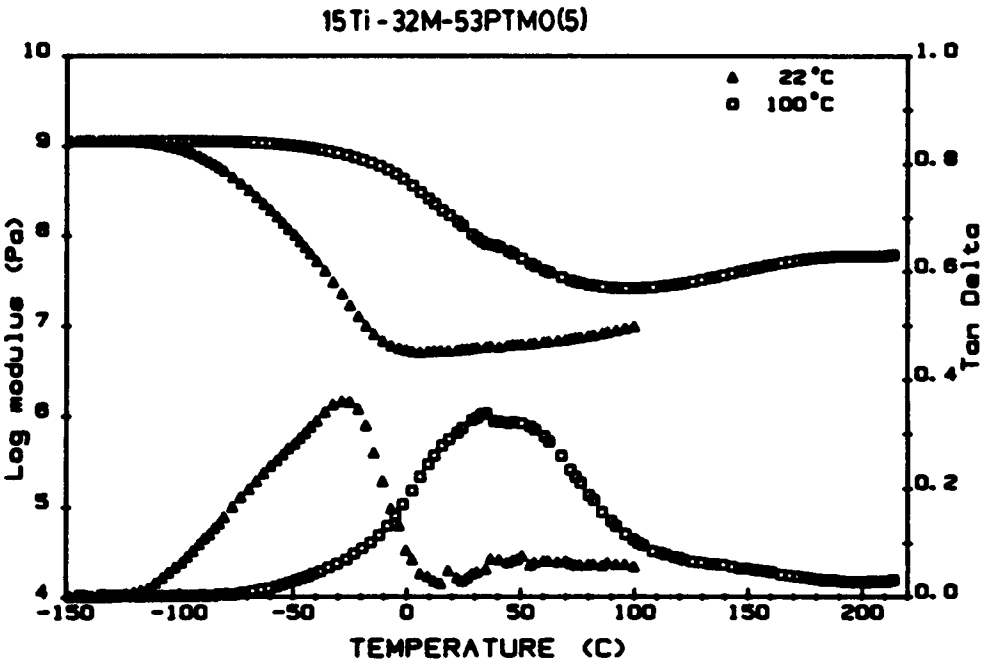

Figure 83. Dynamic mechanical spectra of annealed 15Ti-32M-53PTMO(5) gels: (triangles) 6 days ~22°C, (squares) ~1 hr 100°C

observed shift to higher temperatures of the T_g of the PTMO chains must be due to the triethoxysilane functional groups on the PTMO(5) polymer itself.

7.3.2 Modified Metal Oxides: Metal Acetyl Acetonate Incorporation

One of the fundamental goals of this work was to incorporate metals other than silicon into hybrid sol-gel systems. This was successfully accomplished for Ti using $Ti(i\text{-}pr)_4$. $Al(s\text{-}bu)_3$ incorporation was attempted, using the modified sol-gel scheme developed for $Ti(i\text{-}pr)_4$ incorporation, with only limited success. The $Al(s\text{-}bu)_3$ was prone to react rapidly on exposure to moisture and quickly formed a "useless" (from the author's standpoint) Al_2O_3 powder. This result prompted the exploration of metal compounds other than alkoxides as potential sol-gel precursors. Metal acetylacetonates were chosen as prime candidates to replace the unusable alkoxides. $Al(acac)_3$ once in solution, in contrast to $Al(s\text{-}bu)_3$, provided a stable and relatively easy precursor to incorporate into hybrid sol-gel systems. The same was found for $Zr(acac)_4$ and $Zn(acac)_2$. Furthermore, solutions of the metal acetyl acetonates, because of their acid and water content (from the acidic solution added to dissolve the $M(acac)_n$), do not require a CCC procedure to allow the sol-gel process to take place; simply adding the $M(acac)_n$ solution to the reaction mixture initiates the process.

Gelled films were made using Al, Zr and Zn acetylacetonates to determine whether they could be successfully incorporated into a hybrid polymer modified sol-gel scheme. The metal containing gel compositions listed in Table 22 on page 250 were all prepared for study using the procedure outlined in Chapter III section 3.3.3. The three compositions were observed to gel at different rates, the $Zn(acac)_2$ was the slowest (several days) and the $Zr(acac)_4$ the fastest ($<$1/2 hour at room temperature) with the $Al(acac)_3$ composition in between ($\sim$6 hours). A direct consequence of the gel rate was that the 15Zr-53PTMO(5) composition initially formed a thick gel that trapped large quantities of solvent and was prone to severe shrinking. The linear shrinkage observed after gelation and air-drying (measured by comparing the diameter

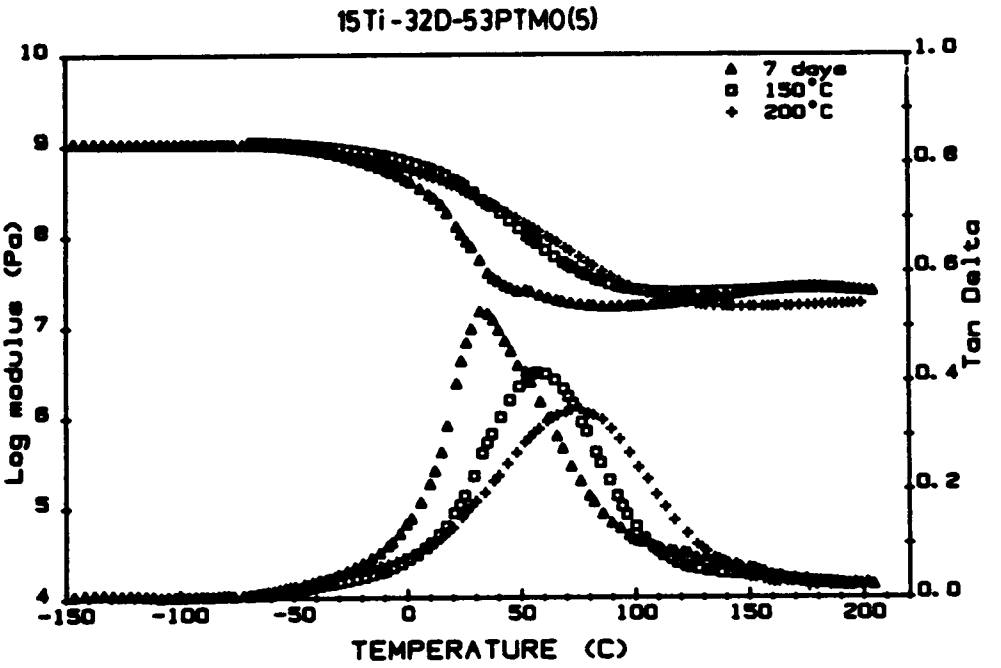

Figure 84. Dynamic mechanical spectra of 15Ti-32D-53PTMO(5) gels: (triangles) 6 days ~22°C, (squares) ~1 hr 150°C, (crosses) ~3 hrs 200°C

of the Petri dish in which the materials were cast to the diameter of the final gel) was a whopping 45.5±0.5% for the 15Zr-53PTMO(5) composition and 24±1% for the 15Al-53PTMO(5) composition but only 8.5±0.0% for the 15Zn-53PTMO(5) composition (which is the slowest gelling system).

Figure 85 on page 262 contains the stress-strain curves for the three different metal acetyl acetonate gels aged 9 days at ~22°C and the corresponding 7 day old 15Ti-53PTMO(5) gel. The data obtained from the tensile strain to break test are listed in Table 24 on page 263. The differences qualitatively observed in the gelation rates of the different metal acetylacetonates are also reflected in the observed tensile behavior. The two slow gelling compositions, 15Zn-53PTMO(5) (A) & 15Al-53PTMO(5) (B), exhibit "elastomeric" stress-strain curves while the rapid gelling 15Zr-53PTMO(5) composition (C) exhibits a steep initial slope and a yield point. These results are substantiated by the dynamic mechanical spectra given in Figure 86 on page 264 for the same materials aged 9 days at ~22°C. The tanδ curves clearly show the 15Zr-53PTMO(5) gel (x's) to be substantially vitrified at ~20°C whereas the other three gels, 15Ti-53PTMO(5) (squares), 15Al-53PTMO(5) (triangles) and 15Zn-53PTMO(5) (crosses), are all comfortably within the glass transition and therefore not vitrified. Additionally, the transition observed in the storage modulus is much smaller for the 15Zr-53PTMO(5) gel than for any of the other gels (as is the observed tanδ transition in Figure 86); this is indirect evidence that the degree of conversion of the sol-gel process is higher in the $Zr(acac)_4$ containing materials than for any of the others.

Thermogravimetric analyses (TGA) were performed on the three metal acetylacetonate compounds, as well as standard 15Ti-53PTMO(5) material, primarily to determine the volatile content in the gelled materials. These experiments were run according to the procedure outlined in Chapter III section 3.4.7. The TGA curves are given in Figure 87 on page 266. The most notable result from the TGA data is that the 15Ti-53PTMO(5) gel (a) does not show any appreciable weight loss until ~200°C. The other gels, 15Zn-53PTMO(5) (b), 15Zr-53PTMO(5) (c) and 15Al-53PTMO (d) all show considerable weight loss beginning at temperatures as low as 75°C. This weight loss, in the temperature region from 0°C to ~225°C, is most likely due

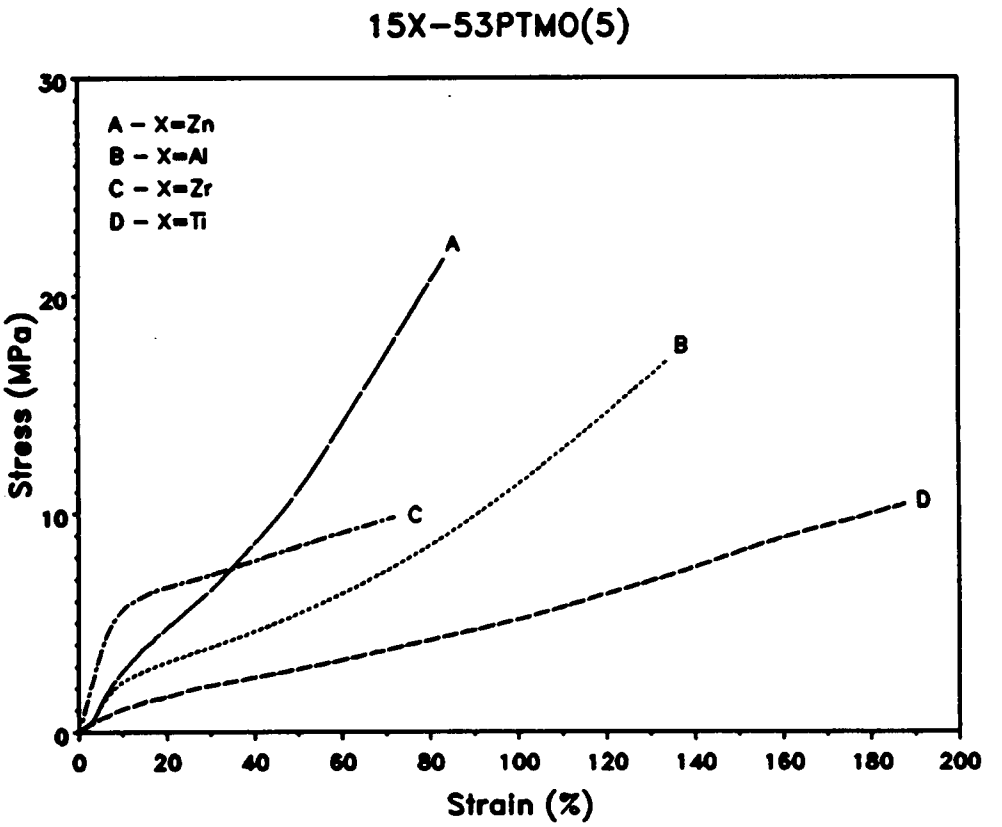

Figure 85. Stress-strain curves of 15X-53PTMO(5) gels

Table 24. Mechanical properties of $M(acac)_n$ modified sol-gel materials

sample	days at 22°C	elongation at break (%)	ultimate strength (MPa)	Young's modulus (MPa)
15Ti-53PTMO(5)	7	185±17	10±2	12±5
15Al-53PTMO(5)	9	132±9	16.2±1.7	29±4
15Zn-53PTMO(5)	9	80±7	19.6±2.2	36±4
15Zr-53PTMO(5)	9	82±11	12.2±2.1	83±14

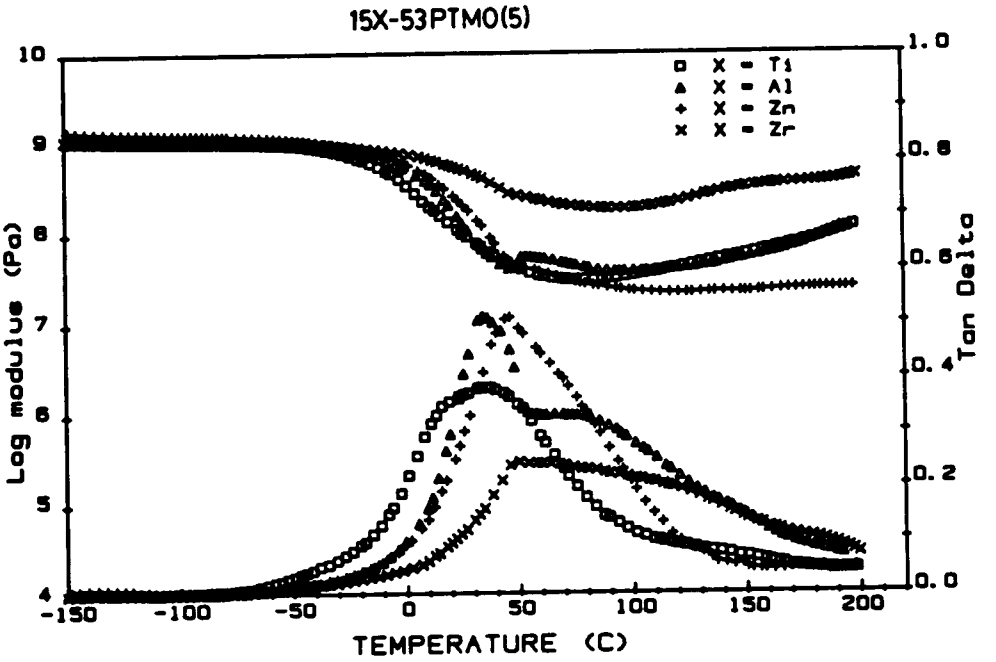

Figure 86. Dynamic mechanical spectra of 15X-53PTMO(5) gels: (squares) X=Ti, (triangles) X=Al, (crosses) X=Zn, (diamonds) X=Zr

to solvent and/or bound organic moieties being removed. At temperatures beyond 200°C the PTMO component is undoubtedly being degraded; it is therefore, not surprising that all of the TGA traces in the 200°C to ~400°C resemble each other with the exception of the 15Zr-53PTMO(5) gel (c) which displays a sharp discontinuity at ~350°C rather than at ~390° as observed for the other gels. Unfortunately, without detailed knowledge of the chemical processes occurring at the elevated temperatures only a qualitative interpretation of the TGA data is possible. However, the TGA curves given in Figure 87 clearly demonstrate that the metal acetylacetonate gels all contain significantly more volatiles or bound organics than do the $Ti(i\text{-}pr)_4$ gels.

7.4 Conclusions From Preliminary Results

Preliminary results from the MTEOS and DMDEOS modified gels presented here, surprisingly, indicate that hybrid sol-gel materials can vitrify somewhat independent of the silicate functionality. This, in turn, indicates that the vitrification observed on aging multifunctional PTMO modified sol-gel materials may be due to the crosslinking of functional groups contained on the polymer rather further reaction of the silicate component. Additionally, it has been demonstrated that metal acetylacetonates can be successfully incorporated into hybrid sol-gel schemes. This allows, potentially, any soluble metal acetylacetonate to be incorporated into hybrid materials made by this route.

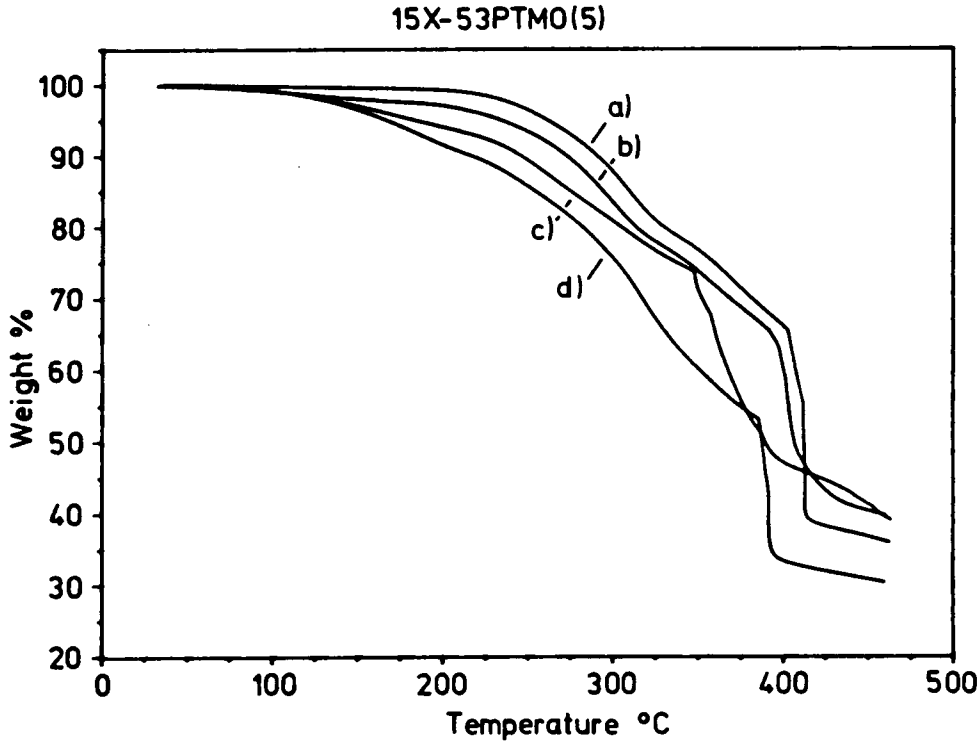

Figure 87. Thermo-gravimetric analysis of 15X-53PTMO(5) gels: a) X=Ti, b) X=Zn, c) X=Zr, d) X=Al

CHAPTER VIII

CONCLUSIONS AND RECOMMENDATIONS

8.1 Summary

A number of goals were established at the outset of this work. These goals can be condensed into two basic mandates: 1) "synthesize" new types of hybrid sol-gel materials incorporating metals other than silicon, 2) characterize the material matrix formed in the new and existing sol-gel systems to determine the structure-property relationships. In the both of these regards, the work undertaken has been relatively successful. Procedures have been developed to make new hybrid sol-gel materials that allowed the incorporation of not only multifunctional silicon alkoxides and titaniumisopropoxide, but several different metal acetylacetonates as well. Characterization of these materials using spectroscopic and mechanical methods provided certain key insights to their structure-property behavior. Specifically, NMR and Raman studies helped to determine the degree of conversion and the chemical composition of the silicate sol-gel matrix formed under acidic conditions. SAXS profiles, in turn, provided information regarding the degree of phase separation and the cor-

relation distance between the phases while tensile stress-strain and dynamic mechanical studies allowed correlation of the observed properties with known structural features.

8.2 Conclusions

In light of the results presented in prior chapters, the following conclusions can be made concerning the sol-gel process in general and the hybrid sol-gel materials studied in particular:

1. The sol-gel process for HCl catalyzed silicon ethoxides using 1/2 the stoichiometric amount of H_2O goes to at least 87% conversion when gelled at ~22°C.
2. The sol-gel process proceeds to equally high degrees of conversion for all multifunctional silicon ethoxide components.
3. Hydrolysis is the limiting reaction (under the above conditions) for silicates of actual functionality $\leq$3.0.
4. Condensation is the limiting reaction (under the above conditions) for silicates of actual functionality $\geq$3.0 (the system is limited by vitrification i. e. it is governed by "TTT" type behavior).
5. Vitrification occurs for multifunctional silicate gels with an actual functionality of $\geq$3.0.
6. Turbidity when observed in multifunctional silicate sol-gels is due to pore structure of sufficient size (~20nm) to scatter visible light (the pore structure is probably a consequence of the post gelation drying rate).
7. The sol-gel process in TEOS-PDMS(1700) hybrid materials (CERAMERs) goes to relatively high conversions (~94%).
8. The sol-gel process run under acidic conditions (using 1/2 the stoichiometric amount of water) results, generally, in the formation of four-membered (D4) silicate rings.

9. Incorporation of $Ti(i\text{-}pr)_4$ into hybrid oligomer/polymer modified sol-gel materials to form monolithic crack-free amorphous gels is possible.
10. Incorporation of $Ti(i\text{-}pr)_4$ imparts a yellow hue to the material and increases the Young's modulus relative to corresponding 0 wt% $Ti(i\text{-}pr)_4$ materials.
11. Functionalized PTMO oligomer/polymer modified sol-gel systems display post gelation aging effects due to, primarily, a slow continuation of the crosslinking process ***by the oligomer/polymer functional groups***.
12. The loss of ultimate properties observed in functionalized oligomer/polymer gels held for long times ($\geq$100 days) at ~22°C or short times at elevated temperatures is probably due to depolymerization of the PTMO.
13. The tensile behavior of the hybrid sol-gel materials is determined by the physical state of the oligomeric/polymeric component. Yielding behavior in the stress-strain curves is the result of a predominantly vitrified PTMO component.
14. Slow gelation of 30 wt% $Ti(i\text{-}pr)_4$ containing PTMO hybrid materials can result in large scale phase separation.
15. Better dispersion of the oxide throughout the material matrix produces higher modulus and higher strength materials.
16. Metal acetylacetonates can be used in the sol-gel process to produce monolithic crack-free gels containing mixed metal oxides.
17. Ti and Zr act as (condensation) catalysts for the sol-gel process.

8.3 Recommendations and Future Directions

NMR and Raman spectroscopy have been somewhat "underused" in this study. Only the most rudimentary information has been extracted from these two analytical techniques. The solid state ^{29}Si NMR has been used to observe and quantify the different silicate structures

in silicate gels; using this information, the degree of conversion of the sol-gel process was determined. Likewise Raman spectra have been interpreted with an eye for determining the degree of hydrolysis and identifying the unreacted sites on the alkoxide components of silicate systems. The solid state NMR and Raman techniques, though, have been generally unable to provide the same type of quantitative information for the PDMS(1700) modified sol-gel systems as was obtained for the multifunctional silicates. The primary reason for this is the overwhelming amount of "modifying" oligomer present in the hybrid gels. Refinement of the CP/MAS parameters to obtain reasonably quantitative spectra, as was successfully accomplished in Chapter IV, holds promise that the solid state ^{29}Si NMR experiment may yet provide quantitative data for hybrid sol-gels with high oligomer content (despite the low concentration of "Q" forming TEOS species). These studies are worth pursuing.

High resolution Raman spectroscopy, in turn, should compliment the NMR data obtained and provide a wealth of information on the nature of the structures formed in hybrid sol-gel materials: especially those containing mixed metal oxides. However, Raman experiments on PDMS hybrid sol-gel materials, in addition to the concentration problem observed in NMR, are generally plagued by spectral overlap (from the PDMS), low observed signal to noise ratios and high background fluorescence due to trapped organics. The use of annealed samples would greatly reduce the fluorescence problem in the Raman spectra as well as "eliminate" the observed aging effects on mechanical properties. Future Raman work (as well as NMR work), therefore, should focus on samples that have been heat treated to remove any residual solvent and/or reaction by-products trapped in the "as gelled" materials. Further investigations should also focus on sol-gel materials of higher silicate content that are not modified with PDMS. Such samples would not result in the same spectral overlap as observed with the PDMS containing materials. Also, high TEOS content gels would alleviate the "concentration" or lack of sensitivity problem by amplifying the silicate signals relative to that of the modifying component.

The data presented in Chapters V-VII for titania containing materials imply that the degree of phase separation between the oligomer modifying component and the inorganic oxide

is sensitive to the gel composition and rate of gelation. Both optical and, in the case of the multifunctional PTMO systems, mechanical properties seem to be affected by the degree of phase separation in the Ti containing hybrid sol-gels. Evidence was discovered that indicates a unique spherelike morphology is formed in certain $Ti(i\text{-}pr)_4$ containing materials. More elaborate and detailed gelation studies, including both SAXS and WAXS, optical microscopy and TEM analysis should be undertaken on, specifically, the 30Ti-50PTMO(2900) SP & LP gels (and the 30 wt% $Ti(i\text{-}pr)_4$ hybrid gels in general) to determine the exact cause and nature of the observed microstructure. NMR studies utilizing different solid state NMR experiments (such as ^1H CRAMPS spin diffusion and static ^1H T_2^* dephasing experiments) should be undertaken to determine the relative mobility in the different components of such phase separated hybrid sol-gel systems, thereby providing an indication of the structure within each phase.

Aging studies should be conducted on ***stabilized*** PTMO hybrid gels. Such studies would confirm (or refute) the conclusion that the loss of ultimate properties on long term aging is the result of PTMO depolymerization. A series of unstabilized PTMO gels that had been extracted could also be observed to determine if a "wash" procedure effectively removes the species responsible for the proposed depolymerization that occurs (primarily residual acid).

Finally, the procedures developed to incorporate metal acetylacetonates into hybrid systems opened the "Pandora's box" of new sol-gel materials. In principle, any metal that forms a soluble acetylacetonate could be utilized in such a process. This "new" chemistry, however, will require much study before the effects of using an acetylacetonate complex (rather than an alkoxide precursor) on the final sol-gel structure are known. For this reason, it is recommended that, in future work, comparisons are made between gelled materials of the same composition made using different starting materials. Gels containing zirconium, for example, could be studied as a function of using $Zr(acac)_4$, zirconyl nitrate hydrate and/or zirconium isopropoxide.

CHAPTER IX

REFERENCES CITED

1. H. Schmidt, H. Scholze, A. Kaiser, **J. Non-cryst. Solids**, 63 (1984) 1.
2. H. Schmidt, B. Seiferling, **Mate. Res. Soc. Symp. Proc.**, 73 (1986) 739.
3. G. Philipp, H. Schmidt, **J. Non-cryst. Solids**, 63 (1984) 283.
4. G. Philipp, H. Schmidt, **J. Non-cryst. Solids**, 82 (1986) 31.
5. H. Schmidt, **J. Non-cryst. Solids**, 73 (1985) 681.
6. H. Scholze, **J. Non-cryst. Solids**, 73 (1985) 669.
7. J. E. Mark, S. J. Pan, **Makromol. Chem. Rapid Comm.**, 3 (1982) 681.
8. C. Y. Jiang, J. E. Mark, **Makromol. Chem.**, 18 (1984) 2609.
9. Y. P. Ning, M. Y. Tang, C. Y. Jiang, J. E. Mark, W. C. Roth, **J. Appl. Polym. Sci.**, 29 (1984) 3209.
10. J. E. Mark, Y. P. Ning, C. Y. Jiang, M. Y. Tang, W. C. Roth, **Polymer**, 26 (1985) 2069.
11. J. E. Mark, J. L. Sullivan, **J. Chem. Phys.**, 66(3) (1977) 1006.
12. M. A. Llorente, J. E. Mark, **Macromolecules**, 13 (1980) 681.
13. S. B. Wang, J. E. Mark, **Polym. Bull.**, 17 (1987) 271.
14. G. L. Wilkes, B. Orler, H. Huang, **Polym. Prep.**, 26(2) (1985) 300.
15. H. Huang, B. Orler, G. L. Wilkes, **Polym. Bull.**, 14(6) (1985) 557.

16. C. S. Parkhurst, L. A. Doyle, L. A. Silverman, S. Singh, M. P. Anderson, D. McClurg, G. E. Wnek, D. R. Uhlmann, **Mat. Res. Soc. Symp. Proc.**, 73 (1986) 769.

17. H. Huang, B. Orler, G. L. Wilkes, **Macromolecules**, 20(6) (1987) 1322.

18. H. H. Huang, R. H. Glaser, G. L. Wilkes, **ACS Symposium Series**, 360 (1988) 354.

19. J. L. Noell, **M.S. Thesis**, Virginia Polytechnic Institute and State University, 1987.

20. H. H. Huang, **Ph.D. Dissertation**, Virginia Polytechnic Institute and State University, 1988.

21. H. Dislich, **J. Non-cryst Solids**, 73 (1985) 599.

22. L. G. Hubert-Pfalzgraf, **New Journal of Chem.**, 11 (1987) 663.

23. L. C. Klein, **Ann. Rev. Mater. Sci.**, 15 (1985) 227.

24. S. Sakka, K. Kamiya, **J. Non-cryst. Solids**, 42 (1980) 403.

25. S. P. Mukherjee, **J. Non-cryst Solids**, 42 (1980) 477.

26. P. J. Flory, Principles of Polymer Chemistry, (Cornell University Press, Ithaca, 1953) 353.

27. M. F. Bechtold, R. D. Vest, L. Plambeck Jr., **J. Am. Chem. Soc.**, 90 (1968) 4590.

28. B. W. Peace, K. G. Mayhan, J. F. Montle, **Polymer**, 14 (1973) 420.

29. R. K. Iler, The Chemistry of Silica, (John Wiley & Sons, New York, 1979).

30. L. C. Klein, G. J. Garvey, **J. Non-cryst. Solids**, 38 & 39 (1980) 45.

31. B. E. Yoldas, **J. Non-cryst. Solids**, 63 (1984) 145.

32. B. E. Yoldas, **J. Non-cryst. Solids**, 83 (1986) 375.

33. I. Artaki, T. W. Zerda, J. Jonas, **J. Non-cryst Solids**, 81 (1986) 381.

34. R. Aelion, A. Loebel, F. Eirich, **J. Am. Chem. Soc.**, 72 (1950) 5705.

35. C. J. Brinker, K. D. Keefer, D. W. Schaefer, C. S. Ashley, **J. Non-Cryst. Solids**, 48 (1982) 47.

36. K. D. Keefer, **Mat. Res. Soc. Symp. Proc.**, 32 (1984) 15.

37. D. W. Schaefer, K. D. Keefer, **Mat. Res. Soc. Symp. Proc.**, 32 (1984) 1.

38. C. J. Brinker, K. D. Keefer, D. W. Schaefer, R. A. Assink, B. D. Kay, C. S. Ashley, **J. Non-cryst. Solids**, 63 (1984) 45.

39. D. W. Schaefer, K. D. Keefer, **Mat. Res. Soc. Symp. Proc.**, 73 (1986) 277.

40. L. C. Klein, G. J. Garvey, **Mat. Res. Soc. Symp. Proc.**, 32 (1984) 33.

41. I. Strawbridge, A. F. Craievich, P. F. James, **J. Non-cryst. Solids**, 72 (1985) 139.

42. I. Artaki, S. Sinha, A. D. Irwin, J. Jonas, **J. Non-cryst. Solids**, 72 (1985) 391.

43. D. W. Schaefer, J. P. Wilcoxon, K. D. Keefer, B. C. Bunker, R. K. Pearson, I. M. Thomas, D. E. Miller, in: Physics and Chemistry of Porous Media, J. Koplik, J. Banavar, K. Winkler, eds. (Am. Inst. of Physics, New York, 1987).

44. L. H. Sommer, C. L. Frye, **J. Am. Chem. Soc.**, 82 (1960) 3796.

45. L. H. Sommer, C. L. Frye, M. C. Musolf, G. A. Parker, P. G. Rodewald, K. W. Michael, Y. Okaya, P. Peplinski, **J. Am. Chem. Soc.**, 83 (1961) 2210.

46. T. H. Lowry, K. S. Richardson, Mechanism and Theory in Organic Chemistry 2nd Ed., (Harper & Row, New York, 1981).

47. G. W. Scherer, C. J. Brinker, E. P. Roth, **J. Non-cryst. Solids**, 72 (1985) 369.

48. D. C. Bradley, R. C. Mehrotra, D. P. Gaur, Metal Alkoxides, (Academic Press, London, 1978).

49. K. Kamiya, K. Tanimoto, T. Yoko, **J. Mat. Sci. Lett.**, 5 (1986) 402.

50. B. E. Yoldas, **J. Mat. Sci.**, 21 (1985) 1087.

51. M. Yamane, S. Inoue, K. Nakazawa, **J. Non-cryst. Solids**, 48 (1982) 153.

52. B. E. Yoldas, **J. Non-cryst. Solids**, 38 & 39 (1980) 81.

53. L. C. Klein, in: Design of New Materials, D. L. Cooke and A. Clearfield, eds. (Plenum Publishing Co., 1987).

54. C. Zhu, L. Hou, F. Gan, Z. Jiang, **J. Non-cryst. Solids**, 63 (1984) 105.

55. M. Nogami, **J. Non-cryst. Solids**, 69 (1985) 415.

56. M. Nogami, M. Tomozawa, **J. Am. Ceram. Soc.**, 69(2) (1986) 99.

57. J-Y. Chane-Ching, L. C. Klein, **J. Am. Ceram. Soc.**, 71(1) (1988) 83.

58. W. Höland, E. R. Plumat, P. H. Duvigneaud, **J. Non-cryst. Solids**, 48 (1982) 205.

59. B. E. Yoldas, **J. Mat. Sci.**, 10 (1975) 1856.

60. C. J. R. Gonzalez-Oliver, P. F. James, H. Rawson, **J. Non-cryst. Solids**, 48 (1982) 129.

61. M. Emili, L. Incoccia, S. Mobilio, G. Fagherazzi, M. Guglielmi, **J. Non-cryst. Solids**, 74 (1985) 129.

62. J. Covino, R. A. Nissan, **Mat. Res. Soc. Symp. Proc.**, 73 (1986) 565.

63. J. Covino, R. A. Nissan, **Mat. Res. Bull.**, 21 (1986) 337.

64. A. Duran, C. Serna, V. Fornes, J. M. Fernandez Navarro, **J. Non-cryst. Solids**, 82 (1986) 69.

65. R. A. Assink, B. D. Kay, **Mat. Res. Soc. Symp. Proc.**, 32 (1984) 301.

66. T. Kawaguchi, H. Hishikura, J. Iura, Y. Kokubu, **J. Non-cryst Solids**, 63 (1984) 61.

67. J. Zarzycki, Ultrastructure Processing of Ceramics, Glasses and Composites, L. L. Hench, D. R. Ulrich eds., (John Wiley & Sons, 1984) 27.

68. T. W. Zerda, I. Artaki, J. Jonas, **J. Non-cryst. Solids**, 81 (1986) 365.

69. L. W. Kelts, N. J. Effinger, S. M. Melpolder, **J. Non-cryst. Solids**, 83 (1986) 353.

70. I. Artaki, M. Bradley, T. W. Zerda, J. Jonas, **J. Phys. Chem.**, 89 (1985) 4399.

71. J. Schaefer, E. O. Stejskal, in: Topics in C-13 NMR Spectroscopy, G. C. Levy ed., (John Wiley & Sons, New York, 1979) 283.

72. C. S. Yannoni, **Acc. Chem. Res.**, 15 (1982) 201.

73. J. R. Lyerla, C. S. Yannoni, C. A. Fyfe, **Acc. Chem. Res.**, 15 (1982) 208.

74. M. Mehring, Principles of High Resolution NMR in Solids 2nd Ed., (Springer-Verlag, Berlin, 1983).

75. K. Beshah, J. E. Mark, J. L. Ackerman, A. Himstedt, **J. Polym. Sci. Polym. Phys. Ed.**, 24 (1986) 1207.

76. F. L. Galeener, **Phys. Rev. B**, 19(8) (1979) 4292.

77. F. L. Galeener, R. A. Barrio, E. Martinez, R. J. Elliot, **Phys. Rev. Lett.**, 53 (1984) 2429.

78. D. R. Tallant, B. C. Bunker, C. J. Brinker, C. A. Balfe, **Mat. Res. Soc. Symp. Proc.**, 73 (1986) 261.

79. L. C. Klein, C. Nelson, K. L. Higgins, **Mat. Res. Soc. Symp. Proc.**, 32 (1984) 293.

80. D. M. Krol, J. G. Van Lierop, **J. Non-cryst. Solids**, 63 (1984) 131.

81. V. Gottardi, M. Guglielmi, A. Bertoluzza, C. Fagnano, M. A. Morelli, **J. Non-cryst. Solids**, 63 (1984) 71.

82. A. Bertoluzza, C. Fagnano, M. A. Morelli, V. Gottardi, M. Guglielmi, **J. Non-cryst. Solids**, 48 (1982) 117.

83. J. C. Debsikdar, **J. Mat. Sci.**, 20 (1985) 4454.

84. W. L. Olson, L. J. Bauer, **Mat. Res. Soc. Symp. Proc.**, 73 (1986) 187.

85. S. Sakka, K. Kamiya, K. Makita, Y. Yamamoto, **J. Non-cryst. Solids**, 63 (1984) 223.

86. B. Coltrain, private communication.

87. J. B. Blum, **Inter. J. Hybrid Microelec.**, 8(3) (1985) 1.

88. D. Gallagher, L. C. Klein, **J. Colloid and Interface Sci.**, 109(1) (1986) 40.

89. Solid state NMR experiments were conducted by Dr. Charles E. Bronnimann at the Regional NMR Center at Colorado State University in Fort Collins Colorado which is funded by NSF grant CHE-8610151.

90. I. D. Gay, **J. Mag. Res.**, 58 (1984) 413.

91. Small-angle x-ray scattering experiments were conducted by Dr. Hao-Hsin Huang in the laboratory of Prof. G. L. Wilkes at Virginia Polytechnic Institute and State University.

92. Raman spectra collected from the SPEX system were run by Dr. Mark Holtz in the laboratory of Prof. R. H. Zallen at Virginia Polytechnic Institute and State University.

93. Raman spectra collected from the ISA system were run by the author (RHG) at the Virginia Vibrational Spectroscopy Center at Virginia Polytechnic Institute and State University which is funded by the NSF.

94. Thermogravimetric analysis was performed by the author (RHG) in the laboratory of Prof. M. E. Davis at Virginia Polytechnic Institute and State University.

95. E. Lippmaa, M. Mägi, A. Samoson, G. Engelhardt, A. -R. Grimmer, **J. Am. Chem. Soc.**, 102 (1980) 4889.

96. G. Engelhardt, H. Jancke, E. Lippmaa, A. Samoson, **J. Organometallic Chem.**, 210 (1981) 295.

97. M. Mägi, E. Lippmaa, A. Samoson, G. Engelhardt, A. -R. Grimmer, **J. Phys. Chem.**, 88 (1984) 1518.

98. E. A. Williams, **Annual Reports on NMR**, (1983) 235.

99. S. Sakka, Y. Tanaka, T. Kokubo, **J. Non-cryst. Solids**, 82 (1986) 24.

100. G. E. Maciel, D. W. Sindorf, **J. Am. Chem. Soc.**, 102 (1980) 7607.

101. D. A. Torchia, **J. Mag. Res.**, 30 (1978) 613.

102. J. K. Gillham, **Polym. Eng. Sci.**, 19(10) (1979) 676.

103. R. Zallen, **The Physics of Amorphous Solids**, (John Wiley & Sons, New York, 1983) 187.

104. P. G. de Gennes, **J. Phys. (Paris)** 37 L1 (1976).

105. D. J. Stauffer, **J. Chem. Soc. Faraday Trans. II** 72 (1976) 1354.

106. P. J. Flory, **J. Am. Chem. Soc.** 63 (1941) 3083.

107. W. H. Stockmayer, **J. Chem. Phys.**, 11 (1943) 45.

108. W. H. Stockmayer, H. Jacobson, **J. Chem. Phys. Lett.**, 11 (1943) 393.

109. H. Jacobson, W. H. Stockmayer, **J. Chem. Phys.**, 18 (1950) 1600.

110. M. Hass, **J. Phys. Chem. Solids**, 31 (1970) 415.

111. S. A. Brawer, W. B. White, **J. Non-cryst. Solids**, 23 (1977) 261.

112. T. Furukawa, W. B. White, **J. Non-Cryst. Solids.**, 38 & 39 (1980) 87.

113. N. Grassie, I. MacFarlane, **Eur. Polym. J.**, 14 (1978) 875.

114. J. E. McGrath private communication.

115. R. W. Lenz, **Organic Chemistry of Synthetic High Polymers**, (John Wiley & Sons, New York, 1967) 745.

The vita has been removed from the scanned document